Electromagnetic Analysis of Electric Machines

First Principles, Modeling, and Design

James L. Kirtley • Christopher H. T. Lee
Sajjad Mohammadi

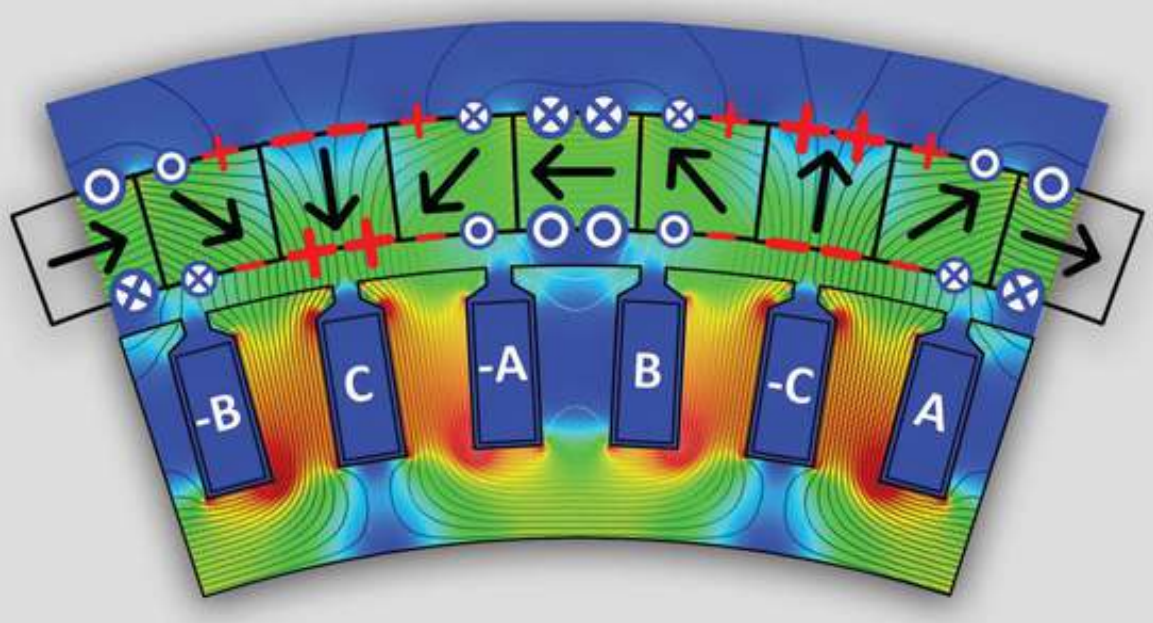

IEEEPress
with website
WILEY

Electromagnetic Analysis of Electric Machines

IEEE Press
445 Hoes Lane
Piscataway, NJ 08854

Electromagnetic Analysis of Electric Machines

First Principles, Modeling, and Design

James L. Kirtley
Massachusetts Institute of Technology
MA, USA

Christopher H. T. Lee
Nanyang Technological University
Singapore

Sajjad Mohammadi
University of Alberta
Canada

IEEE*Press*
WILEY

Published by John Wiley & Sons, Inc., Hoboken, New Jersey.

The manufacturer's authorized representative according to the EU General Product Safety Regulation is Wiley-VCH GmbH, Boschstr. 12, 69469 Weinheim, Germany, e-mail: Product_Safety@wiley.com.

Library of Congress Cataloging-in-Publication Data Applied for:

Hardback ISBN: 9781394315277

Cover Design: Wiley
Cover Image: © Sajjad Mohammadi

Set in 9.5/12.5pt STIXTwoText by Straive, Chennai, India

Contents

About the Authors

James L. Kirtley is a Professor of Electrical Engineering at the Massachusetts Institute of Technology and a recognized expert in electric machines and power systems. A Member of the National Academy of Engineering, Fellow of IEEE and recipient of the IEEE Nikola Tesla Award, he has decades of research and teaching experience. He is the author of *Electric Power Principles*.

Christopher H. T. Lee is an Associate Professor and Assistant Chair (Research) at School of Electrical and Electronic Engineering, Nanyang Technological University, Singapore, with expertise in electric machine analysis and renewable energy integration. He has held research positions at Massachusetts Institute of Technology and serves as an Associate Editor for several IEEE journals. He is a Fellow of IET, United Kingdom and recipient of Nagamori Award.

Sajjad Mohammadi is an Assistant Professor of Electrical Engineering at the University of Alberta, with expertise in electric machines, power magnetics, and power electronic drives. Previously, he was with Apple Inc. He has received several awards, including the George M. Sprowls Outstanding PhD Thesis Award from MIT, where he earned his PhD.

Preface

Electric motors and generators have been central to the world economy since the industrial revolution and have had a major and beneficial impact on just about all aspects of modern lives. And, even though they have been around for well over a century, electromechanical devices are still evolving, improving, and attaining new applications. There is still a need for understanding electromechanical systems, not only so they can be well designed but also so they can be properly applied. Our objective in writing this book is to provide a basis for understanding electromechanical systems, both for design and application.

Evolution of electromechanical systems has involved better understanding of the interactions involved as well as improvements in materials, applications of new materials, advances in heat transfer, and developments of new and different applications. It is not out of bounds to think that all of these driving forces will continue, so that there will continue to be a need for understanding of electromechanics and electromechanical systems, to enable more generations of applications.

In writing this book, we have been influenced in our thinking by the work of Charles Kingsley and Arthur Fitzgerald, joined by Stephen Umans, whose textbook "*Electric Machinery*"[1] is still widely used. Our objective in this book is to provide a more analytical and rigorous framework for understanding and to provide a way of extending our knowledge to devices not yet envisioned. It is our strong conviction that, to understand electric machines and similar electromechanical systems, one must have a firm grasp of the underlying physical principles. In this respect, this book has been heavily influenced by the teaching, at The Massachusetts Institute of Technology, of Herbert Woodson and James Melcher, who developed and taught an undergraduate subject entitled, as was their three volume textbook, "*Electromechanical Dynamics.*"[2] Thus this book is quite heavily analytical in nature. We resort to numerical analysis only when systems cannot be accurately represented by analytical constructs such as partial differential equations.

This book is the descendant of informal notes used in a graduate subject in electric machinery taught by one of us (Kirtley) at MIT[3]. Those notes have evolved over many teachings of that subject, involving several different generations of students and with developments in the technology of electric machinery and power electronics.

The book begins with a concise introduction and then a description of electric and magnetic circuits and electromagnetic fields, forces, and energy flows. A chapter on design synthesis and optimization is intended to set the stage for further analysis. Then the fundamental classes of electric machines are presented with a more rigorous mathematical framework than usual in college textbooks. Within the descriptions of the various classes of machine are developments of analytical

1 Electric Machinery, A.E. Fitzerald, C. Kingsley, S.D. Umans, McGraw-Hill, 2003.
2 Electromechanical Dynamics, H.H. Woodson, J.R. Melcher, Wiley, 1968.
3 https://ocw.mit.edu/courses/6-685-electric-machines-fall-2013/

methods for understanding and modeling of electromechanical devices. The basics of power electronics drives and machine control finish the presentation. In most of the chapters, representative examples and problems appear to challenge the reader.

At the end, it is hoped that a student who uses this book will have developed an intuitive understanding not only of electric machinery, but also of the basic principles on which electric machines work, and that study of this material will lead to the ability to use the fundamentals of electromechanics to develop new types of systems and for applications that we do not yet envision.

About the Companion Website

This book is accompanied by a companion website:

www.wiley.com/go/kirtleyelectric

This website includes:

Problems and Solutions

1

Motors, Generators, and Electromechanics

1.1 Introduction

Electric machinery has had a profound impact on our world, and will continue to be used in many new and existing ways. As a way of generating and transferring motive force, electric power has advantages over other methods. It is easily divisible: one large generating source can provide energy for many smaller loads. It is flexible in arrangement and physical alignment. At the point of use, electricity is clean, relatively safe, and efficient relative to most other means of distributing power, and, unlike hydraulic and pneumatic systems, it doesn't leak. Electric power is consistent with all manner of sources: heat engines, hydraulic power (falling water), wind, and even photons from the sun. Battery technology has evolved to the point where it is possible to store substantial quantities of electric energy to power vehicles and to power stationary devices overnight, when the sun is not shining. It is reasonable to conclude that electric machinery will play a major role in the conversion of many energy uses to carbon-free, sustainable, and renewable sources.

The purpose of this book is to understand not only the existing classes of electric motors and generators but also existing and yet-to-be-invented classes of electromechanical devices. In the text, we delve into a number of analytical techniques. Analytical techniques distinct from some of the numerical methods for analysis of electric machines, notably finite elements, are prominent here. While numerical methods are in a sense more advanced and can, in many circumstances, provide more accurate predictions of performance, in our opinion, the analytical methods contained here will lead to better intuitive understanding. Numerical analysis can follow.

1.2 Motors and Generators

Experimentation with electric motors and generators began in the 1830s with small devices that today we would regard as interesting toys. Progress evolved slowly, but by the 1880s, commercial electric lighting, using commutator machines as generators, had evolved; and by the 1890s, alternating-current generators that permitted high-voltage transmissions were in use. Evolution of these machines to the types we have today largely involved development of materials (conductors, insulation, magnetic steels, and permanent magnets) but also understanding of electromagnetic principles and associated analytical techniques has led to improvements in machine design.

Electric machines come in a very wide variety of types and sizes: from milliwatts to gigawatts. There are three major classes of rotating electric machines used today. Commutator machines are the oldest. They rely on a mechanical switch to align the magnetic flux and current. They are

Electromagnetic Analysis of Electric Machines: First Principles, Modeling, and Design, First Edition.
James L. Kirtley, Christopher H. T. Lee, and Sajjad Mohammadi.

Companion website: www.wiley.com/go/kirtleyelectric

usually thought of as "DC" machines, although one variety of commutator machine, called "universal motor" works with alternating current and actually has a wide range of applications in consumer products such as vacuum cleaners and industrial tools. In some applications, commutator machines employ permanent magnets for providing the interaction flux.

The other widely used classes of electric machines, synchronous and induction, resemble each other in that they incorporate similar winding structures in the stator. They both employ a rotating magnetic current distribution that interacts with a rotating magnetic flux to produce torque. Synchronous machines have a magnet, either an electromagnet or a permanent-magnet structure, to provide that interaction flux. Induction machines generally use the stator to induce both the interaction flux and reaction currents in both the rotor and stator. Induction motors are generally rugged, reliable, and widely used for applications such as pumps, fans, and powering shop equipment. Synchronous generators are used in power plants. Both synchronous and induction motors are used in propulsion of cars, trains, and ships. It is impossible to describe, in the space available, all applications of electric machinery. Suffice it to say that, if it moves, it is likely that an electric motor moves it.

The three major classes of electric machines described so far are not the complete set of useful machines, and one of the purposes of this book is to establish in the reader skills that permit understanding of many other machine types, such as variable reluctance motors, synchronous reluctance motors, and other cleverly designed machines.

Most vehicles employ heat engines for motive power. But even in this area, electric motors are in the ascendancy. Many railroad trains employ electric propulsion: some trains run "under catenary" and have electric motors that turn the wheels. Other trains employ "diesel-electric" propulsion, with the diesel engines driving generators and electric motors driving the wheels. Modern cruise ships employ similar drive mechanisms. At the time of writing of this book, motors and generators thought to be suitable for aircraft propulsion are under development. Mention must be made to electric and hybrid electric automobiles, which are bound to be increasingly important in the near future.

When we refer to electric machines, we tend to think of rotating machines, but there are also linear machines that are used in applications such as propulsion and braking for roller coasters, baggage handling equipment, and moving materials around factories. Linear induction motors are now seeing application in launching airplanes from aircraft carriers.

Most of the machines dealt with here employ the interaction between magnetic flux and a current to produce torque or linear force. There are some machines, called flux switching, variable reluctance, or synchronous reluctance machines, that use variation in reluctance of a magnetic circuit to produce torque or linear force. There are also truly "electric" machines that employ variations in capacitance to produce motion.

Electric machines, or generally electromechanical devices, have various other applications beyond the common ones mentioned above. High-speed motors along with magnetic levitation systems are employed in flywheel energy storages. Photolithography machines in semiconductor technology utilize levitated linear machines having highly precise location, small noise, and low vibration. Robotic joints and mechatronic systems are facilitated by torque-dense actuators along with mechanical gears to reduce speed and increase torque. Electromechanical and electromagnetic devices are present in consumer electronics like cell phones, e.g. wireless charging, haptic engines, and camera voice-coil motors. Satellite systems utilize high-speed motors for the reaction wheels used for altitude control systems (ACS) and actuators in solar and antenna pointing mechanisms. Electric machines are also present in medical devices such as actuators in assistive robotic arms, levitated motors in blood pumps, and, likely in the future, in artificial hearts.

Not all electromechanical devices qualify as motors or generators, and some important electromechanical devices have no electrical current connections. For example, eddy current couplers have found their way into flywheel energy storage systems, high-speed levitated technologies, and precision robotic arms, addressing the need for noncontact torque transfer and minimized mechanical wear. Their use extends to wind turbines, offering inherent vibration filtering and overload protection. Magnetic gears have important advantages over their toothed-wheel equivalents.

1.3 Analytical Modeling for Further Innovations in the Next Generation of Electric Machines

In a world marked by ever-increasing energy consumption and a growing demand for sustainable, economical, and environmentally friendly power and energy systems, there is an urgent need for innovative electromechanical devices with higher efficiency. The evolving landscape of emerging applications, ranging from electric transportation and renewable energy initiatives to robotics and space technology, as well as advancements in other areas such as high-performing wide-bandgap semiconductors allowing for high-frequency compact power electronics and high-temperature superconducting materials facilitating new levitation systems, presents new opportunities and challenges. These developments necessitate the evolution of the next generation of electromechanical devices for the existing and the emerging applications that are not only efficient, compact, and reliable but also lightweight and cost-effective. Addressing these demands with pioneering solutions is fundamental for meeting the evolving needs of our societies and advancing technology.

Despite the convenient use of finite element methods as a powerful technique, which does not even require a deep theoretical knowledge of electromagnetics in many cases, it does not capture many physical aspects of the device, as it acts like a black-box platform. This book takes an analytical approach, delving into the physics and fundamental principles of electromagnetics and electromechanics, with the intention of yielding deeper insights and thereby facilitating the development of novel and application-specific technologies.

1.4 Analytical Modeling for Design Optimizations

Analytical models provide a fast yet sufficiently accurate framework for design optimization, in contrast to the computationally intensive numerical techniques such as Finite Element Modeling (FEM). The approach to the design optimization of electromechanical devices and electric machines in this book is a hybrid strategy, integrating both analytical models and FEM. Consider optimizing an electromechanical device with ten design parameters to be tuned. If each parameter needs to be evaluated for at least ten values within a practical range, there will be $10^{10} = 10{,}000{,}000{,}000$ designs to investigate. Even with a supervised search to reduce the number of iterations, running finite element simulations for each iteration is generally impractical.

Analytical modeling and finite element analysis each have their pros and cons, as summarized in Table 1.1. In essence, analytical models provide intuition and pave the way for further innovation. They are also fast and can easily be incorporated into system-level designs, making them suitable for the initial design stages. On the other hand, finite element methods can account for greater complexities but are computationally inefficient. Therefore, incorporating both approaches in the design process is more effective.

Table 1.1 Comparison of modeling methods.

Analytical Modeling	Finite Element Method (FEM)
Governing equations and insight into fundamental principles of electromechanics	Sort of a black box framework between input and output quantities, no equations
Computationally efficient and very fast	Computationally heavy and time-consuming
Suitable for primary design optimizations and sensitivity analysis	Too heavy for initial design optimizations
Suitable for primary stages of the design within a large search space	Suitable for sanity checks and final stages of the design optimization within a limited search space
Contributing to efficient control system designs	No equations to be employed in control system designs
Requires deep knowledge of electromagnetics, physics, and math	No need for deep knowledge of electromagnetics, physics, and math
Difficult for beginners and people in other fields	Easy tool for beginners and people in other fields
May require geometry simplifications to apply boundary conditions	Can handle complex geometries and boundary conditions
May ignore nonlinearities and complex material properties	Can handle nonlinearities and complex material properties

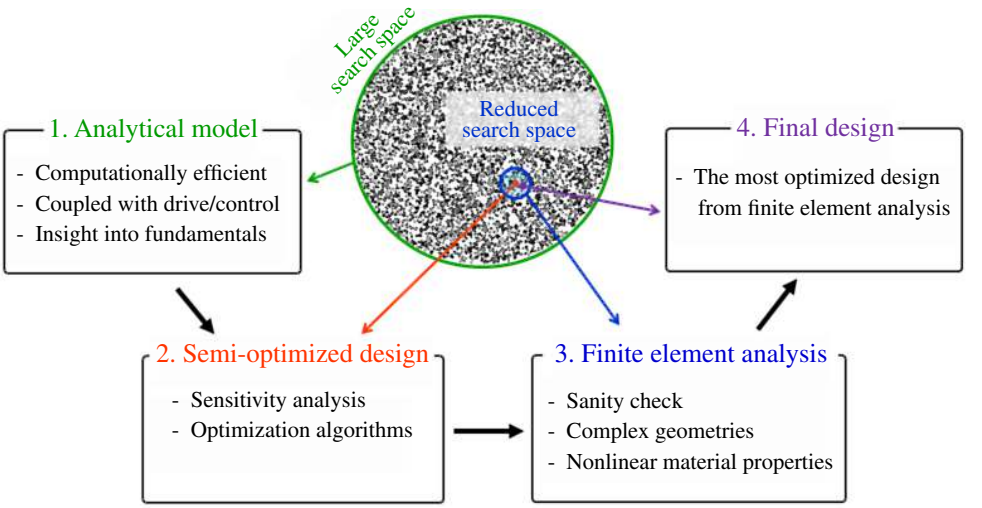

Figure 1.1 The design process.

The design optimization approach proposed, illustrated in Figure 1.1, includes three stages:

1) **Developing an Analytical Model:** This model helps in understanding the fundamental electromechanics and provides a computationally fast solution for optimizations. Each design evaluation using the analytical method typically takes only a few seconds.
2) **Initial Optimization:** Using optimization methods such as genetic algorithms, one searches within the large search space to find a semi-optimized design. This is referred to as the

semi-optimal point because the analytical model may have simplified some geometries or ignored certain material properties.

3) **Refined Search with FEM:** Now a reduced search space with a much smaller range of designs may be analyzed with finite element techniques. Although time-consuming, FEM can handle complex geometries and material properties more accurately than analytical methods.
4) **Final Design:** The final design is obtained from finite element analysis, which may deviate slightly from the semi-optimal point due to the simplifications in the analytical model, but it accounts for the complexities that were ignored within the analytical model.

1.5 Analytical Modeling for Integrated-Design of Electric Machines, Drives, and Other Components

Another attribute of developing analytical models for system components is that it permits the development of performance models that are difficult to derive from FEM. These models permit system-level optimization as different components must interact with each other. A system in which each component is optimized for a particular operating condition will likely not be as effective as one in which all of the components have their parameters set to make the whole system work optimally. This is another argument for an analytical approach to understanding the operation of electromechanical devices.

1.6 Analytical Modeling for Physics-Informed Artificial Intelligence

Artificial intelligence (AI), through machine learning (ML), may be used in the future for machine design. In particular, for specialized designs for similar applications, the use of AI might reduce the costs of "design" and of producing details and drawings. That said, there would be a need for interpretable and generalizable models to be used by AI-based design routines. Analytical models can be developed to integrate physics into the architecture, loss function, or optimization constraints of AI models. This approach bridges the gap between data-driven and physics-based models, enabling them to complement each other, forming an efficient yet accurate framework.

Embedding physics into AI models enhances accuracy, interpretability, reliability, physical plausibility, and the generalizability of predictions. Guided by physical laws, the learning process converges faster and requires less training data. This reduces computational costs and training time, as well as the size and complexity of the model. A physics-based loss term guides the training of the AI/ML model to align with the fundamental principles of physics of the system. This improves the model's ability to generalize to unseen conditions – a significant challenge for traditional ML models during extrapolation. Physics-informed AI is particularly more effective at avoiding overfitting to noisy or outlier data. Analytical models can also be used to train ML models in scenarios where data collection is expensive, such as rare extreme cases that could cause permanent damage to the system (e.g. severe faults in electric machines or power electronics converters).

On the other hand, when only part of the physics is derived, when the developed analytical model lacks accuracy due to unavoidable simplifications such as approximated boundary conditions, or when there exist unmodeled dynamics or ignored material properties, physics-informed AI/ML can address these discrepancies. Physics-informed AI is capable of modeling and characterization of material nonlinearities such as magnetic saturation or hysteresis in motor laminations and magnetic components in power electronics converters. It can also handle non-idealities in the switches

of the drive circuit and account for system variations over time, such as aging of bearings, demagnetization of magnets, or resistance variations due to temperature.

Expression (1.1) is an example of a loss function L for a physics-informed AI model to predict magnetic flux density distribution within an electric machine. In addition to the traditional data loss L_{data}, it includes a loss term $L_{physics}$ to minimize the error from the physics-based analytical model:

$$L = L_{data} + \lambda L_{physics} = \frac{1}{N}\sum_{i=1}^{N}\left(B_i^{ML} - B_i^{data}\right)^2 + \lambda\,\frac{1}{N}\sum_{i=1}^{N}\left(B_i^{ML} - B_i^{physics}\right)^2 \tag{1.1}$$

where λ is a coefficient balancing the contribution of the loss terms, B^{ML} is the predicted value from the ML model, B^{data} is the collected data, and $B^{physics}$ is derived from the analytical model.

As another example, for faster convergence, a neural network model can initially be trained using data generated from analytical equations and then fine-tuned with high-fidelity FEM or experimental data. Alternatively, PIAI models can predict flux density or magnetic potential distribution by embedding Maxwell's equations and boundary conditions as part of the training process or as loss functions, significantly reducing reliance on time-consuming FEM. Below is an example of a physics loss term designed to penalize the violation of Ampere's law, Gauss's law as well as normal and tangential boundary conditions:

$$L_{physics} = \int \underbrace{\|\nabla \cdot B\|^2 + \left\|\nabla \times \frac{B}{\mu_0} - J\right\|^2}_{\text{Gauss's and Ampere's laws}} + \underbrace{\|\hat{n}\cdot(B_1 - B_2)\|^2 + \|\hat{n}\times(B_1 - B_2) - \mu_0 K\|^2}_{\text{Boundary Conditions}} \tag{1.2}$$

where n is the normal unit vector of the boundary, and K is the surface current density.

Physics-informed AI systems can also be applied in thermal modeling to predict temperature distributions in the powertrain components while adhering to the heat diffusion equation by defining a loss function using steady-state form of heat diffusion as:

$$L_{physics} = \|k\nabla^2 T + q\|^2 \tag{1.3}$$

where T, k, and q are temperature, thermal conductivity, and generated heat, respectively.

Additionally, such techniques can be employed to enhance instrumentation reliability. For example, powertrain sensors, which are prone to faults caused by aging or vibrations, can be made more robust and reliable when integrated with ML-based monitoring methods.

1.7 Developed in This Book

The objective of this textbook is to gain an understanding of the various types of electromechanical systems and the means for comprehending the principles of their inner workings. We intend that students of this work will be able to analyze all manner of electromechanical and related devices. This book should be suitable for use in an advanced university subject. It is not intended for a "second" course in electric machinery, since it deals with fundamental principles of electromechanics.

The book starts with the development, from first principles, of the lumped-parameter approximations to reality embedded in circuits. Electric circuit theory is well developed, and its analog, magnetic circuit theory, is useful in understanding the operation of electric motors, which perhaps should more properly be called "magnetic motors". Techniques of field analysis suitable for

understanding electromechanical apparatus are developed, including the rigorous methods of scalar and vector potential, and the heuristic methods of flux tubes and finite elements.

To gain an understanding of electromechanical apparatus, we resort to first principles, as described by Maxwell's equations, Poynting's theorem, and conservation of energy (the first law of thermodynamics). From these basic laws of nature, it is possible to develop ways of calculating force and torque, including the direct Lorentz force law and the indirect Principle of Virtual Work as the basic ways of understanding how electric machines work. Field methods for estimating forces, embodied in the Maxwell stress tensor, are developed at this point. Surface impedances and magnetic diffusion are introduced as important analytical techniques and aids to understanding.

A discussion such as this must also address design techniques, including optimization. This book describes some of the heuristic optimization techniques employed by machine designers. A diversion into the design of transformers, important energy-handling devices that do not involve motion, is used to further understand design, optimization, and situations with multiple "attributes".

Once a basic understanding of the principles of force generation and power flow in electromechanical systems has been developed, the book then describes the major classes of electric motors and generators, starting with synchronous machines, including variable-speed "brushless DC" machines that are really synchronous machines with associated variable frequency drives. The notion of "round rotor" and "salient" machines will be developed and used to show how such machines work.

At this point, a theoretical picture of typical structures in machines, such as slots, air gaps, and windings, is developed. An understanding of the fields, particularly fields in the relative motion "gaps" of machines is developed using the Fourier series of space harmonics.

Analysis of synchronous machine dynamics is developed from field analysis and modeling of the windings and other structures of the machines. This involves the development of rotating-field transformations (Park's equations), approximate pictures of the synchronous machine structures, normalization into "per unit" systems, and interactions with networks. The approximate notions of "transient" and "subtransient" impedances and their importance in machine and system dynamics will be introduced.

At this point, the book makes a diversion into commutator machines, an economically very important class of motor, particularly of small motors. Historically important connections (series, shunt, separately excited) and other structures, such as commutation and compensation windings, which are not, of themselves, of much importance, are discussed because they provide an understanding of the structures and control techniques of other classes of machines. The notions of "base speed", "constant torque region", and "constant power region" will be introduced as variable-speed operation is considered.

Induction motors are developed in detail, using elements from earlier in the book, such as windings, associated space harmonics, and diffusion. Both wound-rotor and "squirrel-cage" structures are important and described. Induction motors and generators are economically and technically important, and they will be described in some detail. Induction motor control, including variable speed drives, volts/Hz control, and field-oriented control, will be developed.

Variable reluctance machines are, as of this writing, not particularly economically important, but they are interesting from a technical viewpoint and have some important attributes, so their structures and operation will be discussed.

Advances in power electronics are driving many advances in electric machine design and application, and a basic understanding of power electronics, including devices and circuits, is essential to the modern machine designer. While this is not a book about power electronics, a chapter is

devoted to the topic, hopefully with enough detail to enable a machine designer to understand the interaction between the motor (or generator) and the system of power electronics that is driving it.

Control of machine/drive systems is necessary for the design and application of electromechanical systems. Elements of control are developed at various points in the text: variable DC machine drives using "choppers", volts/Hz, and "field-oriented" control for induction motors and slip ring injection for wound-rotor induction generators. The final chapter of the book delves into the most important elements of classical control: feedback, feed-forward, responsiveness, disturbance rejection, and stability.

Each chapter will be followed by example problems that might be used by themselves or as templates for homework assignments. Most of these problems were used at MIT in a subject for which most of the material in the book was written.

An appendix will contain a number of scripts that have been written to illustrate and provide some color to concepts in the text. These were written to run under the MATLAB mathematical assistant program. With at most minor edits, they will also run under the newer public-domain program Octave.

It is assumed that the students taking the subject that uses this book will have a working understanding of circuit theory and ordinary and partial differential equations. The physical principles to be discussed are described by Maxwell's equations, Poynting's theorem, the Lorentz force law, and the first law of thermodynamics. As will be shown, not all types of electromechanical systems are amenable to the same form of analysis, so the focus here is on physical understanding. Different methods of analysis will be discussed and compared. In some cases, a direct calculation of force, using the Lorentz force law, which is the interaction of current with magnetic flux density, will suffice. In other cases, energy conservation, which is a consequence of the first law of thermodynamics, can be invoked, and in other cases, the Maxwell stress tensor is appropriate. One feature of the book is an argument that shows the equivalence of multiple versions of force calculation techniques.

It is our hope that students of this book will emerge as important motor designers and appliers after reading and understanding the material contained herein.

2

Circuits and Field Analyses

2.1 Introduction

Magnetic circuits offer, as do electric circuits, a way of simplifying the analysis of magnetic field systems which can be represented as having a collection of discrete elements. In electric circuits, the elements are sources, resistors, and so forth, which are represented as having discrete currents and voltages. These elements are connected together with "wires" and their behavior is described by network constraints (Kirchhoff's voltage and current laws) and by constitutive relationships such as Ohm's law. In magnetic circuits, the lumped parameters are called "Reluctances" (the inverse of "Reluctance" is called "Permeance"). The analog to a "wire" is referred to as a high permeance magnetic circuit element. Of course, high permeability is the analog of high conductivity. By organizing magnetic field systems into lumped parameter elements and using network constraints and constitutive relationships, the analysis of such systems may be simplified.

2.2 Electric Circuits

First, review how electric circuits are defined. Start with two conservation laws: conservation of charge and Faraday's law. From these, with appropriate simplifying assumptions, can be derived the two fundamental circuit constraints embodied in Kirchhoff's laws.

2.2.1 Kirchhoff's Current Law (KCL)

Conservation of charge is, in integral form as:

$$\oiint \vec{J} \cdot \vec{n} da + \int_{volume} \frac{d\rho_f}{dt} \, dv = 0 \tag{2.1}$$

This simply states that the sum of current out of some volume of space and rate of change of free charge in that space must be zero. See Figure 2.1.

Now, a discrete current is the integral of current density crossing through a part of the surface:

$$i_k = -\int_{surface_k} \vec{J} \cdot \vec{n} da$$

and if there is no accumulation of charge within the volume (in ordinary circuits, the nodes are small and do not accumulate charge). As illustrated in Figure 2.2:

$$\oiint \vec{J} \cdot \vec{n} da = -\sum_k i_k = 0 \tag{2.2}$$

Electromagnetic Analysis of Electric Machines: First Principles, Modeling, and Design, First Edition.
James L. Kirtley, Christopher H. T. Lee, and Sajjad Mohammadi.

Companion website: www.wiley.com/go/kirtleyelectric

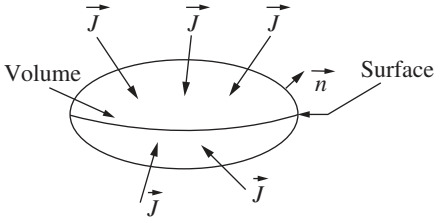

Figure 2.1 Illustration of conservation of charge.

which holds if the sum over the index k includes all current paths into the node. This is, of course, KCL.

2.2.2 Kirchhoff's Voltage Law (KVL)

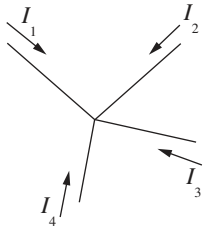

Figure 2.2 Illustration of KCL.

$$\sum_k i_k = 0$$

Faraday's law is, in integral form:

$$\oint \vec{E} \cdot d\vec{\ell} = -\frac{d}{dt} \iint \vec{B} \cdot \vec{n}\, da$$

where the closed loop on the left-hand side of the equation is the edge of the surface of the integral on the right-hand side. (See figure 2.3)

Now define voltage in the usual way, between points a and b for element k:

$$v_k = \int_{a_k}^{b_k} \vec{E} \cdot d\vec{\ell} \tag{2.3}$$

Then, if it is assumed that the right-hand side of Faraday's law is zero (that is, there is no flux linked by the loop of circuit elements), Faraday's law becomes, assuming a complete loop as shown in Figure 2.4:

$$\sum_k v_k = 0 \tag{2.4}$$

This works for circuit analysis because most circuits do not involve magnetic induction in the loops. However, it does form the basis for much head scratching over voltages encountered by "ground loops".

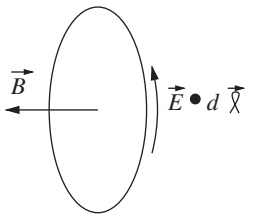

Figure 2.3 Illustration of Faraday's law.

2.2.3 Constitutive Relationship: Ohm's Law

Many of the materials used in electric circuits carry current through a linear conduction mechanism. That is, the relationship between electric field and electric current density (known as Ohm's law) is:

$$\vec{J} = \sigma \vec{E}$$

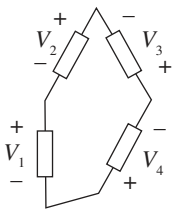

Figure 2.4 Illustration of KVL.

To show how lumped-parameter circuit elements are identified, suppose a cylindrical rod that has constant area and is carrying current over some finite length, as shown in Figure 2.5. Assume this rod is carrying current density J (assume that this rod is connected to something that can carry current, perhaps a wire …). Total current carried by the rod is simply $I = |J|A$.

And then voltage across the element is:

$$v = \int \vec{E} \cdot d\vec{\ell} = \frac{\ell}{\sigma A} I \tag{2.5}$$

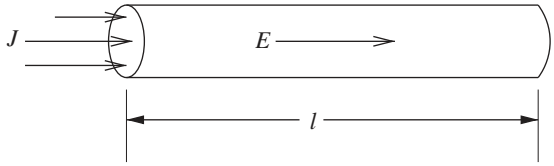

Figure 2.5 Simple rod-shaped resistor.

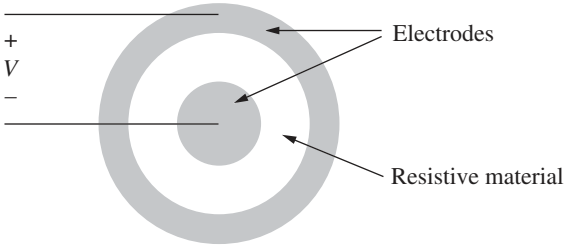

Figure 2.6 Annular resistor.

From which the resistance is simply:

$$R = \frac{V}{I} = \frac{\ell}{\sigma A}$$

Note that, if conductivity σ is very large, electric field $\vec{E}$ must be very small (if current is not very large). The concept of a "wire" interconnecting components is the limit of conductivity approaching infinity, in which current is confined to the wire, and voltage drop along the wire is zero.

The lumped parameter picture can be used even with elements that are more complex. Consider the annular resistor shown in Figure 2.6. This is an end-on view of something which is uniform in cross-section and has depth D in the direction perpendicular to the page. Assume that the inner and outer elements are very good conductors, relative to the annular element in between. Assume further that this element has conductivity σ and inner and outer radii R_i and R_o, respectively.

Now, if this structure is carrying current from the inner to the outer electrode, current density would be:

$$\vec{J} = \vec{i}_r J_r(r) = \vec{i}_r \frac{I}{2\pi D r}$$

Electric field is:

$$E_r = \frac{J_r}{\sigma} = \frac{I}{2\pi D r \sigma}$$

Voltage is:

$$v = \int_{R_i}^{R_o} E_r(r)\, dr = \frac{I}{2\pi\sigma D} \log \frac{R_o}{R_i}$$

So, the resistance of this element is:

$$R = \frac{\log \frac{R_o}{R_i}}{2\pi\sigma D}$$

2.3 Magnetic Circuit Analogs

In the electric circuit, elements for which voltage and current are defined are connected together by elements thought of as "wires", or elements with zero or negligible voltage drop. The interconnection points are "nodes". In magnetic circuits, the analogous thing occurs: Elements for which

magnetomotive force and flux can be defined are connected together by high-permeability magnetic circuit elements (usually iron), which are the analog of wires in electric circuits. Consider Ohm's law above: If conductivity σ is very large, either current density is very large or electric field is very small. In the limit of conductivity approaching infinity, electric field approaches zero, and in circuit theory, "wires" are assumed to have zero voltage. An analog to Ohm's law is the constitutive relationship between magnetic flux density and magnetic field. In some cases, this may be approximated as a linear relationship:

$$\vec{B} = \mu \vec{H}$$

As will be shown anon, this is only an approximation to reality, but in many cases it will suffice, and if the permeability μ can be assumed to be very large, and unless magnetic flux density B is very large, magnetic field H is very small.

2.3.1 Analogy to KCL: Flux Conservation

Gauss's law is:

$$\oiint \vec{B} \cdot \vec{n}\, da = 0$$

which means that the total amount of flux coming out of a region of space is always zero.

Now, define a quantity which is sometimes called simply "flux" or a "flux tube". This might be thought to be a collection of flux lines that can be bundled together. Generally, it is the flux that is identified with a magnetic circuit element. Mathematically, it is:

$$\boldsymbol{\Phi}_k = \iint \vec{B} \cdot \vec{n}\, da$$

In most cases, flux as defined above is carried in magnetic circuit elements which are made of high permeability material, analogous to the "wires" of high-conductivity material which carry current in electric circuits. It is possible to show that flux is largely contained in such high-permeability materials.

If all of the flux tubes out of some region of space ("node") are considered in the sum, they must add to zero:

$$\sum_k \boldsymbol{\Phi}_k = 0 \tag{2.6}$$

2.3.2 Analogy to KVL: Magnetomotive Force (MMF)

Ampere's law is:

$$\oint \vec{H} \cdot d\vec{\ell} = \iint \vec{J} \cdot \vec{n}\, da$$

where, as for Faraday's law, the closed contour on the left is the periphery of the (open) surface on the right. Now define magnetomotive force, in direct analog to "electromotive force", (voltage):

$$F_k = \int_{a_k}^{b_k} \vec{H} \cdot d\vec{\ell}$$

Further, define the current enclosed by a loop to be:

$$F_0 = \iint \vec{J} \cdot \vec{n}\, da$$

Then the analogy to KVL is:

$$\sum_k F_k = F_0 \tag{2.7}$$

Note that the analog is not exact as there is a source term on the right-hand side, whereas KVL has no source term. Note also that sign counts here. The closed integral is taken in such a direction so that the positive sense of the surface enclosed is positive (upward) when the surface is to the left of the contour. (This is another way of stating the celebrated "right-hand rule": If you wrap your right hand around the contour with your fingers pointing in the direction of the closed-contour integration, your thumb is pointing in the positive direction for the surface.)

2.3.3 Analog to Ohm's Law: Reluctance

2.3.3.1 Simple Case

Consider the magnetic circuit situation shown in Figure 2.7. Here, there is a piece of highly permeable material shaped to carry flux across a single air gap. A coil is wound through the window in the magnetic material (this shape is usually referred to as a "core").

Note that in Figure 2.7: If the positive sense of the closed loop is a direction that goes vertically upward through the leg of the core through the coil and then downward through the gap, the current crosses the surface surrounded by the contour in the positive sense. So that the integral of magnetic field around that loop is just equal to the number of turns in the coil times the current, or NI.

2.3.3.2 Flux Confinement

In this case, the highly permeable material is the magnetic analog of a "wire", in that the magnetic field is very small. If permeability approaches infinity, magnetic field H must approach zero.

By focusing on the two regions indicated, a few observations may be made about magnetic circuits. First, consider "region 1" as shown in Figure 2.7. A bit of detail is shown in Figure 2.8.

In this picture, note that magnetic field $\vec{H}$ parallel to the surface must be the same inside the material as it is outside. Consider Ampere's law carried out about a very thin loop consisting of the two arrows drawn at the top boundary of the material in Figure 2.8 with very short vertical paths joining them. If there is no current singularity inside that loop, the integral around it must be zero, which means the magnetic field just inside must be the same as the magnetic field outside. Since the material is very highly permeable and $\vec{B} = \mu\vec{H}$, and "highly permeable" means μ is very large, unless B is really large, H must be quite small. Thus, the magnetic circuit has small magnetic field H and therefore flux densities parallel to and just outside its boundaries are also small.

Figure 2.7 Single air-gapped core.

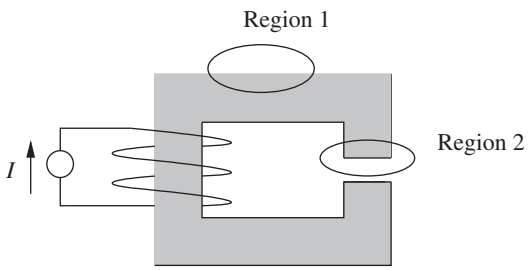

Figure 2.8 Flux confinement boundary: this is "region 1".

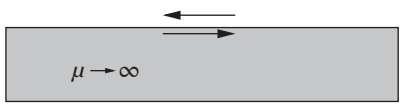

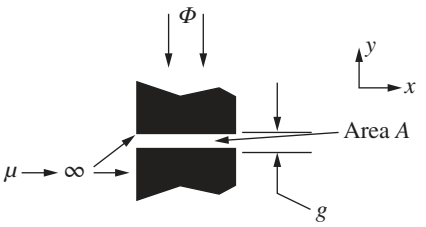

Figure 2.9 Gap boundary.

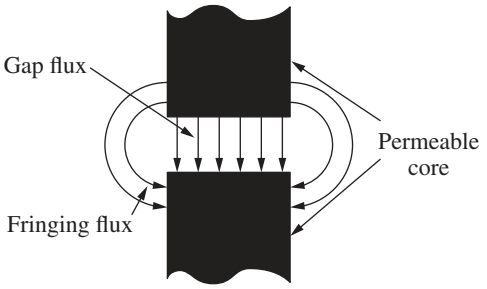

Figure 2.10 Details of flux lines in and around the gap.

2.3.3.3 Magnetic Gap

Consider what is labeled as "region 2" in Figure 2.7, as shown in Figure 2.9. The "gap" is assumed to be relatively small compared with the dimensions in the *x*- and *z*-dimensions that make up the area of the gap. At the surface of the magnetic material, since the magnetic field parallel to the surface must be very small, any flux lines that emerge from the core element must be perpendicular to the surface as shown for the gap region in Figure 2.10. The lines of flux in the gap, being perpendicular to the gap surface, are relatively short. The "fringing fields" outside of the gap are longer and therefore less intense.

For this reason, "fringing fields" are often ignored in considering narrow air gaps.

Assume that some flux is crossing the gap from the upper pole to the lower. That flux is:

$$\Phi = BA$$

where B is the flux density crossing the gap and A is the gap area. Since the permeability of free space is μ_0 (assuming the gap is indeed filled with "free space"), magnetic field intensity is:

$$H = \frac{B}{\mu_0}$$

and gap MMF is just magnetic field intensity times gap dimension. This, of course, assumes that the gap is uniform and thus so is the magnetic field intensity:

$$F = \frac{B}{\mu_0} g$$

which means that the *reluctance* of the gap is the ratio of MMF to flux:

$$\mathfrak{R} = \frac{F}{\Phi} = \frac{g}{\mu_0 A} \tag{2.8}$$

Now, it is possible to produce an equivalent (magnetic) circuit as shown in Figure 2.11, in which the flux crossing the air-gap, represented by the same symbol used for a resistance, is:

$$\Phi = \frac{NI}{\mathfrak{R}}$$

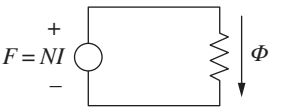

Figure 2.11 Equivalent magnetic circuit.

Figure 2.12 Gapped "C" core.

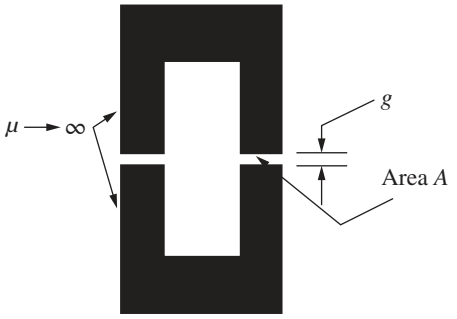

2.3.3.4 Example: C-Core

Consider a "gapped" c-core as shown in Figure 2.12. There are two pieces of highly permeable material shaped generally like "C"s. They have uniform depth in the direction you cannot see. Call that dimension D. Of course, the area $A = wD$, where w is the width at the gap.

Assume the two gaps have the same area. Each of the gaps will have a reluctance.

$$\mathfrak{R} = \frac{g}{\mu_0 A}$$

Suppose a coil with N turns is wound on this core and a current I is carried by the coil.

The magnetic equivalent circuit (MEC) is shown in Figure 2.13. The two gaps are in series and, of course, in series with the MMF source. Since the two fluxes are the same and the MMFs add:

$$F_0 = NI = F_1 + F_2 = 2\mathfrak{R}\Phi$$

And then

$$\Phi = \frac{NI}{2\mathfrak{R}} = \frac{\mu_0 ANI}{2g}$$

The corresponding flux density in each of the two gaps is:

$$B_y = \frac{\mu_0 NI}{2g}$$

2.3.3.5 Example: Core with Different Gaps

As a second example, consider the perhaps oddly shaped core shown in Figure 2.14. Suppose the gap on the right has twice the area as the gap on the left. We would have two gap reluctances:

$$\mathfrak{R}_1 = \frac{g}{\mu_0 A} \quad \mathfrak{R}_2 = \frac{g}{2\mu_0 A}$$

Since the gaps are in series, the flux is the same in each and the total reluctance is:

$$\mathfrak{R} = \mathfrak{R}_1 + \mathfrak{R}_2 = \frac{3}{2}\frac{g}{\mu_0 A}$$

Flux in the magnetic circuit loop is:

$$\Phi = \frac{F}{\mathfrak{R}} = \frac{2}{3}\frac{\mu_0 ANI}{g}$$

And flux density in the two gaps is:

$$B_{y1} = \frac{\Phi}{A} = \frac{2}{3}\frac{\mu_0 NI}{g} \quad B_{y2} = \frac{\Phi}{2A} = \frac{1}{3}\frac{\mu_0 NI}{g}$$

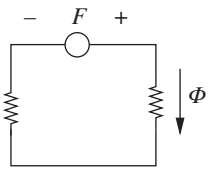

Figure 2.13 Equivalent magnetic circuit: two equal gaps.

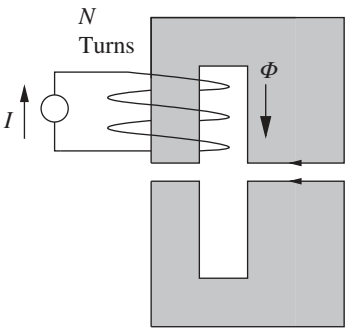

Figure 2.14 Wound, gapped core: different gaps.

2.4 Permanent Magnets

The purpose of this section is to explore the simple model of permanent magnets (PMs) and to develop two ways of looking at permanent magnets that will be useful in analysis of systems employing such magnets.

2.4.1 Permanent Magnetization

A better constitutive relationship between flux density and magnetic field is:

$$\vec{B} = \mu_0(\vec{H} + \vec{M}) \tag{2.9}$$

where M is "magnetization", arising from alignment of magnetic moment of materials. In the linear case, an approximation is that:

$$\vec{M} = \chi_m \vec{H}$$

where χ_m is magnetic susceptibility which is a dimensionless quantity that describes a material's response to an applied magnetic field. And in that case, the permeability is simply $\mu = \mu_0(1 + \chi_m)$.

The problem is usually not so simple, however, as will be shown in subsequent chapters. However, a useful approximation, particularly in the case of permanent magnets, is that:

$$\vec{B} = \mu_0(\vec{H} + \vec{M}_0)$$

where *magnetization* M_0 is fixed. This is very often written as:

$$\vec{B} = \mu_0 \vec{H} + \vec{B}_R$$

And here, the remanent flux density $\vec{B}_R$ is what characterizes the permanent magnet. This is shown graphically in Figure 2.15.

2.4.2 Magnetic Circuits

To illustrate quantitatively how a permanent magnet works in a magnetic circuit, consider the situation illustrated in Figure 2.16. The upper and lower elements are very highly permeable, and there is an "air gap" that is assumed to have permeability μ_0. The vertical dimension of the magnet is h_m and of the gap is g. In this case, all of the action is in the y-direction. Assume the magnet is magnetized in the +y direction. Using Gauss's law, it is easily seen that y-directed flux in the magnet and y-directed flux in the air gap must add to zero. And using Ampere's law, since there

Figure 2.15 Simplified permanent magnet characteristic.

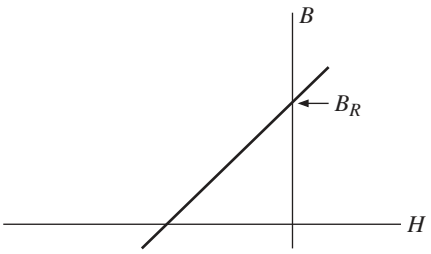

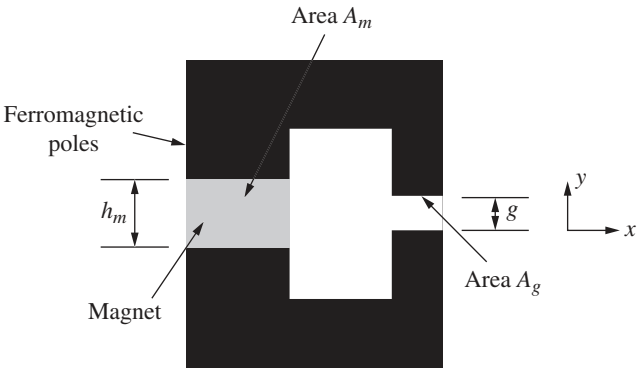

Figure 2.16 Permanent magnet in a magnetic circuit.

is no current in the problem, *y*-directed magnetic field in the magnet times magnet height must balance with field in the gap times the gap height:

$$A_m B_{ym} + A_g B_{yg} = 0$$
$$h_m H_{ym} - g H_{yg} = 0$$

Combining these, we find what is called the unit permeance. That is the dotted line in Figure 2.17.

$$B_{ym} = -\mu_0 \frac{A_g h_m}{A_m g} H_{ym} = -\mu_0 \wp_u H_{ym} \tag{2.10}$$

And, finally, flux densities in magnet and gap are:

$$B_{ym} = B_R \frac{\wp_u}{1 + \wp_u}$$

Figure 2.17 Magnet operating point.

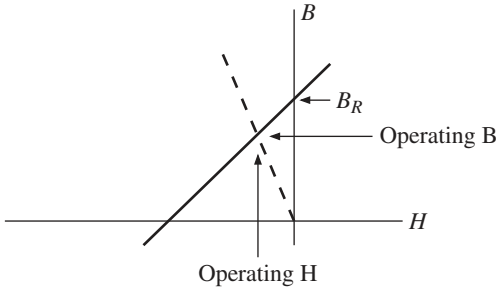

$$B_{yg} = -B_R \frac{\frac{h_m}{g}}{1 + \frac{A_g h_m}{A_m g}}$$

2.4.3 Amperian Current

Noting that, in free space, $\nabla \times \vec{H} = \vec{J}$, one might hypothesize that magnetization might be related to a hypothetical current in this way:

$$\nabla \times \vec{M} = \vec{J}_a$$

That is, the curl of magnetization might be equal to a current-like quantity that could be called *Amperian current*. And indeed, this is a convenient fiction that can be used in boundary value problems to be described anon. For example, consider the boundary between a permanent magnet and free space, shown in simplified form in Figure 2.18.

Using Stokes' theorem,

$$\iint \vec{J}_a \cdot \vec{n}\, da = \oint \vec{M} \cdot d\vec{\ell}$$

Since the boundary between the magnet material and free space is abrupt, the Amperian current will be a surface current. In the z-direction (normal to and out of the paper in this view):

$$K_z = -M_y$$

To illustrate how this Amperian current works, consider the example of Figure 2.16, but with the permanent magnet replaced by a coil of wire carrying a surface current, as illustrated by Figure 2.19. Here, it is clear that the surface current is in the -z direction on the right boundary.

Ampere's and Gauss's laws give:

$$H_{ym} h_m - H_{yg}\, g = h_m K_a$$
$$\mu_0 A_m H_{ym} + \mu_0 A_g H_{yg} = 0$$

Solving this set:

$$B_g = -\mu_0 \frac{\frac{h_m}{g} K_a}{1 + \frac{h_m A_g}{g A_m}}$$

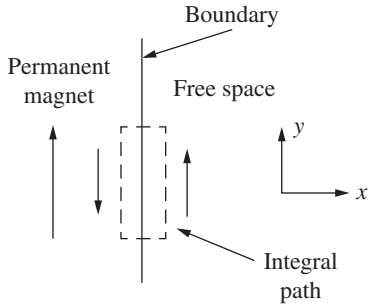

Figure 2.18 Partial magnet boundary.

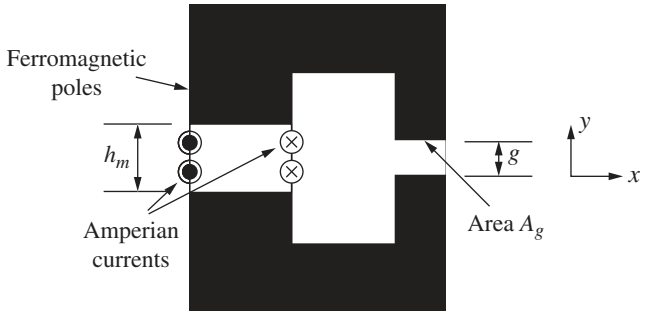

Figure 2.19 Magnet replaced by a coil.

If the Amperian current K_a has the same magnitude as the magnetization M_0 and has the proper sense (right-hand rule), the Amperian current model gives the same flux density in the gap as did the permanent magnet. Note that the use of Amperian current does not get the magnetic field inside the magnet right, but it does get the external fields right. It is interesting to note, and this leads to an understanding of why permanent magnets are so useful, that a magnet with a remanent flux density of 1.2 T (characteristic of modern *NdFeB* magnets) would have Amperian current of about 955 kA/m.

2.4.4 Chu Magnetic Charge

The hypothetical but fictitious magnetic charge was hypothesized by Chu [1] in the following manner:

$$\nabla \cdot \vec{H} = \frac{\rho^*}{\mu_0} \tag{2.11}$$

Then, if flux density B has zero divergence, the fictitious "Chu" charge must be:

$$\frac{\rho^*}{\mu_0} = -\nabla \cdot \vec{M}$$

Applying the divergence theorem to this:

$$\oiint \vec{H} \cdot \vec{n}\, da = \int_{vol} \frac{\rho^*}{\mu_0} dv$$

At the surface of a magnet, as shown by Figure 2.20, if the magnetization is upward, the "Chu charge" will be positive and

$$H_1 - H_2 = \frac{\sigma^*}{\mu_0} = M_0$$

This, too, can be used to describe a permanent magnet. Note that this type of boundary is useful when magnetization is perpendicular to a surface, while the Amperian current is useful when magnetization is parallel to a surface.

Figure 2.20 Magnetic charge as a boundary condition.

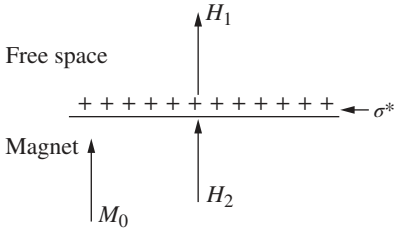

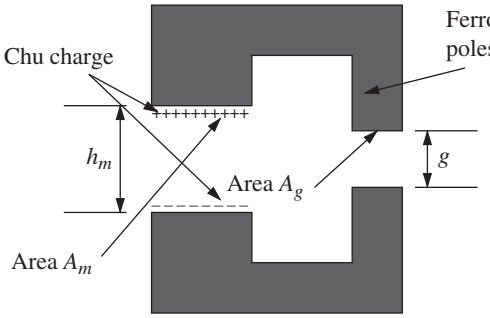

Figure 2.21 Magnet replaced by Chu charge.

Consider the same magnetic circuit problem examined earlier but with the magnet replaced by the appropriate Chu (fictitious) magnetic charge, as shown in Figure 2.21. The governing equations are:

$$H_{ym}A_m + H_{yg}A_g = -\frac{\sigma^*}{\mu_0}A_m$$
$$H_{ym}h_m - H_{yg}g = 0$$

And the magnetic flux density in the gap is the same as before.

2.5 Scalar Potential for Field Analysis

Magnetic fields are vectors that may vary in space. Having multiple components, vectors may be complicated to handle. The use of scalar potential is a way of simplifying field analysis, since, as its name suggests, potential is a single-valued function of space. Generally, the form of a solution is found and applied to boundary conditions. Once that is done, the magnetic fields are computed directly.

In a region with no current, the curl of magnetic field is zero, suggesting that magnetic field might be represented as the gradient of a scalar quantity:

$$\vec{H} = -\nabla\psi$$

Then, since the divergence of magnetic field is also zero, if permeability is constant (as it is in free space):

$$\nabla \cdot \nabla\psi = \nabla^2\psi = 0 \tag{2.12}$$

2.5.1 Scalar Potential in Rectangular Coordinates

In rectangular coordinates, the pertinent expressions are:

$$H_x = -\frac{\partial\psi}{\partial x} \quad H_y = -\frac{\partial\psi}{\partial y} \quad H_z = -\frac{\partial\psi}{\partial z}$$
$$\frac{\partial^2\psi}{\partial x^2} + \frac{\partial^2\psi}{\partial y^2} + \frac{\partial^2\psi}{\partial z^2} = 0 \tag{2.13}$$

In practice, solutions to these equations are found and matched to boundary conditions.

2.5.1.1 An Example in Rectangular Coordinates

To illustrate how this might be useful, consider the simple boundary condition problem illustrated by Figure 2.22. A current sheet located at $y = 0$ has z-directed current $K_z = K_0 \cos ky$. This

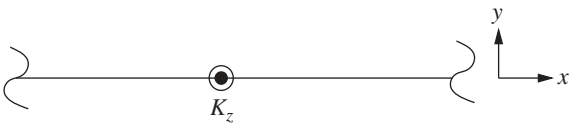

Figure 2.22 Simple boundary condition: current sheet.

is the only boundary condition and the problem is to find magnetic fields above ($y > 0$) and below ($y < 0$) the sheet. It is assumed that the problem is very long in both the z-direction and x-direction.

To start, note that symmetry demands that magnetic field parallel to and just above and below the sheet must be:

$$H_x(x = 0_+) = -\frac{K_0}{2}\cos ky \quad H_x(x = 0_-) = \frac{K_0}{2}\cos ky$$

Then, seeing that $H_x = -\frac{\partial \psi}{\partial x}$, the form of the scalar potential must be

$$\psi(x, y) = \psi_\pm(y) \quad \sin kx \quad \psi(y = 0_\pm) = \pm\frac{K_0}{2k}$$

The Laplacian on the scalar potential is, assuming all is uniform in the z-direction:

$$\nabla^2\psi = 0 = \frac{\partial^2\psi}{\partial x^2} + \frac{\partial^2\psi}{\partial y^2} + \frac{\partial^2\psi}{\partial z^2} \Rightarrow -k^2\psi_\pm \sin kx + \frac{\partial^2\psi_\pm}{\partial y^2}\sin kx = 0$$

This is solved by two possible solutions:

$$\psi(y) = \psi_+ e^{ky} + \psi_- e^{-ky}$$

It should be clear that the solution that grows with y in the positive half of the problem must have zero coefficient and that the solution that grows with negative y in the negative half of the problem must also have zero coefficient, so the total solution is:

$$\psi(x, y > 0) = \frac{K_0}{2k}e^{-ky}\sin kx$$

$$\psi(x, y < 0) = -\frac{K_0}{2k}e^{ky}\sin kx$$

Then, to finish the problem, use $\vec{H} = -\nabla\psi$ or $H_x = -\frac{\partial\psi}{\partial x}$ and $H_y = -\frac{\partial\psi}{\partial y}$
And:

$$y > 0: \qquad H_x = -\frac{K_0}{2}e^{-ky}\cos kx \quad H_y = \frac{K_0}{2}e^{-ky}\sin kx$$

$$y < 0: \qquad H_x = \frac{K_0}{2}e^{ky}\cos kx \qquad H_y = \frac{K_0}{2}e^{ky}\sin kx$$

2.5.2 Scalar Potential in Circular Cylindrical Coordinates

In circular coordinates, the coordinates are radius r, azimuthal angle θ, and axial dimension z. The gradient and Laplacian operators are:

$$\nabla\psi = \vec{i}_r\frac{\partial\psi}{\partial r} + \vec{i}_\theta\frac{1}{r}\frac{\partial\psi}{\partial\theta} + \vec{i}_z\frac{\partial\psi}{\partial z}$$

$$\nabla^2\psi = \frac{1}{r}\frac{\partial}{\partial r}\left(r\frac{\partial\psi}{\partial r}\right) + \frac{1}{r^2}\frac{\partial^2\psi}{\partial\theta^2} + \frac{\partial^2\psi}{\partial z^2} \tag{2.14}$$

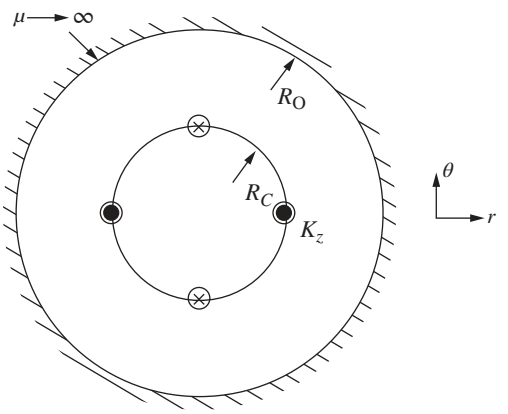

Figure 2.23 Problem in circular cylindrical coordinates.

The mechanism of solving field problems is the same as in rectangular coordinates: First the form of the potential solution is found, then boundary conditions are applied and finally, the gradient is taken to find the fields.

2.5.2.1 Example in Cylindrical Coordinates

Consider the situation shown in Figure 2.23, which looks a bit like an electric machine. A current sheet is located at a circular radius R_C. (There will be some structure on which this is mounted, but assume that to be nonmagnetic.) There is a ferromagnetic boundary at radius R_0. Assume this problem is long enough in the z-direction that we don't have to worry about derivatives in that direction. The current is z-directed and has the value: $K_z = K_0 \cos p\theta$, where p is an integer. The picture is drawn for $p = 2$, which means there are two complete cycles of the sinusoidal current sheet. This will be recognized as a "four pole" geometry.

To start this problem, we can guess that the scalar potential will likely have the form:

$$\psi(r, \theta) = \psi(r) \sin p\theta$$

and this will be confirmed when boundary conditions are applied. The Laplacian applied here is, when the radial amplitude part of the scalar potential is considered:

$$\nabla^2 \psi = \frac{1}{r} \frac{\partial}{\partial r} \left(r \frac{\partial \psi(r)}{\partial r} \right) - \frac{p^2}{r^2} \psi(r) = 0 \tag{2.15}$$

Inserting a "guess" that radial dependence might be proportional to radius to a power into this, it is found that a form for the scalar potential that solved the Laplacian is:

$$\psi(r) = \psi_+ r^p \sin p\theta + \psi_- r^{-p} \sin p\theta$$

This is a two-region problem, with one set of coefficients inside ($r < R_C$, call this region 1) and the other solution outside ($R_C < r < R_O$, call this region 2). Note also that the solution inside must have the coefficient of the -p component be zero to avoid things "blowing up" at the origin:

$$\psi_{1-} = 0$$

The other boundary conditions must be:

1) Fields are perpendicular to the boundary of infinitely permeable iron, so azimuthal field at the outer radius r=R_O must be zero, or

$$H_\theta^2 = 0 \Rightarrow \psi_{2+} R_O^p + \psi_{2-} R_O^{-p} = 0 \Rightarrow \psi_{2-} = -\psi_{2+} R_O^{2p}$$

2) Radial field at the radius of the boundary between regions ($r=R_C$) must be continuous:

$$H_r^2 = H_r^1 \Rightarrow -pR_C^{p-1}\psi_{1+} = -pR_C^{p-1}\psi_{2+} + pR_C^{-p-1}$$

3) Azimuthal field at the radius of the boundary between regions ($r=R_C$) must be discontinuous by the surface's current density:

$$H_\theta^2 - H_\theta^1 = K_z \Rightarrow -pR_C^{p-1}\psi_{2+} - pR_C^{-p-1}\psi_{2-} + pR_C^{p-1}\psi_{1+} = K_0$$

There are three equations and three unknowns, resulting in:

$$\psi_{1+} = \frac{K_0}{2p}R_C^{p+1}R_O^{-2p}\left(1 + \left(\frac{R_O}{R_C}\right)^2\right)$$

$$\psi_{2+} = \frac{K_0}{2p}R_C^{p+1}R_O^{-2p}$$

$$\psi_{2-} = -\frac{K_0}{2p}R_C^{p+1}$$

And the magnetic fields are:

$$H_r^1 = -\frac{K_0}{2}r^{p-1}R_C^{p+1}R_O^{-2p}\left(1 + \left(\frac{R_O}{R_C}\right)^2\right)\sin p\theta$$

$$H_\theta^1 = -\frac{K_0}{2}r^{p-1}R_C^{p+1}R_O^{-2p}\left(1 + \left(\frac{R_O}{R_C}\right)^2\right)\cos p\theta$$

$$H_r^2 = -\frac{K_0}{2}\left(r^{-p-1}R_C^{p+1} + r^{p-1}R_C^{p+1}R_O^{-2p}\right)\sin p\theta$$

$$H_\theta^2 = \frac{K_0}{2}\left(r^{-p-1}R_C^{p+1} - r^{p-1}R_C^{p+1}R_O^{-2p}\right)\cos p\theta$$

2.6 Example: Halbach Magnet Array

A novel array of magnets was developed some years ago by Klaus Halbach to generate flux for a "wiggler" to modify electron beams for applications such as free electron lasers. It is included here to show how methods of electromechanics might be used in other applications.

Imagine an array of long, rectangular magnets as shown in Figure 2.24. The array is assumed to be long in the z direction, relative to the height and width of the magnets. Indicated in the picture are directions of magnetization of the different magnets: Half are magnetized in the vertical direction, half horizontally, and the array is assumed to be repeated to the right and left. For the purpose of analysis, we assume it to be infinite in the x- and z-directions.

A cursory examination of this array would indicate that the vertically oriented magnets and horizontally oriented magnets will produce fields that reinforce below the array and that cancel above the array, and that is the purpose of this arrangement. The objective of this analysis is to show, quantitatively, how this works. Imagine the array is located above a magnetically permeable surface as shown in Figure 2.25. The permeable surface is located at the bottom and is indicated by

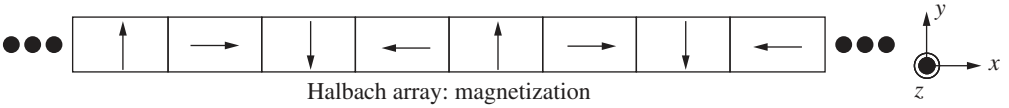

Figure 2.24 Halbach array of magnets.

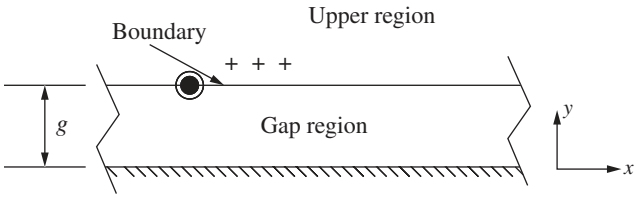

Figure 2.25 Array with a magnetic boundary.

cross-hatching. The array is indicated by "boundary". It is assumed that the space above the array is free space and is semi-infinite in extent.

To understand what is going on here, note that to satisfy both Ampere's law and Gauss's law in free space, both curl and divergence of the magnetic field must be zero. In a space described by Figure 2.25, there are two regions: one below the boundary and one above. Because the lower boundary is ferromagnetic, the x-directed field there must be zero and because the upper region is unbounded, field must decay away. Proper solutions for the fields are, in the "gap" or lower region:

$$H_x = A \sinh ky \cos kx$$

$$H_y = A \cosh ky \sin kx$$

and in the upper, unbounded regions:

$$H_x = Be^{-ky} \cos kx$$

$$H_y = -Be^{-ky} \sin kx$$

Note that these are proper solutions for the field, having zero curl and zero divergence, and the functions are selected so that they match the boundaries. Note these solutions would work for each space harmonic with k replaced by nk. (n being the harmonic order). And of course, $k = \frac{2\pi}{\lambda}$ where λ is the wavelength, or the width of four of the magnets.

Note also that free space is linear, and if the magnets have incremental permeability the same as free space (a decent approximation), the whole problem can be solved as the superposition of two two-region problems, one corresponding to a boundary condition on the upper boundary of the magnets and one corresponding to the lower boundary of the magnets.

The boundaries at the surface of the magnets may be described as either magnetic charge (so-called Chu charge) or as Amperian current, as shown in Figure 2.26. Shown are the boundary conditions at the lower surface of the magnet array. The boundary at the upper surface of the magnets is the same, but with opposite sign.

The magnetization charges and Amperian currents may be represented by their respective Fourier series:

$$K_z = \sum_{n\ odd} K_n \cos nkx \quad K_n = \frac{2}{\pi} \int_{-\frac{\pi}{4}}^{\frac{\pi}{4}} -M_0 \cos nkx\, dkx = -\frac{4}{n\pi} \sin n\frac{\pi}{4}$$

$$M_y = \sum_{n\ odd} M_n \sin nkx \quad M_n = \frac{2}{\pi} \int_{\frac{\pi}{4}}^{\frac{3\pi}{4}} M_0 \sin nkx\, dkx = \frac{4}{n\pi} \sin n\frac{\pi}{2} \sin n\frac{\pi}{4} \tag{2.16}$$

Analysis of this problem may be carried out for each Fourier component. Figure 2.27 shows the Fourier Analysis of the boundaries of Figure 2.26 to harmonic order 29.

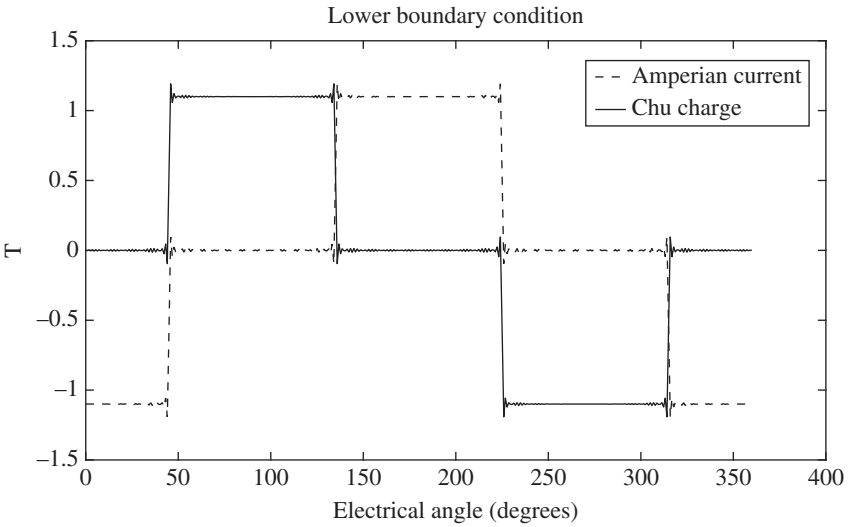

Figure 2.26 Boundary conditions.

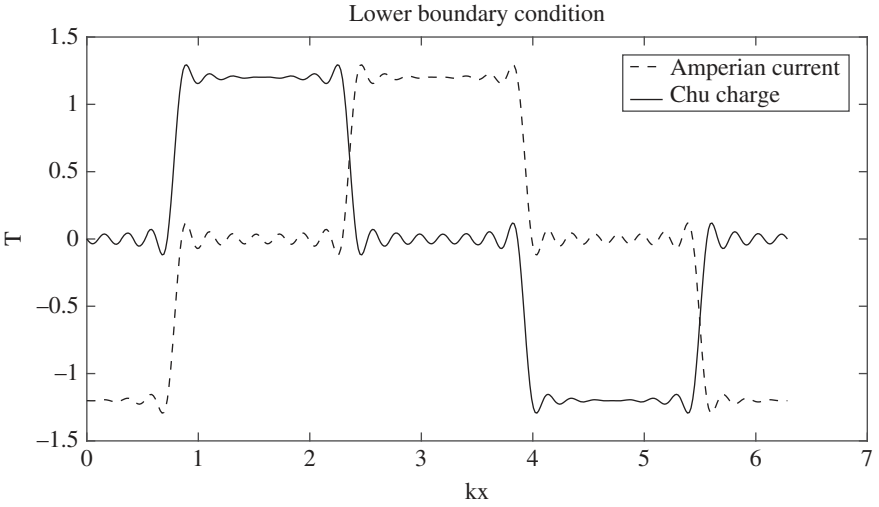

Figure 2.27 Fourier analysis of boundary conditions to harmonic order 29.

At the boundary, the discontinuity of the horizontal component of the field H_x is related to the Amperian current, while the discontinuity of the vertical component of the field H_y is related to the Chu charges. For each component, the boundary conditions are where the upper region and gap meet:

$$H_x^{gap} - H_x^{upper} = K_z \cos kx \quad A_n \sinh nkg - B_n e^{-nkg} = K_n$$
$$H_y^{gap} - H_y^{upper} = -M_y \sin kx \quad A_n \cosh nkg + B_n e^{-nkg} = -M_n$$

The coefficients of these two sets are:

$$A_n = (K_n - M_n)\, e^{-nkg}$$
$$B_n = K_n \sinh\ nkg + M_n \cosh nkg$$

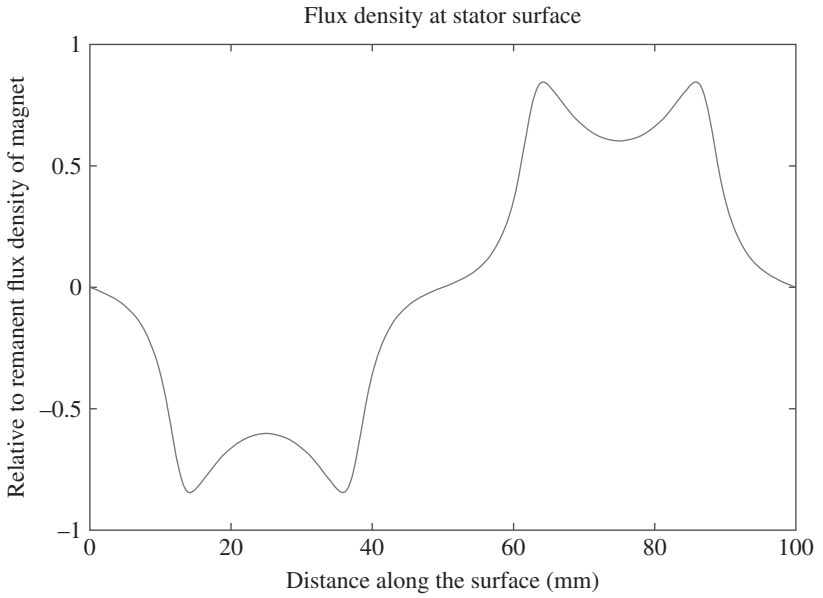

Figure 2.28 Flux density, relative to remanent flux density of magnets.

At the lower boundary ($y = 0$), where an armature winding would be, we find the total solution to be, for flux density:

$$B_y(x) = -\sum_{n\ odd} B_0 \frac{4}{n\pi} \sin n\frac{\pi}{4} \left(1 + \sin n\frac{\pi}{2}\right) (e^{-nkg} - e^{-nk(g+h))}) \sin nkx \tag{2.17}$$

where B_0 is the remanent flux density of the magnets and h is magnet thickness.

For an example case of individual magnet width of 25 mm, or wavelength of 100 mm, magnet thickness of 10 mm, and gap of 2 mm, Flux density at the surface at $y = 0$ is plotted in Figure 2.28.

2.7 Problems

2.1

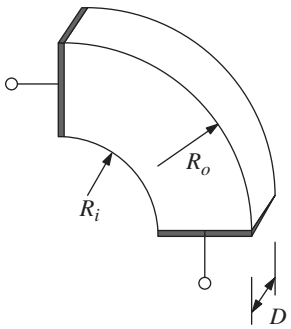

A quarter-circle of material with conductivity σ is shown in the figure above. The ends are connected electrically to contacts of very highly conductive material. The inner and outer radii of the thing are R_i and R_o, and the width is D.
What is the resistance between the two contacts?

2.2

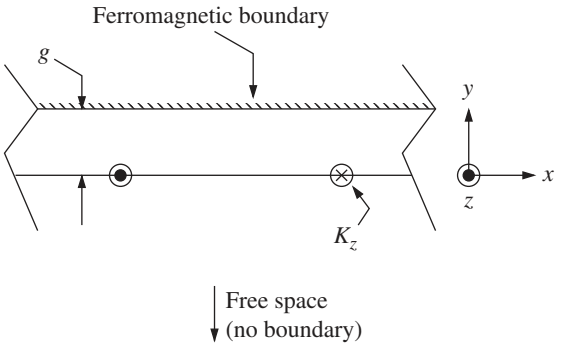

A current sheet is suspended through means not shown at a distance g below a ferromagnetic surface. The sheet has current in the z-direction:

$$K_z = Re\{K_0 e^{-jkx}\}$$

The ferromagnetic boundary is made of infinitely permeable material. Below the surface is "free space", with no boundary at all for several wavelengths, so you may assume there is no boundary down there at all. The problem is large in both x and z directions.

a) What is the x-direct H field just above and just below the current sheet?
b) What is the y-directed H field at the surface of the ferromagnetic boundary?
c) What is the y-directed H field at the position of the current sheet?
d) What are the x- and y-directed H fields in the region below the current sheet?

2.3

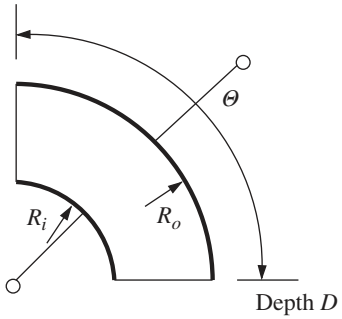

The same quarter circle of material shown in Problem 2.1 is shown in the figure above. But in this case, the electrical contacts are on the inner and outer radii. The contacts are made of highly conductive material connected electrically to the material.
What is the resistance between the terminals?

2.4

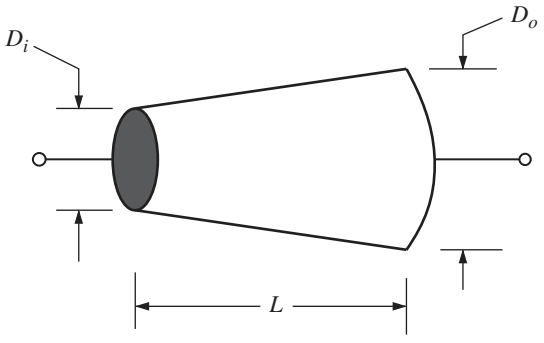

A tapered, circular rod of conductive material, of length L and tapered from one end to the other, from diameter D_i to diameter D_o, has conductivity σ. Highly conductive contacts cover each end.
What is the resistance between terminals?

2.5

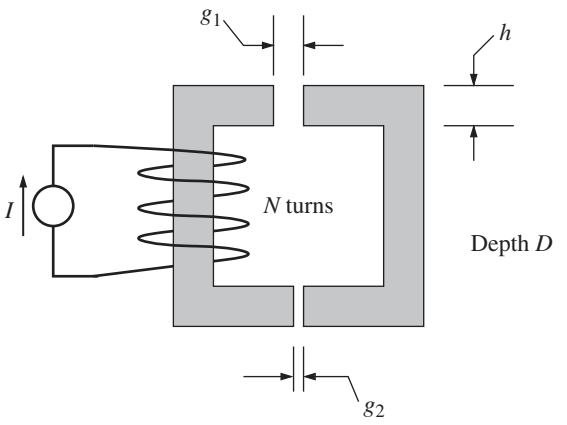

Two pieces of highly permeable material shaped roughly like "C"s form a magnetic circuit. They have width h and depth D, and face each other across gaps with different spacings, g_1 and g_2. This thing is excited by a coil that has ampere-turns NI. Ignore fringing.
What is the magnetic field in each of the two gaps?

2.6

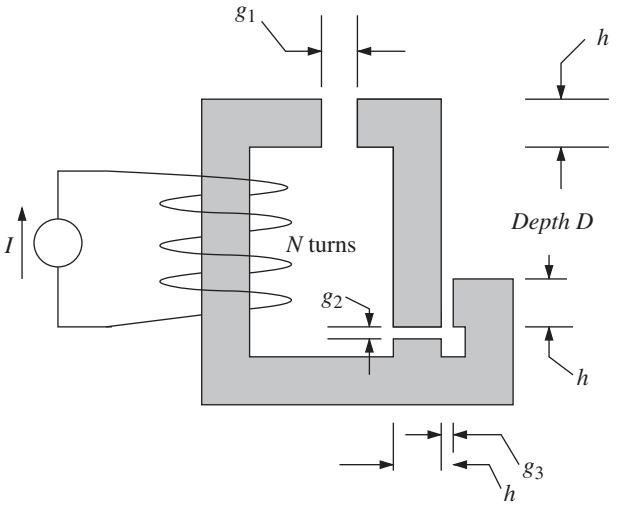

A magnetic circuit somewhat similar to that of Problem 2.5 is shown in the figure above. This one has three gaps. All of the gaps are the same width and depth, but may have different spacings. The magnetic circuit is excited by a coil with ampere turns NI.
What are the fields in the three gaps?

2.7

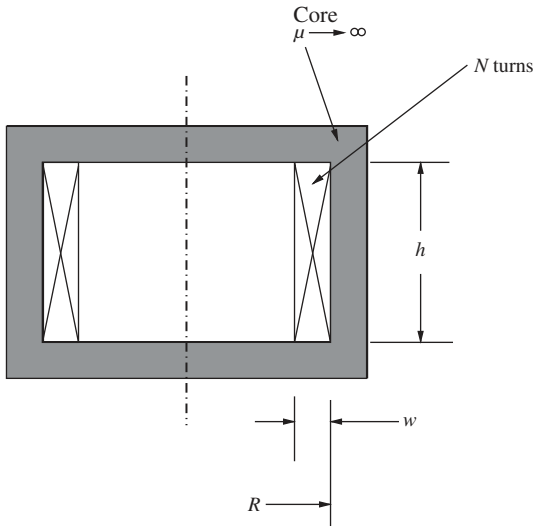

The magnetic circuit shown in the figure above is shaped like a can of soup. It is a thick cylinder with inner radius R with thick disks at top and bottom. Just inside the cylinder is a coil of N turns that occupies the whole of the axial dimension and a relatively thin layer ($w \ll R$) just inside the magnetic cylinder. Both the cylinder and the end caps are highly permeable (assume infinitely permeable). One can see that the magnetic field produced by this coil will be purely axial and uniform.
What is the inductance of the coil?

2.8

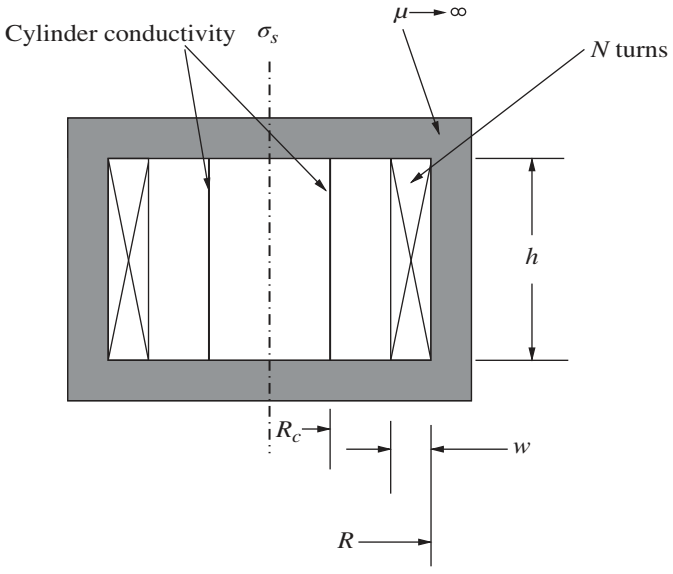

The same magnetic cylinder of Problem 2.7 now has a conductive cylinder of radius R_c and surface conductivity σ_s inserted. This cylinder will obviously link flux from the coil.

a) Convince yourself that this situation can be modeled by the equivalent circuit shown here:

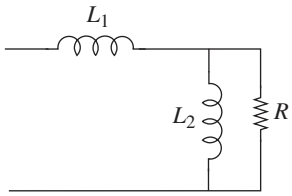

b) What are the values of the two inductances and resistance? (Hint: What do you expect to see if a current of very high frequency is applied to the terminals?)
c) Find and sketch (or use a mathematical assistant to plot) the terminal impedance magnitude and angle as a function of frequency. Assume the coil has resistance R_c, and this value is substantially less than the value of R in the equivalent circuit.

2.9

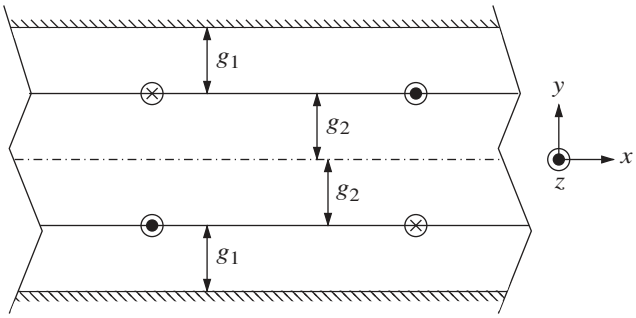

Two current sheets are suspended between two highly permeable magnetic surfaces. They are spaced apart by a distance $2g_2$, and the spacing from each current sheet to the proximate ferromagnetic surface is g_1. So, the distance between magnetic surfaces is $2g_2 + 2g_1$. For convenience, we pick the surface equidistant between current sheets as $y = 0$. Current in the upper sheet is in the $+z$ direction and is $K_z = K_0 \sin kx$. Current in the lower sheet is the same, but direction is reversed: $K_z = -K_0 \sin kx$.

a) Before starting to work on this problem analytically, sketch what you think the magnetic field lines will look like.
b) Now formulate the problem: What are the boundary conditions? Can you use symmetry to simplify the problem?
c) Find expressions for magnetic fields in the x- and y-directions at:
   - The upper ferromagnetic boundary
   - The center of the problem ($y = 0$)
   - The region above the upper current sheet: $g_2 < y < g_1 + g_2$
   - The region below the upper current sheet: $0 < y < g_2$

2.10

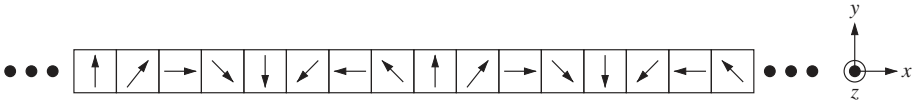

The figure above can be compared with Figure 2.24 of this chapter. It shows a Halbach Array with four magnet orientations per pole. It yields a magnetic field that is a bit more sinusoidal than the two magnets per pole shown in Figure 2.24. The objective of this exercise is to look into that.

a) Note that the analysis of this kind of magnet array uses a mix of Amperian currents and fictitious (Chu) magnetic charge. This array has magnets with the magnetization at a 45° angle, so those magnets have a mix of Amperian and magnetic charge boundaries. Do a sketch of the two types of boundary conditions on the upper and lower boundaries. See Figure 2.27 of this chapter.
b) Now find the Fourier series for each of the boundaries (Amperian current and magnetic charge).
c) Now you should be able to, following the derivation in the text, find the magnetic field in the region below the array.
d) Using your favorite mathematical assistant, compare the flux density produced by this magnet array with that of the two magnet per pole array in the text. Use the same dimensions: Wavelength = 100 mm, magnet thickness of 10 mm, a magnetic surface 2 mm below the lower surface of the magnet array, and a remanent flux density of 1 T.

Reference

1 Fano, R.M., Chu, L.J., and Adler, R.B. (1963). *Electromagnetic Fields, Energy and Forces*. Wiley.

3

Electromagnetic Forces and Energy Flows

3.1 Introduction

Electric machinery comes in many different types and a strikingly broad range of sizes, from those little haptic machines that cause cell phones to vibrate (yes, rotating electric machines are used for that purpose) to turbine generators with ratings upward of a gigawatt. Most of the machines with which we are familiar are rotating, but linear electric motors are widely used, including shuttle drives in weaving machines, equipment handling, and amusement park rides, and even launching aircraft from carriers. It is our purpose in this chapter to develop an analytical basis for understanding how all of these different machines work. It is our contention that an understanding of the fundamentals of energy conversion will be required to make further advances in electric machinery in the future.

This chapter discusses some of the fundamental processes involved in electric machinery. In the section on energy conversion processes, we examine two major ways of estimating electromagnetic forces: those involving thermodynamic arguments (conservation of energy) and field methods (e.g. Maxwell stress tensor). In between these two explications is a bit of description of electric machinery, primarily there to motivate the description of field-based force calculating methods.

The section of the chapter dealing with losses is really about eddy currents in both linear and non-linear materials and about semi-empirical ways of handling iron losses and exciting currents in machines.

3.2 Energy Conversion Process

In a motor, the energy conversion process can be thought of in simple terms. In "steady state", electric power input to the machine is just the sum of electric power inputs to the different phase terminals (Figure 3.1):

$$P_e = \sum_i v_i i_i \tag{3.1}$$

Mechanical power is torque times speed:

$$P_m = f^e \frac{dx}{dt} \tag{3.2}$$

And the sum of the losses is the difference between input and output power:

$$P_d = P_e - P_m \tag{3.3}$$

Electromagnetic Analysis of Electric Machines: First Principles, Modeling, and Design, First Edition.
James L. Kirtley, Christopher H. T. Lee, and Sajjad Mohammadi.

Companion website: www.wiley.com/go/kirtleyelectric

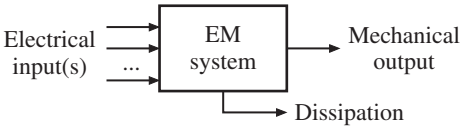

Figure 3.1 Electromechanical converter. *Source*: Adapted from [1].

It will sometimes be convenient to employ the fact that, in most machines, dissipation is small enough to approximate mechanical power with converted electrical power. In fact, there are many situations in which the loss mechanism is known well enough that it can be idealized away. The "thermodynamic" arguments for force density take advantage of this and employ a "conservative" or lossless energy conversion system.

3.3 Energy Approach to Electromagnetic Forces

To start, consider some electromechanical system which has two sets of "terminals", electrical and mechanical, as shown in Figure 3.2. If the system stores energy in magnetic fields, the energy stored depends on the state of the system, defined by (in this case) two of the identifiable variables: flux (λ), current (i), and mechanical position (x). In fact, with only a little reflection, you should be able to convince yourself that this state is a single-valued function of two variables and that the energy stored is independent of how the system was brought to this state.

It is possible to choose the variables in such a way that electrical power *into* this conservative system is:

$$P^e = vi = i\frac{d\lambda}{dt} \tag{3.4}$$

Similarly, mechanical power *out* of the system is:

$$P^m = f^e\frac{dx}{dt} \tag{3.5}$$

The difference between these two expressions is the rate of change of magnetic energy stored in the system:

$$\frac{dW_m}{dt} = P^e - P^m \tag{3.6}$$

It is then possible to compute the change in energy required to take the system from one state to another by:

$$W_m(a) - W_m(b) = \int_b^a id\lambda - f^e dx \tag{3.7}$$

where the two states of the system are $a = (\lambda_a, x_a)$; $b = (\lambda_b, x_b)$.

Since the energy stored in the system is described by the states λ and x, the total differential of stored energy is:

$$dW_m = \frac{\partial W_m}{\partial \lambda}d\lambda + \frac{\partial W_m}{\partial x}dx \tag{3.8}$$

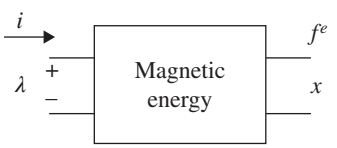

Figure 3.2 Energy interaction with electrical and mechanical terminals.

If the system is described by two (and only two) variables λ and x, the total differential of energy is described by (3.9):

$$dW_m = id\lambda - f^e dx \tag{3.9}$$

So that we can make a direct equivalence between the derivatives and:

$$f^e = -\frac{\partial W_m}{\partial x} \tag{3.10}$$

In the above equation, it is important to keep λ as an independent variable. This generalizes in the case of multiple electrical terminals and/or multiple mechanical terminals. For example, a situation with multiple electrical terminals will have:

$$dW_m = \sum_k i_k d\lambda_k - f^e dx \tag{3.11}$$

And (3.10) still holds to find force.

In the case of rotary motion, as opposed to linear motion, in place of force f^e and displacement x, use torque T^e and angular displacement θ.

In many cases, we might consider a system that is electrically linear, in which case inductance is a function only of the mechanical position x.

$$\lambda = L(x)\, i \tag{3.12}$$

In this case, assuming that the energy integral is carried out from $\lambda = 0$ (so that the part of the integral carried out over x is zero),

$$W_m = \int_0^\lambda \frac{1}{L(x)} \lambda d\lambda = \frac{1}{2}\frac{\lambda^2}{L(x)} \tag{3.13}$$

This makes

$$f^e = -\frac{1}{2}\lambda^2 \frac{\partial}{\partial x}\frac{1}{L(x)} \tag{3.14}$$

Note that in this case, this is numerically equivalent to:

$$f^e = -\frac{1}{2}\lambda^2 \frac{\partial}{\partial x}\frac{1}{L(x)} = +\frac{1}{2}\left(\frac{\lambda}{L(x)}\right)^2 \frac{\partial L}{\partial x} = \frac{1}{2} i^2 \frac{\partial L}{\partial x} \tag{3.15}$$

This is just the opposite in sign to what results if one were to naively substitute $\lambda = L(x)\, i$ in (3.13) before differentiating.

3.3.1 Multiply Excited Systems

There may be (and in most electric machine applications, there will be) more than one source of electrical excitation (more than one coil). In such systems, we may write the conservation of energy expression as:

$$dW_m = \sum_k i_k d\lambda_k - f^e dx \tag{3.16}$$

which simply suggests that electrical input to the magnetic field energy storage is the sum (in this case, over the index k) of inputs from each of the coils. To find the total energy stored in the system, it is necessary to integrate over all of the coils (which may and in general will have mutual inductance).

$$W_m = \int \underline{i} \cdot d\underline{\lambda} \tag{3.17}$$

Note that, in (3.17), current and flux are multi-valued and so are noted as vectors. And thus, care must be taken in carrying out the integration so that each element of the path through flux space assumes the correct value of current in each coil. If the system is conservative, the energy W_m is uniquely specified, so the actual path taken in carrying out this integral will not affect the path of the resulting energy. For a bit more about this, look at Section 3.3.4, on the simple synchronous machine model.

3.3.2 Co-energy

We often will describe systems in terms of inductance rather than their reciprocal, so that current, rather than flux, appears to be the relevant variable. It is convenient to derive a new energy variable, which we will call co-energy, by:

$$W'_m = \sum_i \lambda_i i_i - W_m \tag{3.18}$$

And in this case, it is quite easy to show that the energy differential is, for a single mechanical variable, simply:

$$dW'_m = \sum_k \lambda_k di_k + f^e dx \tag{3.19}$$

So that force produced is

$$f_e = \frac{\partial W'_m}{\partial x} \tag{3.20}$$

3.3.3 Example: Simple Solenoid

Consider the magnetic actuator shown in cartoon form in Figure 3.3. The actuator consists of a circular rod of ferromagnetic material (very highly permeable) that can move axially (the z-direction) inside of a stationary piece, also made of highly permeable material. A coil of N turns carries a current i. The rod has a radius R and spacing from the end of the stator is the variable dimension x. At the other end, there is a radial clearance between the rod and the stator, g. Assume $g \ll R$. If the axial length of the radial gaps is $l = R/2$, the area of the radial gaps is the same as the area of the variable gap between the rod and the stator.

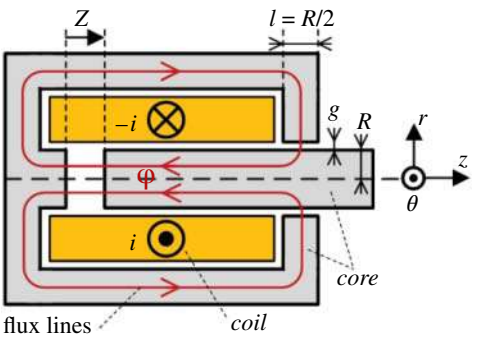

Figure 3.3 Solenoid actuator.

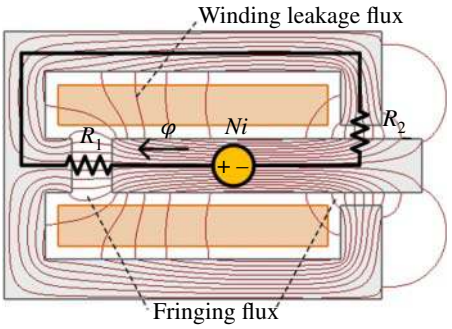

Figure 3.4 Flux lines by FEM simulation and corresponding magnetic equivalent circuit.

The flux lines simulated by finite element method (FEM) and the magnetic equivalent circuit (MEC) are given in Figure 3.4. The permeances of the axial variable gap and the radial clearance gap are:

$$\mathcal{P}_1 = \frac{1}{\mathcal{R}_1} = \frac{\mu_0 \pi R^2}{z} \tag{3.21}$$

$$\mathcal{P}_2 = \frac{1}{\mathcal{R}_2} = \frac{2\mu_0 \pi R l}{g} = \frac{\mu_0 \pi R^2}{g} \tag{3.22}$$

The inductance of the coil and the flux linkage can be obtained using total permeance or total reluctance as follows:

$$L = \frac{N^2}{\mathcal{R}_t} = N^2 \mathcal{P}_t \Rightarrow L = \frac{N^2}{\mathcal{R}_1 + \mathcal{R}_2} = N^2 \frac{\mathcal{P}_1 \mathcal{P}_2}{\mathcal{P}_1 + \mathcal{P}_2} = \frac{\mu_0 \pi R^2 N^2}{g + z} \tag{3.23}$$

$$\lambda(z, i) = L(z)\ i = \frac{\mu_0 \pi R^2 N^2}{g + z} i \tag{3.24}$$

Magnetic energy is:

$$W_m = \int_0^{\lambda_0} i\, d\lambda = \int_0^{\lambda_0} \frac{\lambda}{L(z)}\ d\lambda = \frac{1}{2} \frac{\lambda^2}{L(z)} \tag{3.25}$$

Finally, force of electric origin is:

$$f^e = -\frac{\partial W_m}{\partial x} = -\frac{\lambda_0^2}{2} \frac{d}{dx} \left(\frac{1}{L(x)} \right) = -\frac{{\lambda_0}^2}{2} \frac{1}{\mu_0 \pi R^2 N^2} \tag{3.26}$$

By substitution of $\lambda = L(x)i$, the total force is simply:

$$f^e = -\frac{1}{2} \frac{\mu_0 \pi R^2 N^2}{(g + z)^2} i_0^2 \tag{3.27}$$

The other method to calculate force is employing co-energy as follows:

$$W'_m = \int_0^{i_0} \lambda\, di = \int_0^{i_0} L(z)\, i\, di = \frac{1}{2} L(z)\ i_0^2 \tag{3.28}$$

Then, the same relationship for force is obtained as:

$$f^e = \frac{\partial W'_m}{\partial z} = \frac{1}{2} i_0^2 \frac{dL(z)}{dz} = -\frac{1}{2}\ \frac{\mu_0 \pi R^2 N^2}{(g + z)^2} i_0^2$$

3.3.4 Synchronous Machine

Consider a simple electric machine example shown in Figure 3.5 in which there is a single winding on a rotor (field winding) and a polyphase armature with three identical coils spaced at uniform locations about the periphery of stator. If the rotor is round, we can describe the flux linkages as:

$$\begin{aligned}
\lambda_a &= L_a i_a + L_{ab} i_b + L_{ab} i_c + M\cos(p\theta)\, i_f \\
\lambda_b &= L_{ab} i_a + L_a i_b + L_{ab} i_c + M\cos\left(p\theta - \frac{2\pi}{3}\right) i_f \\
\lambda_c &= L_{ab} i_a + L_{ab} i_b + L_a i_c + M\cos\left(p\theta + \frac{2\pi}{3}\right) i_f \\
\lambda_f &= M\cos(p\theta)\, i_a + M\cos\left(p\theta - \frac{2\pi}{3}\right) i_b + M\cos\left(p\theta + \frac{2\pi}{3}\right) i_c + L_f i_f
\end{aligned} \tag{3.29}$$

This system can be simply described in terms of co-energy. With multiple excitations, it is important to exercise some care in taking the co-energy integral (to ensure that it is taken over a valid path in the multi-dimensional space). In our case, there are actually five dimensions, but only four are important since we can position the rotor with all currents at zero, so there is no contribution to co-energy from setting rotor position. Suppose the rotor is at some angle and that the four currents have values i_{a0}, i_{b0}, i_{c0}, and i_{f0}. One of many correct path integrals to take would be:

$$\begin{aligned}
W'_m = &\int_0^{i_{a0}} L_a i_a di_a \\
&+ \int_0^{i_{b0}} (L_{ab} i_{a0} + L_a i_b)\, di_b \\
&+ \int_0^{i_{c0}} (L_{ab} i_{a0} + + L_{ab} i_{b0} + L_a i_c)\, di_c \\
&+ \int_0^{i_{f0}} \left(M\cos(p\theta)\, i_{a0} + M\cos\left(p\theta - \frac{2\pi}{3}\right) i_{b0} + M\cos\left(p\theta + \frac{2\pi}{3}\right) i_{c0} + L_f i_f\right) di_f
\end{aligned} \tag{3.30}$$

The result is:

$$\begin{aligned}
W'_m = &\frac{1}{2} L_a \left(i_{a0}^2 + i_{b0}^2 + i_{c0}^2\right) + L_{ab}(i_{a0}\, i_{b0} + i_{a0}\, i_{c0} + i_{b0}\, i_{c0}) \\
&+ M i_{f0}\left(i_{a0}\cos(p\theta) + i_{b0}\cos\left(p\theta - \frac{2\pi}{3}\right) + i_{c0}\cos\left(p\theta + \frac{2\pi}{3}\right)\right) + \frac{1}{2} i_{f0}^2
\end{aligned} \tag{3.31}$$

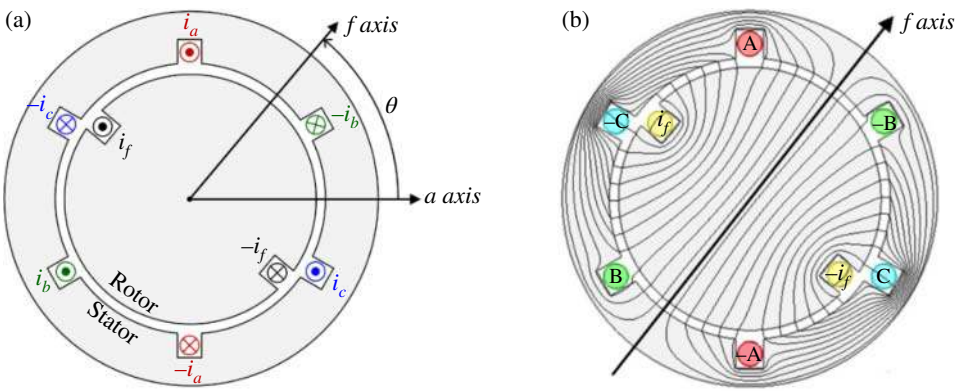

Figure 3.5 Three-phase two-pole wound-field round-rotor synchronous machine (a) and finite element simulations for the flux lines generated by a current in the field winding (b).

Note that we are assuming here that there are no variations in stator self or mutual inductances with rotor position and no variation of field self-inductance with rotor position. This is usually referred to as "round rotor". Torque is found by:

$$T^e = \frac{\partial W'_m}{\partial \theta} = -pMi_{f0}\left(i_{a0}\sin(p\theta) + i_{b0}\sin\left(p\theta - \frac{2\pi}{3}\right) + i_{c0}\sin\left(p\theta + \frac{2\pi}{3}\right)\right) \tag{3.32}$$

3.3.5 Current-Driven Synchronous Machine

Assume that this machine is driven with stator and field currents:

$$\begin{aligned} i_{a0} &= I_a\cos(\omega t) \\ i_{b0} &= I_a\cos\left(\omega t - \frac{2\pi}{3}\right) \\ i_{co} &= I_a\cos\left(\omega t + \frac{2\pi}{3}\right) \\ i_{f0} &= I_f \end{aligned} \tag{3.33}$$

And assume the rotor is turning at *synchronous speed*: $p\theta = \omega t + \delta_i$.

Carrying out a few trigonometric expressions, we find that torque is simply:

$$T^e = -\frac{3}{2}pMI_aI_f\sin\delta_i \tag{3.34}$$

And this is indeed one way of looking at a synchronous machine, which produces steady torque if the rotor speed and currents all agree on frequency. Torque is related to the current torque angle δ_i. Figure 3.6 shows a "phasor" diagram for this situation. The vectors represent complex amplitudes of the variables, or alternatively, their position in space as a "snapshot" at some given time. As it turns out, such machines are not generally run against current sources, but we will take up actual operation of such machines later.

3.3.6 Generalization to Continuous Media

Now, consider a system with not just a multiplicity of circuits but a continuum of current-carrying paths. In that case, we could identify the co-energy as:

$$W'_m = \int_{area}\int \lambda(\vec{a})\, d\vec{J}\cdot d\vec{a} \tag{3.35}$$

where that area is chosen to cut all of the current-carrying conductors. This area can be picked to be perpendicular to each of the current filaments since the divergence of current is zero. The flux λ is calculated over a path that coincides with each current filament (such paths do exist since current also has zero divergence). Then the flux is:

$$\lambda(\vec{a}) = \int \vec{B}\cdot d\vec{a} \tag{3.36}$$

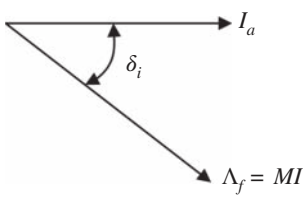

Figure 3.6 Phasor diagram for current-driven synchronous motor.

If we use the vector potential $\vec{A}$ for which the magnetic flux density is $\vec{B} = \nabla \times \vec{A}$, the flux linked by any one of the current filaments is $\lambda(\vec{a}) = \oint \vec{A} \cdot d\vec{\ell}$, where $d\vec{\ell}$ is the path of the current filament. This implies directly that the co-energy is:

$$W'_m = \int_{area} \int_J \oint \vec{A} \cdot d\vec{\ell} d\vec{J} \cdot d\vec{a}$$

Since it is possible to make $d\vec{\ell}$ coincide with $d\vec{a}$ and be parallel to the current filaments,

$$W'_m = \int_{vol} \int_J \vec{A} \cdot d\vec{J}\, dv \tag{3.37}$$

3.3.7 Permanent Magnets

Often, systems with permanent magnets are approached in a relatively ad-hoc way, by being made equivalent to a current that produces the same magnetomotive force (MMF) as the magnet itself.

The constitutive relationship for a permanent magnet relates the magnetic flux density B to magnetic field H and the property of the magnet itself, the magnetization M:

$$\vec{B} = \mu_0(\vec{H} + \vec{M}) \tag{3.38}$$

The effect of the magnetization is to act as if there were a current (called the *Amperian current*), with density:

$$\vec{J} = \nabla \times \vec{M} \tag{3.39}$$

Note that this Amperian current "acts" just like ordinary current in making magnetic flux density. Magnetic co-energy is:

$$W'_m = \int_{vol} \int_M \vec{A} \cdot \nabla \times d\vec{M} dv = \int_{vol} \int_M (\nabla \times \vec{A} \cdot d\vec{M})\, dv - \int_{vol} \int_M \nabla \cdot (\vec{A} \times d\vec{M}) dv \tag{3.40}$$

where the vector identity $\nabla \cdot (\vec{C} \times \vec{D}) = \vec{D} \cdot (\nabla \times \vec{C}) - \vec{C} \cdot (\nabla \times \vec{D})$ is used. Then, noting $\vec{B} = \nabla \times \vec{A}$, magnetic co-energy becomes:

$$W'_m = -\oiint \int_M \vec{A} \times d\vec{M} d\vec{a} + \int_{vol} \int_M \vec{B} \cdot d\vec{M} dv \tag{3.41}$$

The first of these integrals (closed surface) vanishes if it is taken over a surface just outside the magnet, where M is zero. Thus, the magnetic co-energy in a system with only a permanent magnet source is

$$W'_m = \int_{vol} \int_M \vec{B} \cdot d\vec{M} dv \tag{3.42}$$

Adding current-carrying coils to such a system is done in the obvious way.

3.4 Field Description of Energy Flow: Poynting's Theorem

Here is another method for deducing forces in electromagnetic field systems. Start with the celebrated Poynting's theorem, which states that electromagnetic energy flow, noted by the symbol S, is simply the cross-product of electric and magnetic fields:

$$\vec{S} = \vec{E} \times \vec{H} \tag{3.43}$$

Noting the units of electric field are volts/meter and the units of magnetic field are amperes per meter, the units of the Poynting vector are volt-amperes per meter squared, and if the fields are in phase with one another, the units become watts per square meter.

Suppose we are interested in finding the energy flow (power) into some region of space bounded by a surface we call A. That flow would be noted by:

$$P = -\oiint \vec{S} \cdot \vec{n} da$$

If we use the divergence theorem, $\oiint \vec{S} \cdot \vec{n} da = \int_{vol} \nabla \cdot \vec{S} dv$, we find:

$$P = -\int_{vol} \nabla \cdot (\vec{E} \times \vec{H})\, dv$$

Then, using the vector identity $\nabla \cdot (\vec{E} \times \vec{H}) = \vec{H} \cdot (\nabla \times \vec{E}) - \vec{E} \cdot (\nabla \times \vec{H})$ and then noting two of Maxwell's equations, Faraday's law and Ampere's law:

$$\nabla \times \vec{E} = -\frac{\partial \vec{B}}{\partial t}$$
$$\nabla \times \vec{H} = \vec{J}$$

We arrive at a second expression for power:

$$P = \int_{vol} \left(\vec{H} \cdot \frac{\partial \vec{B}}{\partial t} + \vec{E} \cdot \vec{J} \right) dv \tag{3.44}$$

The two terms in the integral are local effects, and we will interpret them as, respectively, change in stored energy and dissipation or converted power. To start, consider free space, in which $\vec{B} = \mu_0 \vec{H}$. In this situation, $\vec{H} \cdot \frac{\partial \vec{B}}{\partial t} = \frac{d}{dt} \frac{1}{2} \mu_0 |\vec{H}|^2$, which is clearly the rate of change of energy stored in magnetic fields. The second observation is that if current density is governed by Ohm's law: $\vec{J} = \sigma \vec{E}$, then $\vec{E} \cdot \vec{J} = \sigma |\vec{E}|^2$ is dissipation. But what if there is material motion? To understand this, we need to go back to Faraday's law:

$$\nabla \times \vec{E} = -\frac{\partial \vec{B}}{\partial t}$$

Applying Stokes' theorem to Faraday's law results in the integral form:

$$\oint \vec{E} \cdot d\vec{\ell} = -\iint \frac{\partial \vec{B}}{\partial t} \cdot \vec{n} da$$

where the integral of electric field $\vec{E}$ is taken at the edge of the surface over which the normal component of flux density $\vec{B}$ is taken. This might be interpreted as being the integral of electric field around the periphery is the rate of change of flux through the area. If that is the case, then even if the edge of the surface is moving, the expression becomes:

$$\oint \vec{E}' \cdot d\vec{\ell} = -\frac{d}{dt} \iint \vec{B} \cdot \vec{n} da$$

where now the electric field $\vec{E}'$ is the electric field at the edge of the surface. Now, if that edge is moving, the time derivative of the integral becomes:

$$\frac{d}{dt} \iint \vec{B} \cdot \vec{n}\, da = \iint \frac{\partial \vec{B}}{\partial t} \cdot \vec{n}\, da - \oint \vec{v} \times \vec{B} \cdot d\vec{\ell}$$

where $\vec{v}$ is the velocity of the edge of the surface. The integral of electric field then becomes:

$$\oint \vec{E}' \cdot d\vec{\ell} = -\iint \frac{\partial \vec{B}}{\partial t} \cdot \vec{n} da + \oint \vec{v} \times \vec{B} \cdot d\vec{\ell} = \oint (\vec{E} + \vec{v} \times \vec{B}) \cdot d\vec{\ell} \tag{3.45}$$

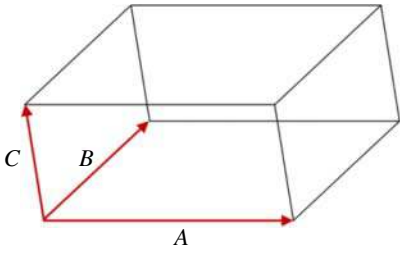

Figure 3.7 Illustration of scalar triple product.

from which we can conclude that electric field at the edge of the (possibly) moving surface would be:

$$\vec{E}' = \vec{E} + \vec{v} \times \vec{B} \tag{3.46}$$

In this case, the term

$$\vec{E} \cdot \vec{J} = \vec{E}' \cdot \vec{J} - \vec{v} \times \vec{B} \cdot \vec{J}$$

The first part of this is dissipation, as current density $\vec{J} = \sigma \vec{E}'$. The second part is a scalar triple product between three vectors. As illustrated by Figure 3.7, a scalar triple product is the equivalent of the volume of a parallelogram defined by the three vectors, so that $\vec{A} \times \vec{B} \cdot \vec{C} = \vec{A} \cdot \vec{B} \times \vec{C}$ and then using the fact that reversing the order of a cross product simply changes its sign: $\vec{B} \times \vec{J} = -\vec{J} \times \vec{B}$. This then becomes a conversion between electrical and mechanical power:

$$-\vec{v} \times \vec{B} \cdot \vec{J} = -\vec{v} \cdot \vec{B} \times \vec{J} = \vec{v} \cdot \vec{J} \times \vec{B} \tag{3.47}$$

where we now have found the Lorentz force law.

$$\vec{F} = \vec{J} \times \vec{B} \tag{3.48}$$

Velocity times force is converted to mechanical power.

3.4.1 Rotary Machine: The Faraday Disk and Fields in Motion

Shown in Figure 3.8 is an impractical but yet interesting device. A disk of conductive material is mounted on a shaft so it can rotate. Sliding electrical contacts on the inner and outer radii make contact with the disk. Note that these contacts are continuous around both the inner and outer surfaces so that this device is azimuthally continuous. Somehow, the whole thing is immersed in an axial magnetic flux density B. A few more details of the device from the axial and cross-section views are shown in Figure 3.9.

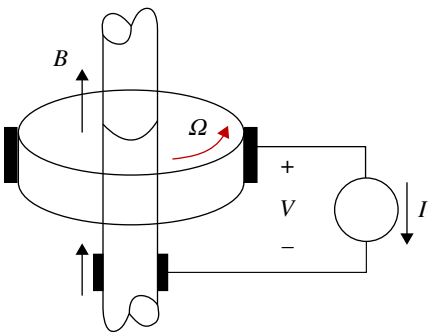

Figure 3.8 The Faraday disk in cartoon form.

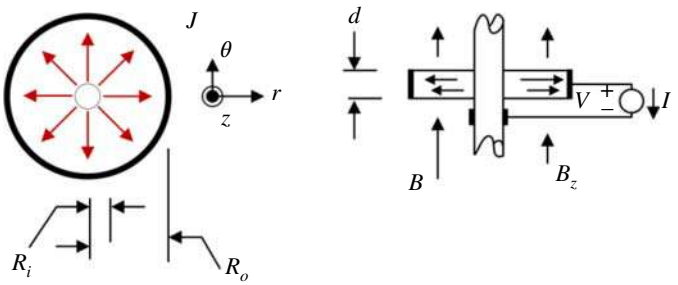

Figure 3.9 Dimensions of the Faraday disk.

Assuming the current to be distributed uniformly because of the continuous sliding contacts, there will be a current in the disk that is radially directed and of magnitude:

$$\vec{J} = \vec{i}_r \frac{I}{2\pi rd}$$

Note that as expected, this current density is inversely proportional to radius and so has no divergence. Torque produced by the interaction of this current with the axial magnetic flux density by using the *Lorentz force law*:

$$\vec{F} = \vec{J} \times \vec{B}$$

In this case, the force is azimuthally directed:

$$\overline{F} = \vec{i}_r \times \vec{i}_z \frac{I}{2\pi rd} B_z = -\vec{i}_\theta \frac{IB_z}{2\pi rd}$$

Then torque is the integral of this force over the thickness, circumference, and radius of the disk:

$$T = d \times \int_{R_i}^{R_o} 2\pi r \times r \times \frac{-B_z I}{2\pi rd} dr = \int_{R_i}^{R_o} -B_z I r dr = -B_z I \frac{R_o^2 - R_i^2}{2}$$

Now, we know that this thing must convert mechanical power to electrical (if the signs are as indicated). And that power converted must be:

$$P_g = B_z I \Omega \frac{R_0^2 - R_i^2}{2}$$

And because this power is proportional to current, it must be that this power can be represented as the interaction of a speed-dependent voltage with the terminal current. So, a suitable model for the interaction is likely as shown in Figure 3.10. The voltage is, to produce the same power:

$$E_b = -B_z \frac{R_o^2 - R_i^2}{2} \ \Omega$$

This can be double-checked by actually deriving voltage produced. The resistance is also to be estimated.

Figure 3.10 Speed-dependent voltage source.

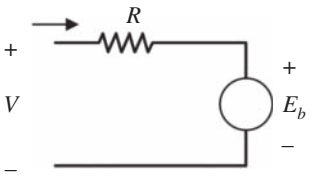

Noting that the electric field in the material of the disk is the resistive drop from the current:

$$\vec{E}' = \vec{i}_r E_r = \vec{i}_r \frac{J_r}{\sigma}$$

Then, noting from (3.36), the electric field in the stationary frame is:

$$\vec{E} = \vec{E}' - \vec{u} \times \vec{B} = \vec{i}_r \frac{I}{2\pi d\sigma r} - \vec{i}_\theta \times \vec{i}_z r\Omega B_z$$

and the voltage at the terminals is:

$$V = \left(\frac{I}{2\pi d\sigma r} - B_z \Omega r \right) dr = I \frac{\left(\ln\left(\frac{R_o}{R_i}\right) \right)}{2\pi d\sigma} - B_z \Omega \frac{R_o^2 - R_i^2}{2}$$

So, using Faraday's law, the "internal" or generated voltage is the same as was surmised from the first law (conservation of energy), and the resistance of the model is:

$$R = \frac{\ln\left(\frac{R_o}{R_i}\right)}{2\pi d\sigma}$$

3.5 Field Description of Forces: Maxwell Stress Tensor

Begin by contending that forces of electromagnetic origin, since they are transferred by electric and magnetic fields, are the result of only the fields and may be calculated once the fields are known. In fact, if a surface can be established that fully encases a material body, the force on that body can be shown to be the integral of a force density, or traction, over that surface. That the traction derived by taking the cross product of surface current density and flux density on the air-gap surface of a machine actually makes sense in view of the empirically derived Lorentz force law: Given a (vector) current density and a (vector) flux density. In the absence of magnetic materials (those with permeability different from that of free space), the observed force on a conductor is

$$\vec{F} = \vec{J} \times \vec{B}$$

where $\vec{J}$ is the vector describing current density (A/m^2) and $\vec{B}$ is the magnetic flux density (T). This is actually enough to describe the forces we see in many machines, but since electric machines have permeable magnetic material and since magnetic fields produce forces on permeable material even in the absence of macroscopic currents, it is necessary to observe how force appears on such material. A suitable empirical expression for force density is:

$$\vec{F} = \vec{J} \times \vec{B} - \frac{1}{2}(\vec{H} \cdot \vec{H})\nabla\mu \tag{3.49}$$

where $\vec{H}$ is the magnetic field intensity and μ is the permeability. Now, note that current density is the curl of magnetic field intensity, so that:

$$\begin{aligned} \vec{F} &= (\nabla \times \vec{H}) \times \mu\vec{H} - \frac{1}{2}(\vec{H} \cdot \vec{H})\nabla\mu \\ &= \mu(\vec{H} \cdot \nabla)\vec{H} - \frac{1}{2}(\vec{H} \cdot \vec{H})\nabla\mu \end{aligned} \tag{3.50}$$

And, since $(\nabla \times \vec{H}) \times \vec{H} = (\vec{H} \cdot \nabla)\vec{H} - \frac{1}{2}\nabla(\vec{H} \cdot \vec{H})$,

$$\begin{aligned} \vec{F} &= -\frac{1}{2}\mu\nabla(\vec{H} \cdot \vec{H}) - \frac{1}{2}(\vec{H} \cdot \vec{H})\nabla\mu \\ &= \mu(\vec{H} \cdot \nabla)\,\vec{H} - \nabla\,\frac{1}{2}\mu(\vec{H} \cdot \vec{H}) \end{aligned} \tag{3.51}$$

This expression can be written by components:

$$F_i = \mu \sum_k \left(H_k \frac{\partial}{\partial x_k} \right) H_i - \frac{\partial}{\partial x_i} \left(\frac{1}{2} \mu \sum_k H_k^2 \right) \tag{3.52}$$

The same can be done for the divergence of flux density:

$$\nabla \cdot \vec{B} = \sum_k \frac{\partial}{\partial x_k} \mu H_k = 0$$

$$\mu \sum_k \left(H_k \frac{\partial}{\partial x_k} \right) H_i = \sum_k \frac{\partial}{\partial x_k} \mu H_i H_k - \sum_k H_i \frac{\partial}{\partial x_k} \mu H_k$$

But since the last term is zero,

$$F_k = \frac{\partial}{\partial x_i} \left(\mu H_i H_k - \frac{\mu}{2} \delta_{ik} \sum_n H_n^2 \right) \tag{3.53}$$

where the "Kronecker Delta", $\delta_{ik} = 1$ if $i = k$ and $\delta_{ik} = 0$ otherwise. Note that this force is in the form of a divergence of a tensor:

$$F_k = \frac{\partial T_{ik}}{\partial x_k}$$

$$\vec{F} = \nabla \cdot \underline{T} \tag{3.54}$$

In this case, the force on some object that can be surrounded by a closed surface can be found by using the divergence theorem:

$$\vec{f} = \int_{vol} \vec{F} dv = \int_{vol} \nabla \cdot \underline{T} dv = \oiint \underline{T} \cdot \vec{n} da \tag{3.55}$$

or surface traction is $\tau_i = \sum_k T_{ik} n_k$, where n is the surface normal vector, then the total force in direction i is just:

$$f_i = \oiint \tau_i da = \oiint \sum_k T_{ik} n_k da \tag{3.56}$$

The interpretation of all of this is less difficult than the notation suggests. This field description of forces gives a simple picture of surface traction, the force per unit area on a surface. Integrating this traction over the area of some body yields the whole force on the body. Note one more thing about this notation. Sometimes, when subscripts are repeated as they are here, the summation symbol is omitted. Thus,

$$\tau_i = \sum_k T_{ik} n_k = T_{ik} n_k \tag{3.57}$$

3.5.1 Example: Linear Induction Machine

Figure 3.11 shows a highly simplified picture of a single-sided linear induction motor. This is not how most linear induction machines are actually built, but it is possible to show through symmetry arguments that the analysis we can carry out here is actually valid for other machines of this class.

This machine consists of a stator (the upper surface) which is represented as a surface current on the surface of a highly permeable region. The moving element consists of a thin layer of conducting material on the surface of a highly permeable region. The moving element (or "shuttle") has a

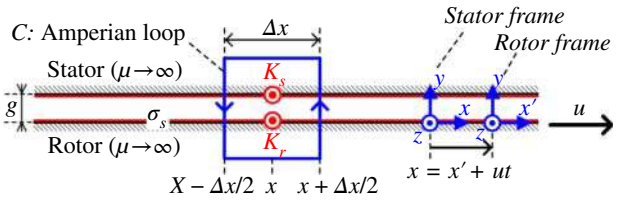

Figure 3.11 Simple model of a single-sided linear induction machine.

velocity u with respect to the stator and that motion is in the x direction. The stator surface current density is assumed to be:

$$K_s = \mathrm{Re}\left\{\underline{K}_s e^{j(\omega t - kx)}\right\}$$

It is a traveling wave where ω is the electrical frequency of the stator generating the rotating magnetic field and k is the wave number defined by the pole-pair pitch of the stator λ as follows:

$$k = \frac{2\pi}{\lambda}$$

Viewed from the shuttle for which the dimension in the direction of motion is $x' = x - ut$, the relative frequency is:

$$x = x' + ut; \omega_s = \omega - ku \quad \Rightarrow \quad \omega t - kx = (\omega - ku)\, t - kx' = \omega_s t - kx'$$

where $\omega_s = \omega - ku$ is the slip frequency. Now, since the shuttle surface can support a surface current and is excited by magnetic fields which are in turn excited by the stator currents, it is reasonable to assume that the form of rotor current is the same as that of the stator:

$$K_r = \mathrm{Re}\left\{\underline{K}_r e^{j(\omega_s t - kx')}\right\}$$

The block diagram given in Figure 3.12 describes how the induction machine works. The initial excitation is from the stator current density K_s (representative of stator three-phase winding) which, through Ampere's law, initially develops the magnetic field H_y, which induces the current density K_r in the rotor through Faraday's law. At steady state, it is both K_s and K_r that contribute to the generation of the total field H_y in the gap, and it is this total field (not only the part generated by stator current) that induces currents in the rotor.

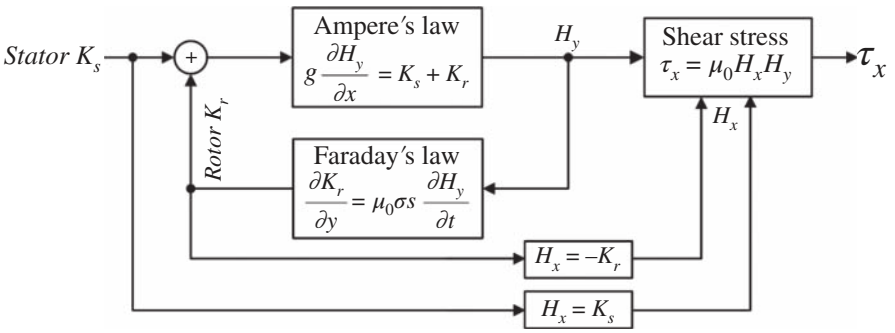

Figure 3.12 Block diagram of the operating principles and the modeling approach of the induction machine.

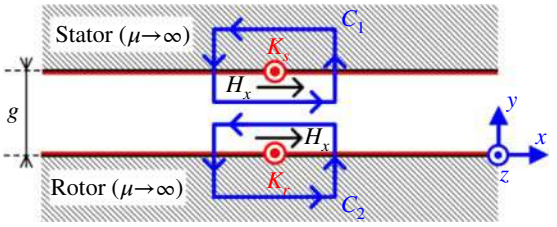

Figure 3.13 Ampere's law applied to the linear induction motor.

From the closed loop C in Figure 3.13, Ampere's law can be written as:

$$\oint_C H.dl = I_{enc} \Rightarrow H_y|_{x+\Delta x}\, g - H_y|_{x-\Delta x}\, g = \Delta x\,(K_s + K_r)$$

From the definition of derivative:

$$\lim_{\Delta x\to 0} g\frac{H_y|_{x+\Delta x} - H_y|_{x-\Delta x}}{\Delta x} = K_s + K_r \Rightarrow g\frac{\partial H_y}{\partial x} = K_s + K_r$$

which is, in complex amplitude:

$$\underline{H}_y = \frac{\underline{K}_s + \underline{K}_r}{-jkg}$$

On the other hand, the total magnetic field in the air-gap H_y, through Faraday's law, induces current density K_r in the rotor's conductive sheet. Assuming the problem is uniform in the z-direction:

$$\nabla \times \left(E'_z \hat{a}_z\right) = -\frac{\partial(B_x\hat{a}_x + B_y\hat{a}_y)}{\partial t} \Rightarrow \frac{\partial E'_z}{\partial y}\hat{a}_x - \frac{\partial E'_z}{\partial x}\hat{a}_y = -\frac{\partial B_x}{\partial t}\hat{a}_x - \frac{\partial B_y}{\partial t}\hat{a}_y$$

From the y-components on the two sides, we have:

$$\frac{\partial E'_z}{\partial y} = \frac{\partial B_y}{\partial t} \xrightarrow{B_y=\mu_0 H_y} \frac{\partial E'_z}{\partial y} = \mu_0\frac{\partial H_y}{\partial t} \Rightarrow -jk\,\underline{E}'_z = j\omega_s\mu_0\underline{H}_y \Rightarrow \underline{E}'_z = -\frac{\mu_0\omega_s}{k}\underline{H}_y$$

According to Ohm's law:

$$\underline{K}_r = -\frac{\mu_0\omega_s\sigma_s}{k}\underline{H}_y$$

The two unknowns H_y and K_r can be obtained through the 2-by-2 system of equations formed by Ampere's and Faraday's laws. A bit of algebraic manipulation yields:

$$\underline{K}_r = \frac{-j\frac{\mu_0\omega_s\sigma_s}{k^2 g}}{1 + j\frac{\mu_0\omega_s\sigma_s}{k^2 g}}\underline{K}_s$$

$$\underline{H}_y = \frac{j}{kg}\frac{1}{1 + j\frac{\mu_0\omega_s\sigma_s}{k^2 g}}\underline{K}_s$$

The equation of K_r indicates that $K_s = 0$ at zero slip frequency and $K_r = -K_s$ at $\omega_s = +\infty$.

This equation of H_y looks like a magneto motive force K_s divided by a complex reluctance, leading to field H_y. It is seen that the induced current in rotor K_r is zero if the slip frequency is zero, i.e. if the rotor moves at the speed of the traveling field.

$$\omega_s = \omega - ku = 0 \Rightarrow u = \frac{\omega}{k}$$

To find surface traction, the Maxwell stress tensor can be evaluated at the surface of stator or rotor where H_x can be obtained using boundary conditions shown in Figure 3.13. If the Amperian loops get small enough, $H_y\ dl$ on the two vertical sides of the Amperian loop cancels out. The upper horizontal branch is also zero in the infinitely permeable iron, leaving the lower branch related to the surface current. On the surface of stator, using the Amperian loop C_1, we obtain:

$$H_x|_{y=g} - H_x|_{iron} = K_s;\ H|_{iron} = 0 \Rightarrow H_x|_{y=g} = K_s$$

On the surface of rotor, using the Amperian loop C_2, we obtain:

$$H_x|_{iron} - H_x|_{y=0} = K_r;\ H|_{iron} = 0 \Rightarrow H_x|_{y=0} = -K_r$$

On the surface of stator, the x-directed magnetic field is simply $H_x = K_s$. Thus, the traction is:

$$\tau_x = \mu_0 H_x H_y$$

$$< \tau_x > = \frac{\mu_0}{2}\mathrm{Re}\left\{ \underline{H}_x\Big|_{y=g}\ \underline{H}_y^*\Big|_{y=g} \right\} = \frac{\mu_0}{2}\mathrm{Re}\left\{ \underline{K}_z\ \underline{H}_y^*\Big|_{y=g} \right\} = \frac{\mu_0}{2}\frac{1}{kg}\frac{\frac{\mu_0\omega_s\sigma_s}{k^2g}}{1+\left(\frac{\mu_0\omega_s\sigma_s}{k^2g}\right)^2}|\underline{K}_s|^2 \tag{3.58}$$

As an alternative way, the Maxwell stress tensor can be evaluated at the rotor's surface, where the x-directed magnetic field is simply $H_x = -K_r$. Thus, the traction is:

$$< \tau_x > = \frac{\mu_0}{2}\mathrm{Re}\left\{ \underline{H}_x\Big|_{y=0}\ \underline{H}_y^*\Big|_{y=0} \right\} = \frac{\mu_0}{2}\mathrm{Re}\left\{ -\underline{K}_r\ \underline{H}_y^*\Big|_{y=0} \right\}$$

Now, if we consider electromagnetic power (Poynting's theorem), in the y-direction: $S_y = E_z H_{x'}$, and since in the frame of the shuttle: $\underline{E'}_z = -\frac{\omega_s}{k}\mu_0 \underline{H}_y$

$$< S'_y \geq -\frac{1}{2}\frac{\omega_s}{k}\frac{\mu_0}{kg}\frac{\frac{\mu_0\omega_s\sigma_s}{k^2g}}{1+\left(\frac{\mu_0\omega_s\sigma_s}{k^2g}\right)^2}|\underline{K}_z|^2 = -\frac{\omega_s}{k} < \tau_x > \tag{3.59}$$

Similarly, evaluated in the frame of the stator:

$$< S_y > = -\frac{\omega}{k} < \tau_x >$$

This shows what we already suspected: the electromagnetic power flow from the stator is the force density on the shuttle times the wave velocity. The electromagnetic power into the shuttle is the same force density times the "slip" velocity. The difference between these two is the power converted to mechanical form and it is the force density times the shuttle velocity.

3.6 Surface Impedance and Eddy Currents

The purpose of studying "eddy currents" in electric machines, including surface impedances, is to understand frequency-dependent losses in machine conductors, induced current losses in magnets and in structural and magnetic flux-carrying components of electric machines.

Eddy currents in linear materials can often be handled rigorously, but eddy currents in saturating materials are more difficult and are often handled in a heuristic fashion. We present here both

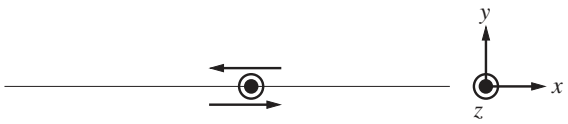

Figure 3.14 Convention for surface impedance.

analytical and semi-empirical ways of dealing with such losses. We start with surface impedance: the ratio of tangential electric field to surface current.

$$Z_s = \frac{E_t}{K_t}$$

In this description, the "surface current" K_t should be understood to be the total current flowing in a semi-infinite region of space, and therefore

$$K_t = -\vec{n} \times H_{\|}$$

Referring to Figure 3.14, in which the normal vector is in the "y" direction and surface current is in the z direction, the surface impedance is, if one is:

$$\underline{Z}_s = \frac{\underline{E}_z}{\mp \underline{H}_x}$$

depending on whether one is "looking" down or up. That is, if the region of interest is below the surface at $y = 0$, the vector normal to the region of interest is in the $+y$ direction and the surface current in the $+z$ direction yields a magnetic field just above the surface in the $-x$ direction. Conversely, if one is looking "up", the normal vector is in the $-y$ direction and surface current in the $+z$ direction yields a field in the $+x$ direction.

This model simplifies the analysis of fields in conductors by reducing the problem to boundary conditions on the surface, rather than solving for the fields throughout the volume of the material. This is important not just in calculating machine losses but also in describing how some machines operate. The surface impedance tells you how much voltage per unit length you need to apply to get the electrons moving at the surface, given the magnetic field produced by the moving electrons. It blends the material's resistance and reactance into a single measure that varies with frequency. The real part (resistance) of surface impedance represents the actual energy loss due to the resistance of the material. It relates to how much energy is converted into heat or other forms. The imaginary part (reactance) represents the energy storage in the magnetic fields surrounding the conductor (inductance). Reactance dictates how the phase of the current lags or leads the voltage.

Note that, in the prior example, loss in the surface of the moving element is:

$$P_d = - < S'_y \geq = \frac{\omega_s}{k} \frac{1}{2} \mathrm{Re} \left\{ \mu_0 \underline{H}^*_x \underline{H}_y \right\}$$

And power flow out of the stator is:

$$P_d = - < S_y > = \frac{\omega}{k} < \tau_x > = \frac{\omega}{k} \frac{1}{2} \mathrm{Re} \left\{ \mu_0 \underline{H}^*_x \underline{H}_y \right\}$$

And, since $\underline{E}'_z = -\frac{\omega_s}{k} \mu_0 \underline{H}_{y'}$, we can cast $P_d = \frac{1}{2} \mathrm{Re} \left\{ \underline{E}'_z \underline{H}^*_x \right\}$. And the surface impedance is $\underline{Z}_s = \frac{\underline{E}'_z}{\underline{H}_x}$, then

$$P_d = \frac{1}{2} |\underline{H}_x|^2 \mathrm{Re}\{\underline{Z}_s\}$$

In the next section, we look at the previously studied linear induction machine in multiple ways in which we calculate the surface impedance Z_s at the surface of rotor (conductive material), then

we transfer it to the surface of stator to get the impedance at the surface of stator, which will be employed in calculating shear stress:

$$< \tau_x > = \frac{\mu_0}{2} \mathrm{Re}\left\{ \underline{H}_x^* \underline{H}_y \right\} = \frac{\mu_0}{2} |\underline{H}_x|^2 \mathrm{Re}\left\{ \frac{\underline{H}_y}{\underline{H}_x} \right\} = \pm \frac{k}{2\omega} |\underline{H}_x|^2 \mathrm{Re}\{\underline{Z}_s\}$$

Also, the average normal stress T_{yy} for the vertical force can be obtained as:

$$< T_{yy} > = \frac{\mu_0}{4} \left\{ |\underline{H}_y|^2 - |\underline{H}_x|^2 \right\} = \frac{\mu_0}{4} |\underline{H}_x|^2 \left\{ \left| \frac{\underline{H}_y}{\underline{H}_x} \right|^2 - 1 \right\} = \frac{\mu_0}{4} |\underline{H}_x|^2 \left\{ \left| \frac{\underline{Z}_s}{\frac{\mu_0 \omega}{k}} \right|^2 - 1 \right\}$$

3.6.1 Uniform Conductors

Consider the situation shown in Figure 3.15. A slab of material with uniform conductivity and permeability is situated with its bottom surface at $y = 0$. At the lower surface of the material exists a "surface impedance" noted as Z_0. At the top surface of the material, there is a magnetic field parallel to the surface that is of the form:

$$H_{xs} = \mathrm{Re}\{\underline{H}_s e^{(j\omega t - kx)}\} \tag{3.60}$$

The surface impedance Z_0 is the boundary condition at the bottom surface. The surface impedance Z_h will be a boundary condition for the next layer. The ratio of the magnetic field H_{x0} at the bottom of the layer to the magnetic field at the top H_{xh} is a transfer ratio that can be used to evaluate shielding by that layer of material. Note also that the transfer of surface impedance and transfer ratio can be used to evaluate the performance of multiple layers of material. Note that because B_y and H_x are both continuous across the boundary, so are the surface impedances. The frequencies for the diffusion problem are local, so, for example, in the linear induction motor, the proper frequency to use is the slip frequency.

First comes the derivation of a diffusion equation. Assume permeability and conductivity are both uniform over the layer.

Start with Ampere's law and Faraday's law:

$$\nabla \times \vec{H} = \vec{J}$$

$$\nabla \times \vec{H} = -\frac{\partial \vec{B}}{\partial t}$$

Assume that all of the important variables are in a traveling wave with an argument $e^{j(\omega t - kx)}$.

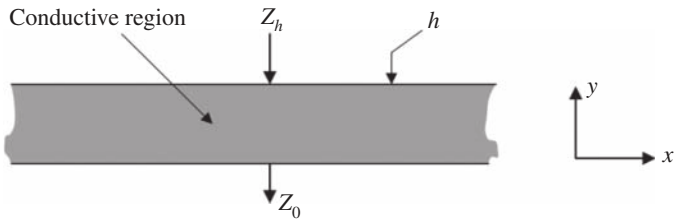

Figure 3.15 Layer of uniform conductor.

Then the electric field can be found by:

$$(\nabla \times \vec{E})_y = \begin{vmatrix} \vec{a}_x & \vec{a}_y & \vec{a}_z \\ \frac{\partial}{\partial x} & \frac{\partial}{\partial y} & \frac{\partial}{\partial z} \\ E_x & E_y & E_z \end{vmatrix}_y = -\frac{\partial E_z}{\partial x} = jk\underline{E_z} = -j\omega\underline{B_y}$$

Or

$$\underline{E_z} = -\frac{\omega}{k}\mu\underline{H_y} \tag{3.61}$$

Now take the curl of Ampere's law:

$$\nabla \times \nabla \times \vec{H} = \nabla \times \vec{J} = \nabla \times \sigma\vec{E} = -\sigma\mu\frac{\partial \vec{H}}{\partial t}$$

Since $\nabla \times \nabla \times \vec{H} = \nabla(\nabla \cdot \vec{H}) - \nabla^2\vec{H}$ and $\nabla \cdot \vec{H} = 0$, a diffusion equation results:

$$\nabla^2\vec{H} = \mu\sigma\frac{\partial \vec{H}}{\partial t} \tag{3.62}$$

In this situation, if $\vec{H} = \mathrm{Re}\{\underline{\vec{H}}(y)\, e^{j(\omega t - kx)}\}$, the diffusion equation devolves to:

$$\frac{\partial^2\vec{H}}{\partial y^2} - k^2\underline{\vec{H}} = j\omega\mu\sigma\underline{\vec{H}}$$

This indicates that H must be proportional to $e^{\pm\gamma y}$, where $\gamma^2 = k^2 + j\omega\mu\sigma$. A suitable form for the fields in this situation is:

$$\begin{aligned} H_x &= \mathrm{Re}\{(\underline{H}_+ e^{\gamma y} + \underline{H}_- e^{-\gamma y})e^{j(\omega t - kx)}\} \\ H_y &= \mathrm{Re}\left\{j\frac{k}{\gamma}(\underline{H}_+ e^{\gamma y} - \underline{H}_- e^{-\gamma y})e^{j(\omega t - kx)}\right\} \end{aligned} \tag{3.63}$$

It is left as an exercise to show that, for this form of magnetic field, the divergence of magnetic field is zero and that the curl of magnetic field is equal to current density:

$$\nabla \times \vec{H}_z = J_z$$

To derive the impedance facing the top of the layer, start with the impedance faced by the bottom of the layer:

$$\underline{Z}_0 = \mu\frac{\omega}{k}\frac{\underline{H_y}}{\underline{H_x}} = \frac{\underline{E_z}}{-\underline{H_x}} = \mu\frac{\omega}{k}j\frac{k}{\gamma}\frac{\underline{H}_+ - \underline{H}_-}{\underline{H}_+ + \underline{H}_-} \tag{3.64}$$

Using shorthand $\underline{\Gamma} = \frac{\underline{H}_-}{\underline{H}_+}$

$$\underline{Z}_0 = j\mu\frac{\omega}{\gamma}\frac{1 - \underline{\Gamma}}{1 + \underline{\Gamma}} \tag{3.65}$$

Solving for Γ,

$$\Gamma = \frac{j\mu\frac{\omega}{\gamma} - \underline{Z}_0}{j\mu\frac{\omega}{\gamma} + \underline{Z}_0}$$

Then at the top surface,

$$\underline{Z}_h = j\mu\frac{\omega}{\gamma}\frac{e^{\gamma h} - \Gamma e^{-\gamma h}}{e^{\gamma h} + \Gamma e^{-\gamma h}}$$

Substituting for Γ and doing some "plug and grind", an expression for impedance at the top surface, in terms of frequency, material properties, and impedance at the bottom surface is:

$$\underline{Z}_h = j\mu\frac{\omega}{\gamma}\frac{j\mu\frac{\omega}{\gamma}\sinh\gamma h + \underline{Z}_0\cosh\gamma h}{j\mu\frac{\omega}{\gamma}\cosh\gamma h + \underline{Z}_0\sinh\gamma h} \tag{3.66}$$

There are a few special cases. If the region in question has zero conductivity (as in air), $\gamma = k$ and the expression is:

$$\underline{Z}_h = j\mu\frac{\omega}{k}\frac{j\mu\frac{\omega}{k}\sinh kh + \underline{Z}_0\cosh kh}{j\mu\frac{\omega}{k}\cosh kh + \underline{Z}_0\sinh kh} \tag{3.67}$$

If the bottom surface is ferromagnetic, $|Z_0| \to \infty$, the impedance at the top surface is:

$$\underline{Z}_h = j\mu\frac{\omega}{k}\coth\gamma h \tag{3.68}$$

And, if the bottom surface is facing "free space" in the $-y$ direction, the component of H that grows in the negative direction, $H_- = 0$, and then

$$\underline{Z}_0 = j\mu_0\frac{\omega}{k} \tag{3.69}$$

Note also that a transfer coefficient, the ratio of magnetic field at the bottom of a region to field at the top of the region, can be derived:

At the bottom surface, $\underline{H}_x(y=0) = \underline{H}_+(1+\underline{\Gamma})$

At the top surface, $\underline{H}_x(y=h) = \underline{H}_s = \underline{H}_+(e^{\gamma h} + \underline{\Gamma e^{-\gamma h}})$

The transfer coefficient is:

$$\begin{aligned}\underline{T} = \frac{\underline{H}_0}{\underline{H}_s}T = \frac{\underline{H}_0}{\underline{H}_h} &= \frac{1+\frac{j\mu\frac{\omega}{\gamma}-\underline{Z}_0}{j\mu\frac{\omega}{\gamma}+\underline{Z}_0}}{e^{\gamma h}+e^{-\gamma h}\frac{j\mu\frac{\omega}{\gamma}-\underline{Z}_0}{j\mu\frac{\omega}{\gamma}+\underline{Z}_0}} \\ &= \frac{j\mu\frac{\omega}{\gamma}+\underline{Z}_0+j\mu\frac{\omega}{\gamma}-\underline{Z}_0}{e^{\gamma h}\left(j\mu\frac{\omega}{\gamma}+\underline{Z}_0\right)+e^{-\gamma h}\left(j\mu\frac{\omega}{\gamma}-\underline{Z}_0\right)} = \frac{j\mu\frac{\omega}{\gamma}}{j\mu\frac{\omega}{\gamma}\cosh\ \gamma h+\underline{Z}_0\sinh\ \gamma h}\end{aligned} \tag{3.70}$$

This relationship can be useful if shielding is important.

3.6.2 Example: The Linear Machine and Limiting Cases

The foregoing expressions are useful in situations ranging from estimating shielding and dissipation in conductive layers used for shielding conductors, performance of linear machines to levitation systems. First, consider the linear motor pictured in Figure 3.16, part c. First is the full model, considering both the thickness of the shuttle conductive layer and the width of the air-gap. From above, we have the impedance at the surface of the air-gap:

$$Z_r = j\mu_0\frac{\omega_s}{k}\coth\gamma h$$

Then, the impedance presented to the surface current is:

$$\underline{Z}_r = j\mu_0\frac{\omega_s}{k}\frac{j\mu_0\frac{\omega_s}{k}\sinh k(g_e-h)+\underline{Z}_r\ \cosh k(g_e-h)}{j\mu_0\frac{\omega_s}{k}\cosh k(g_e-h)+\underline{Z}_r\ \sinh k(g_e-h)}$$

Power density input to the surface is:

$$\langle p\rangle = \frac{1}{2}|K_s|^2\mathrm{Re}\{\underline{Z}_s\}$$

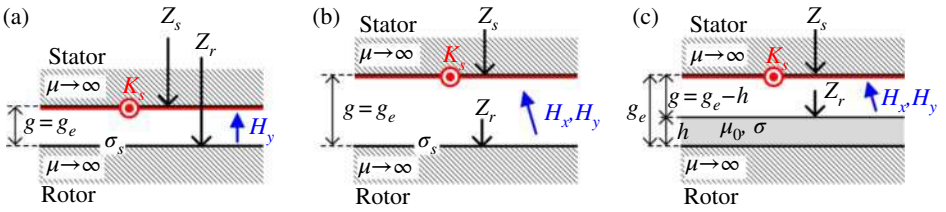

Figure 3.16 Modeling of induction machine by impedance transfer theory: (a) surface conductivity for a thin conductive sheet and only *y*-directed fields in a narrow air-gap, (b) surface conductivity for a thin conductive sheet and both *x* and *y* fields in a large air-gap, and (c) diffusion for a thick conductive sheet and both *x* and *y* fields in a large air-gap.

and resulting shear stress density is that dissipation divided by slip velocity:

$$\langle \tau_s \rangle = \frac{\langle p \rangle}{\frac{\omega_s}{k}} = \frac{1}{2}\frac{k}{\omega_s}|K_s|^2 \mathrm{Re}\{\underline{Z}_s\}$$

There are some interesting and useful limits. In the case in which the conductor is thin, so that γ_h is small, if k is negligible:

$$Z_r \to j\mu_0 \frac{\omega_s}{\gamma^2 h} \to \frac{j\mu_0\omega_s}{(k^2 + j\omega_s\mu_0\sigma)h} \to \frac{1}{\sigma h} = \frac{1}{\sigma_s}$$

In the case of a narrow air-gap,

$$Z_s = j\mu_0\frac{\omega_s}{k}\frac{j\mu_0\frac{\omega_s}{k}\sinh kg_e + Z_r\cosh kg_e}{j\mu_0\frac{\omega_s}{k}\cosh kg_e + Z_r\sinh kg_e} \to j\mu_0\frac{\omega_s}{k}\frac{j\mu_0\frac{\omega_s}{k}kg_e + Z_r}{j\mu_0\frac{\omega_s}{k} + Z_r kg_e}$$

If k_h can be neglected, this is:

$$Z_s = j\mu_0\frac{\omega_s}{k}\frac{Z_r}{j\mu_0\frac{\omega_s}{k} + kg_e Z_r} = \frac{j\mu_0\frac{\omega_s}{k^2 g_e}Z_s}{j\mu_0\frac{\omega_s}{k^2 g_e} + Z_s} = Z_g \parallel Z_r$$

where g_e is the magnetic gap and $Z_g = j\mu_0\frac{\omega}{k^2 g_e}$ is the "gap impedance".

If these two approximations are used in the expression for power transferred across the gap, they yield:

$$\langle p \rangle = \frac{\omega}{k}\frac{\mu_0}{2}\frac{1}{kg}|K_s|^2\frac{\mu_0\frac{\omega\sigma_s}{k^2 g_e}}{1+\left(\mu_0\frac{\omega\sigma_s}{k^2 g_e}\right)^2}$$

which is the same as (3.59).

3.7 Magnetic Materials

Electric machines employ ferromagnetic materials to carry magnetic flux from and to appropriate places within the machine. Such materials have properties that are interesting, useful, and problematical, and the designers of electric machines must deal with this stuff. The purpose of this note is to introduce the most salient properties of the kinds of magnetic materials used in electric machines.

We will be concerned here with materials which exhibit magnetization: flux density is something other than $\vec{B} = \mu_0\vec{H}$. Generally, we will speak of hard and soft magnetic materials. Hard materials

are those in which the magnetization tends to be permanent, while soft materials are used in magnetic circuits of electric machines and transformers. Since they are related, we will find ourselves talking about them either at the same time or in close proximity, even though their uses are widely disparate.

3.7.1 Magnetization

It is possible to relate, in all materials, magnetic flux density to magnetic field intensity with a constitutive relationship of the form:

$$\vec{B} = \mu_0(\vec{H} + \vec{M}) \tag{3.71}$$

where magnetic field intensity H and magnetization M are the two important properties. In linear magnetic material, magnetization is a simple linear function of magnetic field:

$$\vec{M} = \chi_m \vec{H}$$

So that the flux density is also a linear function:

$$\vec{B} = \mu_0(1 + \chi_m) \quad \text{or} \quad \mu = \mu_0\left(1 + \chi_m\right) \tag{3.72}$$

Note that in the most general case, the magnetic susceptibility χ_m might be a tensor, leading to flux density being non-colinear with magnetic field intensity. But such a relationship would still be linear. Generally, this sort of complexity does not have a major impact on electric machines.

3.7.2 Saturation and Hysteresis

In useful magnetic materials, this nice relationship is not correct and we need to take a more general view. We will not deal with the microscopic picture here, except to note that the magnetization is due to the alignment of groups of magnetic dipoles, the groups often called domains. There are only so many magnetic dipoles available in any given material, so that once the flux density is high enough, the material is said to saturate, and the relationship between magnetic flux density and magnetic field intensity is non-linear.

In most useful magnetic materials, the magnetic domains tend to be somewhat "sticky", and a more-than-incremental magnetic field is required to get them to move. This leads to the property called "hysteresis", both useful and problematical in many magnetic systems.

Hysteresis loops take many forms; a generalized picture of one is shown in Figure 3.17. Salient features of the hysteresis curve are the remnant magnetization B_r and the coercive field H_c. Note that the actual loop that will be traced out is a function of field amplitude and history. Thus, there are many other "minor loops" that might be traced out by the B–H characteristic of a piece of material, depending on just what the fields and fluxes have done and are doing.

Hysteresis is important for two reasons. First, it represents the mechanism for "trapping" magnetic flux in a piece of material to form a permanent magnet. We will have more to say about that anon. Second, hysteresis is a loss mechanism. To show this, consider some arbitrary chunks of material for which we can characterize an MMF and a flux:

$$F = NI = \int \vec{H} \cdot d\vec{\ell}$$

$$\boldsymbol{\Phi} = \int \frac{V}{N}\, dt = \iint \vec{B} \cdot d\vec{A}$$

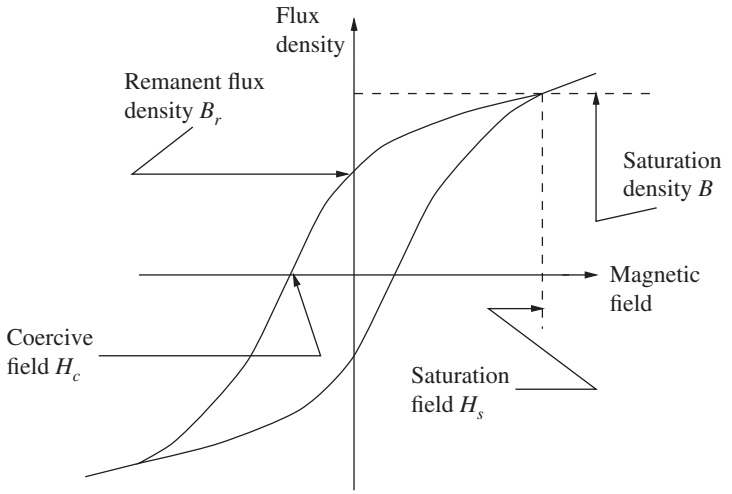

Figure 3.17 Hysteresis loop nomenclature.

Energy input to the chunk of material over some time period is:

$$w = \int VIdt = \int Fd\Phi = \int_t \int \vec{H} \cdot d\vec{\ell} \iint d\vec{B} \cdot d\vec{A} dt$$

Now, imagine carrying out the second (double) integral over a continuous set of surfaces which are perpendicular to the magnetic field H. (This IS possible!) The energy becomes:

$$w = \int_t \int_{vol} \vec{H} \cdot d\vec{B} d\ vol\ dt$$

Done over a complete cycle of some input waveform, that is:

$$w = \int_{vol} W_m\, d\ vol$$

$$W_m = \oint \vec{H} \cdot d\vec{B} \tag{3.73}$$

That last expression simply expresses the area of the hysteresis loop for the particular cycle.

Generally, for most electric machine applications, magnetic material characterized as "soft" is used, having as narrow a hysteresis loop (and therefore as low a hysteretic loss) as possible. At the other end of the spectrum are "hard" magnetic materials, which are used to make permanent magnets. The terminology comes from steel, in which soft, annealed steel material tends to have narrow loops and hardened steel tends to have wider loops. However, permanent magnet technology has advanced to the point where the coercive forces possible in even cheap ceramic magnets far exceed those of the hardest steels.

3.7.3 Conduction, Eddy Currents, and Laminations

Steel, being a metal, is an electrical conductor. Thus, when time-varying magnetic fields pass through it, they cause eddy currents to flow, and of course, those produce dissipation. In fact, for almost all applications involving "soft" iron, eddy currents are the dominant source of loss. To reduce the eddy current loss, magnetic circuits of transformers and electric machines are almost

invariably laminated, or made up of relatively thin sheets of steel. To further reduce losses, the steel is alloyed with elements (often silicon) which reduce the electrical conductivity.

There are several approaches to estimating the loss due to eddy currents in steel sheets and in the surface of solid iron, and it is worthwhile to look at a few of them. It should be noted that this is a "hard" problem, since the behavior of the material itself is difficult to characterize.

3.7.4 Complete Penetration in a Thin Lamination

Consider a stack of laminations. In particular, consider one sheet in the stack represented in Figure 3.18. It has thickness t, conductivity σ, and permeability μ. We will study the induced eddy currents and the associated losses for low-frequency and high-frequency cases.

If the "skin depth" is much greater than the sheet thickness, so that magnetic field penetrates the sheet completely, as shown in Figure 3.19. In this case, the induced eddy currents are directly obtained from the average time-varying field B_0 in the material, while the impact of the reaction fields generated by the induced eddy currents B_e on the initial field B_0 is ignored.

Assume that the applied magnetic flux density B_0 is parallel to the surface of the sheets and is sinusoidal in time:

$$\vec{B} = \hat{a}_z \mathrm{Re}\{\sqrt{2}B_0\, e^{j\omega t}\}$$

Faraday's law can be used to determine the electric field and therefore, current density in the sheet. If the problem is uniform in the x- and z-directions,

$$\nabla \times (E_x \hat{a}_x) = -\frac{\partial (B_z \hat{a}_z)}{\partial t} \quad \Rightarrow -\frac{\partial E_x}{\partial y}\hat{a}_z = -\frac{\partial B_z}{\partial t}\hat{a}_z \quad \Rightarrow \quad \frac{\partial E_x}{\partial y} = \frac{\partial B_z}{\partial t} \quad \Rightarrow \quad \frac{\partial J_x}{\partial y} = \sigma \frac{\partial B_z}{\partial t}$$

In the phasor domain, we have:

$$J_x(y) = j\omega\sigma B_0 y$$

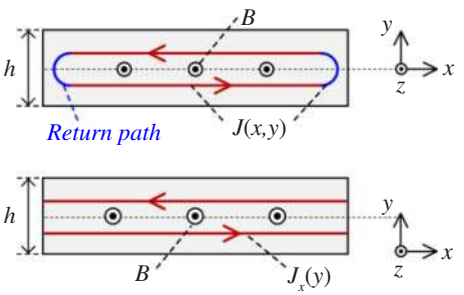

Figure 3.18 Lamination section for loss calculation.

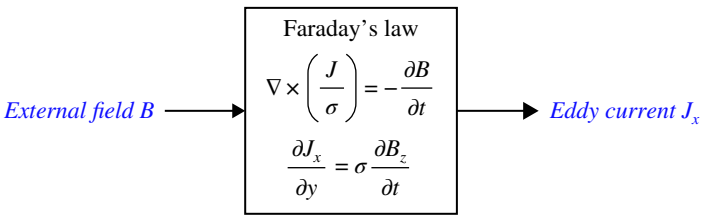

Figure 3.19 Eddy current J_x induced by average field B_0 while reaction fields are ignored.

Local power dissipated is, noting we are working in RMS amplitudes:

$$P_d(y) = \frac{|J|^2}{\sigma} = \omega^2 B_0^2 \sigma y^2$$

It is seen that, as we ignore reaction fields, the above equation does not depend on the permeability of laminations μ. To find average (over the thickness of the lamination) power dissipated, integrate over the thickness of the lamination:

$$< P_d > = \frac{2}{h}\int_0 P_d(y)\, dy = \frac{2}{h}\omega^2 B_0^2 \sigma \int_0^{h/2} y^2 dy = \frac{1}{12}\sigma\omega^2 B_0^2 h^2$$

Pay attention to the orders of the various terms here: power is proportional to the square of flux density and to the square of frequency. It is also proportional to the square of the lamination thickness (this is average volume power dissipation).

As an aside, consider a simple magnetic circuit made of this material, with some length ℓ and area A, so that volume of material is ℓA. Flux linked by a coil of N turns would be:

$$\Lambda = N\Phi = NAB_0$$

And voltage is $\underline{V} = j\omega\Lambda$. Total power dissipated in this core would be:

$$P_c = A\ell \frac{1}{12}\sigma\omega^2 B_0^2 h^2 = \frac{V^2}{R_c}$$

where the equivalent core resistance is now:

$$R_c = \frac{12AN^2}{\ell\sigma h^2} \tag{3.74}$$

3.7.5 Solid Ferromagnetic Material

Consider the geometry described by Figure 3.20. A solid slab of ferromagnetic material, such as iron, is shown. Assume that the problem is "long" in both the x and z dimensions, and that the slab is deep. We will discover what "deep" means as we go along. This is an analog of a conductive surface that is several skin depths in depth. This is a non-linear problem, but one that is sometimes encountered. We also consider that the wavelength is long ($k \to 0$). The problem was worked by MacLean and Agarwal [2, 3]. They assumed that the magnetic field at the surface of the flat slab of material was sinusoidal in time and of high enough amplitude to saturate the material. This is true if the material has high permeability and the magnetic field is strong. The assumed saturation curve is shown in Figure 3.21.

What happens is that the impressed magnetic field saturates a region of material near the surface, leading to a magnetic flux density parallel to the surface. The depth of the region affected changes with time, and there is a separating surface (in the flat problem, this is a plane) that moves away from the top surface in response to the change in the magnetic field. An electric field is developed to move the surface, and that magnetic field drives eddy currents in the material.

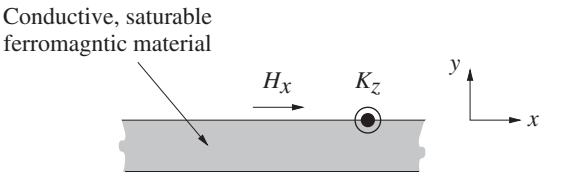

Figure 3.20 Solid iron problem.

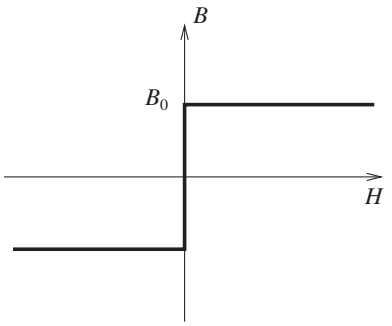

Figure 3.21 Abrupt saturation curve.

Assume that the material has a perfectly rectangular magnetization curve as shown in Figure 3.21, so that flux density in the x-direction is:

$$B_x = B_0 sign(H_x)$$

The flux per unit width in the z-direction is:

$$\boldsymbol{\Phi} = \int_0^{-\infty} B_x dy$$

Faraday's law becomes:

$$E_z = \frac{\partial \boldsymbol{\Phi}}{\partial t}$$

While Ampere's law, in conjunction with Ohm's law is:

$$\frac{\partial H_x}{\partial y} = \sigma E_z$$

McLean suggested a solution to this set in which there is a "separating surface" at depth ζ as shown in Figure 3.22. At any given time:

$$H_x = H_s(t)\left(1 + \frac{y}{\zeta}\right)$$

$$J_z = \sigma E_z = \frac{H_s}{\zeta}$$

That is, in the region between the separating surface and the top of the material, electric field E_z is uniform and magnetic field H_x is a linear function of depth, falling from its impressed value at the surface to zero at the separating surface. Now, electric field is produced by the rate of change

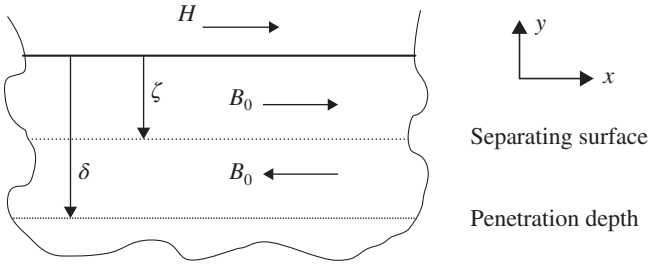

Figure 3.22 Separating surface and penetration depth.

of flux, which is:

$$E_z = \frac{\partial \boldsymbol{\Phi}}{\partial t} = 2B_0 \frac{\partial \zeta}{\partial t}$$

Eliminating E and rearranging:

$$2\zeta \frac{\partial \zeta}{\partial t} = \frac{H_x}{\sigma B_0}$$

If the impressed magnetic field is sinusoidal, this becomes:

$$\frac{\mathrm{d}\zeta^2}{\mathrm{d}t} = \frac{H_0}{\sigma B_0} |\sin \omega t|$$

This is solved by assuming that $\zeta = 0$ at $t = 0$,

$$\zeta = \sqrt{\frac{2H_0}{\omega \sigma B_0}} \sin \frac{\omega t}{2} \quad 0 < \omega t < \pi$$

The separating surface always moves in the downward direction (as we have drawn it), so at each half cycle a new surface is created: the old one just stops moving at a maximum position, or penetration depth:

$$\delta = \sqrt{\frac{2H_0}{\omega \sigma B_0}}$$

This penetration depth is analogous to the "skin depth" of the linear theory. However, the fields really do penetrate to this depth and stop there. The resulting electric field is:

$$E_z = \frac{2H_0}{\sigma \delta} \cos \frac{\omega t}{2} \quad 0 < \omega t < \pi$$

This may be Fourier analyzed: noting that if the impressed magnetic field is sinusoidal, only the time fundamental component of electric field is important, so that:

$$E_z = \frac{8}{3\pi} \frac{H_0}{\sigma \delta} (\cos \omega t + 2 \sin \omega t + \ldots)$$

Complex surface impedance is the ratio between the complex amplitude of electric and magnetic fields, which becomes:

$$\underline{Z}_s = \frac{\underline{E}_z}{\underline{H}_x} = \frac{8}{3\pi} \frac{1}{\sigma \delta} (2 + j) \tag{3.75}$$

Thus, in practical applications, ferromagnetic surfaces can be handled much as are linear conductive surfaces, by establishing a skin depth and assuming that current flows within that skin depth of the surface. The resistance is modified by the factor of $\frac{16}{3\pi}$ and the "power factor" of this surface is about 89% (as opposed to a linear surface where the "power factor" is about 71%.

Agarwal suggests using a value for B_0 of about 75% of the saturation flux density of the steel.

3.8 Semi-Empirical Method of Handling Iron Loss

Neither of the models described so far is fully satisfactory in describing the behavior of laminated iron, because losses are a combination of eddy current and hysteresis losses. The rather simple model employed for eddy currents is precise because of its assumption of abrupt saturation.

The hysteresis model, while precise, would require an empirical determination of the size of the hysteresis loops anyway. So, most often it is necessary to resort to empirical loss data. Manufacturers of lamination steel sheets will publish data, usually in the form of curves, for many of their products. There are a few ways of looking at the data.

A low-frequency flux density vs. magnetic field ("saturation") curve was shown in Figure 3.17.

A measure of the incremental permeability is the slope of that curve:

$$\mu' = \frac{dB}{dH}$$

In some machine applications, either the "total" inductance (ratio of flux to MMF) or "incremental" inductance (slope of the flux to MMF curve) is required. In the limit of low frequency, these numbers may be useful.

For designing electric machines, however, a second way of looking at steel may be more useful. This is to measure the real and reactive power as a function of magnetic flux density and frequency. In principle, this data is immediately useful. In any well-designed electric machine, the flux density in the core is distributed fairly uniformly and is not strongly affected by eddy currents, etc., in the core. Under such circumstances, one can determine the flux density in each part of the core. With that information, one can go to the published empirical data for real and reactive power and determine core loss and reactive power requirements.

Manufacturers publish core loss and "apparent" power per unit mass as a function of induction (B, usually peak) for their various grades of electrical sheet steel. The use of this data is quite straightforward. If the flux density in a machine is estimated for each part of the machine and the mass of steel calculated, then with the help of this chart, a total core loss and apparent power can be estimated. Then the effect of the core may be approximated with a pair of elements in parallel with the terminals, with:

$$R_c = \frac{q|V|^2}{P}$$

$$X_c = \frac{q|V|^2}{Q}$$

where q is the number of phases, P is real power, and Q is reactive power, estimated from real and "apparent" power by

$$Q = \sqrt{P_a^2 - P^2}$$

In practical machine design, there may be regions of the core for which flux density is different, for example, the teeth and core "back iron". To calculate total real and reactive power, one would find real and reactive power per unit mass (from the published data) for each region and then multiply by the mass of each region.

"Looking up" this data is a bit awkward for design studies, so it is often convenient to do a "curve fit" to the published data. There are a large number of possible ways of doing this. One method that has been found to work reasonably well for silicon iron is an "exponential fit", often attributed to Steinmetz:

$$P \simeq P_0 \left(\frac{B}{B_0}\right)^{\varepsilon_B} \left(\frac{f}{f_0}\right)^{\varepsilon_F} \tag{3.76}$$

where P_0, B_0, and f_0 are "base", or reference quantities and the two exponentials describe the slopes of the curves on log–log coordinates. Note from Figure 3.23 that the curve exponential does not necessarily fit the data very closely.

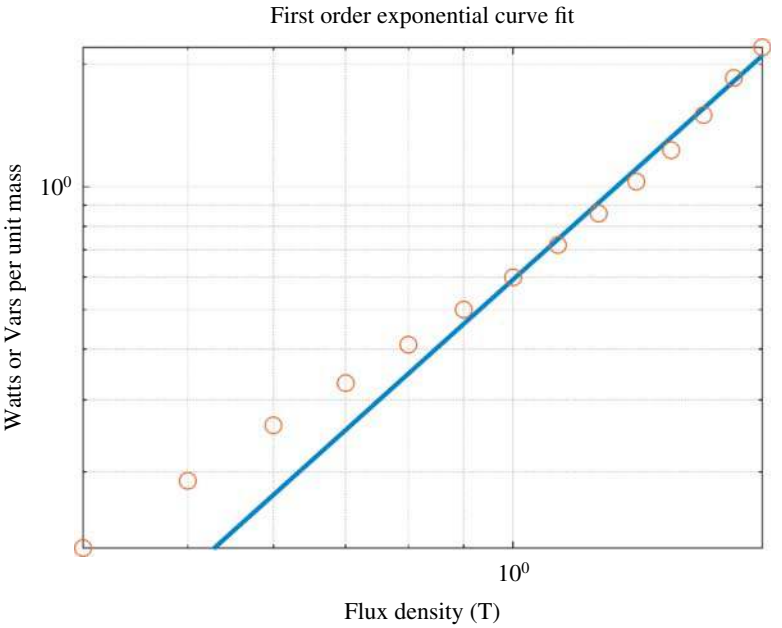

Figure 3.23 Steinmetz fit for core loss in 29-gauge, fully processed M-19 sheet steel at 60 Hz.

3.9 Problems

3.1 A two-coil rotary system with the coils on the stator and permanent magnets on the rotor has self- and mutual flux linkages of:

$$\begin{bmatrix}\lambda_1\\ \lambda_2\end{bmatrix} = \begin{bmatrix}L_1 & 0\\ 0 & L_2\end{bmatrix}\begin{bmatrix}i_1\\ i_2\end{bmatrix} + \begin{bmatrix}\lambda_0\cos\theta\\ \lambda_0\sin\theta\end{bmatrix}$$

Assume values of the inductances to be $L_1 = L_2 = 100$ mH and the constant flux is $\lambda_0 = 1$ Wb. The angle θ is the physical angle of the rotor.

Find and plot the answers to the following questions. Your plots should show two complete rotations of the system. Time origin is not important.

a) With the rotor turning at a constant speed of 50 Hz, coil 1 open and coil 2 carrying a constant current of 5 A, what are:
   - Torque produced?
   - Voltage in coil 1?

b) With coil 2 shorted and coil 1 open, what is torque produced? (For this part, you should assume flux $\lambda_2 = 0$. Why can you do this?)

c) With both coils connected to resistors so the total resistance (coil plus resistor) is 10 Ω, torque is constant. (Why?). Assuming steady state operation, calculate this torque as a function of speed over the range zero to 100 Hz.

3.2 A two-coil rotary system with one coil on the stator and one coil on the rotor has a flux/current relationship:

$$\begin{bmatrix}\lambda_1\\ \lambda_2\end{bmatrix} = \begin{bmatrix}L_1 & M\cos\theta\\ M\cos\theta & L_2\end{bmatrix}\begin{bmatrix}i_1\\ i_2\end{bmatrix}$$

Assume values of the inductances to be $L_1 = L_2 = 200$ mH $M = 150$ mH. Note this system has a coupling coefficient less than one: $M^2 < L_1 L_2$. It is rotated at a constant speed of

3600 RPM (60 Hz). Current in coil 1 is held constant at 5A. It has been on long enough to be in steady state operation.
Find and plot the answers to the following questions. Your plots should show two complete rotations of the system. Time origin is not important.

a) What torque does this system produce?
b) What is the voltage (ignore resistance) across the terminals of coil 1? Under three cases:
   1. Current in coil 2 is held constant at 5 A
   2. Flux linked by coil 2 is constrained to be zero (this is what would be approximately true were the terminals of coil 2 to be shorted, assuming the resistance of coil 2 is neglectable)
   3. Coil 2 is shorted through a resistor so that the total resistance (including the coil itself) is 10 Ω

3.3 This problem is related to a "coil gun" problem that is sometimes used to motivate freshmen to think electrical technology is "neat". A permanent magnet can move through a plastic tube, which for our purposes, we will assume to be frictionless. A coil of wire is wrapped around the tube.

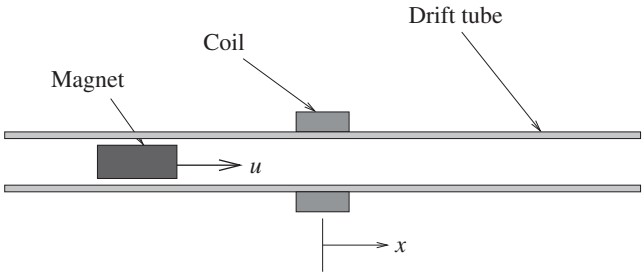

In an experiment, the permanent magnet is made to move through the tube with a velocity of 5 m/s. The coil is open and its voltage is measured to be this:

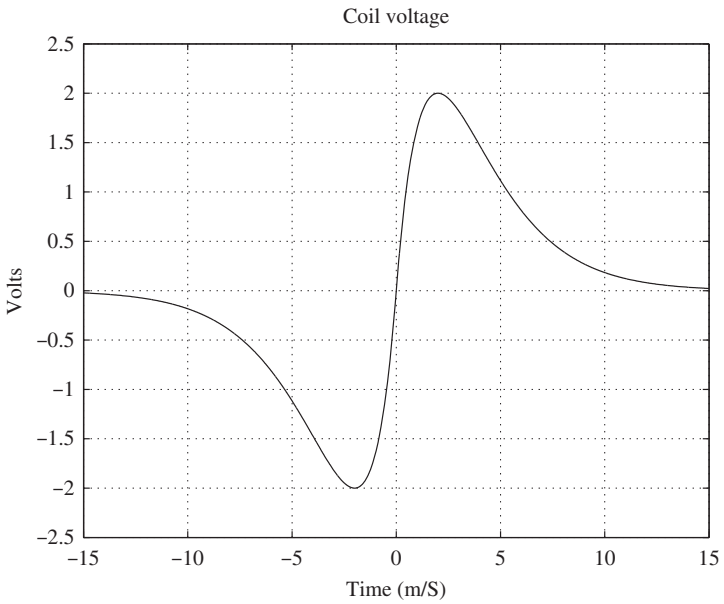

As it turns out, a very good approximation for this voltage is:

$$v(t) = Ate^{-a|t|}$$

where the peak voltage of 2 V is reached at 2 m/s. Note that we have set time $t = 0$ to be when the magnet is in the middle of the coil, and this is the point in time when the voltage is going through zero.

1) Convince yourself that force exerted on the magnet by current in the coil is

$$f(x) = ID(x) = I\frac{d\lambda}{dx}.$$

2) Find $D(x)$ from the information given here.
3) If the magnet is held stationary at position x and current is fixed at value I, find the force on the magnet. Find and plot this force as a function of position for $-10\text{ cm} < x < 10\text{ cm}$ and for $I = 10\text{A}$.
4) Convince yourself that this force tends to push the magnet away from the center of the coil. Find the energy imparted to the magnet, as a function of position, starting from the center of the coil ($x = 0$).
5) The magnet has a mass of 50 g. If the coil current is held at 10A and the magnet is released from the position $x = 1$ mm, find its velocity as a function of position.
6) The coil has a current held at 10 A. The magnet is injected into the left-hand end of the tube with a velocity of 1.5 m/s. How fast is it going when it passes through the center of the tube?
7) The same experiment is done, but this time the coil current is reversed so the magnet is attracted, rather than repelled, to the center. Now, how fast is it going when it passes through the center of the coil?

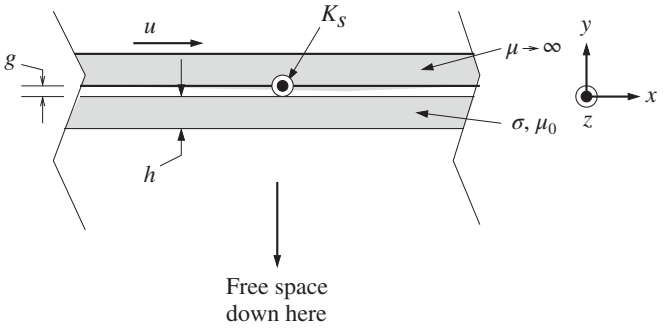

3.4 Shown in the picture above is a cartoon of a levitated device. A magnetic slab has a surface current $K_s = \text{Re}\{\underline{K}_s e^{-jkx'}\}$, where x' is the dimension with reference to the slab itself. The slab and its current are moving to the right with velocity u. Below is a slab of non-magnetic but conducting stuff of thickness h. The objective of this problem is to find the forces acting on the moving slab. (Hint: There will be a drag force and there should be a levitation force.)

A) What is the surface impedance looking downward from the bottom of the conductive slab?
B) Using the diffusion models presented in the chapter, find the "drag" force on the moving slab and current. This may be left in the form of an algorithm, so that it could be programmed into, say, MATLAB or Octave.
C) Find a closed form for the drag force, assuming that the slab and the air-gap are both thin. Assume a surface conductivity for the fixed slab.

References

1 Woodson, H.H. and Melcher, J.R. (1968). *Electromechanical Dynamics*. Wiley.
2 MacLean, W. (1954). Theory of strong electromagnetic waves in massive iron. *Journal of Applied Physics* 25 (10).
3 Agarwal, P.D. (1959). Eddy-current losses in solid and laminated iron. *Transactions of the American Institute of Electrical Engineers* 78: 169–171.

4

Design Synthesis, Optimization, and Modeling

4.1 Introduction

The notion of "optimization" is, at first blush, fairly straightforward: it is finding a set of machine dimensions, materials, methods of assembly, and so forth that constitute the "best" machine. In principle, it should be possible to figure out which machine is best and perhaps even to teach a computer program to seek out the *optimal* machine.

There are a few problems with this, however. The first and most difficult problem is that there is usually no way of knowing what the "best" machine is, a priori. All physical systems have a variety of attributes, and usually, tradeoffs need to be made between them. Even if an appropriate set of tradeoffs has been made so that there is a scalar objective function, the design space is complicated by the existence of integer and integer-like variables and complex limits.

4.2 Design Synthesis

Illustrated in Figure 4.1 is a schematic representation of the design process. This is an iterative process in which sets of designs are evaluated and compared with previous designs. It is to be expected that in synthesizing a machine design, one would go around this loop several (or many) times. Eventually, the design stops improving and is considered "finished".

4.2.1 Specifications: Requirements and Attributes

Here is some nomenclature:

- Requirements are specifications which must be met by a design. They would include things such as rated power, limitations on tip speed and temperature, perhaps lower limits on efficiency and power factor.
- Attributes are things which, all other things being equal, are to be either minimized or maximized. These would include cost (to be minimized), efficiency (to be maximized), etc.
- Feasibility is a binary ("go/no-go") variable which determines if a machine will work at all. For example, a design might entail a violation of material stress limits, thermal heating limits, etc.
- Design Variables are machine dimensions and material properties which fully specify a machine design.

Electromagnetic Analysis of Electric Machines: First Principles, Modeling, and Design, First Edition.
James L. Kirtley, Christopher H. T. Lee, and Sajjad Mohammadi.

Companion website: www.wiley.com/go/kirtleyelectric

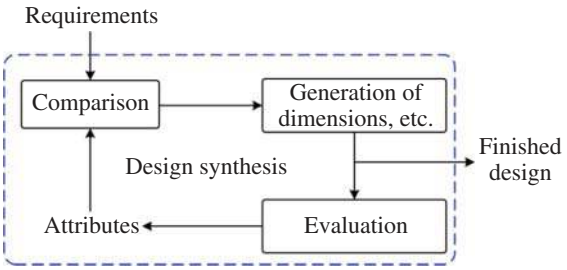

Figure 4.1 Design synthesis.

Note that the distinction between requirements and attributes is not really clean: a requirement can be a limit on an attribute. However, in order to perform "optimization", it is necessary to have at least one attribute which can be maximized.

The design process consists of two fundamental steps. One is generation of a set of design variables that constitutes a design; the other is evaluation of that design to establish feasibility and attributes. A machine that is feasible meets the requirements, and of course, it makes sense to discuss the attributes only of feasible machines.

One way of setting up the process illustrated by Figure 4.1 is to use a design evaluator, with an expert machine designer serving to perform the synthesis step. So, for example, if a candidate machine has a power output that is too small, the designer might set the rotor length to be a bit larger and then run the evaluator again. This process works fairly well, particularly as the expertise of the designer improves. But there are two issues: one is that success depends on having an expert designer. The other, and perhaps the more important issue is that the expertise of the designer will tend to restrict designs to a narrow range of parameters, so that all designs from that designer will be about the same.

One method that might be considered is to evaluate all possible designs. This is clearly not practical in practice. As the number of dimensions and material combinations becomes large, the number of combinations to be evaluated becomes unreasonably large. And there is always the question: over what range of dimensions does one search? So other methods of design must be developed.

There have been developed, in recent years, heuristic techniques to automate both the design evaluation and synthesis steps, so that the computer can produce finished (or nearly finished) designs. These methods go by a number of names, including "genetic algorithms", "synthetic annealing", "particle swarm", and many others. All of these are basically random search routines that use what is often called "Monte Carlo" techniques, after the city in Monaco where there is a lot of "rolling of dice".

If it is possible to establish an "optimal" objective function, the process of evaluation can be fairly straightforward. The objective function might be expressed as:

$$F = \sum_k w_k a_k \tag{4.1}$$

where F is the objective function to be maximized, w_k is the "weight" of attribute k, and a_k is the value of the attribute k. And actually, this process can go both ways, as F might be something to be minimized, as a combination of "costs". If an analytic expression for each of the attributes can be had, optimization is simply finding the spot in the design space where the first derivative of F is zero for each of the design variables. This rarely works in real situations for two reasons. First, analytic expressions for attributes are often not derivable. Second, the derived objective function may not be *convex*, meaning that there may not be a single spot in the design space where all of the derivatives of the objective function with respect to the design variables go through zero.

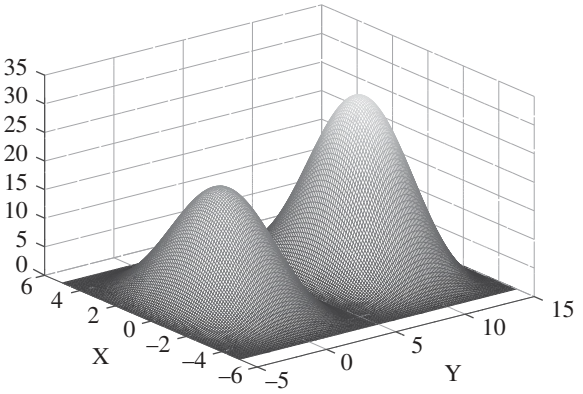

Figure 4.2 Surface with multiple optimal points.

If an analytic expression for F is not possible and convex, an evaluation of F at any given point in the design space can usually be had. And one way of finding the "optimal" design, using "Monte Carlo" techniques, would be to start at some point in the design space, perturb the design variables by adding or subtracting a random number to each one and re-evaluating. If the new spot is "better", adopt that as the design. If not, stay at the old spot. Do the perturbation again. This process can go on until after some number of cycles, the design does not improve, one concludes that the optimum has been reached. This works, but consider the surface shown in Figure 4.2. A "hill climbing" routine as described here might get trapped in the "local" optimum. No ready solution to this is proposed here, aside from starting with a "wide net" and progressively taking smaller steps.

4.2.2 Monte Carlo–Based Synthesis

There are many heuristic schemes for doing optimal design; too many to be fully categorized here. However, it is probably useful to consider the difference between deterministic and random search processes. Deterministic search methods include grid search and hill-climbing techniques. Random search methods are variations on "rolling the dice" and are therefore called "Monte Carlo". One way of searching the design space is to evaluate all possible designs and then pick, somehow, the best one. A variation on this would be to use a "grid" search, evaluating all of the designs that are at intersections of a coarse grid in the design space. Then the grid could be re-oriented to be located around one or a few of the most promising nodes and to have shorter intervals between points. This process can be carried out until the grid spacing becomes small enough that the designer is confident that the "optimal" machine has been reached.

A second way of doing a deterministic search is to use a "hill climbing" routine, which starts at some point in design space and evaluates the gradient at that point. The design evaluator figures out which way is "up", and moves in that direction, usually with a fairly large step. If the next point is indeed better than the first, the gradient is evaluated and the process is repeated. If it is not better, usually the prior point is used with a reduced step size. This method, of course, depends on having the ability to evaluate the gradient of the objective function.

Grid search routines become computationally infeasible in design spaces with large dimensionality. Hill climbing routines don't work well in situations in which some variables are integer in nature (such as the number of turns or the type of steel to be used). Further, hill-climbing techniques very often cannot handle situations in which there are local optima, since if a hill climber starts up the wrong hill, it has no way of knowing that it has found an inferior solution. Because of this, random search routines are often used for optimization of complex designs.

It should be noted that Monte Carlo search techniques work well in both of the situations that befuddle hill climbers: they can handle mixed continuous/integer variable situations and they can often be set up so they are not troubled by local optima.

4.3 The Pareto Surface and Dominance

There will usually not be a single attribute to be maximized, so it is necessary to carry out tradeoffs. Consider the situation illustrated in Figure 4.3. Here we have two attributes, labeled in the figure as "costs", to reinforce the notion that the "best" machine would be at the origin. Suppose "cost 1" is manufacturing cost and "cost 2" is the inverse of efficiency and so would represent the cost of operating losses.

There will be a feasibility frontier, shown as the solid curve in the figure. No machines can be made closer to the origin than this curve. We should note that the design process can be distilled into finding that curve and the machines whose attribute set lies on or very close to it. Now consider some specific cases. The circles labeled "A" and "B" are on that feasibility frontier. Neither of these machines is clearly better than the other, and the choice between them must be made by tradeoff of the attributes. Machine "A" would be best for a machine that does not run very much, while machine "B" would probably be best for a machine that operates a lot, due to energy costs. Machines "C" and "D" are not on the design frontier, and are actually better examples of the sorts of machines that would be generated by a synthesis program. Note that we cannot, a priori, say that these machines are inferior to either "A" or "B". However, we can see that machine "E" is inferior to machine "B" (it is both less efficient and costs more). We say that machine "E" is *dominated* by machine "B". Note that a synthesis process carried out for enough steps would eventually find designs very close to the frontier, so that designs "C" and "D" would eventually become dominated.

Here are the steps one might build into code to implement a design evaluator:

1) Start with a known "feasible" design: one that meets all design requirements (such as thermal, voltage limits, and mechanical stress limits).
2) Establish a list of feasible designs: initially this list will be empty, but will be filled in subsequent steps. The length of this list is not easy to specify, and will likely be determined by experience.
3) Generate a random set of design perturbations and apply them to the design. As with the length of the list of designs, the size of the random perturbations (standard deviation of each variable) is likely determined by experience.
4) In evaluation of the new design,
   a) first check to see that it is feasible.
   b) If it is feasible, compare this design to all other designs in the list.

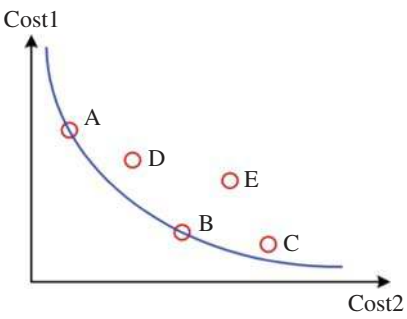

Figure 4.3 The Pareto surface.

i) If it is dominated (that is, if any design in the list is better in all attributes, the candidate design is discarded). Go back to step 3.
ii) If the candidate design is *better* than any design in the list, that is, superior in all attributes, it is dominant and is added to the list. Any designs that it dominates are discarded. Go back to step 3.

c) If it is not feasible, go back to step 3.

5) The number of iterations to be used is also a matter of experience. Note that if only two or possibly three attributes are used, the Pareto surface can be visualized. If the non-dominated designs form a smooth surface, it is likely that they are close to the limit of feasibility, meaning enough trials have been done. This becomes much harder if the number of attributes is large.

4.4 Design Example: A Single-Phase Transformer

4.4.1 Description

Consider a simple electrical device: a transformer. This consists of two coils of a conductor (typically a good conductor such as copper in the form of wire) wound around a magnetic "core". The transformer couples the two coils together. In most cases, the two coils of wire have a different number of turns and so "transform" voltage and current. The device described here is similar to a common distribution transformer used in electric utility systems. Transformers like this come in a very wide variety of sizes and for a wide variety of applications. Shown in Figure 4.4 is the symbol typically used in circuit diagrams. Here, N_1 and N_2 are the number of turns in each coil, and voltages and currents are noted in the conventional way.

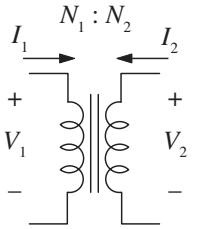

Figure 4.4 Ideal transformer circuit model.

The "ideal" transformer has the following characteristic:

$$\frac{V_1}{N_1} = \frac{V_2}{N_2}$$
$$N_1 I_1 + N_2 I_2 = 0 \tag{4.2}$$

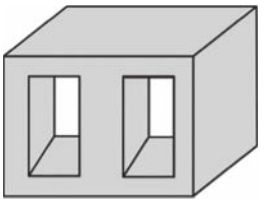

Figure 4.5 Transformer core.

Now look at the physical embodiment of the transformer. First, the core is shown in isometric form in Figure 4.5. It is made of a highly permeable material. To start, we will assume that the core has permeability $\mu \to \infty$. This core is typically made of laminations of electrical sheet steel, either "E" and "I" shape in the plane of the front surface, or of four "C" cores, also of electrical sheet steel. The two winding coils are wound around the central "leg" of the core, typically in a concentric fashion.

Shown in Figure 4.6 are the dimensions of the core "windows" and the magnetic core legs, and how the windings are situated. We assume here semicircular forms for the windings outside of the core legs.

Finally, a detail of the window is shown in Figure 4.7. The two windings each occupy half of the window.

Note that the central leg of the transformer is twice as wide as the two side legs. This ensures that flux density is the same in the central and wide legs. Note that Gauss's law:

$$\oiint \vec{B}.\vec{n}\, da = 0$$

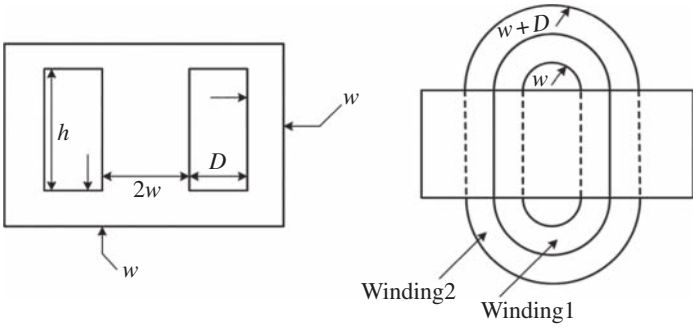

Figure 4.6 Dimensions of the transformer.

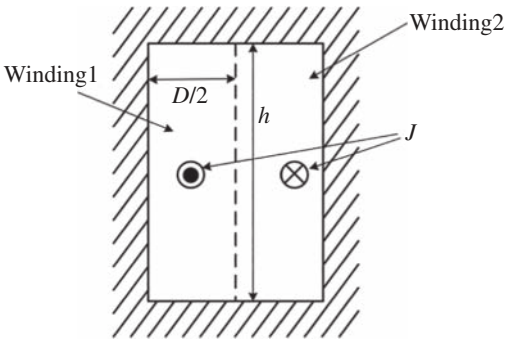

Figure 4.7 Cross-section of the transformer window.

is satisfied if the flux density in the center leg splits and goes down the side legs equally.

Note Ampere's law:

$$\oint \overline{H} \cdot d\overline{\ell} = \iint \overline{J} \cdot \overline{n} da$$

An integral carried out over a contour that is in the shaded area around the window must indicate that the total ampere-turns in the window is zero ($N_1 I_1 + N_2 I_2 = 0$). This means that the current in one winding (ampere-turns) must be equal to and in the opposite direction from the current (ampere-turns) in the other winding. This is because if the permeability of the magnetic material is very high, because $\overline{B} = \mu \overline{H}$, magnetic field $\overline{H}$ must be nearly zero all the way around the window. Now, to understand voltage, consider a somewhat more detailed view of one of the coils, shown in cartoon view in Figure 4.8.

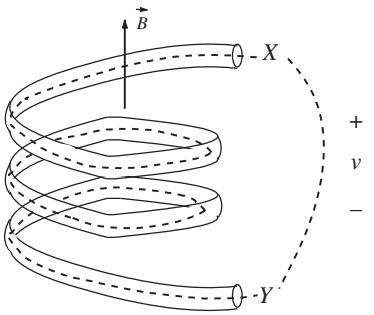

Figure 4.8 Cartoon view of a coil.

Invoking Faraday's law:

$$\oint \overline{E} \cdot d\overline{\ell} = -\frac{d}{dt} \iint \overline{B} \cdot \overline{n} da$$

Using the dotted line shown in Figure 4.8, the closed integral can be seen to be made up of two integrals:

$$\oint \overline{E} \cdot d\overline{\ell} = \int_Y^X \overline{E} \cdot d\overline{\ell} + \int_X^Y \overline{E} \cdot d\overline{\ell}$$

The first integral is, as shown in the figure, through the wire, and if that is a good conductor, the electric field may be approximated as zero, while the second integral defines the terminal voltage:

$$V = \int_X^Y \overline{E} \cdot d\overline{\ell}.$$

Note that the definition of the circular integral is going in a counter-clockwise direction around the area, defined by a normal vector, on the right-hand side. This means the reference direction for magnetic flux density $\overline{B}$ is downward, as represented in Figure 4.8, or the opposite direction of the flux density shown. The voltage induced in the coil is the rate of change of flux density $\overline{B}$ as shown in the figure. If the flux is in the core, it will be uniform, and then voltage induced is:

$$V = NA\frac{dB}{dt} = N\frac{d\phi}{dt} = \frac{d\lambda}{dt} \tag{4.3}$$

where now flux is:

$$\phi = \iint \overline{B} \cdot \overline{n} da = 2w\ell B \tag{4.4}$$

And each coil voltage divided by number of turns is:

$$\frac{V}{N} = \frac{d\phi}{dt} = j\omega\phi \tag{4.5}$$

4.4.2 Rating

Note that the volt-ampere rating of the transformer is, if the voltage and current are noted as peak quantities:

$$VA = \frac{1}{2} V I = \frac{1}{2}\frac{V}{N} NI \tag{4.6}$$

This voltage will be limited by operating flux density in the core: from the expression just above,

$$\left|\frac{V}{N}\right| = \omega\phi = \omega 2w\ell B_s \tag{4.7}$$

where B_s (called "saturation" flux density) is the peak operating flux density for the core material.

Similarly, the operating current is current density in the wires times the winding factor, which gives current density in the slot, times the area per winding (half the window):

$$NI = J_c \lambda_w h \frac{D}{2} \tag{4.8}$$

where J_c is the operating current density in the conductors, generally limited by heating.

The rating, in volt-amperes, is therefore:

$$VA = \frac{1}{2}\frac{V}{N} NI = \omega w\ell h \frac{D}{2} \lambda_w J_c B_s \tag{4.9}$$

Note the VA rating of the transformer is proportional to the fourth power of linear dimension (assuming constant shape), while the mass would be proportional to the cube of dimension, so that these devices tend to have a higher rating per unit mass as they get bigger.

4.4.3 Equivalent Circuit Model

Development of an equivalent circuit is useful in system studies, in which the circuit model is embedded in a larger circuit diagram that describes a system. Note that the assumption that winding resistance is zero is not really correct. A correction to the circuit of the transformer can be made by estimating the true winding resistance. Assuming the wire area is uniform, the resistance of a length of wire is simply:

$$R = \frac{l_w}{\sigma A_w} \tag{4.10}$$

The wire area can be estimated by noting that the window area is subdivided by the N turns of each winding, and the conductor area is the window area per conductor times a space factor (λ_w) that allows for things like insulation, wire shape, and perhaps other details:

$$\begin{aligned} A_{w1} &= \frac{Dh}{2N_1}\lambda_{w1} \\ A_{w2} &= \frac{Dh}{2N_2}\lambda_{w2} \end{aligned} \tag{4.11}$$

Assuming that winding 1 is on the inside, and the end windings are circular as shown in Figure 4.6, the length of each winding is:

$$\begin{aligned} \ell_{w1} &= N_1\left(2\ell + 2\pi\left(w + {}^{D}/_{4}\right)\right) \\ \ell_{w2} &= N_2\left(2\ell + 2\pi\left(w + {}^{3D}/_{4}\right)\right) \end{aligned} \tag{4.12}$$

Then resistances of the two windings are:

$$\begin{aligned} R_1 &= 2N_1^2\frac{2\ell + 2\pi\left(w + {}^{D}/_{4}\right)}{\sigma Dh\ \lambda_{w1}} \\ R_2 &= 2N_2^2\frac{2\ell + 2\pi\left(w + {}^{3D}/_{4}\right)}{\sigma Dh\ \lambda_{w2}} \end{aligned} \tag{4.13}$$

where σ is electrical conductivity of the wire.

The core of the transformer will exhibit loss due to the flux density. This is a complex issue that will be dealt with in a subsequent chapter, but for the moment, assume that the loss density per unit mass of the core material may be approximated by:

$$P_{fe} = P_0\left(\frac{B}{B_0}\right)^2 \tag{4.14}$$

This is not exact, but will do for now. If that is the case, noting that the flux density in the core is related to terminal voltage by:

$$B = \frac{V_1}{2w\ell N_1\omega} = \frac{V_2}{2w\ell N_2\omega} \tag{4.15}$$

Then loss per unit mass of the core is:

$$P_{fe} = \frac{P_0}{B_0^2}\frac{V_1^2}{(2wlN_1\omega)^2} \tag{4.16}$$

And total core mass is:

$$M_{fe} = \rho_{fe}\ell\left((4w + 2D)(2w + h) - 2Dh\right) \tag{4.17}$$

Since total loss in the core is $P_C = P_{fe}M_{fe}$, and noting that this is proportional to the square of voltage, it is possible to define a parallel core resistance:

$$R_{fe} = \rho_{fe}\ell \left[(4w + 2D)(2w + h) - 2Dh\right] \left(2w\ell\omega N_1\right)^2 {}^{B_0^2}/_{P_0} \tag{4.18}$$

This is an approximation to reality, because core loss is not always quadratic in flux density and frequency.

Note that there will be some magnetic stored energy from magnetic fields in the window and around the end turns. The fields around the end turns are beyond our scope right now, but within the window, we know the magnetic field in the windows, given some current in the windings, must be z-directed (vertical) and will have a variation in the x-direction as shown in Figure 4.9. Note that the magnetic field must be zero on both sides of the window because each side has a highly permeable surface. The current in winding 2 is in the opposite direction from the current in winding 1 and the number of ampere-turns is the same.

The straightforward approach to finding leakage inductance is to note that energy stored in an inductor is $\frac{1}{2}LI^2$. Energy density is $\frac{\mu_0}{2}|H|^2$. Given that there are two windows, the total energy in both windows on the winding 1 side is:

$$W_1 = 2h\ell \int_0^{\frac{D}{2}} \frac{\mu_0}{2}\left(\frac{2N_1I_1}{D}\right)^2\left(\frac{2x}{D}\right)^2 dx = \frac{4}{3}\mu_0\frac{h\ell}{D}N_1^2I_1^2 \tag{4.19}$$

Then the inductance associated with each winding would be:

$$\begin{aligned} L_{l1} &= \frac{8}{3}\mu_0\frac{h\ell}{D}N_1^2 \\ L_{l2} &= \frac{8}{3}\mu_0\frac{h\ell}{D}N_2^2 \end{aligned} \tag{4.20}$$

All of these can be used in an equivalent circuit for the transformer as shown in Figure 4.10.

Figure 4.9 Magnetic field in window.

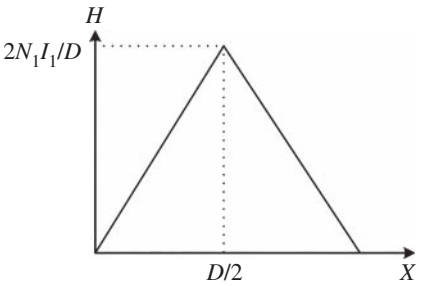

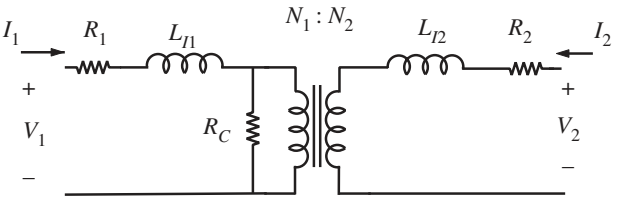

Figure 4.10 Transformer equivalent circuit.

4.4.4 Cost of Losses

The cost of iron and the cost of copper are fairly straightforward to evaluate: they are just the price in \$/kg times the mass in kilograms. There may be a cost of assembly (labor) as well, but that is beyond the scope of this discussion. To evaluate the cost of loss, recognize that the present value of a continuous stream of expenditure is:

$$P = \int_0^T pe^{-rt}dt = p\frac{1-e^{-rT}}{r} \tag{4.21}$$

where p is the continuous stream of expense, r is the interest rate, and T is lifetime. Note that for very long lifetime, P becomes just p/r.

If d is dissipation in watts and c is price of one kilowatt hour, $p = dc \times 10^{-3} \times 8766 = 8.766 \times d \times c$ where 8766 is the number of hours per year and p is the cost of dissipation in \$ per watt per year. A price of $c = \$0.15$ per kilowatt hour would yield a price per watt of loss of about \$1.31 per watt per year. If an interest rate of 5% per year and a lifetime of 40 years is considered, the loss evaluation would be \$22.65 per watt.

4.5 Problems

This problem is to design a reactor (an inductor intended for use in AC systems to absorb reactive power). To do this, we will use one of two types of core. The first, shown in Figure 4.11, consists of two C-cores made of very highly permeable material, separated by a gap. (The gap is the same on both sides). A winding goes through the "window" enclosed by the two cores, and will have some number of turns (call the number N). This core is uniform in the dimension perpendicular to the page. Call that dimension D.

It will be most economical to divide the winding into two parts: one around the core legs on one side and the other around the other core leg. (You might want to consider why this is!). For the purpose of this exercise, assume the end turns have a semi-circular shape.

A second option for the core is a single-gap core, as shown in Figure 4.13. It consists of flat steel sheets with the gap built in. There may be clever ways of overlapping the laminations so that the winding can be fabricated and then the core assembled within and around it. Note that the width of the center leg is usually just twice the width of the side legs, and the top and bottom legs are the same width as the side. This makes flux about uniform in the magnetic circuit.

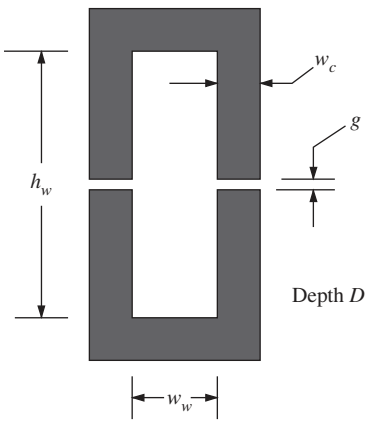

Figure 4.11 Two C-Cores.

Often, "C" cores are tape wound around a rectangular mandrel and then cut to form the two "C" shaped parts. The C-cores are typically gapped with non-conducting, non-magnetic spacers.

Before starting on the main exercise, there will be some preparatory exercises to get us started. But first, some parameters to start.

Assume the conductivity of the material to be used for the winding is IACS, which is 5.81×10^7 s/m. Also, assume a "winding" factor (ratio of conductor area to total window area) of 0.5. Assume also that the density of the winding material is that of copper (8400 kg/m^3).

For the purpose of this exercise, assume the core material has the following parameters at 60 Hz:

- Core loss at 60 Hz and peak flux density of 1 T : 0.62 W/kg
- Core loss exponent is 2.4.
- Core density is 7200 kg/m^3

4.1 Assume the following dimensions for a reactor made with two C-cores, as shown in Figure 4.11.

a) Gap g = 6 mm;
b) Core and gap width $w_c = 4$ cm;
c) Core and gap depth $D = 5$ cm;
d) Number of turns = 600
   - What is the inductance and reactance at 60 Hz?
   - What is the peak flux density in the core if terminal voltage is 440 V (RMS)?
   - What is the reactive power absorbed and current?

4.2 Now assume further dimensions:

a) Window width $w_w = 5$ cm.
b) Window height $h_w = 10$ cm.
   - If the number of turns is 600 and the winding just fills the window, with a winding space factor of 0.5, if the superficial current density is 5 A/mm^2, what is the terminal current?
   - Assuming the same circular end turns pictured in Figure 4.12, what is the average length of a turn? With 600 turns, what is the total length of the winding?
   - With a winding space factor of 0.5, what is the area of each turn? What is the resistance of the winding?

4.3 Assuming the flux density in the core is 1.2 T, peak, what is the core loss in watts?

Figure 4.12 Single-gap core.

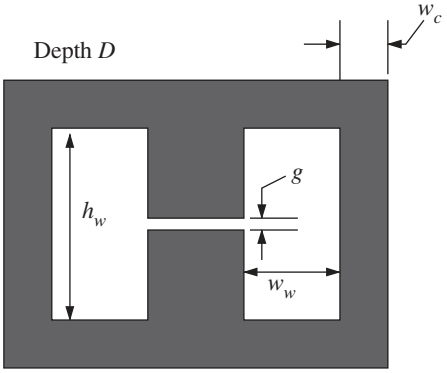

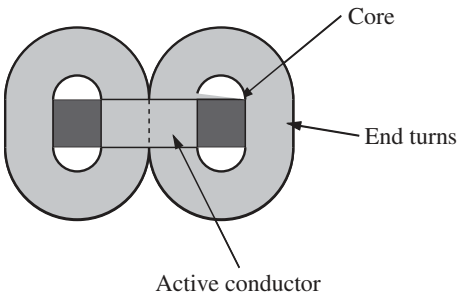

Figure 4.13 End turns: view from the top.

4.4 Now write a script that takes as input the core and window dimensions, the number of turns and winding factor, voltage, and frequency and that outputs reactive power, winding, and core loss.

4.5 Modify your script to take as an input the required reactive power drawn, and calculate the required gap.

4.6 Now for the main act: The reactor you are to design is to operate at 60 Hz, with a terminal voltage of 600 V, RMS. It is to absorb 10 kVA of reactive power. You should limit the current density in the core window(s) to 5 A/mm^2 (peak), and limit the peak flux density in the core to 1.7 T. Write a script in the same form as the script attribute.m in the appendix to Chapter 4 that accepts dimensions and returns, as attributes. Total reactor weight and total loss at the operating condition of $V = 600$ Volts, RMS, drawing 10 kVAR. Use this with the other scripts in the appendix to find a Pareto curve, trading these two attributes against each other.

4.7 Assume a reasonable cost for losses, and for copper and core mass; see if you can find an "optimal" design for your reactor.

Appendix 4.A Simple Design Example with Code

Code that implements the calculations described here is provided below. This exercise is included here because the distribution transformer is easy to understand, and so all steps in the design evaluation can be included. This code is believed to be correct, but it comes with no assurances or warranties.

The design and optimization exercise is carried out with four variables in the design space. These are the core leg width (w), the window width (D), the window height (h), and the core length (ℓ).

The transformer is assumed to operate at a fixed flux density. This simplifies the calculation of core losses, as they are simply a multiple of core mass. For a given VA rating, the required window current density is:

$$J_w = \frac{VA}{\omega D \ell h w B_c} \tag{4.22}$$

And this may be used both directly as a limit in the calculation and in the loss calculation.

The code included here is in the language used by the MATLAB program. It also runs under the public domain Octave. It is organized as follows:

- The script attribut.m does the evaluations and some output. It is called with three parameters:
  - *D* is a vector that contains the variable design space.
  - *B* is a vector that contains all of the fixed parameters.
  - DEBUG is an integer that controls output: if it is zero, attribute does not print anything; if it is one, attribute prints summary output; attribut.m returns two outputs.
  - *A* is the list of *attributes*. In this case, there are six.
  - *C* is 1 if the design is acceptable (i.e. does not violate any limits), and zero if the design is unacceptable (violates one or more limits).
- The script msetup.m is run first and, as its name suggests, sets up the problem. It contains one acceptable design embodied in the four variable inputs, all of the fixed inputs, and some housekeeping variables, such as the number of "shots" to run, the number of designs to keep in the list, and space for designs.
- The script nda.m runs the show: it "rolls the dice" for each design shot, uses attribut.m to do the calculations, and determines dominance. It also keeps the list of non-dominated designs.
- mdd.m prints the list of designs.
- dsort.m sorts and then prints the designs in order of one of the attributes.
- tdet.m prints details of one of the designs.
- ropt.m does a Monte Carlo optimization, attempting to maximize the first of the list of attributes.

```
function[A, C] = attribut(D, B, DEBUG)

% attribut.m: design of a single phase transformer
% for use with nda.m
% Copyright 1997, 2023  James L. Kirtley Jr.
%

% Requires the following input variables:

% Here are the fixed variables, defined in B[]
VC = B(1);                  % cost of losses, $/watt
VA = B(2);                  % transformer rating
om = B(3);                  % electrical frequency
Jmax = B(4);                % maximum allowed current density
Bc = B(5);                  % core flux density, T, RMS
Pc = B(6);                  % core loss density, w/kg
sig = B(7);                 % winding conductivity
lam = B(8);                 % winding space factor
f = B(9);                   % loading factor
P_iron = B(10);             % price of iron, $/kg
P_cu = B(11);               % price of copper, $/kg;

% Here are the continuous variables to search, defined in D[]
w = D(1);                   % core leg width
h = D(2);                   % window height
d = D(3);                   % window width
l = D(4);                   % core length

% Here are the discrete variables to search, defined in DI[]
% none in this version

% Here are a few constants
muzero=pi*4e-7;                % free-space permeability
rhos = 7462;                   % mass density of magnetic steel
rhoc = 8960;                   % mass density of copper
tol = 1e-3;                    % convergence tolerance
```

```
% DEBUG determines how the program behaves
% DEBUG = 0 generates no external output: used for NDA
% DEBUG = 1 generates screen output

% Calculation of performance
J = VA/(om*w*l*h*d*Bc);                % required current density

if J>Jmax
  A = [0 0 0 0 0 0];
  C=0;
  return
end

C=1;
Volc = l*(2*d+4*w)*(2*w+h)-2*d*h*l;     % volume of core steel
Volw = h*2*d*l+h*pi*((w+d)^2-w^2);    % volume of winding

Msteel = rhos*Volc;                    % mass of core steel
Mcopper = rhoc*lam*Volw;               % mass of winding copper
Dissc = Pc*Msteel;                     % Steel dissipation
Dissw = J^2*Volw/(sig*lam);           % winding dissipation at rated point
Cost_fe = Msteel*P_iron;               % cost of core iron
Cost_cu = Mcopper*P_cu;                % cost of winding copper
Cost_e = (Dissc + f*Dissw)*VC;         % cost of losses

mass = Msteel + Mcopper;
cost = Cost_fe+Cost_cu+Cost_e;

A = [1/cost 1/mass 1/Dissc 1/Dissw 1/Msteel 1/Mcopper];
if DEBUG == 0,
  return
  end
  fprintf('Single Phase Transformer\n')
  fprintf('Core Length = %8.0f mm\n', 1000*l)
  fprintf('Core thickness = %8.0f mm\n', 1000*w)
  fprintf('Windown height = %8.0f mm\n', 1000*h)
  fprintf('Window width = %8.0f mm\n', 1000*d)
  fprintf('Total Mass = %8.3f kg\n', mass)
  fprintf('Mass of core iron = %8.3f kg\n', Msteel)
  fprintf('Mass of winding copper = %8.3f kg\n', Mcopper)
  fprintf('Steel Dissipation = %8.0f W\n', Dissc)
  fprintf('Winding Dissipation = %8.0f W\n', Dissw)
  fprintf('Cost of core steel = $ %8.2f\n',Cost_fe)
  fprintf('Cost of winding copper = $ %8.2f\n', Cost_cu)
  fprintf('Cost Eveluation of Loss = $ %8.2f\n', Cost_e)
  fprintf('Total Cost = $ %8.2f\n', cost)
  fprintf('Total Mass = %8.2f kg\n', mass)
```

```
% msetup.m
% Setup Script for single phase transformer
% Copyright 2023  James L. Kirtley Jr.
%

NA = 6;                % attributes
ND = 4;                  % continuous design space
NDE = 24;                   % designs to keep
NITER = 100000;                 % shots to try
```

```
% Variables Inputs:
% Mean Values
w = .05;                        % core thickness
d = .05;                        % window width
h = .2;                       % window height
l = .1;                       % core length

% mean value vector
DM = [w d h l];

% Standard Deviations
w = .02;                      % core thickness
d = .02;                      % window width
h = .05;                      % window height
l = .05;                      % core length

DS = [w d h l];

% Lower Limit
w = .02;                      % core thickness
d = .02;                      % window width
h = .05;                      % window height
l = .05;                      % core length

DL = [w d h l];
% Upper Limit
w = .1;                       % core thickness
d = .1;                       % window width
h = .4;                       % window height
l = .2;                       % core length

DU = [w d h l];

% Here are the fixed variables, defined in B[]
VC = 20.43;                   % cost of losses, $/watt
VA = 5e4;                     % transformer rating
om = 120*pi;                  % electrical frequency
Jmax = 3e6;                   % maximum allowed current density
Bc = 1.13;                    % core flux density, T, RMS
Pc = 1.4884;                  % core loss density, w/kg
sig = 5.881e7;                % winding conductivity
lam = .5;                     % winding space factor
f = .2;                       % loading factor
P_iron = 1.00;                % price of iron, $/kg
P_cu = 50.00;                 % price of copper, $/kg;
% Price of copper and iron need to be revisited

B = [VC VA om Jmax Bc Pc sig lam f P_iron P_cu];
% Here are the matrices that NDA will fill out

MA = zeros(NDE, NA);      % design attributes across rows
MD = zeros(NDE, ND);      % design variables (continuous)
MAOpt = zeros(NDE, NA);      % scratchpad for optimized machine
```

```
[A, C] = attribut(DM, B, 1)
% nda.m
% Copyright 1997, James L. Kirtley Jr.
```

```
% Requires an attribute generating function called this way:
% [A, g] = attribut(D, B, Out)
% A is a vector of attributes of size NA
%   Attributes are all positive and goodness is in increase
% g is a scalar that is 0 if a design is not viable and 1 if it is
% D is a vector of design variables that ndi will manipulate
%   it is of size ND
% B is a vector of design variables that will remain fixed
% Out = 1 will cause the thing to print
% DL, DU, DS and DM are starting points for the vector D
% DL and DU are lower and upper limit points
% DM is the median value to be used in generating D
% DS is a vector of standard deviation to be used in generating D
% DIN is the vector of ranges of the elements of DI
% NDE is the number of design points to be accumulated
% NITER is the total number of shots to be tried
% Output will be accumulated in two matrices
% MA [NA, NDE] holds the attributes of all designs
% MD [ND, NDE] holds the design variables
% These matrices are declared in the setup program, so
% that NDA can be run over again
multi_dom = 0;                  % so we don't get an error message

for i = 1:NITER,
  D = DM + DS .* randn(1, ND);    % generate a random input
  if sum([DL>D DU<D]) == 0,        % if design is in range, continue
    %fprintf('in range\n')

    [A, g] = attribut(D, B, 0);   % generate design
    if g~= 0,                       % if viable, do dominance check
      inserted = 0;               % used later
      multi_dom = 0;
      for nd=1:NDE,                 % dominance check
          %sum(A>MA(nd, :))
       if sum(A>MA(nd,:))== 0    % design is dominated
         break,
       end;
       %if ((sum(MA(nd,:)>A) == 0) && (sum(MA(nd, :)) >0 )),% design
                                                              % dominates
       if sum(MA(nd, :) > A ) == 0,
         if inserted == 0;         % this is the first dominated design
           inserted = 1;
           MA(nd, :) = A;          % it goes here
           MD(nd, :) = D;          % save design too!
           fprintf('Replacing Design    %5.0f At Step %5.0f\n', nd, i);
         else
           multi_dom = 1;               % flag need for cleanup later
           MA(nd, :) = zeros(size(A));  % clobber dominated design
           MD(nd, :) = zeros(size(D));
         end                            % end of if inserted
       end                              % end of dominating design
      end                               % end of check loop
    end                                 % end of dominance check
    if multi_dom == 1;                  % need to clean up matrices
      for nd = 1:NDE,                   % scan attribute matrix
        if sum(MA(nd, :)) == 0          % hole found
          for ndd = nd:NDE,             % scan rest of file
            if sum(MA(ndd, :)) > 0;     % first non-zero design
```

```
            fprintf('Design %5.0f Is Dominated At Step %5.0f \n',…
            MA(nd, :) = MA(ndd, :);    % copy upward
            MD(nd, :) = MD(ndd, :);
            MA(ndd, :) = zeros(size(A));% and erase
            MD(ndd, :) = zeros(size(D));
            multi_dom = 0;
            break;                 % only move one design
          end                      % end if nonzero
        end                        % end of scan rest of design
      end                          % end if hold found
    end                            % end scan attribute matrix
  end                              % end cleanup
end                                % end of input range check
end                                % that's all folks!
```

```
% mdd.m
% This script displays transformer details
% For use with permanent motor scripts and the NDA
% Copyright 2023  James L. Kirtley Jr.
%A = [1/cost 1/mass 1/Dissc 1/Dissw 1/Msteel 1/Mcopper];
clc
fprintf('Summary Motor/Generator Attributes\n');
fprintf('           Cost       Mass      Dissc      Dissw    Massc    Massw\n');
fprintf('            $          kg         W          W        kg      kg\n');
for r = 1:NDE,
  Cost = 1/MA(r,1);
  Mass = 1/MA(r,2);
  Dissc= 1/MA(r,3);
  Dissw= 1/MA(r,4);
  Msteel = 1/MA(r,5);
  MCopper = 1/MA(r,6);
  fprintf('%7.0f   %7.2f   %7.2f   %7.0f   %7.0f   %7.1f   %7.1f\n',...
           r, Cost,Mass,Dissc,Dissw,Msteel,MCopper);
      end
```

```
% dsort.m
% this script sorts the output by an attribute and prints attributes
% vs. design index number
fprintf('Design Sorter\n')
fprintf('Attribute 1 is 1/cost\n')
fprintf('Attribute 2 is 1/mass\n')
fprintf('Attribute 3 is 1/copper dissipation\n')
fprintf('Attribute 4 is 1/steel dissipation\n')
fprintf('Attribute 5 is 1/steel mass\n')
fprintf('Attribute 6 is 1/copper mass\n')
n = input('Which Attribute? ==>');
c = n+1;
[Y, I] = sortrows(MA, n);    %
fprintf(' #         $          kg         W            W         kg
kg \n')
for k = 1:length(I)
    if Y(k, 2) > 0
        cost = 1/Y(k, 1);
        mass = 1/Y(k, 2);
        DC = 1/Y(k, 3);
        DW = 1/Y(k, 4);
        Mfe = 1/Y(k, 5);
        Mcu = 1/Y(k, 6);
```

```
        fprintf('%3.0f  %10.3f   %10.4f     %10.1f     %10.2f
%10.2f    %10.2f\n', ...
        I(k), cost, mass, DC, DW, Mfe, Mcu)
    end
end
% here is the A vector we are displaying
%A = [eff 1/Mtot 1/dT 1/Ro 1/ltot];
```

```
% tdet.m: details of transformer design
ind = input('which one?==>');
D = MD(ind, :)
[A, C] = attribut(D, B, 1)
```

```
ropt.m
% Copyright 1997, James L. Kirtley Jr.

% This program is intended to operate in conjunction with nda.m
% Requires an attribute generating function called this way:
% [A, g] = attribut(D, DI, B, Out)
% A is a vector of attributes of size NA
%   Attributes are all positive and goodness is in increase
% ropt tries to maximize A(1), which should be the objective function
% g is a scalar that is 0 if a design is not viable and 1 if it is
% D is a vector of design variables that ndi will manipulate
%   it is of size ND
% DI is a vector of integer variables to be varied randomly
%   it is of size NI
% B is a vector of design variables that will remain fixed
% Out = 1 will cause the thing to print
% DL, DU, DS and DM are starting points for the vector D
% DL and DU are lower and upper limit points
% DM is the median value to be used in generating D
% DS is a vector of standard deviation to be used in generating D
% DIN is the vector of ranges of the elements of DI
% NDE is the number of design points to be accumulated
% NITER is the total number of shots to be tried
% Output from nda is accumulated in two matrices
% MA [NA, NDE] holds the attributes of all designs
% MD [ND, NDE] holds the design variables
% MDI [NI, NDE] holds the integer design variables

NCYCLES = input('How many reduction cycles? ==>');
NITER = input('How many shots per cycle? ==>');
RF = input('What reduction in STDEV/cycle? ==>');
N = input('Which design do we start from? ==>');

DM = MD(N,:);               % this is the starting point design
%DI = MDI(N,:);                % use the integer variables as is

%[A, g] = attribut(DM, DI, B, 1);        % generate design
[A, g] = attribut(DM, B, 1);       % generate design
V=A(1);                   % starting point

for i = 1:NITER,

  D = DM + DS .* randn(1, ND);        % generate a random input
  if sum([DL>D DU<D]) == 0,        % if design is in range, continue
```

```
%    [A, g] = attribut(D, DI, B, 0);    % generate design
    [A, g] = attribut(D, B, 0);   % generate design

    if g~= 0,              % if viable, check objective value
      if A(1) > V,            % indicates improvements
        DM = D;               % save design for later
      end                % end dominance check
    end                  % end viability check
  end                  % end range check
end                    % end first iteration

% now we refine only the continuous variables: DI is fixed

for ic = 1:NCYCLES,
  fprintf('\nCycle Number %4.0f\n',ic)

  DS = DS .* RF;           % reduce STD of search

  for i = 1:NITER,

    D = DM + DS .* randn(1, ND);  % generate a random input
    if sum([DL>D DU<D]) == 0,     % if design is in range, continue
%     [A, g] = attribut(D, DI, B, 0);  % generate design
          [A, g] = attribut(D, B, 0);  % generate design

      if g~= 0,           % if viable, check objective value
        if A(1) > V,          % indicates improvements
          DM = D;          % save design for later
          V = A(1);           % this is the new reference design
        end                % end dominance check
      end                  % end viability check
    end                   % end range check
  end                  % end iteration
%  [A, g] = attribut(DM, DI, B, 1);  % display results of this cycle
    [A, g] = attribut(DM, B, 1);  % display results of this cycle
end
```

5

Synchronous and Brushless DC Machines

5.1 Introduction

Synchronous machines constitute one of the major classes of electric machine, with myriad applications. Turbine generators, including the very largest machines, are of this class. Much smaller motors, including servomotors, are typically synchronous machines with permanent magnet excitation. Vehicle propulsion motors are often synchronous, with either field winding or permanent magnet excitation. We first encountered synchronous machines in Chapter 3, but here the text will go into much greater depth. First, the synchronous machine is treated as if its windings are current sheets, with sinusoidal winding patterns. Second, a more realistic view is taken of this class of machine, and operation and limits are investigated. Later chapters will consider details shared by synchronous machines and other classes of machines, including windings and dynamic models.

5.2 Current Sheet Description

The objective here is to develop a simple but physically meaningful model of the synchronous machine, one of the major classes of electric machines. This model is useful because of its simplicity, and it can be viewed from several different directions. This model will help develop an understanding of analysis of machines, particularly in cases where one or another analytical picture is more appropriate than others. Both operation and sizing will be of interest here.

Along the way, machine windings will be approached from two points of view. In this chapter, the windings are approximated as sinusoidal distributions of current and flux linkages. In the next chapter, a more realistic and detailed winding model is developed.

Figure 5.1 shows a cut through the cross-section of the machine. The "rotor" is a solid cylinder with a sinusoidal current source on its outer surface. The "stator" is a hollow cylinder with a current source on its inner surface. The two elements are concentric, with a relatively narrow gap between them. This is variously referred to as the "air gap" or "relative rotation gap". The "rotor" and "stator" bodies are made of highly permeable material, with permeability $\mu \to \infty$ and the relative rotation gap is assumed to have the permeability of free space. For the moment, it is assumed that the gap is narrow: $g \ll R$, where g is the clearance between the outside of the rotor and the inside of the stator and R is the outer radius of the rotor. The whole apparatus has length that is finite but that is also assumed to be relatively long compared with the gap dimension.

Electromagnetic Analysis of Electric Machines: First Principles, Modeling, and Design, First Edition.
James L. Kirtley, Christopher H. T. Lee, and Sajjad Mohammadi.

Companion website: www.wiley.com/go/kirtleyelectric

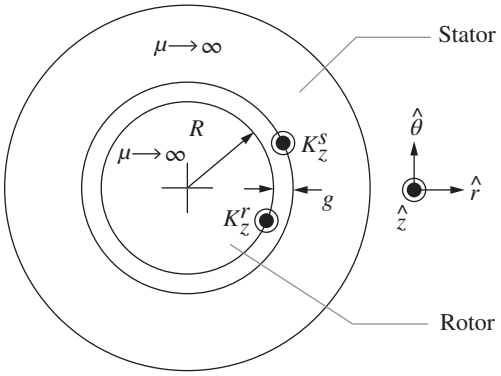

Figure 5.1 Elementary synchronous machine model: axial view.

Assume that the rotor and stator have current distributions that are axially (z) directed and sinusoidal:

$$K_z^S = K_S \cos\, p\theta$$
$$K_z^R = K_R \cos\, p(\theta - \phi) \tag{5.1}$$

where ϕ is the rotation angle of the rotor. The integer "p" is the number of pole pairs.

The current distribution on the rotor is fixed with respect to the rotor. If the assumption that $g \ll R$ holds true, it is not difficult to show that the radial flux density B_r is nearly uniform across the gap (i.e. not a function of radius) and, using Ampere's Law:

$$\frac{\partial B_r}{\partial R\theta} = -\mu_0 \frac{K_z^S + K_z^R}{g}$$

Then the radial magnetic flux density is:

$$B_r = -\frac{\mu_0 R}{pg}(K_S \sin p\theta + K_R \sin p(\theta - \phi)) \tag{5.2}$$

Now it is possible to compute the traction on rotor and stator surfaces by recognizing that the surface current distributions are the azimuthal magnetic fields: at the surface of the stator, $H_\theta = -K_z^S$ and at the surface of the rotor, $H_\theta = K_z^R$. So, at the surface of the rotor, traction is:

$$\tau_\theta = T_{r\theta} = -\frac{\mu_0 R}{pg}(K_S \sin p\theta + K_R \sin p\ (\theta - \phi))K_R \cos p(\theta - \phi)$$

The average of this is:

$$\langle \tau_\theta \rangle = -\frac{\mu_0 R}{2pg} K_S K_R \sin p\phi \tag{5.3}$$

The same exercise done at the surface of the stator yields the same result (with opposite sign). Torque is:

$$T = 2\pi R^2 \ell \langle \tau_\theta \rangle = -\frac{\mu_0 \pi R^3 \ell}{pg} K_S K_R \sin p\phi \tag{5.4}$$

A few observations are in order at this point:

1) For a given value of surface currents K_S and K_R, torque goes as the third power of linear dimension. That implies that the achieved shear stress is constant with machine size. And the ratio of machine torque density to machine volume is constant.

2) If, on the other hand, gap is held constant, torque goes as the fourth power of machine volume. Since the volume of the machine goes as the third power, this implies that torque capability goes as the 4/3 power of machine volume.
3) Actually, this understates the situation since the assumed surface current densities are the products of volume current densities and winding depth, which one would expect to increase with machine size. As machine radius grows, one would expect both stator and rotor surface current densities to grow. Thus, machine torque (and power) densities tend to increase somewhat faster than linearly with machine volume.
4) The current distributions want to align with each other. In actual practice, what is done is to generate a stator current distribution which is not static as implied here but which rotates in space:

$$K_z^S = K_S \cos\,(p\theta - \omega t)$$

and this pulls the rotor along.
5) For a given pair of current distributions, there is a maximum torque that can be sustained, but as long as the torque that is applied to the rotor is less than that value, the rotor will adjust to the correct angle.

5.2.1 Continuous Approximation to Winding Patterns

It would be useful to produce those surface current distributions with physical windings. In fact, it is not possible to do exactly that, but conceptually it is possible to approximate a physical winding with a turns distribution that would look like:

$$n_S = \frac{N_S}{2R}\cos p\theta$$

$$n_R = \frac{N_R}{2R}\cos p(\theta - \phi) \tag{5.5}$$

Note that this implies that N_S and N_R are the total number of turns on the rotor and stator, i.e.:

$$p\int_{-\frac{\pi}{2p}}^{\frac{\pi}{2p}} n_S R\ d\theta = N_S$$

Then the surface current densities are as stated above, with:

$$K_S = \frac{N_S I_S}{2R} \quad K_R = \frac{N_R I_R}{2R} \tag{5.6}$$

So far, nothing is different, but with an assumed number of turns, it is possible to proceed to computing inductances. It is important to remember what these assumed winding distributions mean: they are the density of wires along the surface of the rotor and stator. A positive value implies a wire with sense in the $+z$ direction, a negative value implies a wire with sense in the $-z$ direction. That is, if terminal current for a winding is positive, current is in the $+z$ direction if n is positive, in the $-z$ direction if n is negative. In fact, such a winding would be made of elementary coils with one half (the negatively going half) separated from the other half (the positively going half) by a physical angle of $\frac{\pi}{p}$. So the flux linked by that elemental coil would be:

$$\Phi_i(\theta) = \int_{\theta-\frac{\pi}{p}}^{\theta} \mu_0 H_r(\theta')\ \ell R d\theta' \tag{5.7}$$

If only the stator winding is excited, radial magnetic field is:

$$H_r = -\frac{N_S I_S}{2gp} \sin\ p\theta \tag{5.8}$$

and thus the elementary coil flux is:

$$\boldsymbol{\Phi}_i(\theta) = \frac{\mu_0 N_S I_S \ell R}{p^2 g} \cos p\theta \tag{5.9}$$

This is flux linked by an elementary coil to get flux linked by a whole winding. It is necessary to "add up", or integrate, the flux linkages of all of the elementary coils. In the continuous approximation to the real coil, this is found by integrating over the coil distribution:

$$\lambda_S = p \int_{-\frac{\pi}{2p}}^{\frac{\pi}{2p}} \boldsymbol{\Phi}_i(\theta)\ n_S(\theta)\ R\ d\theta = \mu_0 \frac{\pi}{4} \frac{\ell R N_S^2}{gp^2} I_S$$

which implies a self-inductance for the stator winding:

$$L_S = \mu_0 \frac{\pi}{4} \frac{\ell R N_S^2}{gp^2} \tag{5.10}$$

The same process can be used to find self-inductance of the rotor winding (with appropriate changes of spatial variables):

$$L_R = \mu_0 \frac{\pi}{4} \frac{\ell R N_R^2}{gp^2}$$

To find the mutual inductance between the two windings, excite one and compute flux linked by the other:

$$M(\phi) = \mu_0 \frac{\pi}{4} \frac{\ell R N_S N_R}{gp^2} \cos p\phi \tag{5.11}$$

It is straightforward to compute torq ue using conventional methods. Assuming both windings are excited, magnetic coenergy is:

$$W'_m = \frac{1}{2} L_S I_S^2 + \frac{1}{2} L_R I_R^2 + M(\phi)\ I_S I_R$$

And then torque is:

$$T = \frac{\partial W'_M}{\partial \phi} = -\mu_0 \frac{\pi}{4} \frac{\ell R N_S N_R}{gp} I_S I_R \sin p\phi$$

And then substituting for $N_S I_S$ and $N_R I_R$:

$$N_S I_S = 2RK_S$$
$$N_R I_R = 2RK_R$$

The same expression for torque is obtained as with the field approach (above).

5.3 Classical Synchronous Machine Model

Now it is possible to examine the simplest model of a polyphase synchronous machine. Suppose the machine has a rotor that is the same as the one considered above, but the stator has three separate windings, identical but with spatial orientation separated by an electrical angle of 120° or 2π/3 radians (electrical). The three stator windings will have the same self-inductance (call it L_a). With

a little bit of examination, it can be seen that the three stator windings will have mutual inductance, and that inductance will be characterized by the cosine of 120°. Since the physical angle between any pair of stator windings is the same, so are the mutual inductances between pairs of phase windings:

$$L_{ab} = L_{ac} = L_{bc} = -\frac{1}{2}L_a$$

where, of course, the phases are identified as *a*, *b,* and *c*.

There will also be a mutual inductance between the rotor and each phase of the stator. Using M to denote the magnitude of that inductance, and noting the angular displacement of the various phase windings:

$$M = \mu_0 \frac{\pi}{4} \frac{\ell R N_a N_f}{p^2 g}$$
$$M_{af} = M \cos p\phi$$
$$M_{bf} = M \cos\left(p\phi - \frac{2\pi}{3}\right)$$
$$M_{cf} = M \cos\left(p\phi + \frac{2\pi}{3}\right)$$

As is shown in Chapter 3, torque for this system is:

$$T = -pMi_a\ i_f\ \sin(p\phi) - pMi_b\ i_f\ \sin\left(p\phi - \frac{2\pi}{3}\right) - pMi_c\ i_f\ \sin\left(p\phi + \frac{2\pi}{3}\right)$$

5.3.1 Balanced Operation

Suppose the machine is operated in this fashion: the rotor turns at a constant velocity, the field current is held constant, and the three stator currents are sinusoids in time, with the same amplitude and with phases that differ by 120°.

$$p\phi = \omega t + \delta_i$$
$$i_f = I_f$$
$$i_a = I \cos \omega t$$
$$i_b = I\ \cos\left(\omega t - \frac{2\pi}{3}\right)$$
$$i_c = I \cos\left(\omega t + \frac{2\pi}{3}\right)$$

Straightforward (but tedious) manipulation yields an expression for torque:

$$T = -\frac{3}{2} p\ M\ I\ I_f \sin \delta_i \tag{5.12}$$

Operated in this way, with balanced currents and with the mechanical speed consistent with the electrical frequency ($p\Phi = \omega t$), the machine exhibits a constant torque. The phase angle δ_i is called the torque angle, but it is important to use some caution, as there is more than one torque angle.

Now, look at the machine from the electrical terminals. Flux linked by Phase A will be:

$$\lambda_a = L_a I_a + L_{ab} I_b + L_{ac} I_c + M\ I_f \cos p\phi$$

Noting that the sum of phase currents is, under balanced conditions, zero and that the mutual phase–phase inductances are equal, this simplifies to:

$$\lambda_a = (L_a - L_{ab}) i_a + M I_f\ \cos p\phi = L_d i_a + M\ I_f \cos p\phi$$

where the notation $L_d = L_a - L_{ab}$ denotes "synchronous" inductance.

If the machine is turning at a speed consistent with the electrical frequency, it is said to be operating synchronously, and it is possible to employ complex notation in the sinusoidal steady state.

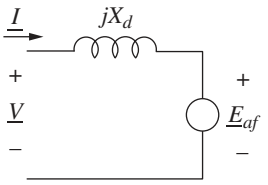

Figure 5.2 Round rotor synchronous motor equivalent circuit.

Then, note:

$$i_a = I\cos(\omega t + \theta_i) = \mathrm{Re}\{I\}e^{j(\omega t+\theta_i)}$$

Flux is, in complex notation:

$$\lambda_a = \mathrm{Re}\{\underline{\Lambda}_a e^{j\omega t}\}$$

And other complex notation:

$$\underline{I} = Ie^{j\theta_i}$$

$$\underline{I}_f = I_f e^{j\theta_m}$$

Terminal voltage is:

$$v_a = \frac{d\lambda_a}{dt} = \mathrm{Re}\{j\omega\ e^{j\omega t}\}$$

This system is described by the equivalent circuit shown in Figure 5.2.

where the internal voltage is:

$$\underline{E}_{af} = j\omega M\ I_f e^{j\theta_m} \tag{5.13}$$

If this machine is connected to a voltage source (that is, if V is of fixed magnitude and has frequency consistent with the internal voltage), current is:

$$\underline{I} = \frac{\underline{V} - E_{af}e^{j\delta}}{jX_d} \tag{5.14}$$

where $X_d = \omega L_d$ is the *synchronous reactance*.

Then real and reactive power (in Phase A) are:

$$\begin{aligned} P + jQ &= \frac{1}{2}\underline{V}\,\underline{I}^* \\ &= \frac{1}{2}\underline{V}\left(\frac{\underline{V} - E_{af}e^{j\delta}}{jX_d}\right)^* \\ &= \frac{1}{2}\frac{|\underline{V}|^2}{-jX_d} - \frac{1}{2}\frac{V\,E_{af}e^{-j\delta}}{-jX_d} \end{aligned} \tag{5.15}$$

This makes real and reactive power:

$$\begin{aligned} P_a &= -\frac{1}{2}\frac{V\ E_{af}}{X_d}\sin\delta \\ Q_a &= \frac{1}{2}\frac{V^2}{X_d} - \frac{1}{2}\frac{V\ E_{af}}{X_d}\cos\delta \end{aligned} \tag{5.16}$$

Considering all three phases, real power is

$$P = -\frac{3}{2}\frac{V\,E_{af}}{X_d}\sin\delta \tag{5.17}$$

Torque produced is just power divided by rotational speed, which is $\Omega = \omega/p$.

Torque vs. angle curves are plotted in Figure 5.3 for a six pole, approximately one MW synchronous machine with terminal voltage of 600 V, line-line, RMS, and with a synchronous reactance of about 0.72 Ω. The curves are plotted for internal voltage (E_{af}) of 620 V, 775 V, and 930 V per phase, respectively, RMS.

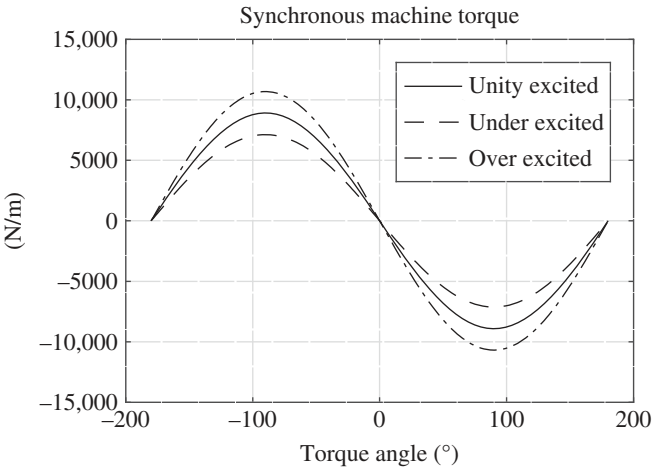

Figure 5.3 Torque vs. angle for a synchronous machine.

5.4 Operation of Motors and Generators

Vector diagrams, sometimes referred to as "phasor diagrams" that describe operation of the machine may be constructed by considering Kirchhoff's voltage law for the elements of Figure 5.2. For example, for a motor in which the field current is adjusted to make the terminal power factor unity (that is, for zero reactive power flow), that phasor diagram would look like what is shown in Figure 5.4. Note that, for a motor in which torque is positive, the torque angle is negative.

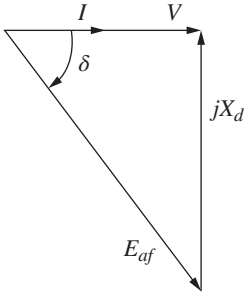

Figure 5.4 Phasor diagram of a motor at unity power factor.

It is possible, in a synchronous machine, to set the field current to different levels. Higher values of field current result in higher peak torque capability, as shown in Figure 5.3. But in most cases, torque is fixed by the load (in the case of a motor) or the prime mover (in case of a generator), so if the field current is sufficient, torque is not affected. What is affected by the value of field current is reactive power, reflected in the phase angle of the terminal current. Shown in Figure 5.5 are phasor diagrams for under- and over-excited operation of the same motor as in Figure 5.4.

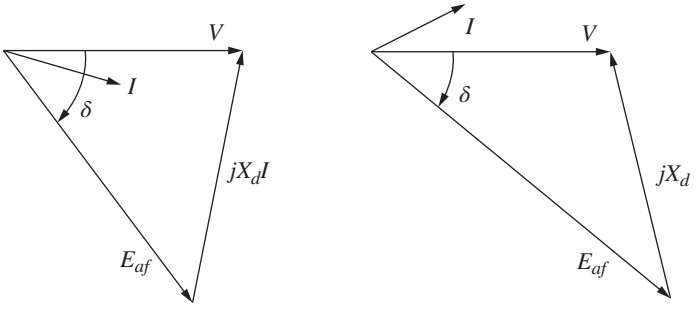

Figure 5.5 Phasor diagrams for under- and over-excited synchronous motor.

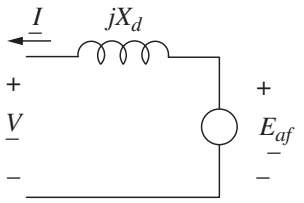

Figure 5.6 Equivalent circuit diagram for a round rotor synchronous generator.

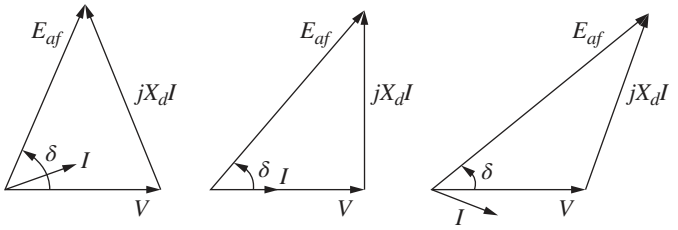

Figure 5.7 Phasor diagrams for under-excited, unity-excited, and over-excited generator.

Generators are typically not much different from motors, but it is customary to reverse the sign convention of current, as shown in Figure 5.6.

Operational phasor diagrams for generators are drawn in a similar fashion to those for motors, but note that the torque angle is positive, and the sign of reactive voltage drop is reversed (Figure 5.7).

5.5 Reconciliation of Torque Angles

It is shown above that it is possible to predict power and/or torque characteristics of a synchronous machine from two points of view: first, by knowing currents in the rotor and stator, torque is:

$$T = -\frac{3}{2} pM\ I\ I_f\ \sin\delta_i \tag{5.18}$$

From the circuit point of view, torque is:

$$T = -\frac{3}{2}\frac{p}{\omega}\frac{V\,E_{af}}{X_d}\sin\delta \tag{5.19}$$

It is possible to show that these two expressions are, in fact, consistent. Consider the phasor diagram of Figure 5.8, which shows a phasor diagram for a slightly over-excited motor. Plotted also are fluxes for that motor, which are lagging by 90° from their voltages. The current torque angle

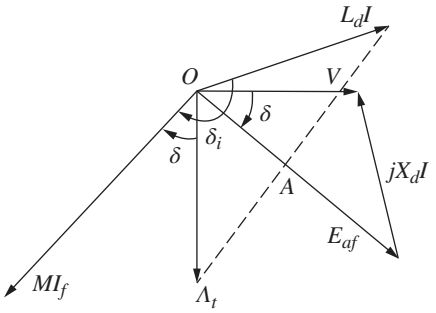

Figure 5.8 Proof of consistency.

and voltage torque angle are shown. A dotted line is drawn from the tip of the flux produced by armature current, $L_d I$ and terminal flux Λ_t. Where that dotted line crosses the internal voltage phasor E_{af} is called "point A". The distance |OA| is $|OA| = L_d I \sin\delta_i = \Lambda_t \sin\delta$. Then, noting that terminal voltage $V = \omega\Lambda_t$, $E_{af} = \omega M I_f$, and $X_d = \omega L_d$, straightforward substitution yields:

$$\frac{3}{2}p\frac{V\,E_{af}}{\omega X_d}\sin\delta = \frac{3}{2}pM\;I\;I_f\sin\delta_i \tag{5.20}$$

5.6 Per-Unit Systems

Per-unit systems are a notational device that, in addition to being convenient, is also conceptually helpful. It is also widely used in understanding operation of electric power systems. The basic notion is quite simple: for most variables, a note a base quantity is established and then, by dividing the variable by the base, a per-unit version of that variable exists. Generally, that base quantity is tied to some aspect of normal operation. So, for example, the base voltage and current usually correspond with machine rating. If base voltage and current are phase values, and RMS, the power base becomes:

$$P_B = 3V_B I_B \tag{5.21}$$

and a base impedance is:

$$Z_B = \frac{V_B}{I_B} \tag{5.22}$$

Note that in the foregoing, it was assumed that voltage is taken as RMS, line-to-neutral, and current as in the line. There are, conceptually, other ways of doing this. For example, in a three-phase system, base voltage could have been taken as line-to-line and current as in a delta connection:

$$V_{B\Delta} = \sqrt{3}\;V_B \quad I_{B\Delta} = \frac{I_B}{\sqrt{3}} \tag{5.23}$$

In that case, the base power would be unchanged, but the base impedance would differ by a factor of three.

$$P_B = 3V_{B\Delta}I_{B\Delta} = 3V_B I_B \quad Z_{B\Delta} = 3Z_B \tag{5.24}$$

However, if one is consistent with actual impedances (note that a delta connection of elements of impedance $3Z$ is equivalent to a wye connection of impedances Z), the per-unit impedances of a given system are not dependent on the particular connection. In fact, one of the major advantages of using a per-unit system is that per-unit values are uniquely determined, while ordinary variables can be line-line, line-neutral, RMS, peak, etc.

As it turns out, base quantities are often specified as line-line voltage and base power, so that:

$$I_B = \frac{P_B}{\sqrt{3}\;V_{B\Delta}} \quad Z_B = \frac{V_B}{I_B} = \frac{1}{3}\;\frac{V_{B\Delta}}{I_{B\Delta}} = \frac{V^2{}_{B\Delta}}{P_B} \tag{5.25}$$

Thus, written in per-unit notation, real and reactive power for a synchronous machine operating in steady state are:

$$p = -\frac{v\;e_{af}}{x_d}\sin\delta \quad q = \frac{v^2}{x_d} - \frac{v\;e_{af}}{x_d}\cos\delta \tag{5.26}$$

These are, of course, in motor reference coordinates, and represent real and reactive power into the terminals of the machine.

5.6.1 Normal Operation

The synchronous machine is used, essentially interchangeably, as a motor and as a generator. Note that, as a motor, this type of machine produces torque only when it is running at synchronous speed. Many synchronous motors are started as induction machines on their damper cages (sometimes called starting cages). And, of course, with power electronic drives, the machine can often be considered to be "in synchronism" even down to zero speed.

In operation against a constant frequency voltage, real power is dictated by the load (if a motor) or the prime mover (if a generator). Thus, if the internal or "field" voltage e_{af} is varied, the torque angle will also be adjusted. Reactive power is determined by the real power and by field current, and so it will vary, even with constant real power, as field current is adjusted.

5.6.2 Capability

It is often necessary to determine the "capability" of a synchronous machine, particularly a synchronous generator. The limits to operation are related to both armature current and field current, and stability depends on having enough torque capability.

Figure 5.9 shows one way of representing the capability of a synchronous machine, in this case a generator. The construction of this figure is made by taking the phasor diagram of Figure 5.7, rotating it 90°, and flipping it horizontally. Note that, while the phasor diagrams usually used are of voltage, they are isomorphic to current, and if the armature current is multiplied by voltage, what emerges is real and reactive power. Shown in this figure is a vector that describes real and reactive power and the torque angle δ. This vector maps real and reactive power as described in the expressions above. It starts at location $q = -\frac{v^2}{x_d}$ and swings a vector of length $\frac{ve_{af}}{x_d}$ over an angle δ. Real power is on the horizontal axis, reactive power on the vertical. Ordinary operation of this generator would be confined to within the limits indicated. The "field limit" as indicated is related to how much current the field winding can handle. The armature limit is a segment of a circle around the origin, and reflects that, for a given terminal voltage, armature current is proportional to $\sqrt{P^2 + Q^2}$.

There are three easily noted limits to capability. The upper limit is a circle (the one traced out by that vector) which is referred to as field capability. The second limit is a circle that describes

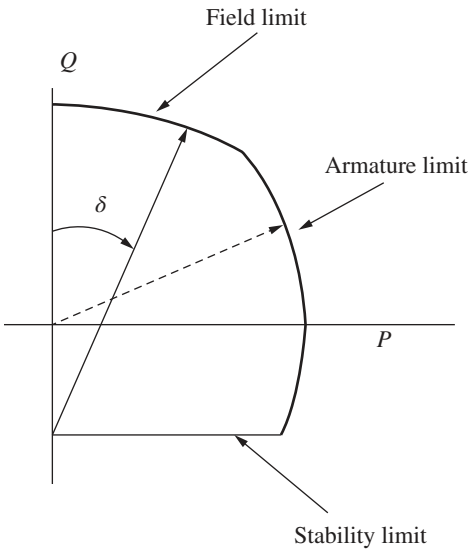

Figure 5.9 Exemplary capability curve for a generator.

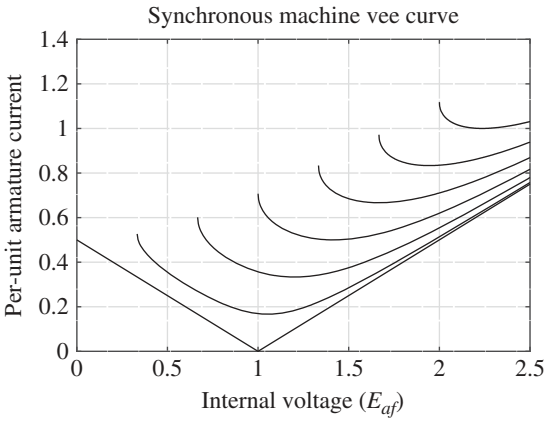

Figure 5.10 Vee curves: $x_d = 2.0$.

constant $|p + jq|$. This is, of course, related to the magnitude of armature current and so this limit is called armature capability. The final limit is related to machine stability, since the torque angle cannot go beyond 90° if the machine is to remain in stable operation. In actuality, there are often other limits that can be represented on this type of chart. For example, large synchronous generators typically have a problem with heating of the stator iron when they attempt to operate in highly under-excited conditions (q strongly negative), so that one will often see another limit that prevents the operation of the machine near its stability limit.

5.6.3 Vee Curve

Another way of describing the limitations of a synchronous machine is embodied in the *Vee Curve*. An example is shown in Figure 5.10. This is a cross-plot of magnitude of armature current with field current. Note that the field and armature current limits are straightforward (and are the right-hand and upper boundaries, respectively, of the chart). The machine stability limit is what terminates each of the curves at the upper left-hand edge. Note that each curve has a minimum at unity power factor.

5.7 Salient Pole Machines: Two-Reaction Theory

So far, what has been described are referred to as "round rotor" machines, in which stator reactance is not dependent on rotor position. This is a pretty good approximation for large turbine generators and many smaller two-pole machines, but it is not a good approximation for many synchronous motors nor for slower speed generators. For many such applications, it is more cost-effective to wind the field conductors around steel bodies (called poles), which are then fastened onto the rotor body, with bolts or dovetail joints. These produce magnetic anisotropies into the machine which affect its operation. The theory which follows is an introduction to two-reaction theory and consequently for the rotating field transformations that form the basis for most modern dynamic analyses.

Figure 5.11 shows a very schematic axial view of a salient pole machine, intended primarily to show how to frame this analysis. As with the round rotor machine, the stator winding is located in slots (not shown) in the surface of a highly permeable stator core annulus. The field winding is wound around steel pole pieces fastened in some way (not shown) to a ferromagnetic shaft. The stator current sheet is separated into two components: one aligned with and one in quadrature

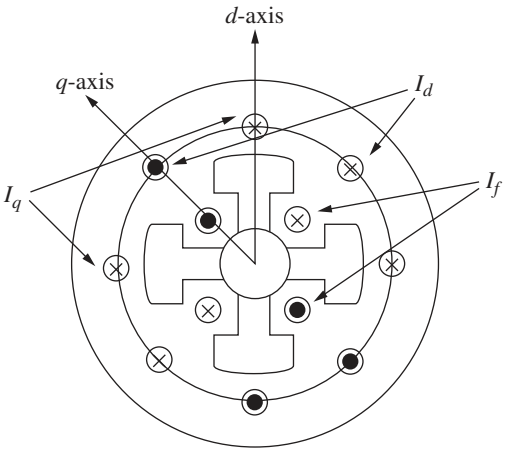

Figure 5.11 Cartoon of a salient pole synchronous machine.

to the field. Remember that these two current components are themselves (linear) combinations of the stator phase currents. A formal derivation of the transformation between phase currents and the *d*- and *q*-axis components will appear in Chapter 7. Note this figure shows a four-pole machine configuration, so the *q*-axis, which is 90 electrical degrees ahead of the *d*-axis, is 45 mechanical degrees ahead.

The key here is to separate MMF and flux into two orthogonal components that can be treated as sinusoidal. The two components are aligned with the direct axis and with the quadrature axis of the machine. The direct axis is aligned with the field winding, while the quadrature axis leads the direct by 90 *electrical* degrees. Then, if ϕ is the angle between the direct axis and the axis of phase a, flux linking phase a is:

$$\lambda_a = \lambda_d \cos\phi - \lambda_q \sin\phi \tag{5.27}$$

Then, in steady state operation, if $V_a = \frac{d\lambda_a}{dt}$ and $\phi = \omega t + \delta$,

$$V_a = -\omega\lambda_d \sin\phi - \omega\lambda_q \cos\phi \tag{5.28}$$

So that voltages on the two axes are:

$$\begin{aligned} V_d &= -\omega\lambda_q \\ V_q &= \omega\lambda_d \end{aligned} \tag{5.29}$$

This implies that the "voltage" vector is leading the "flux" vector by 90°.

If the machine is magnetically linear, those fluxes are given by:

$$\begin{aligned} \lambda_d &= L_d I_d + M\, I_f \\ \lambda_q &= L_q I_q \end{aligned} \tag{5.30}$$

Note that, in general, L_d is not equal to L_q. In wound-field synchronous machines, usually $L_d > L_q$. The reverse is true for most salient (buried magnet) permanent magnet machines.

Referring to Figure 5.12, the terminal voltage can be resolved into *d*- and *q*-axis components:

$$\begin{aligned} V_d &= V\sin\delta = -\omega L_q I_q \\ V_q &= V\cos\delta = \omega L_d I_d + \omega M\, I_f \end{aligned} \tag{5.31}$$

Figure 5.12 Resolution of voltage.

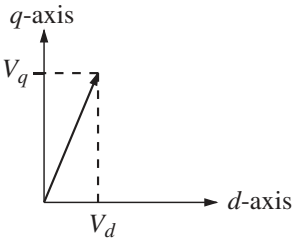

which can be solved for the currents:

$$I_d = \frac{V\cos\delta - E_{af}}{X_d}$$
$$I_q = -\frac{V\sin\delta}{X_q} \tag{5.32}$$

where $X_d = \omega L_d$ $X_q = \omega L_q$ and $E_{af} = \omega M I_f$.

Note that the V_d V_q frame lends itself readily to complex notation:

$$\underline{V} = V_d + jV_q \quad \underline{I} = I_d + jI_q$$

Complex power is then:

$$P + jQ = \frac{3}{2}V\,I^* = \frac{3}{2}\{(V_dI_d + V_qI_q) + j(V_qI_d - V_dI_q)\}$$
$$P = -\frac{3}{2}\left(\frac{V\,E_{af}}{X_d}\sin\delta + \frac{V^2}{2}\left(\frac{1}{X_q} - \frac{1}{X_d}\right)\sin 2\delta\right)$$
$$Q = \frac{3}{2}\left(\frac{V^2}{2}\left(\frac{1}{X_q} + \frac{1}{X_d}\right) - \frac{V^2}{2}\left(\frac{1}{X_q} - \frac{1}{X_d}\right)\cos 2\delta - \frac{V\,E_{af}}{X_d}\cos\delta\right) \tag{5.33}$$

A phasor diagram for a salient pole machine is shown in Figure 5.13. This is a little different from the equivalent picture for a round-rotor machine, in that stator current has been separated into its *d*- and *q*-axis components, and the voltage drops associated with those components have been drawn separately. It is helpful to recognize that the internal voltage E_{af} can be expressed as:

Figure 5.13 Phasor diagram for salient synchronous motor.

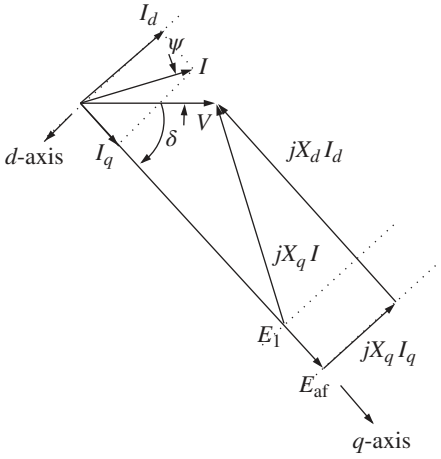

$E_{af} = E_1 + (X_d - X_q)I_d$, where the voltage E_1 is on the quadrature axis. Then the operating point is found by:

$$\delta = -\tan^{-1}\left(\frac{X_q\ I\ \cos\psi}{V + X_q\ I\ \sin\psi}\right)$$
$$E_1 = \sqrt{(V + X_q I\ \sin\psi)^2 + (X_q I\ \cos\psi)^2} \tag{5.34}$$

5.8 Relating Rating to Size

It is possible, even with the simple model developed so far, to establish a quantitative relationship between machine size and rating, depending (of course) on elements such as useful flux and surface current density. To start, note that the rating of a machine (motor or generator) is:

$$|P + jQ| = q\ V\ I \tag{5.35}$$

where q is the number of phases, V is the RMS voltage in each phase, and I is the RMS current in each phase. To establish machine rating, it is necessary to establish voltage and current, and this is done separately.

5.8.1 Voltage

For the moment, assume a sinusoidal approximation for turns density:

$$n_a(\theta) = \frac{N_a}{2R}\cos p\theta \tag{5.36}$$

and that working radial flux density is:

$$B_r(\theta) = B_0 \sin p(\theta - \phi)$$

To compute flux linked by the winding (and consequently to compute voltage), it is necessary to compute flux linked by an incremental coil:

$$\lambda_i(\theta) = \int_{\theta}^{\theta + \frac{\pi}{p}} \ell B_r(\theta')\ R d\theta'$$

Then flux linked by the whole coil is:

$$\lambda_a = p\int_{-\frac{\pi}{2p}}^{\frac{\pi}{2p}} \lambda_i(\theta)\ n_a(\theta)\ d\theta = \frac{\pi}{4}\ \frac{2\ell R N_a}{p} B_0 \cos p\phi$$

This is instantaneous flux linked when the rotor is at angle φ. If the machine is operating at some electrical frequency ω with a phase angle so that $p\varphi = \omega t + \delta$, the RMS magnitude of terminal voltage is:

$$V_a = \frac{\omega}{p}\frac{\pi}{4} 2\ell R N_a \frac{B_0}{\sqrt{2}} \tag{5.37}$$

Note that useful peak flux density that can be used is limited by the fraction of machine periphery that is teeth (i.e. not used by slots): $B_0 \leq B_s(1 - \lambda_s)$, where λ_s is the peripheral fraction that is slots and B_s is the useful (saturation limited) flux density in the teeth.

5.8.2 Current

The (RMS) magnitude of the current sheet produced by a current of (RMS) magnitude I is:

$$K_z = \frac{q}{2}\frac{N_a I}{2R}$$

And then the current is, in terms of the current sheet magnitude:

$$I = 2RK_z\frac{2}{qN_a}$$

Note that the surface current density is, in terms of area current density J_s, slot space factor λ_s, and slot depth h_s:

$$K_z = \lambda_s J_s h_s$$

so that terminal current in terms of dimensions and useful current density:

$$I = \frac{4R}{qN_a}\lambda_s h_s J_s \tag{5.38}$$

5.8.3 Rating

Assembling these expressions, machine rating becomes:

$$|P + jQ| = qVI = \frac{\omega}{p}2\pi R^2 \ell \frac{B_s}{\sqrt{2}}\lambda_s(1-\lambda_s)h_s J_s \tag{5.39}$$

This expression is actually fairly easily interpreted. The product of slot factor times one minus slot factor optimizes rather quickly to 1/4 (when $\lambda_s = 1/2$). The expression can be interpreted as:

$$|P + jQ| = A_s u_s \tau^*. \tag{5.40}$$

where the interaction area is $A_s = 2\pi R\ell$, the surface velocity of the interaction is $u_s = \frac{\omega}{p}R$, and that fragment of the expression that "looks like" traction is:

$$\tau^* = h_s J_s \frac{B_s}{\sqrt{2}}\lambda_s(1-\lambda_s) \tag{5.41}$$

Note that this is not quite traction since the current and magnetic flux may not be ideally aligned, and this is why the expression incorporates reactive as well as real power. This is not quite yet the whole story. The limit on B_s is easily understood to be caused by saturation of magnetic material. The other important element on shear stress density, $h_s J_s$ is a little more involved.

5.8.4 Role of Reactance

The per-unit, or normalized synchronous reactance, is:

$$x_d = X_d\frac{I}{V} = \frac{\mu_0 R}{pg}\frac{\lambda_s}{1-\lambda_s}\sqrt{2}\frac{h_s J_s}{B_s} \tag{5.42}$$

While this may be somewhat interesting by itself, it becomes useful if it is solved for $h_s J_s$:

$$h_s J_s = x_d g\frac{p(1-\lambda_s)B_s}{\mu_0 R\lambda_s\sqrt{2}} \tag{5.43}$$

That is, if x_d is fixed, $h_s J_a$ (and so power) are directly related to air-gap g. Now, to get a limit on g, one must answer the question of how far the field winding can "throw" effective air-gap flux? To

understand this question, it is necessary to calculate the field current to produce rated voltage, at no load, and then the excess of field current is required to accommodate load current.

Under rated operation, per-unit field voltage is:

$$e_{af}^2 = v^2 + \left(x_d i\right)^2 + 2x_d i \ \sin\psi \tag{5.44}$$

5.8.5 Field Winding

From the foregoing, at rated conditions (unity per-unit voltage and current), given a value for x_d and ψ, per-unit internal voltage e_{af} is also fixed. Then the field current required can be calculated by first estimating field winding current for "no-load operation":

$$B_r = \frac{\mu_0 N_f I_{fnl}}{2gp}$$

and rated field current is $I_f = I_{fnl} e_{af}$, or rated field current is:

$$N_f I_f = \frac{2gp(1-\lambda_s)B_s}{\mu_0} e_{af} \tag{5.45}$$

Further, field current is a result of field current density:

$$N_f I_f = \frac{N_{RS}}{2} A_{RS} J_f$$

where N_{RS} is the number of the rotor slots, and A_{RS} is rotor slot area $A_{RS} = w_R h_R$, where h_R is slot height and w_R is slot width: $w_R = \frac{2\pi R}{N_{RS}}\lambda_R$. Then the field current is:

$$N_f \ I_f = \pi R \lambda_R h_R J_f$$

This yields a value for air-gap as limited by reactance:

$$g = \frac{\pi}{2} \frac{\mu_0 R \lambda_R h_R J_f}{p(1-\lambda_s)B_s e_{af}} \tag{5.46}$$

and this, in turn, yields a useful limit on armature surface current density, based on reactance and useful field current:

$$h_s J_s = \frac{\pi}{2\sqrt{2}} \frac{x_d}{e_{af}} \frac{\lambda_R}{\lambda_s} h_R J_f \tag{5.47}$$

Note that the ratio of x_d/e_{af} can be quite small (if the per-unit reactance is small), will never be a very large number for any practical machine, and is generally less than one. As a practical matter, it is unusual for the per-unit synchronous reactance of a machine to be larger than about 2 or 2.25 per-unit. What this indicates should be obvious: either the rotor or the stator of a machine can produce the dominant limitation on shear stress density (and so on rating). The best designs are "balanced", with both limits being reached at the same time.

5.9 Permanent Magnet Synchronous Machines

The discussion of synchronous machines has, so far, focused on wound field machines. Permanent magnets have had substantial application as the field source in synchronous machines, and such machines have seen substantial application as servomotors and propulsion motors for transportation vehicles: cars, trains, motorcycles, and other applications. At the time of this

writing, permanent magnet–excited motors were under development for potential propulsion of aircraft. There are, of course, many ways of building permanent magnet motors, but only a few will be considered in this chapter. Once these are understood, rating evaluations of most other geometrical arrangements should be fairly straightforward.

5.9.1 Surface Magnet Machines

Figure 5.14 shows the basic magnetic morphology of the motor with magnets mounted on the surface of the rotor and an otherwise conventional stator winding. This sketch does not show some of the important mechanical aspects of the machine, such as the means for fastening the permanent magnets to the rotor, so one should look at it with a bit of caution. In addition, this sketch and the other sketches to follow are not necessarily to a scale that would result in workable machines. This figure shows an axial section of a four-pole ($p = 2$) machine. The four magnets are mounted on a cylindrical rotor "core", or shaft, made of ferromagnetic material. Typically, this would simply be a steel shaft. In some applications, the magnets may be simply bonded to the steel. For applications in which a glue joint is not satisfactory (e.g. for high-speed machines), some sort of rotor banding or retaining ring structure is required.

The stator winding of this machine is *conventional*, very much like that of a wound field synchronous motor or an induction motor, consisting of wires located in slots in the surface of the stator core. The stator core itself is made of laminated ferromagnetic material (probably silicon iron sheets), the character and thickness of the sheets determined by operating frequency and efficiency requirements. They are required to carry alternating magnetic fields, so must be laminated to reduce eddy current losses. This sort of machine is simple in construction. Note that the operating magnetic flux density in the air-gap is nearly the same as in the magnets, so that this sort of machine cannot have air-gap flux densities higher than that of the remanent flux density of the magnets. If low-cost ferrite magnets are used, this means relatively low induction and consequently relatively low efficiency and power density. (Note the qualifier "relatively" here!) Note, however, that with modern, high-performance permanent magnet materials in which remanent flux densities can be on the order of 1.2–1.4 T, air-gap working flux densities can be

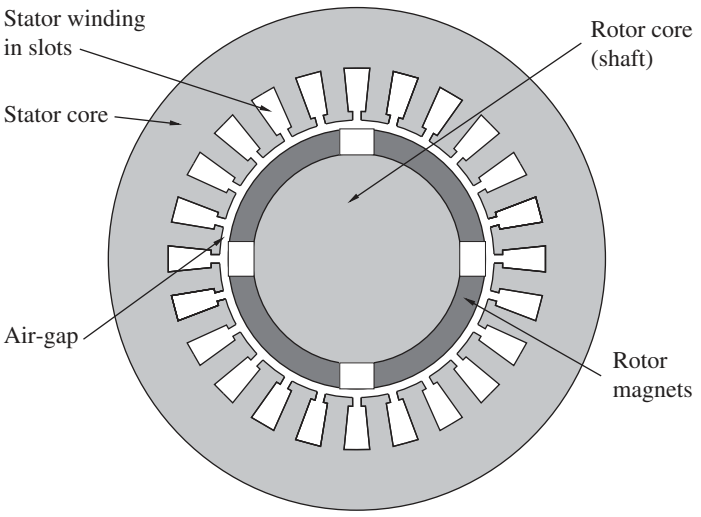

Figure 5.14 Axial section of a surface mount permanent magnet synchronous machine.

on the order of 1 T. With the requirement for slots to carry the armature current, this may be a practical limit for air-gap flux density anyway. It is also important to note that the magnets in this design are really in the "air gap" of the machine, and therefore are exposed to all of the time- and space-harmonics of the stator winding MMF. Because some permanent magnets have electrical conductivity (particularly the higher-performance magnets), any asynchronous fields will tend to produce eddy currents and consequent losses in the magnets.

5.9.2 Interior Magnet Machines

Interior magnet designs have been developed to counter several apparent or real shortcomings of surface-mount motors:

- Flux concentrating designs allow the flux density in the air-gap to be higher than the flux density in the magnets themselves.
- In interior magnet designs, there is some degree of shielding of the magnets from high order field variations by winding harmonics and slot openings.
- There are control advantages to some types of interior magnet motors, afforded by relatively large negative saliency which enhances "flux weakening" for high-speed operation, in rather direct analogy to what is done in DC machines.
- Some types of internal magnet designs have (or claim) structural advantages over surface mount magnet designs.

The geometry of one type of internal magnet motor is shown (crudely) in Figure 5.15. The permanent magnets are oriented so that their magnetization is azimuthal. They are located between wedges of magnetic material (the pole pieces) in the rotor. Flux passes through these wedges, going radially at the air-gap, then azimuthally through the magnets. The central core of the rotor must be non-magnetic to prevent "shorting out" the magnets. No structure is shown at all in this drawing, but quite obviously, this sort of rotor is a structural challenge. Shown is a six-pole machine. Typically, one does not expect flux concentrating machines to have small pole

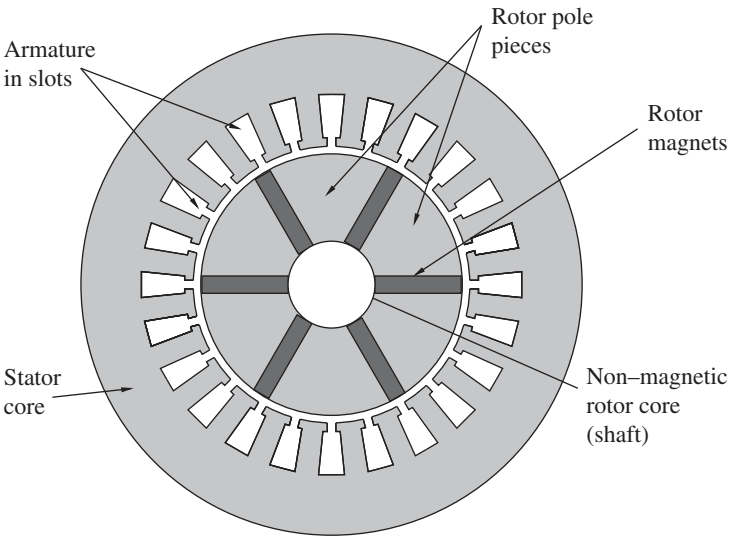

Figure 5.15 Flux concentrating interior magnet motor.

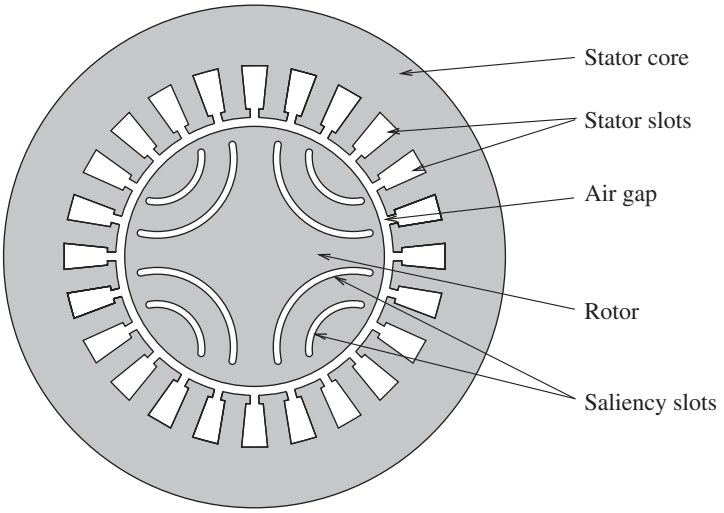

Figure 5.16 Negatively salient interior permanent magnet motor.

numbers, because it is difficult to get more area inside the rotor than around the periphery. On the other hand, a machine built in this way but without substantial flux concentration will still have saliency and magnet shielding properties.

A second morphology for an internal magnet motor is shown in Figure 5.16. This geometry has also been proposed for highly salient synchronous machines without permanent magnets: such machines would run on the saliency torque and are called *synchronous reluctance* motors. However, the saliency slots may be filled with permanent magnet material, giving them some internally generated flux as well. The rotor iron tends to short out the magnets, so that the "bridges" around the ends of the permanent magnets must be relatively thin. These structural elements are normally saturated.

5.9.3 Rating

In determining the rating of a machine, two separate sets of parameters must be considered. The first set, the elementary rating parameters, consists of the machine inductances, internal flux linkage, and stator resistance. From these and a few assumptions about base and maximum speed, it is possible to get a first estimate of the rating and performance of the motor.

Refer back to the equivalent circuit of a single phase of a synchronous machine shown in Figure 5.2. This is the same as any other round-rotor synchronous machine, but the internal voltage E_{af} is proportional to rotor speed. Most motors are three-phase, but it is not difficult to extend the analysis to an arbitrary number of phases. The circuit shows an internal voltage E_{af} and a reactance X_d which together with the terminal current I determine the terminal voltage V. In this picture, armature resistance is ignored. This has a minor effect on results which may be corrected for in a straightforward way once the basics are understood. If the machine is running in the sinusoidal steady state, the major quantities are of the form:

$$E_{af} = \omega\lambda_a \cos(\omega t + \delta)$$
$$V_t = V \cos \omega t$$

The machine is in synchronous operation if the internal and external voltages are at the same frequency and have a constant (or slowly changing) phase relationship (δ). The relationship between the major variables may be visualized by the phasor diagram shown in Figure 5.4. The internal voltage is just the time derivative of the internal flux from the permanent magnets, and the voltage drop in the machine reactance is also the time derivative of flux produced by armature current in the air-gap and in the "leakage" inductances of the machine. By convention, the angle ψ is positive when current I lags voltage V and the angle δ is positive when internal voltage Eaf leads terminal voltage V. In Figure 5.5, which depicts a motor, δ is negative and both signs of ψ are shown.

If there are q phases, the time average power produced by this machine is simply:

$$P = \frac{q}{2} V I \cos\psi$$

For most polyphase machines operating in what is called "balanced" operation (all phases doing the same thing with uniform phase differences between phases), torque (and consequently power) is approximately constant. Since we have ignored power dissipated in the machine armature, it must be true that power absorbed by the internal voltage source is the same as terminal power, or:

$$P = \frac{q}{2} E_{af} I \cos(\psi - \delta)$$

Since converted power is: $P = (\omega/p)T$, where T is torque and ω/p is mechanical rotation speed, torque is:

$$T = \frac{q}{2} p \lambda_a I \cos(\psi - \delta) \tag{5.48}$$

In principle, then, to determine the torque and hence power rating of a machine, it is only necessary to determine the internal flux, the terminal current capability, and the speed capability of the rotor. In fact, it is almost that simple. Unfortunately, the existence of saliency in buried magnet machines complicates matters, and this makes it necessary to look at the machine from the d-q point of view. Note that instantaneous power is:

$$P = \frac{3}{2} V_d I_d + \frac{3}{2} V_q I_q \tag{5.49}$$

And since

$$V_d = -\omega \lambda_q$$
$$V_q = \omega \lambda_d$$

Power and therefore torque are:

$$P = \omega \frac{3}{2} (\lambda_d I_q - \lambda_q I_d)$$
$$T = \frac{3}{2} p (\lambda_d I_q - \lambda_q I_d) = \frac{3}{2} p (\lambda_f + (L_d - L_q) I_d) I_q \tag{5.50}$$

5.9.4 Negatively Salient Machines: Operation

For high-performance drives, it is assumed that the power supply, generally an inverter, can supply currents in the correct spatial relationship to the rotor. This involves determining the rotor position (the instantaneous value of θ) and establishing the proper proportion of phase currents to establish current in the proper direction and magnitude. This means determining the values of I_d and I_q. The inverse Park's transformation is used to determine the instantaneous values required for phase

currents. This is the essence of what is known as "field oriented control", or putting stator currents in the correct location in space to produce the required torque.

There are three things to consider here:

- Armature current is limited, generally by heating,
- A second limit is the voltage capability of the supply, particularly at high speed, and
- If the machine is operating within these two limits, what is the optimal placement of currents? (that is, how to get the most torque per unit of current to minimize losses).

The discussion of current placement is carried out using the i_d, i_q plane. Operation in the steady state implies a single point on this plane, and translation of the current pair i_d, i_q to the required phase currents i_a, i_b, i_c is done using the inverse Park's transform. (To be discussed in depth in Chapter 7.)

A simple illustration is shown in Figure 5.17. The thermally limited armature current capability is represented as a circle around the origin, since the magnitude of armature current is just the length of a vector from the origin in this space. In general, for permanent magnet machines with buried magnets, $L_d < L_q$, so the optimal operation of the machine will be with negative I_d. A derivation of the optimal placement of currents will be derived below, and it will, in general, follow a curve in the I_d, I_q plane as shown.

To simplify the mathematics involved in this estimation, reactances, fluxes, currents, and torques are normalized into a per-unit system. First, define the base flux to be simply $\lambda_B = \lambda_f$ and the base current I_B to be the armature capability. Then the two per-unit reactances are:

$$x_d = \frac{L_d I_B}{\lambda_B} \quad x_q = \frac{L_q I_B}{\lambda_B} \tag{5.51}$$

Consider what would happen if the terminals of the machine were to be short-circuited so that $v = 0$. If the machine is operating at sufficiently high speed so that armature resistance is negligible, armature current would be simply:

$$i_d = -\frac{1}{x_d} \quad i_q = 0 \tag{5.52}$$

This is noted as the "short circuit" point in Figure 5.17.

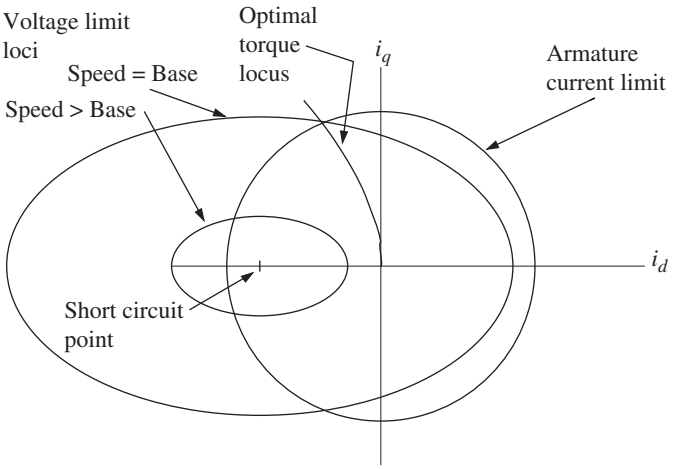

Figure 5.17 *d-q* plane current placement.

If the base torque is defined as $T_B = p\frac{3}{2}\lambda_B I_B$, then the per-unit torque is, in terms of the other per-unit quantities:

$$t_e = \left(1 - (x_q - x_d)i_d\right) i_q \tag{5.53}$$

It is fairly straightforward (but tedious) to show that the locus of current-optimal operation (that is, the largest torque for a given current magnitude or the smallest current magnitude for a given torque) is along the curve:

$$\begin{aligned} i_d^{opt} &= -\sqrt{\frac{i_a^2}{2} + 2\left(\frac{1}{4(x_q - x_d)}\right)^2 - \frac{1}{2(x_q - x_d)}\sqrt{\left(\frac{1}{4(x_q - x_d)}\right)^2 + \frac{i_a^2}{2}}} \\ i_q^{opt} &= \sqrt{\frac{i_a^2}{2} - 2\left(\frac{1}{4(x_q - x_d)}\right)^2 + \frac{1}{2(x_q - x_d)}\sqrt{\left(\frac{1}{4(x_q - x_d)}\right)^2 + \frac{i_a^2}{2}}} \end{aligned} \tag{5.54}$$

This curve is also shown in Figure 5.17.

The "rating point" will be the point along this curve when $i_a = 1$, or where this curve crosses the armature capability circle in the i_d, i_q plane. It should be noted that this set of expressions only works for salient machines. For non-salient machines, of course, torque-optimal current is on the q-axis. In general, for machines with saliency, the "per-unit" torque will not be unity at the rating, so that the rated, or "Base Speed" torque is not the "Base" torque, but $T_r = T_b \times t_e$ where t_e is calculated at the operating point (that is, $i_a = 1$ and i_d and i_q are "optimal").

Direct and quadrature axis voltages are:

$$\begin{aligned} V_d &= -\omega\ \lambda_q = -\omega\ L_q I_q \\ V_q &= \omega\ \lambda_d = \omega(\lambda_f + L_d\ I_d) \end{aligned} \tag{5.55}$$

Normalized (in per-unit), using the definitions of (5.51) and noting the base voltage to be:

$$V_B = \omega_0 \lambda_B = \omega_0 \lambda_f \tag{5.56}$$

these are:

$$\begin{aligned} v_d &= -\frac{\omega}{\omega_0} x_q i_q \\ v_q &= \frac{\omega}{\omega_0}(1 + x_d i_d) \end{aligned}$$

which means fluxes are:

$$\begin{aligned} \psi_d &= 1 + x_d i_d \\ \psi_q &= x_q i_q \end{aligned}$$

Operating at a point in the i_d, i_q plane means a flux magnitude:

$$|\psi|^2 = (1 + x_d i_d)^2 + (x_q i_q)^2 \tag{5.57}$$

This defines an ellipse in the i_d, i_q plane. The center of this ellipse is at the "short circuit" point defined by (5.52), and its size is dependent on the per-unit flux: $\psi = \frac{V}{\omega \lambda_B}$. Because this normalized flux is inversely proportional to speed, as speed increases, the size of this ellipse decreases, as shown in Figure 5.17.

The *Base Speed* is the speed at which this ellipse crosses the point where the optimal current curve crosses the armature capability. Operation at the highest attainable torque (for a given speed above this base speed) generally implies *d*-axis currents that are higher than those on the optimal current locus. What is happening here is that the (negative) *d*-axis current serves to reduce effective machine flux and hence voltage, which is limiting q-axis current. Thus, operation above the base speed is often referred to as "flux weakening".

The strategy for picking the correct trajectory for current in the i_d, i_q plane depends on the value of the per-unit reactance x_d. For values of $x_d > 1$, it is possible to produce some torque at *any* speed. For values of $x_d < 1$, there is a speed for which no point in the armature current capability is within the voltage limiting ellipse, so that useful torque has gone to zero. Generally, the maximum torque operating point is the intersection of the armature current limit and the voltage limiting ellipse.

5.10 Problems

5.1 A two-coil rotary system with the coils on the stator and permanent magnets on the rotor has self-and mutual flux linkages of:

$$\begin{bmatrix}\lambda_1\\ \lambda_2\end{bmatrix} = \begin{bmatrix}L_1 & 0\\ 0 & L_2\end{bmatrix}\begin{bmatrix}i_1\\ i_2\end{bmatrix} + \begin{bmatrix}\lambda_0\cos\theta\\ \lambda_0\sin\theta\end{bmatrix}$$

Assume values of the inductances to be $L_1 = L_2 = 100$ mH and the constant flux is $\lambda_0 = 1$ Wb. The angle θ is the physical angle of the rotor.

Find and plot the answers to the following questions. Your plots should show two complete rotations of the system. Time origin is not important.

a) With the rotor turning at a constant speed of 50 Hz, Coil 1 open and Coil 2 carrying a constant current of 5 A, what are:
   - Torque produced?
   - Voltage in coil 1?

b) With Coil 2 shorted and Coil 1 open, what is torque produced?

c) (For this part, you should assume flux $\lambda_2 = 0$. Why can you do this?)

d) With both coils connected to resistors, so the total resistance (coil plus resistor) is 10 Ω, torque is constant. (Why?) Assuming steady state operation, calculate this torque as a function of speed over the range zero to 100 Hz.

5.2 A two-coil rotary system with one coil on the stator and one coil on the rotor has a flux/current relationship:

$$\begin{bmatrix}\lambda_1\\ \lambda_2\end{bmatrix} = \begin{bmatrix}L_1 & M\cos\theta\\ M\cos\theta & L_2\end{bmatrix}\begin{bmatrix}i_1\\ i_2\end{bmatrix}$$

Assume values of the inductances to be $L_1 = L_2 = 200$ mH $\quad M = 150$ mH. Note this system has a coupling coefficient less than one: $M^2 < L_1 L_2$. It is rotated at a constant speed of 3600 RPM (60 Hz). Current in Coil 1 is held constant at 5 A. It has been on long enough to be in steady state operation.

Find and plot the answers to the following questions. Your plots should show two complete rotations of the system. Time origin is not important.

a) What torque does this system produce?
b) What is the voltage (ignore resistance) across the terminals of Coil 1, under three cases:
   1. Current in Coil 2 is held constant at 5 A
   2. Flux linked by Coil 2 is constrained to be zero (This is what would be approximately true were the terminals of Coil 2 to be shorted, assuming the resistance of Coil 2 is negligible)
   3. Coil 2 is shorted through a resistor so that the total resistance (including the coil itself) is 10 Ω.

5.3 This problem concerns a synchronous generator. Here is what we know about the machine. It is "round rotor", meaning the stator winding inductances are not a function of rotor position and:

- The rating of this machine is 600 MVA with a terminal voltage of 24 kV, RMS, phase–phase. This means that phase voltage is about 13,856 V, RMS.
- The machine is capable of reaching full MVA at a power factor of 0.85, overexcited.
- This is a two-pole, 60 Hz, three-phase machine.
- Under test at rated speed and with the stator winding open, field current required to produce rated terminal voltage is AFNL = 2000 A.
- Also, under test with the stator winding terminals shorted together, field current required to produce rated terminal current in the winding is AFSI = 4000 A.

  In working this problem, you may neglect armature winding resistance, and pretend there is no saturation of the magnetic circuit.
  1. What is the armature current rating of the machine, per phase?
  2. What is the field-to-phase mutual inductance of this machine?
  3. What is the synchronous inductance of the machine?
  4. Draw a phasor diagram of operation of this machine for operation at rated terminal voltage and current at unity power factor. How much field current is required for such operation?
  5. Draw a phasor diagram of operation of this machine for operation at rated terminal voltage and power factor (0.85, current lagging). What is field current required for such operation?
  6. What is the real power capability of this machine when it is operating at power factors of 0.2, 0.4, and 0.6, underexcited? Keep in mind that synchronous machines have a stability limit when operating under-excited. For "round rotor" machines, this stability limit is reached when torque angle $\delta = 90°$.
  7. Compounding curves describe field current required as a function of real power for fixed values of power factor. Using your favorite mathematical assistant, find and plot compounding curves for this machine for power factors of 0.2, 0.4, 0.6, 0.8, both under- and over-excited, and for unity power factor. Be sure to observe the stability limit you just figured for the underexcited curves and the overall current limit for the stator winding.

5.4 Generate and plot a vee curve diagram for the turbogenerator described in Problem 5.3. This is a plot of armature current magnitude $|I_a|$ vs. field current If for real values of output power of 0, 20%, 40%, 60% and 80% of rated. Be sure to observe and show limits for armature and field current and for stability in the under-excited region.

5.5 This problem concerns a large two-pole synchronous generator that has the following parameters, expressed in per-unit:

Machine rating	800 MVA
Rated terminal voltage	24 kV (RMS, line-line)
Field current for rated no-load voltage	2000A
Synchronous, *d*-axis reactance *xd*	2.0 per-unit
Synchronous, *q*-axis reactance *xq*	1.8

a) What is field current required for operation of this machine at rated volt-amperes (800 MVA), and 85%, lagging, power factor?
b) What is the field current when the machine is operating at its under-excited stability limit, with 85% leading power factor and rated volt-amperes? (Hint: the power angle is not exactly 90° at the stability limit for a salient machine.)

5.6 Brushless machine
A permanent magnet synchronous machine with surface magnets and a conventional three-phase stator structure has the following dimensions and parameters:

Rotor radius	35	mm
Active length	100	mm
Relative rotation (magnetic) gap	1.0	mm
Magnet height	3.0	mm
Number of pole pairs	3	
Number of stator slots	36	
Number of stator turns/P	20	
Magnet angular width	150	electrical degrees
Winding format	5/6 pitch	

Note: "rotor radius" is to the outer surface of the magnets, and "gap" is the total dimension between the magnets and stator surface, which may include some (nonmagnetic) structure which is not of interest to us here. Assume the magnets are made of NdFeB material with a peak "energy product" of 40 MG-Oe and an incremental permeability of μ_0.

This machine is turned through some external mechanism at a speed of 6000 RPM. The terminals are left open-circuited.

- What are the magnitude and frequency of the fundamental and first four higher-order harmonic voltages? Use the simple model for gap factor: $B_r = B_{rem}\frac{h_m}{h_m+g}$
- Plot the terminal voltage waveform for one revolution of the rotor. Remember to get the phase (sign, really) of the different components consistent with each other.

5.7 Salient PM machine
This problem concerns a buried magnet permanent magnet motor, perhaps suitable for use as a starter-generator for an engine. Basic data on this machine is:

Peak internal flux (phase)	0.009	Wb
Direct axis inductance	60	μHy
Quadrature axis inductance	240	μHy
Number of poles	12	

The machine is to be operated with a power supply that can produce a phase voltage of 17.2 V, RMS (consistent with a 42 V DC rail), and a terminal current limit of 125 A, RMS. The machine can operate over a speed range of 0–6000 RPM.

1) Find the locus of current that optimally produces torque for this machine. Plot I_d vs. I_q.
2) What is the base speed for this machine? This is the speed at which the power supply voltage just matches the required back voltage when the machine is producing torque optimally.
3) What IS the maximum torque it can make?
4) Draw and label (or get your computer to do this) the phasor diagram for operation at this base condition. What is the power factor at this operating point?

Compute and plot the torque vs. speed and power vs. speed capability of this.

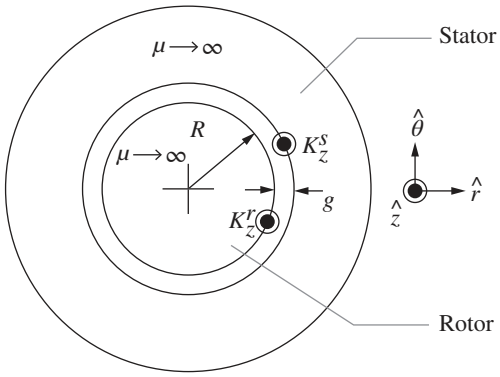

5.8 Air-gap geometry

Assume the geometry of Figure 5.1 of this chapter, repeated here. The gap clearance is ½ mm and gap radius is 5 cm. If stator current $K_z^S = 0$ is zero and rotor surface current $K_z^R = 10,000 \cos 2\theta$ A/m

1) What is radial magnetic flux density in the air gap?
2) If azimuthal flux density in the core must be limited to 1.7 T, how deep must the stator core be?

5.9 Torque

For the same geometry as Problem 5.8, assume the rotor can turn, so that $K_z^R = 10,000 \cos 2(\theta - \phi)$ where ϕ is the rotor position, and $K_z^S = 10,000 \cos 2\theta$ A/m, what is torque as a function of rotor angle ϕ?

5.10 Assuming the geometry of Problem 5.8, with a sinusoidally distributed winding with turns density:

$$n_S = \frac{N_s}{2} \cos 2\theta$$

What is the inductance of that winding?

6

Winding Analysis

6.1 Introduction

Virtually all electric machines have windings that carry current and link flux. The chapters of this book that deal with different classes of machines (synchronous, induction, commutator) all make reference to the windings that are essential parts of those machines. The purpose of this chapter is to deal analytically with generic windings that are common to multiple classes of electric machines. Windings of the type dealt with here are in the stators of most classes of machines and in the rotors of some. As will be shown, space harmonics are often important in understanding how electric machines operate.

6.2 Physical Description: Windings in Slots

Figure 6.1 shows a cartoon view of an axial cross-section of a 12-slot stator. Actually, what is shown is the shape of a thin sheet of steel, or a lamination that is used to make up the magnetic circuit. The stator core and associated teeth are made of thin sheets to control eddy current losses. Thickness varies according to frequency of operation, but in machines for 50 or 60 Hz (the vast bulk of machines made for industrial use), lamination thickness is typically 0.35 to 0.5 mm (0.014″ to 0.02″). These are stacked to make the magnetic circuit of the appropriate length. Windings are carried in the slots of this structure.

Figure 6.1 shows trapezoidal slots with teeth of approximately uniform cross-section over most of their length but wider extent near the air gap. The tooth ends, in combination with the relatively narrow slot depression region, help control certain parasitic losses in the rotor of many machines by improving uniformity of the air-gap fields, increasing the air-gap permeance, and helping hold the windings in the slots. The kind of slots shown in this figure are typically "scramble wound," with generally round wires inserted through the narrow slot top. In some machines, typically large machines, "form wound" coils are used. These are often made of rectangular conductors that are formed and bonded together to make a rigid structure that is inserted into the slots, which consequently must be straight-sided. In such a case, the teeth have a non-uniform cross-section. In both cases, some sort of "wedge" is used to retain the windings in the slots. The description that follows will hold for both types of machines.

To simplify the discussion, imagine the slot/tooth region to be "straightened out" as shown in Figure 6.2. This shows a three-phase, two-pole winding in the twelve slots. Such a winding would

Electromagnetic Analysis of Electric Machines: First Principles, Modeling, and Design, First Edition.
James L. Kirtley, Christopher H. T. Lee, and Sajjad Mohammadi.

Companion website: www.wiley.com/go/kirtleyelectric

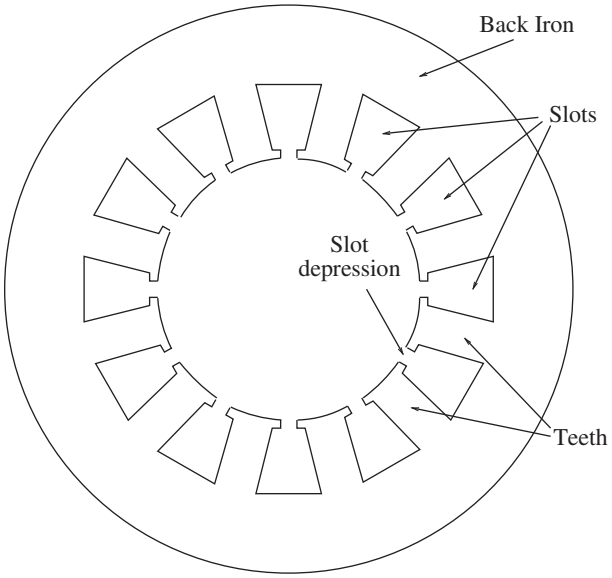

Figure 6.1 Stator cross-section.

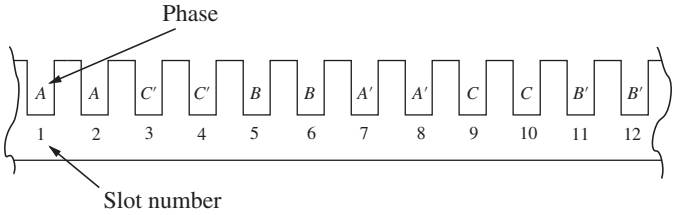

Figure 6.2 Full pitch winding plan.

have two slots per pole per phase. The two coils of phase A would be wound in slots 1 and 2, with the opposite sides in slots 7 and 8. That is, each side of the coils would be six slots apart. An alternate view of this same winding structure, showing only the Phase A winding, is shown in Figure 6.3. The teeth appear as dark rectangles and the winding in a lighter shade. The winding sequence is indicated by arrows. End turns can be seen connecting the two "straight section" parts of the

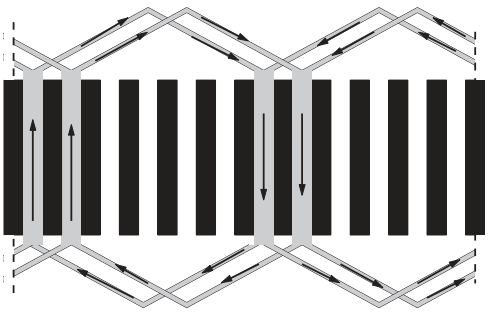

Figure 6.3 Radial view of full pitch winding.

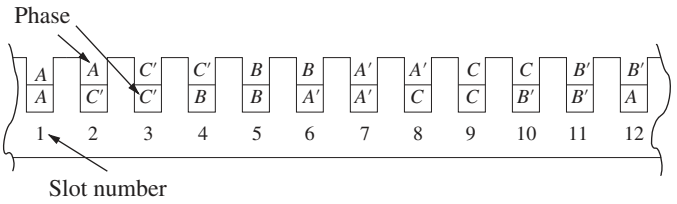

Figure 6.4 Partial pitch winding plan.

winding. Also note that, as the winding is unrolled for the purpose of providing a view, the dotted lines illustrate where the drawing has been cut, so the end turns that cross that cut don't just end: They continue from one end of the figure to the other.

Machines are seldom wound as shown in Figure 6.2 for a variety of reasons. It is usually advantageous in reducing the length of the end turns and to reducing space-harmonic effects in the machine to wind the machine with "short-pitched" windings as shown in Figure 6.4. Each phase in this case consists of four coils (two per slot). The four coils of Phase A would span between slots 1 and 6, slots 2 and 7, slots 7 and 12, and slots 8 and 1. Each of these coil spans is five slots, so this choice of winding pattern is referred to as "Five-Sixths" pitch. But it could be short pitched by two slots, in which case the pattern would be referred to as "Two-Thirds".

This cartoon-figure machine stator (which could represent either a synchronous or induction motor or generator) has both breadth and pitch. It has "breadth" because there is more than one slot per pole per phase, and it has "pitch" which is less than "full pitch." What follows in this chapter is a protocol for estimating the important air-gap fields and inductances.

6.3 Magnetomotive Force and Flux

To start, consider a full-pitch, concentrated winding as shown in schematic form in Figure 6.5. Assuming that the winding has a total of N turns over p pole-pairs, and is carrying current I. Magnetomotive force (MMF) drives the magnetic field across the air gap. MMF has units of Amperes, and it is, as a function of azimuthal position. The Fourier series for gap MMF would be:

$$F = -\sum_{n=1,odd}^{\infty} \frac{4}{n\pi} \frac{N\,I}{2p} \sin np\theta \tag{6.1}$$

Figure 6.5 Primitive geometry.

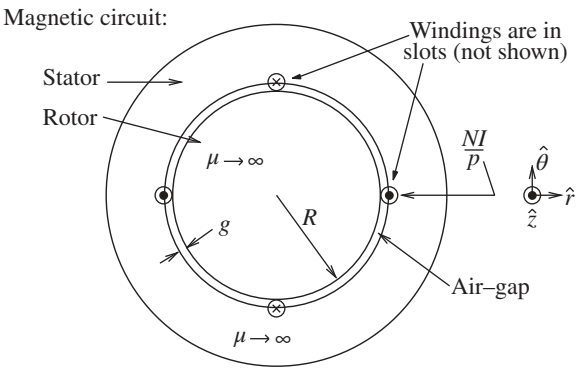

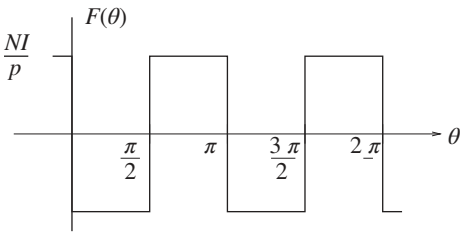

Figure 6.6 Air-gap MMF.

This distribution is a square wave in θ, as shown in Figure 6.6. If the air gap is narrow as shown in Figure 6.5, that is, $g \ll R$, the magnetic flux density in the air gap would be:

$$\vec{B} = -\vec{i}_r \sum_{n=1,odd}^{\infty} \frac{\mu_0}{g} \frac{4}{n\pi} \frac{N\,I}{2p} \sin np\theta \tag{6.2}$$

Note that a real winding, as shown above, won't be concentrated as in this example. Generally, it is possible to express the difference with a winding factor, as will be described below. But first, it is necessary to consider polyphase windings. Figures 6.2 and 6.4 show three-phase winding schemes. Note that the Phase B winding is displaced from Phase A by −120° and Phase C is also displaced from Phase B by the same amount. Suppose the three-phase windings have currents that are balanced and positive sequence:

$$I_a = I\cos(\omega t)$$
$$I_b = I\cos\left(\omega t - \frac{2\pi}{3}\right)$$
$$I_c = I\cos\left(\omega t + \frac{2\pi}{3}\right)$$

If this is the excitation, the flux density in the air gap is:

$$\vec{B} = -\vec{i}_r \sum_{n=1,odd}^{\infty} \frac{\mu_0}{g} \frac{4}{n\pi} \frac{N\,I}{2p} \left(\sin np\theta\ \cos\omega t + \sin n\left(p\theta - \frac{2\pi}{3}\right)\cos\left(\omega t - \frac{2\pi}{3}\right) + \sin n\left(p\theta + \frac{2\pi}{3}\right)\cos\left(\omega t + \frac{2\pi}{3}\right)\right) \tag{6.3}$$

After working through the trigonometry, which is modestly messy, the magnetic flux density is found to be:

$$\vec{B} = -\vec{i}_r \sum_n \frac{3}{2} \frac{\mu_0}{g} \frac{4}{n\pi} \frac{N\,I}{2p} \sin(np\theta - \omega t) \quad \text{for } n = 1, 7, 13, \ldots$$

$$\vec{B} = -\vec{i}_r \sum_n \frac{3}{2} \frac{\mu_0}{g} \frac{4}{n\pi} \frac{N\,I}{2p} \sin(np\theta + \omega t) \quad \text{for } n = 5, 11, \ldots \tag{6.4}$$

That is, for the space fundamental ($n = 1$) and higher harmonics of the order $6k+1$ (k is an integer), the field rotates in the forward direction at a speed inversely proportional to the harmonic order. For harmonics of the orders $6k-1$, the field rotates backward, also with a speed inversely proportional to the harmonic order. For negative sequence currents, for which I_b and I_c are reversed in order, the roles are reversed, and the $6k+1$ order harmonics go backward and $6k-1$ harmonics go forward. For zero sequence currents: $I_a = I_b = I_c = I\cos\omega t$, the flux density is nonzero only for the triplen harmonics (order $3k$, k an integer).

$$\vec{B} = -\vec{i}_r \sum_{n=3,6,9\ldots}^{\infty} 3\frac{\mu_0}{g} \frac{4}{n\pi} \frac{N\,I}{2p} \sin np\theta\ \cos\omega t \tag{6.5}$$

The pulsating sine wave can, of course, be split into one component rotating forward and another backward: $\sin np\theta \cos \omega t = \frac{1}{2}\sin(np\theta - \omega t) + \frac{1}{2}\sin(np\theta + \omega t)$.

A winding on the rotor, such as a field winding of a synchronous machine, would produce an air-gap field:

$$\vec{B} = -\vec{i}_r \sum_{n=1,odd}^{\infty} \frac{\mu_0}{g}\frac{4}{n\pi}\frac{N_f\, I_f}{2p}\sin np\theta' = -\vec{i}_r \sum_{n=1,odd}^{\infty} \frac{\mu_0}{g}\frac{4}{n\pi}\frac{N_f\, I_f}{2p}\sin n\ (p\theta - \omega t) \tag{6.6}$$

The next step is to find the flux linked. If air-gap flux density is of the form:

$$B_r = \sum_n B_n \sin(np\theta \pm \omega t)$$

Flux linked by a single turn, full-pitched winding is:

$$\boldsymbol{\Phi} = \int_0^{\frac{\pi}{p}} B_r R\ell\, d\theta \tag{6.7}$$

which, for this flux density, is:

$$\boldsymbol{\Phi} = 2R\ell \sum_n \frac{B_n}{np}\cos \omega t \tag{6.8}$$

This permits the calculation of self and mutual inductances, since winding flux is simply $\lambda = N\phi$.

The end of this is a set of expressions for various inductances. As shown at the beginning of this chapter, most windings are not full pitched or concentrated. Fortunately, these shortcomings can be accommodated by the use of winding factors.

The simplest and perhaps best definition of a winding factor is the ratio of flux linked by an actual winding to flux that would have been linked by a full-pitch, concentrated winding with the same number of turns. That is: $k_w = \lambda_{actual}/\lambda_{full-pitched}$.

It is relatively easy to show, using reciprocity arguments, that the winding factors are also the ratio of effective MMF produced by an actual winding to the MMF that would have been produced by the same winding were it to be full pitched and concentrated. The argument goes as follows: mutual inductance between any pair of windings is reciprocal. That is, if the windings are designated one and two, the mutual inductance is flux induced in winding one by current in winding two, and it is also flux induced in winding two by current in winding one. Since each winding has a winding factor that influences its linking flux, and since the mutual inductance must be reciprocal, the same winding factor must influence the MMF produced by the winding. The winding factors are often expressed for each space harmonic, although sometimes, when a winding factor is referred to without reference to a harmonic number, what is meant is the space factor for the space fundamental.

Two winding factors are commonly specified for ordinary, regular windings. These are usually called *pitch* and *breadth* factors, reflecting the fact that often windings are not full pitched, which means that individual turns do not span a full π electrical radians and that the windings occupy a range or breadth of slots within a phase belt. The breadth factors are ratios of flux linked by a given winding to the flux that would be linked by that winding were it full pitched and concentrated. These two winding factors are discussed in a little more detail below. What is interesting to note is that the winding factor of any given winding is the product of the pitch and breadth factors: $k_w = k_b k_p$.

6.4 Inductance

With winding factors as defined here, it is possible to define winding inductances. For example, the synchronous inductance of a winding will be the apparent inductance of one phase when the polyphase winding is driven by a balanced set of currents. This is, approximately, for a three-phase winding:

$$L_d = \sum_{n=1,5,7,\ldots}^{\infty} \frac{3}{2}\frac{4}{\pi}\frac{\mu_0 N^2 R\ell k_{wn}^2}{p^2 n^2 g} \tag{6.9}$$

This expression is approximate because it ignores the asynchronous interactions between higher-order harmonics and the rotor of the machine.

Zero-sequence inductance is the ratio of flux to current if a winding is excited by zero-sequence currents, as in:

$$L_0 = \sum_{n=3,9,\ldots}^{\infty} 3\frac{4}{\pi}\frac{\mu_0 N^2 R\ell k_{wn}^2}{p^2 n^2 g} \tag{6.10}$$

Mutual inductance, as between a field winding (f) displaced by an angle ϕ and an armature winding (a), is:

$$M(\phi) = \sum_{n=1,odd}^{\infty} \frac{4}{\pi}\frac{\mu_0 N_f N_a k_{fn} k_{an} R\ell}{p^2 n^2 g}\cos np\phi \tag{6.11}$$

6.4.1 Winding Factors

The winding factor can, for regular winding patterns, be expressed as the product of a pitch factor and a breadth factor, each of which can be estimated separately.

The pitch factor is found by considering the flux linked by a less-than-full-pitched winding. Consider the situation in which radial magnetic flux density is $B_r = B_n \sin(np\theta - \omega t)$. A winding with pitch α (see Figure 6.7, which illustrates this for a two-pole [$p = 1$] winding) will link flux:

$$\lambda = N\ell \int_{\frac{\pi-\alpha}{2p}}^{\frac{\pi+\alpha}{2p}} B_n \sin(np\theta - \omega t)\ R\ d\theta = \frac{2NR\ell}{np}\ \sin\left(\frac{n\pi}{2} - \omega t\right)\ \sin\frac{n\alpha}{2}$$

Noting that for a full-pitch coil, $\alpha = \pi$, the pitch factor for the n^{th} harmonic is then:

$$k_{pn} = \sin\frac{n\pi}{2} \tag{6.12}$$

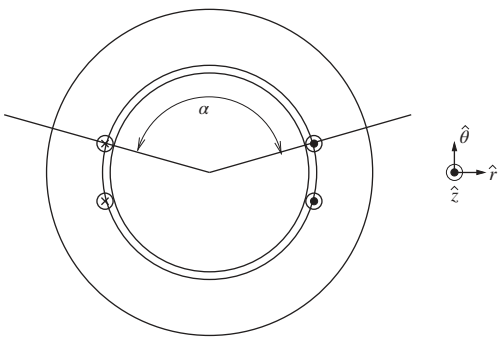

Figure 6.7 Illustration of short pitch winding.

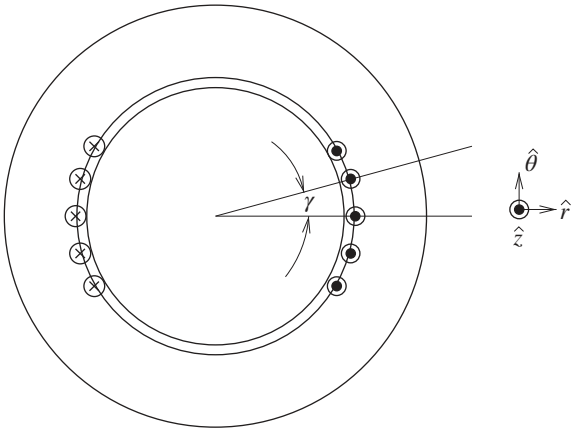

Figure 6.8 Distributed coils and coil breadth.

Now for the breadth factor. This describes the fact that a winding may consist of a number of coils, each linking flux slightly out of phase with the others. A regular winding will have a number (say m) of coil elements, separated by electrical angle γ, which is the *electrical* angle between slots. Figure 6.8 shows five coils separated by that angle γ.

A full-pitch coil with one side at angle ξ will, in the presence of magnetic flux density $B_r = B_n \sin(np\theta - \omega t)$, link flux:

$$\lambda = N\ell \int_{\frac{\xi}{p}}^{\frac{\pi-\xi}{p}} B_n \sin(np\theta - \omega t)\ R\, d\theta = \frac{2N\ell RB_n}{np} Re\left\{e^{j(\omega t - n\xi)}\right\}$$

The coils link fluxes that differ in phase, so the addition of flux is as shown in vector form in Figure 6.9. If the winding is distributed into m sets of slots and the slots are evenly spaced apart by angle γ, the angular position of each slot will be:

$$\xi_i = i\gamma - \frac{m-1}{2}\gamma$$

and the number of turns in each slot will be $\frac{N}{mp}$ so that actual flux linked will be:

$$\lambda = \frac{2N\ell RB_n}{n} \frac{1}{mp} \sum_{i=0}^{m-1} Re\left\{e^{(j\omega t - n\xi_i)}\right\}$$

From this, the breadth factor is:

$$k_{bn} = \frac{1}{m} \sum_{i=0}^{m-1} Re\left\{e^{-jn\xi_i}\right\} = Re\left\{\frac{1}{m} \sum_{i=0}^{m-1} e^{-jn\left(i\gamma - \frac{m-1}{2}\gamma\right)}\right\}$$

That can be re-cast as:

$$k_{bn} = \frac{e^{jn\gamma\frac{m-1}{2}}}{m} \sum_{i=0}^{m-1} e^{-jni\gamma}$$

Figure 6.9 Addition of flux phasors.

Focus on the sum: It is known that any converging geometric sum has the value:

$$\sum_{i=0}^{\infty} x^i = \frac{1}{1-x}$$

And then using the truncated sum:

$$\sum_{i=0}^{m-1} = \sum_{i=0}^{\infty} - \sum_{i=m}^{\infty}$$

Then the sum above can be written as:

$$\sum_{i=0}^{m-1} e^{jni\gamma} = (1 - e^{jnm\gamma}) \sum_{i=0}^{\infty} e^{jni\gamma} = \frac{(1 - e^{jnm\gamma})}{(1 - e^{jn\gamma})}$$

Then, using the definition of sine, the breadth factor is:

$$k_{bn} = \frac{\sin \frac{nm\gamma}{2}}{m \sin \frac{n\gamma}{2}} \tag{6.13}$$

6.4.2 Concentric Coils

For reasons of manufacturing economy, many electric motors are now wound with concentric coils, which do not fit easily into the pitch- and breadth-factor description given here. Such windings are called *concentric* because they can be described as being symmetric about an azimuthal position in the machine. They are commonly used in integral horsepower induction motors because they can be machine inserted. Such windings may also produce more sinusoidal waveforms. An example of the distinction between regular and concentric windings is shown in Figure 6.10. In each figure, one of the phase windings is highlighted and current flow directions are shown.

Typically, a phase winding would consist of some number of coils with (possibly) different numbers of turns in each. Assuming all of the coils are symmetrical about a common centerline, it is possible to describe them with a single winding factor analogous to either the pitch or breadth factor. Each of the coils will have a *coil throw*, or separation between the coil sides of some number of slots, and each coil will have a different coil throw.

If a complete phase winding has N_c coils, indexed by i, each of which has $N_s(i)$ turns and a coil throw of $N_t(i)$, the electrical angle between coils would be:

$$\alpha_i = \frac{2\pi p}{N_{slots}} N_i i$$

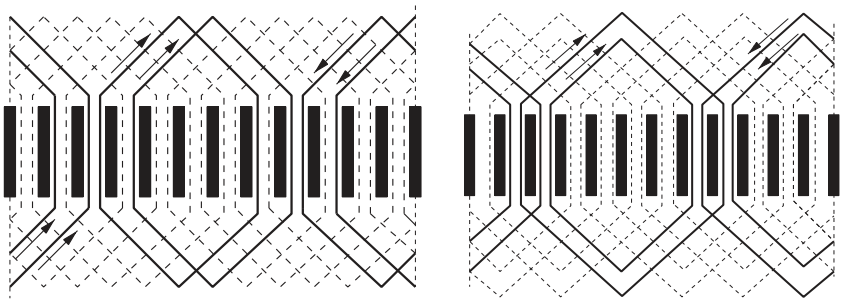

Figure 6.10 "Lap" vs. "concentric" windings.

The winding factor of that phase winding would be calculated similarly to the pitch factor for a "regular" winding, but with the pitch factors of the different coils weighted by their numbers of turns:

$$k_{wn} = \frac{\sum_{i=1}^{N_c} N_s(i) \sin\left(n\frac{\alpha_i}{2}\right)}{\sum_{i=1}^{N_c} N_s(i)} \tag{6.14}$$

6.4.3 Examples of Concentric Coils

To illustrate how concentric coils might be used in a machine, we use as an example a 36-slot, 4-pole induction motor. Such a machine would have 3 slots per pole per phase. Suppose a machine design were to call for 48 turns per coil times 3 coils per pole pair or a total of 288 turns per phase. Note this could be accomplished with a 2-layer lap winding with 24 turns per coil. With one turn short-pitched, the number of turns in the slots of each phase would be 24-48-48-24. The resulting overlap with the other two phases would result in 48 half turns in each slot.

A concentric winding for this case would be as shown in Figure 6.11. On the left is a representation of the complete winding, showing all three phases. On the right is a representation of one phase only, with three coils, each with 48 turns and having coil throws of 7, 9, and 11 slots, respectively. This one would have only two sets of coils, and would therefore have *consequent poles*. Because of the smaller number of coils, this winding would have an advantage in manufacturing cost, but it has higher order space harmonics that are larger than the short-pitched lap winding.

A somewhat more complicated winding scheme that has somewhat shorter end turns is accomplished by winding each of the four poles separately, so that there are four coil sets. Note that with three slots per pole per phase, there are two separate coils in some of the slots (the "middle" slot in the three slots per pole per phase). Thus, the middle coil has 24 turns in it, but since there are two such coils in this middle slot, there are still 48 conductors in that slot. This winding variation has four pole windings. It is represented, only for one phase, in Figure 6.12.

One interesting feature of concentric coils is that the number of turns in each coil can be varied to make the MMF more nearly sinusoidal. This is a bit like "short-pitching" in what we term "regular" windings. Figure 6.13 shows an alternative winding scheme that does this. Here, there are 4 coils per pole pair per phase; 2 coils have 48 turns, and 2 coils have 24 turns. The 24-turn coils overlap with similar coils in the other phases so that every slot has 48 conductors in it. Note that the inner and outer coils of the four-coil group share slots with the other phases. Note this winding has the same number of turns in each slot as does the short-pitched lap winding and consequently has the same winding factors.

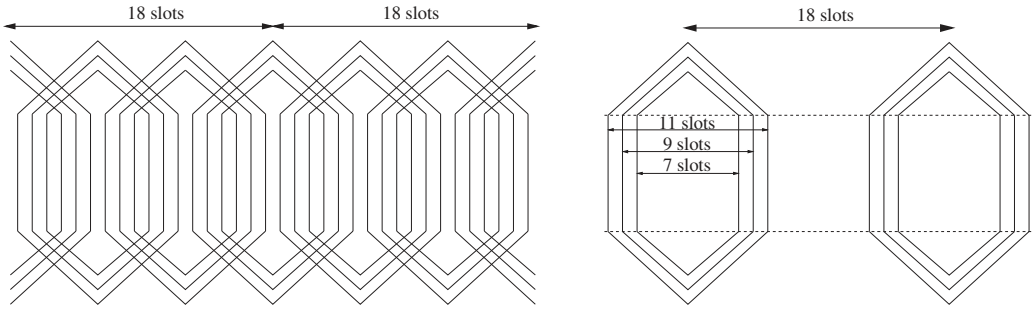

Figure 6.11 Consequent pole winding.

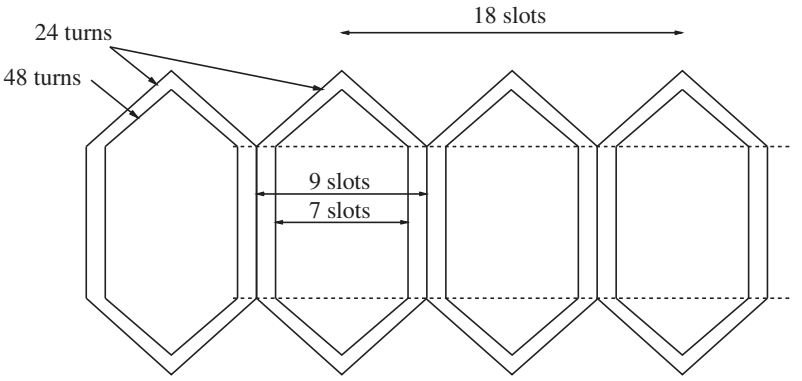

Figure 6.12 Non-consequent pole winding scheme.

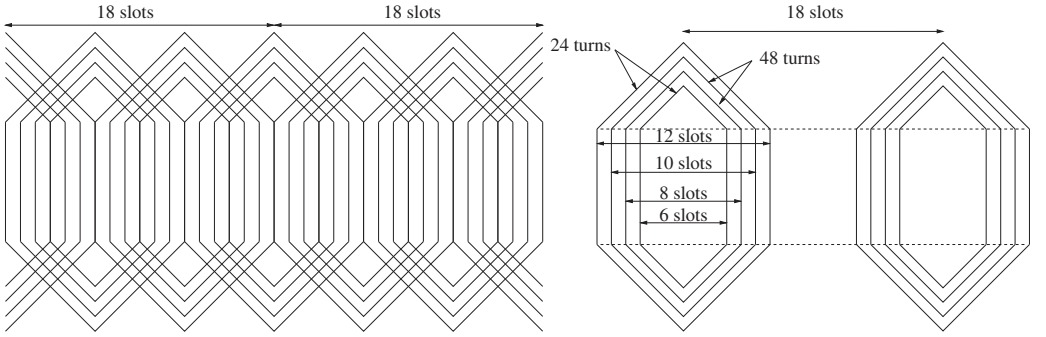

Figure 6.13 Four-coil consequent pole winding.

6.4.4 Concentrated, Partial Pitch Windings

One particular type of "concentric" winding is the concentrated, partial pitch winding as used in machines like the one illustrated in Figure 6.14. This sort of winding is used mainly in permanent magnet motors, and this figure illustrates a situation with consequent poles as well. That is, there is no phase A′, but flux from Phase A must return through the other two phases. Note that this does, indeed, work, as the three-phase fluxes add to zero. In this case, if the gap between teeth is small, the electrical angle subtended by each pole face would be 120°, so the "pitch" factor would be:

$$k_p = \sin\left(\frac{120}{2}\right) = 0.866 \tag{6.15}$$

Of course, there is no relevant breadth factor here, or the breadth factor is unity. In this configuration, there are two coils per phase, and they link flux in the same electrical phase. This is not universally true: there are configurations in which coils in series may not be strictly in time phase, so breadth factor may have to be considered. But those machines are beyond our scope. Making up for the somewhat reduced pitch factor is the fact that the end turns of this sort of machine can be quite short, as they do not overlap with end turns of other coils.

6.4.5 Higher-Phase Order

So far, only three-phase machines have been considered. Higher numbers of phases can and are sometimes used for electric machines. As an example, consider the machine shown in Figure 6.15,

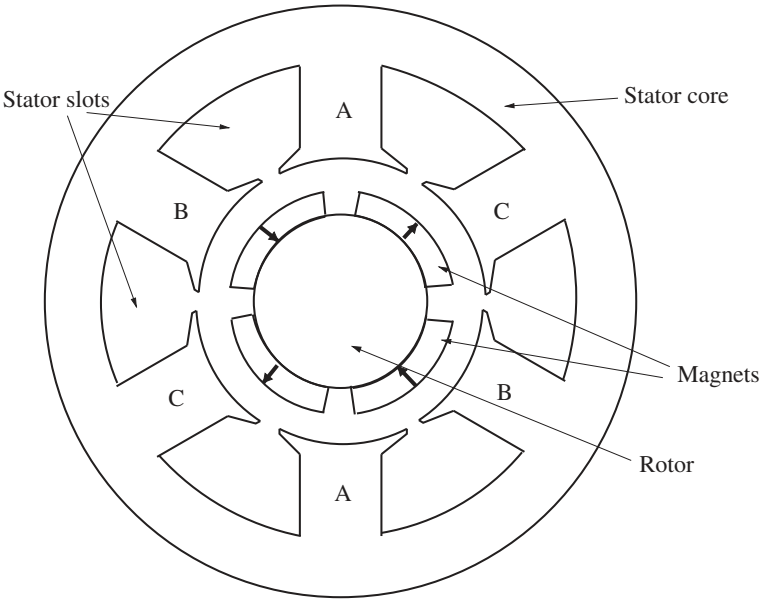

Figure 6.14 Three-phase, four-pole machine with concentrated, partial pitch winding.

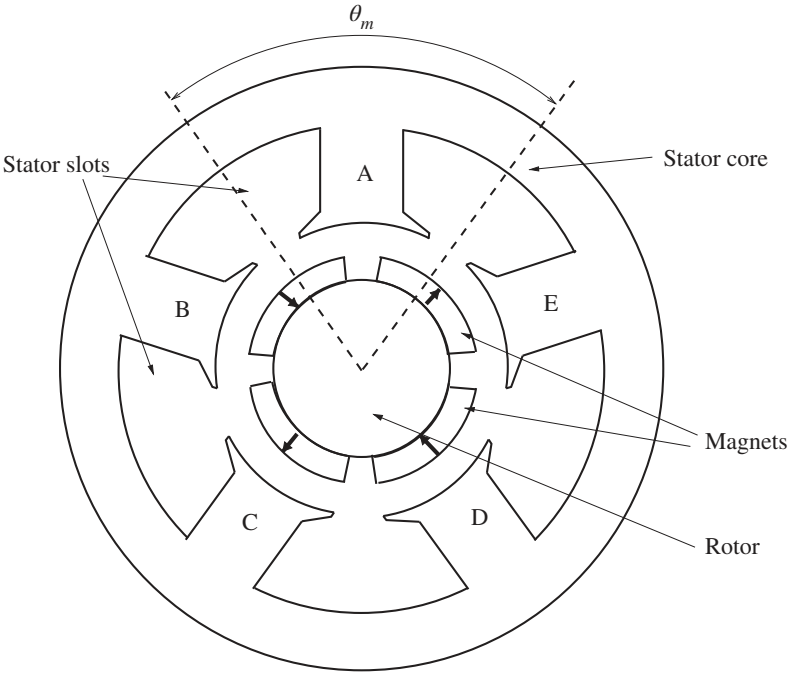

Figure 6.15 Five-phase, four-pole machine.

which shows in cartoon form a four-pole, five-phase machine. A full explication of machines with more than three phases is beyond the scope of this text, but it is possible to point out a few salient issues.

With stator teeth (or, if one prefers, pole pieces) that subtend nearly the available periphery per pole (that is actually wider than is shown in the figure), the mechanical angle of the poles would be

$$\theta_m = \frac{360^\circ}{5} = 72^\circ$$

So that the pitch factor is:

$$k_p = \sin\left(\frac{p\theta_m}{2}\right) = \sin\left(\frac{2 \times 72^\circ}{2}\right) = 0.951$$

For three phases, rotation of the various space harmonics is described by Equations (6.3) and (6.4) above. For higher number of phases, the gap MMF could be described as, for each space harmonic n, as the sum of MMFs from all phases, if N_ϕ is the number of phases:

$$F_n = \sum_{k=0}^{N_\phi - 1} \angle F_n \cos\left(\omega t - k\frac{2\pi}{N_\phi}\right) \cos n\left(p\theta - k\frac{2\pi}{N_\phi}\right) \tag{6.16}$$

This can be broken down into traveling waves:

$$F_n = \sum_{k=0}^{N_\phi - 1} \frac{\angle F_n}{2}\left(\cos\left(\omega t + np\theta + k(1+n)\,\frac{2\pi}{N_\phi}\right) + \cos\left(\omega t - np\theta + k(1-n)\,\frac{2\pi}{N_\phi}\right)\right) \tag{6.17}$$

The result depends on the space harmonic order:

$$\begin{aligned}
&\text{if } (1+n) = k \times N_\phi \ (k \text{ integer}) \quad \text{and } (1-n) \neq kN_\phi \\
&\qquad F_n = \frac{N_\phi}{2} \angle F_n \cos(\omega t + np\theta) \\
&\text{if } (1-n) = k \times N_\phi \ (k \text{ integer}) \quad \text{and } (1+n) \neq kN_\phi \\
&\qquad F_n = \frac{N_\phi}{2} \angle F_n \cos(\omega t - np\theta)
\end{aligned} \tag{6.18}$$

So, for a three-phase machine, we have forward traveling waves for $n = 1, 7, 13$, etc., and backward traveling waves for $n = 5, 11$, etc. For the five-phase machine, forward waves are for space harmonics of order $n = 1, 6, 11, 16, 21, \ldots$ and backward waves for $n = 4, 9, 14, 19, \ldots$ Note that the condition for space harmonic order is sometimes met for even harmonics, which are normally zero for ordinary windings, but not necessarily so for concentrated pole, partial pitch windings with consequent poles, as shown in Figure 6.15.

6.4.6 Sequences

Most of this discussion assumes that currents in the polyphase windings are of (normal) positive sequence. Consider the two phasor diagrams shown in Figure 6.16. In a three-phase system, the positive sequence is A, B, C, with 120 electrical degrees between the three phases. Positive sequence results in a rotation in the positive direction. Negative sequence reverses the order of phases and results in rotation in the negative direction. (Which is why, if a motor turns in the wrong direction, exchanging two of the phase leads will fix the problem.) If all three phase windings have

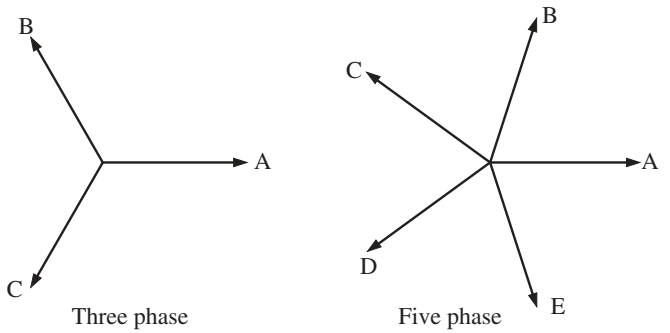

Figure 6.16 Phasor diagrams for three and five phases.

currents in phase with each other, this is called "zero sequence." In zero sequence, as described by Equation (6.5), the space fundamental and many of the space harmonics cancel, leading to a pulsating pattern of harmonic fields. In three-phase machines, the fields from zero sequence are of order 3 and multiples of 3 ("triplens"). It is possible to show that all patterns of current can be made up of these three "sequences," called *symmetrical components*. Negative sequence currents impose fields rotating backward and so at relatively high frequencies in the rotor surface, and in the reverse direction, and so have negative impact on machines, through production of reverse torque and rotor heating.

Five-phase systems have five sequences: (A, B, C, D, E); (A, C, E, B, D); (A, D, B, E, C); (A, E, D, C, B); and all five in phase (zero sequence). The first of these sets is positive sequence, so currents rotate forward at synchronous speed; the fourth is negative sequence (reverse at synchronous speed) and the two others are rotations at twice synchronous speed, forward and backward.

6.5 Stator Slot Leakage

Currents in the stator slots produce fluxes that link the stator conductors but not the rotor. To estimate these fluxes, refer to the slot geometry shown in Figure 6.17. This shows a possibly unrealistic straight-sided stator slot. Typical in induction machines is for such slots to be trapezoidal in shape. A more careful field analysis shows that this analysis will be no more than a few percent in error if the slot width used in the calculation is the slot top (the end of the slot closest to the air gap). There are five important dimensions here: the slot height h, width w, and the slot depression height d and width u, and (not shown) length ℓ. To estimate slot leakage inductance, assume some current in the slot, calculate the magnetic energy that results and then use $w_m = {}^1\!/_2 L_\ell I^2$.

Figure 6.17 Stator slot geometry.

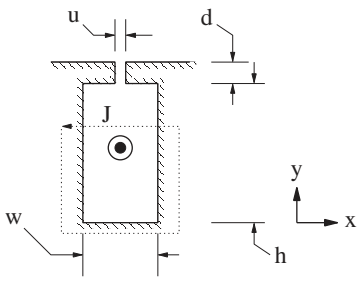

If there are N conductors in the slot, each carrying current I, the current density in the slot is:

$$J = \frac{NI}{h\ w}$$

Using Ampere's law around a loop (shown dotted in the figure), magnetic field in the x direction at height y from the bottom of the slot is:

$$H_x = -\frac{NI}{w}\frac{y}{h}$$

In the slot depression:

$$H_{xd} = -\frac{NI}{u}$$

Magnetic energy stored in the slot and slot depression are then:

$$w_m = w\ell \int_0^h \frac{1}{2}\mu_0 H_x^2 dy + ud\ell \frac{1}{2}\mu_0 H_{xd}^2 = \frac{1}{2}\ell\mu_0\left(\frac{1}{3}\frac{h}{w} + \frac{d}{u}\right)N^2 I^2$$

Noting the slot permeance as:

$$\wp_s = \ell\mu_0\left(\frac{1}{3}\frac{h}{w} + \frac{d}{u}\right) \tag{6.19}$$

Total inductance in the slot is $L_\ell = \wp_s N^2$

There are many different forms of stator winding, and this discourse won't be able to disclose them all, but for the purpose of this discussion, assume an ordinary two-layer winding consisting of coils of N_c turns each, with two half coils in each slot. For such a winding, if there are m slots per pole per phase and p pole pairs and if the winding is short-pitched by N_{sp} slots, there will be $2p(m - N_{sp})$ slots per phase with two coils from the same phase and $2pN_{sp}$ slots per phase sharing another phase. (Assume here a three-phase machine.) Total number of turns in each phase would then be $N_a = 2pmN_c$. Then the "self" slot leakage inductance must be:

$$L_{s\ell} = \wp_s\left(4N_c^2 2p(\ m - N_{sp}) + 2pN_{sp}N_c^2\right)$$

Since there are a total of pN_{sp} "mutual" slots between each pair of phases, and the sense of the windings is opposite, the mutual component of slot leakage is:

$$L_{m\ell} = -\wp_s pN_{sp}N_c^2$$

Total slot leakage is:

$$L_\ell = L_{s\ell} - L_{m\ell} = \wp_s pN_c^2(8m - 5N_{sp}) \tag{6.20}$$

6.6 Problems

Problems 6.1–6.5: These problems are based on the structure shown in the Figure 6.18. Assume the thing has length $\ell = 10$ cm, rotor radius $R = 6.3$ cm, air gap $g = 0.3$ mm, and use the fact that $g \ll R$. This is a four-pole machine ($p = 2$). This is actually an approximation to a real traction motor. But we will approach it in a couple of very approximate ways.

6.1 Assume that there is a single coil around each pole as shown in Figure 6.18. Thus, there are four "slots" with two coil halves in each slot. Compute and plot the magnetic flux density

Figure 6.18 Four-pole concentrated coils.

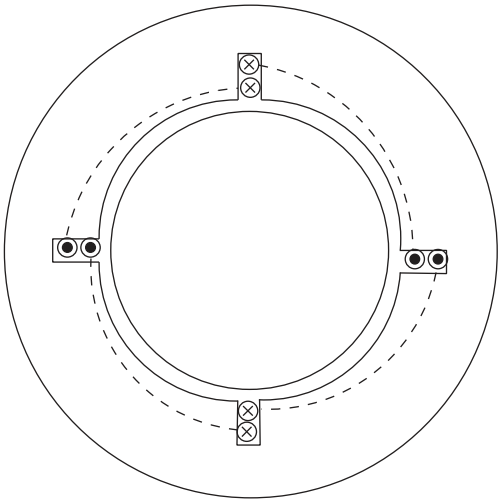

produced across the air gap. Assume each coil has 16 turns and that the coils are connected in series. The winding is carrying a current of 14 A. Assume that slot width is negligible and that the permeability of both rotor and stator iron is high enough that it can be ignored.

6.2 Express the air-gap flux density as a Fourier series. Get your favorite mathematical assistant to plot the sum of the first several terms of this series (Orders 1, 3, 5, 7, 11, 13). That is, the sum of the first six nonzero *space harmonics*. Compare the sum of the Fourier series with the "exact" solution. (Ignore the width of the slots.)

6.3 Assume now a three-phase version of this winding structure. Now there are 12 slots and the 3 phases are appropriately placed. Draw the flux density at the time that current in Phase A peaks. (Current in phases B and C are minus one-half of the current in Phase A.)

6.4 Compute and plot the Fourier series for the situation of Problem 6.3.

6.5 Considering separately the first, third, fifth, and seventh space harmonics. Assume that there is a three-phase winding, driven by a balanced set of currents:

$$I_a = I\cos\omega t, I_b = I\cos(\omega t - 2\pi/3), I_c = I\cos(\omega t + 2\pi/3)$$

Show that the first and seventh space harmonic fields rotate forward, that the fifth harmonic field rotates backward, and that the third harmonic field is zero.

6.6 Assume something closer to an actual three-phase winding, located in 48 slots. This yields $m = 4$ slots per pole per phase, each coil having $N_c = 4$ turns. (What is the angular spacing between slots if this is to be a regular three-phase winding?) With current $I = 14$ A in each coil of one phase, find the amplitude of the space harmonics of order $n = 1$, $n = 5$, and $n = 7$ for the magnetic flux density produced across the air gap for these cases:

- The winding is full pitched
- The winding is short pitched by one slot

- The winding is short pitched by two slots
- The winding is short pitched by three slots
- The winding is short pitched by four slots

6.7 If you consider only the space fundamental, what is the synchronous reactance of the complete three-phase winding?

6.8 Calculate, for the motor described above, the pitch and breadth factors for each of the windings: full pitch, 11/12 pitch, 5/6 pitch, 9/12 pitch, 2/3 pitch. Do this for each of the space harmonics of order 1, 5, 7, 11, 13, 23, and 25. Calculate the "synchronous" reactance components for each of the space harmonics for which you have winding factor.

6.9 Consider a winding structure that is 2-pole and has 36 slots. Diameter is 10 cm and length is 20 cm. Gap clearance is 0.5 mm. Each phase winding is concentric, and the coils of Phase A have the following number of turns: 2-2-4-4-4-4-2-2.

a) Draw a picture of this winding and convince yourself that a three-phase, two-pole winding will fit into a 36-slot stator.
b) If the air-gap flux density is sinusoidal and has a peak value of 1.0 T, what is the voltage induced in one phase of this winding if the field is rotating at 30,000 RPM?
c) Compute the synchronous reactance of a three-phase winding at a frequency of 500 Hz. (Consider only the space fundamental.)
d) Compute the winding factors for harmonics of order 1, 5, 7, 35, and 37.

6.10 This problem is about a five-phase, two-pole winding in 30 slots. Assume a rotor diameter of 10 cm, rotor length of 20 cm, and gap of 0.5 mm.

a) Draw a phasor diagram for a balanced, five-phase set of currents.
b) Assume a full-pitched winding with 30 turns per phase. What is the inductance of one phase?
c) Compute the synchronous inductance of this structure. Note that the factor of 1.5 used in three-phase machines is not applicable to five phases. What is the correct factor?
d) In a three-phase winding, with balanced current excitation, the lowest order harmonic that rotates forward is first, and the next order forward rotating harmonic is seventh. The lowest negatively rotating harmonic is the fifth. And all of the triplens (order of three, six, nine, etc.) have zero amplitude. What are the comparable orders for this five-phase winding?

6.11 A three-phase, two-pole winding in 36 slots has a number of turns in a concentric winding of 2-2-4-4-4-4-2-2. Note that this has the same number of turns in each slot as would a six slot per pole per phase, two-layer winding with 2 turns per coil and a short pitch of 2 slots.

a) Compute the winding factors for harmonics of order 1, 5, and 7, assuming a concentric winding.
b) Compute the pitch and breadth factors for the same harmonics, assuming six slots per pole per phase ($m = 6$) and short pitch by two slots. Do you get the same winding factor?

6.12 This problem concerns a three-phase, four-pole winding in 48 slots with 72 turns per phase.

a) Make a sketch of this winding, assuming it to be full pitch.
b) What are the winding factors for space harmonics of order 1, 5, 7, 23, and 25?

c) Get the same winding factors for a short pitch of two slots.
d) Get the same winding factors for a short pitch of four slots.

Now the winding is to be re-distributed as a concentric winding with turns of 6-12-18-18-12-6.

a) Convince yourself that this is a valid winding by showing that the three phases fit together with a total of 18 turn halves per slot.
b) Compute the winding factor for harmonics of order 1, 5, 7, 23, and 25.

7

Synchronous Machine Dynamic Models

7.1 Introduction

This chapter develops models useful for calculating the dynamic behavior of synchronous machines. It starts with a commonly accepted picture of the synchronous machine, assuming that the rotor can be fairly represented by three equivalent windings: one being the field and the other two are *d*- and *q*-axes "damper" windings, representing the effects of rotor body, wedge chain, amortisseur, and other current-carrying paths. In some cases, deliberately included damper windings are included in synchronous machines.

While a synchronous machine is assumed here, the results are fairly directly applicable to induction machines. Also, extension to situations in which the rotor representation must have more than one extra equivalent winding per axis is straightforward.

To start, refer to Figure 7.1, which shows six coils. There are three-phase windings of the *stator*. On the *rotor* are the field winding, which is assumed to have a direct current supply, and two equivalent damper windings; one on the direct axis and therefore coupled to the field, and one on the quadrature axis, leading the field by 90 electrical degrees. Not shown in the figure, but generally assumed, the two damper windings are shorted through their own resistances.

7.2 Phase Variable Model

Fluxes in the six windings (or equivalent windings) are, in terms of currents:

$$\begin{bmatrix} \underline{\lambda}_{ph} \\ \underline{\lambda}_{R} \end{bmatrix} = \begin{bmatrix} \underline{L}_{ph} & \underline{M} \\ \underline{M}^{T} & \underline{L}_{R} \end{bmatrix} \begin{bmatrix} \underline{I}_{ph} \\ \underline{I}_{R} \end{bmatrix} \tag{7.1}$$

where phase and rotor fluxes (and similarly currents) are:

$$\underline{\lambda}_{ph} = \begin{bmatrix} \lambda_a \\ \lambda_b \\ \lambda_c \end{bmatrix} \quad \underline{\lambda}_{R} = \begin{bmatrix} \lambda_f \\ \lambda_{kd} \\ \lambda_{kq} \end{bmatrix}$$

and the inductance matrix has three sub-matrices. The first of these describes the armature winding self and mutual inductances:

$$\underline{L}_{ph} = \begin{bmatrix} L_a & L_{ab} & L_{ac} \\ L_{ab} & L_b & L_{bc} \\ L_{ac} & L_{bc} & L_c \end{bmatrix} \tag{7.2}$$

Electromagnetic Analysis of Electric Machines: First Principles, Modeling, and Design, First Edition.
James L. Kirtley, Christopher H. T. Lee, and Sajjad Mohammadi.

Companion website: www.wiley.com/go/kirtleyelectric

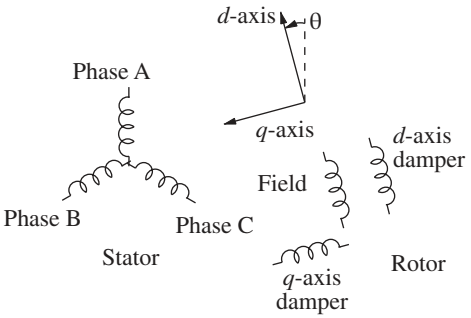

Figure 7.1 Elements of the machine model.

Where, for a machine that might have some saliency:

$$\begin{aligned}
L_a &= L_{a0} + L_2 \cos 2\theta \\
L_b &= L_{a0} + L_2 \cos 2\left(\theta - \frac{2\pi}{3}\right) \\
L_c &= L_{a0} + L_2 \cos 2\left(\theta + \frac{2\pi}{3}\right) \\
L_{ab} &= L_{ab0} + L_2 \cos 2\left(\theta - \frac{\pi}{3}\right) \\
L_{bc} &= L_{ab0} + L_2 \cos 2\theta \\
L_{ac} &= L_{ab0} + L_2 \cos 2\left(\theta + \frac{\pi}{3}\right)
\end{aligned} \tag{7.3}$$

Note that, in this last set of expressions, a particular form for the mutual inductances has been assumed. This is seemingly restrictive, because it constrains the form of phase-to-phase mutual inductance variations with rotor position. The coefficient L_2 is actually the same in all six of these last expressions. As it turns out, this assumption does not unduly restrict the accuracy of the model very much. We will have more to say about this a bit later.

The rotor inductances are relatively simply stated:

$$\underline{L}_R = \begin{bmatrix} L_f & L_{fkd} & 0 \\ L_{fkd} & L_{kd} & 0 \\ 0 & 0 & L_{kq} \end{bmatrix} \tag{7.4}$$

And the stator to rotor mutual inductances are:

$$\underline{M} = \begin{bmatrix} M\cos\theta & L_{akd}\cos\theta & -L_{akq}\sin\theta \\ M\cos\left(\theta - \frac{2\pi}{3}\right) & L_{akd}\cos\left(\theta - \frac{2\pi}{3}\right) & -L_{akq}\sin\left(\theta - \frac{2\pi}{3}\right) \\ M\cos\left(\theta + \frac{2\pi}{3}\right) & L_{akd}\cos\left(\theta + \frac{2\pi}{3}\right) & -L_{akq}\sin\left(\theta + \frac{2\pi}{3}\right) \end{bmatrix} \tag{7.5}$$

7.3 Two-Reaction Theory

The first step in the development of a suitable model is to transform the armature winding variables to a coordinate system in which the rotor is stationary. Equivalent armature windings are identified in the direct and quadrature axes. The direct axis armature winding is the equivalent of one of the phase windings, but aligned directly with the field. The quadrature winding is situated so that its axis leads the field winding by 90 electrical degrees. The transformation used to map the armature currents, fluxes, and so forth onto the direct and quadrature axes is the celebrated

Park's transformation, named after Robert H. Park, an early investigator into transient behavior in synchronous machines. The mapping takes the form:

$$\begin{bmatrix} u_d \\ u_q \\ u_0 \end{bmatrix} = \underline{u}_{dq} = \underline{\underline{T}}\underline{u}_{ph} = \underline{\underline{T}} \begin{bmatrix} u_a \\ u_b \\ u_c \end{bmatrix} \tag{7.6}$$

where the transformation and its inverse are:

$$\underline{\underline{T}} = \frac{2}{3}\begin{bmatrix} \cos\theta & \cos\left(\theta - \frac{2\pi}{3}\right) & \cos\left(\theta + \frac{2\pi}{3}\right) \\ -\sin\theta & -\sin\left(\theta - \frac{2\pi}{3}\right) & -\sin\left(\theta + \frac{2\pi}{3}\right) \\ \frac{1}{2} & \frac{1}{2} & \frac{1}{2} \end{bmatrix}$$

$$\underline{\underline{T}}^{-1} = \begin{bmatrix} \cos\theta & -\sin\theta & 1 \\ \cos\left(\theta - \frac{2\pi}{3}\right) & -\sin\left(\theta - \frac{2\pi}{3}\right) & 1 \\ \cos\left(\theta + \frac{2\pi}{3}\right) & -\sin\left(\theta + \frac{2\pi}{3}\right) & 1 \end{bmatrix} \tag{7.7}$$

This transformation maps balanced sets of phase currents into constant currents in the d-q frame. That is, if the rotor angle is $\theta = \omega t + \theta_0$, and the phase currents are:

$$I_a = I\cos\omega t \quad I_b = I\cos\left(\omega t - \frac{2\pi}{3}\right) \quad I_c = I\cos\left(\omega t + \frac{2\pi}{3}\right)$$

The transformed set of currents is:

$$I_d = I\cos\theta_0 \quad I_q = -I\sin\theta_0$$

Now apply this transformation to the top half of the complete machine flux/current relationship:

$$\underline{\lambda}_{ph} = \underline{\underline{L}}_{ph}\underline{I}_{ph} + \underline{\underline{M}}\underline{I}_R \tag{7.8}$$

The material in this subsection is framed in terms of three-phase ($q = 3$) machine theory, but it is actually generalizable to an arbitrary number of phases. Assume a machine whose three-phase armature can be characterized by internal fluxes and inductances that are functions of rotor position. Stator fluxes are:

$$\underline{\lambda}_{ph} = \underline{\underline{L}}_{ph}\underline{I}_{ph} + \underline{\lambda}_R \tag{7.9}$$

The transformed flux is obtained by pre-multiplying this whole expression by the transformation matrix. Phase current may be obtained from d to q current by multiplying by the inverse of the transformation matrix. Thus:

$$\underline{\lambda}_{dq} = \underline{\underline{T}}\,\underline{\lambda}_{ph} = \underline{\underline{T}}\,\underline{\underline{L}}_{ph}\underline{\underline{T}}^{-1}\underline{I}_{dq} + \underline{\underline{T}}\,\underline{\underline{M}}\,\underline{I}_R \tag{7.10}$$

The same process carried out for the lower half of the flux–current relationship yields:

$$\underline{\lambda}_R = \underline{\underline{M}}^T\underline{\underline{T}}^{-1}\underline{I}_{dq} + \underline{\underline{L}}_R\underline{I}_R \tag{7.11}$$

The fully transformed flux–current relationship is:

$$\begin{bmatrix} \underline{\lambda}_{dq} \\ \underline{\lambda}_{R} \end{bmatrix} = \begin{bmatrix} \underline{L}_{dq} & \underline{L}_{C} \\ \frac{3}{2}\underline{L}_{C} & \underline{L}_{R} \end{bmatrix} \begin{bmatrix} \underline{I}_{dq} \\ \underline{I}_{R} \end{bmatrix} \tag{7.12}$$

where the two new sub-matrices are:

$$\underline{L}_{dq} = \begin{bmatrix} L_d & 0 & 0 \\ 0 & L_q & 0 \\ 0 & 0 & L_0 \end{bmatrix} \quad \underline{L}_{C} = \begin{bmatrix} M & L_{akd} & 0 \\ 0 & 0 & L_{akq} \\ 0 & 0 & 0 \end{bmatrix} \tag{7.13}$$

where the component inductances are:

$$L_d = L_{a0} - L_{ab0} + \frac{3}{2}L_2 \quad L_q = L_{a0} - L_{ab0} - \frac{3}{2}L_2 \quad L_0 = L_{a0} + 2\,L_{ab0} \tag{7.14}$$

Note that some algebraic manipulation has been left out here.

The apparently restrictive assumptions embedded in the form of armature inductances have resulted in the very simple form of the expressions for the *d*, *q,* and 0 inductances. In particular, they result in three mutually independent sets of fluxes and currents. While there may be some concern about the restrictiveness of these expressions, note that the orthogonality between the *d*- and *q*-axes is not unreasonable. In fact, because these axes are orthogonal in space, it seems reasonable that they should not have mutual flux linkages. Given this decoupling, the flux/current relationships can be expressed for the three axes as:

$$\begin{bmatrix} \lambda_d \\ \lambda_{kd} \\ \lambda_f \end{bmatrix} = \begin{bmatrix} L_d & L_{akd} & M \\ \frac{3}{2}L_{akd} & L_{kd} & L_{fkd} \\ \frac{3}{2}M & L_{fkd} & L_f \end{bmatrix} \begin{bmatrix} I_d \\ I_{kd} \\ I_f \end{bmatrix}$$

$$\begin{bmatrix} \lambda_q \\ \lambda_{kq} \end{bmatrix} = \begin{bmatrix} L_q & L_{akq} \\ \frac{3}{2}L_{akq} & L_{kq} \end{bmatrix}$$

$$\lambda_0 = L_0 I_0 \tag{7.15}$$

The principal consequence of these assumptions is the decoupling of the zero-sequence component of flux from the *d*- and *q*-axis components. We are not in a position at this time to determine the reasonableness of this. However, it should be noted that departures from this form (that is, coupling between the "direct" and "zero" axes) must be through higher harmonic fields that will not couple well to the armature, so that any such coupling will be weak.

7.3.1 Speed Voltage

Next, armature voltage is given by:

$$\underline{V}_{ph} = \frac{d\underline{\lambda}_{ph}}{dt} + \underline{R}_{ph}\underline{I}_{ph} = \frac{d}{dt}\underline{T}^{-1}\underline{\lambda}_{dq} + \underline{R}_{ph}\underline{T}^{-1}\underline{I}_{dq} \tag{7.16}$$

And the transformed armature voltage must be:

$$\underline{V}_{dq} = \underline{T}\,\underline{V}_{ph} = \underline{T}\,\frac{d}{dt}\left(\underline{T}^{-1}\underline{\lambda}_{dq}\right) + \underline{T}\,\underline{R}_{ph}\underline{T}^{-1}\,\underline{I}_{dq} \tag{7.17}$$

The component parts of this expression are:

$$\underline{T}\frac{d}{dt}\left(\underline{T}^{-1}\underline{\lambda}_{\underline{dq}}\right) = \frac{d\underline{\lambda}_{\underline{dq}}}{dt} + \left(\underline{T}\frac{d}{dt}\underline{T}^{-1}\right)\lambda_{dq}$$

$$\underline{T}\frac{d}{dt}\underline{T}^{-1} = \begin{bmatrix} 0 & -\frac{d\theta}{dt} & 0 \\ \frac{d\theta}{dt} & 0 & 0 \\ 0 & 0 & 0 \end{bmatrix}$$

$$\underline{T}\,\underline{R}_{ph}\underline{T}^{-1} = \underline{T}\begin{bmatrix} R_a & 0 & 0 \\ 0 & R_a & 0 \\ 0 & 0 & R_a \end{bmatrix}\underline{T}^{-1} = \begin{bmatrix} R_a & 0 & 0 \\ 0 & R_a & 0 \\ 0 & 0 & R_a \end{bmatrix} \tag{7.18}$$

So that the voltages are, using $\frac{d\theta}{dt} = \omega$

$$V_d = \frac{d\lambda_d}{dt} - \omega\lambda_q + R_a I_d$$

$$V_q = \frac{d\lambda_q}{dt} + \omega\lambda_d + R_a I_q \tag{7.19}$$

7.4 Power and Torque

Instantaneous power is given by:

$$P = V_a I_a + V_b I_b + V_c I_c = \frac{3}{2}V_d I_d + \frac{3}{2}V_q I_q + 3V_0 I_0$$

which is, in turn,

$$P = \frac{3}{2}\omega(\lambda_d I_q - \lambda_q I_d) + \frac{3}{2}\left(\frac{d\lambda_d}{dt} + \frac{d\lambda_q}{dt}\right) + 3\frac{d\lambda_0}{dt} \tag{7.20}$$

Noting that electrical speed ω and shaft speed Ω are related by $\omega = p\Omega$ and that the expression above describes electrical terminal power as the sum of shaft power and rate of change of stored energy, it is possible to deduce that torque is given by:

$$T = \frac{3}{2}p(\lambda_d I_q - \lambda_q I_d) \tag{7.21}$$

7.5 Per-Unit Normalization

Per-unit Systems were introduced in Chapter 5, but require some amplification here to get the "base" quantities right. There are some nuances in normalization when considering coupling between the stator and rotor. The first step in normalization is to establish a set of base quantities. In most cases, voltage, current, flux, power, impedance, and torque are normalized, but time and frequency are not. Note that the base quantities are not independent of each other. In fact, for the armature, specify three quantities: voltage (V_B), current (I_B), and frequency (ω_0). Given these, the other base quantities are:

$$\text{Base } \textit{Power} \quad P_B = \frac{3}{2}V_B I_B$$

$$\textit{Base} \text{ Impedance} \quad Z_B = \frac{V_B}{I_B}$$

$$\text{Base Flux} \quad \lambda_B = \frac{V_B}{\omega_0}$$
$$\text{Base } \textit{Torque} \quad T_B = \frac{p}{\omega_0} P_B \tag{7.22}$$

Note that, for this purpose, base voltage and current are expressed as peak quantities. Base voltage is taken on a phase basis (line to neutral for a wye connected machine), and base current is similarly taken on a phase basis (line current for a wye connected machine). Normalized, or per-unit quantities are derived by dividing the ordinary variable (with units) by the corresponding base. For example, per-unit flux is:

$$\psi = \frac{\lambda}{\lambda_B} = \frac{\omega_0 \lambda}{V_B} \tag{7.23}$$

In this derivation, per-unit quantities will usually be designated by lowercase letters. Two notable exceptions are flux, where the letter ψ is used, and torque, where the upper-case T is used, risking confusion.

Note that there will be base quantities for voltage, current, and frequency for each of the different coils represented in our model. While it is reasonable to expect that the frequency base will be the same for all coils in a problem, the voltage and current bases may be different. The normalized flux/current relationship for the d-axis becomes:

$$\begin{bmatrix} \psi_d \\ \psi_{kd} \\ \psi_f \end{bmatrix} = \begin{bmatrix} \frac{\omega_0 I_{dB}}{V_{db}} L_d & \frac{\omega_0 I_{kB}}{V_{db}} L_{akd} & \frac{\omega_0 I_{fB}}{V_{db}} M \\ \frac{\omega_0 I_{dB}}{V_{kb}} \frac{3}{2} L_{akd} & \frac{\omega_0 I_{kB}}{V_{kb}} L_{kd} & \frac{\omega_0 I_{fB}}{V_{kb}} L_{f\,kd} \\ \frac{\omega_0 I_{dB}}{V_{fb}} \frac{3}{2} M & \frac{\omega_0 I_{kB}}{V_{fb}} L_{fkd} & \frac{\omega_0 I_{fB}}{V_{fb}} L_f \end{bmatrix} \begin{bmatrix} I_d \\ I_{kd} \\ I_f \end{bmatrix} \tag{7.24}$$

This becomes, noting the normalized reactances:

$$\begin{bmatrix} \psi_d \\ \psi_{kd} \\ \psi_f \end{bmatrix} = \begin{bmatrix} x_d & x_{akd} & x_{ad} \\ x_{akd} & x_{kd} & x_{fkd} \\ x_{ad} & x_{fkd} & x_f \end{bmatrix} \begin{bmatrix} I_d \\ I_{kd} \\ I_f \end{bmatrix} \tag{7.25}$$

Note the transformed system in ordinary variables does not appear to be reciprocal, and it doesn't have to be. To make the normalized system reciprocal, there are constraints on the base quantities:

$$\frac{3}{2} V_{dB} I_{dB} = V_{fB} I_{fB} = V_{kB} I_{kB} \tag{7.26}$$

These expressions imply the same power base on all of the windings of the machine. This is so because the armature base quantities V_{dB} and I_{dB} are stated as peak values, while the rotor base quantities are stated as DC values. Thus, power base for the three-phase armature is 3/2 times the product of peak quantities, while the power base for the rotor is simply the product of those quantities.

The quadrature axis, which may have fewer equivalent elements than the direct axis and which may have different numerical values, yields a similar structure. Without going through the details, the per-unit flux/current relationship for the q-axis is:

$$\begin{bmatrix} \psi_q \\ \psi_{kq} \end{bmatrix} = \begin{bmatrix} x_q & x_{akq} \\ x_{akq} & x_{kq} \end{bmatrix} \begin{bmatrix} i_q \\ i_{kq} \end{bmatrix} \tag{7.27}$$

The per-unit voltage equations are:

$$v_d = \frac{1}{\omega_0}\frac{d\psi_d}{dt} - \frac{\omega}{\omega_0}\psi_q + r_a\, i_d$$
$$v_q = \frac{1}{\omega_0}\frac{d\psi_q}{dt} + \frac{\omega}{\omega_0}\psi_d + r_a\, i_q \tag{7.28}$$

Note that none of the other circuits in this model have speed voltage terms, so their voltage expressions are exactly what one might expect:

$$v_f = \frac{1}{\omega_0}\frac{d\psi_f}{dt} + r_f i_f \qquad v_0 = \frac{1}{\omega_0}\frac{d\psi_0}{dt} + r_a i_0$$
$$0 = \frac{1}{\omega_0}\frac{d\psi_{kd}}{dt} + r_{kd} i_{kd} \quad 0 = \frac{1}{\omega_0}\frac{d\psi_{kq}}{dt} + r_{kq} i_{kq} \tag{7.29}$$

It should be noted that the damper winding circuits represent closed conducting paths on the rotor, so the two voltages v_{kd} and v_{kq} are always zero.

Per-unit torque is simply:

$$T_e = \psi_d i_q - \psi_q i_d \tag{7.30}$$

7.6 Mechanical Dynamics

To represent the dynamic behavior of the machine, including electromechanical dynamics involving rotor inertia, the rotor dynamics are described by the two ordinary differential equations:

$$\frac{J}{p}\frac{d\omega}{dt} = T^e + T^m$$
$$\frac{d\delta}{dt} = \omega - \omega_0 \tag{7.31}$$

where T^e and T^m are electrical and mechanical torques in ordinary variables, and the angle δ is rotor phase angle with respect to a synchronous reference frame rotating with frequency ω_0.

It is customary to define an "inertia constant" which is not dimensionless but which nevertheless fits into the per-unit system of analysis. This constant uses the symbol H and is the ratio of rotational kinetic energy at base speed to the base power. It has units of seconds:

$$H = \frac{\frac{1}{2}J\left(\frac{\omega_0}{p}\right)^2}{P_B} \tag{7.32}$$

Then the per-unit expression for differential of speed is:

$$\frac{2H}{\omega_0}\frac{d\omega}{dt} = T_e + T_m \tag{7.33}$$

where now T_e and T_m are per-unit torques.

7.7 Equal Mutual's Base

In normalizing the differential equations that make up the model, a number of *base* quantities have been used. For example, in deriving the per-unit flux–current relationship for the direct axis, are six base quantities: V_B I_B V_{fB} I_{fB} V_{kB} and I_{kB} Imposing reciprocity on the flux–current relationship results in two constraints on these six variables. Presumably, the two armature base quantities

will be fixed by machine rating. That leaves two more "degrees of freedom" in selection of base quantities. Note that the selection of base quantities will affect the reactance matrix.

While there are different schools of thought on just how to handle these degrees of freedom, A commonly used convention is to employ what is called the "equal mutuals" base system. The two degrees of freedom are used to set the field and damper base impedances so that all three mutual inductances are equal: $x_{akd} = x_{fkd} = x_{ad}$. With this, the d-axis flux–current relationship becomes:

$$\begin{bmatrix} \psi_d \\ \psi_{kd} \\ \psi_f \end{bmatrix} = \begin{bmatrix} x_d & x_{ad} & x_{ad} \\ x_{ad} & x_{kd} & x_{ad} \\ x_{ad} & x_{ad} & x_f \end{bmatrix} \begin{bmatrix} I_d \\ I_{kd} \\ I_f \end{bmatrix} \tag{7.34}$$

The flux–current relationship of the d-axis is represented by the equivalent circuit of Figure 7.2, if the "leakage" inductances are defined to be:

$$\begin{aligned} x_{al} &= x_d - x_{ad} \\ x_{kdl} &= x_{kd} - x_{ad} \\ x_{fl} &= x_f - x_{ad} \end{aligned} \tag{7.35}$$

Many of the interesting features of the electrical dynamics of the synchronous machine may be discerned from this circuit. While a complete explication of this system is beyond the scope of this note, it is possible to make a few observations.

7.8 Transient and Subtransient Approximations

Figure 7.2 is composed of resistors and inductors, and therefore its impedance (and admittance as well) will have alternating poles and zeros. It will, in the frequency domain, have an impedance of the form:

$$x(s) = \frac{\psi_d(s)}{i_d(s)} = x_d \frac{P_n(s)}{P_d(s)} \tag{7.36}$$

Both the numerator and denominator polynomials in the Laplace operator*s* will be second order. (You may convince yourself of this by writing an expression for terminal impedance.) Since this is a "diffusion" type circuit, having only resistances and inductances, all poles and zeros must be on the negative real axis of the s-plane, as shown in Figure 7.3. The per-unit inductance is, then:

$$x(s) = x_d \frac{\left(1 + T'_d s\right)\left(1 + T''_d s\right)}{\left(1 + T'_{do} s\right)\left(1 + T''_{do} s\right)} \tag{7.37}$$

The two time constants T'_d and T''_d are the reciprocals of the zeros of the impedance, which are the poles of the admittance. These are called the *short circuit* time constants. The other two time constants T'_{do} and T''_d are the reciprocals of the poles of the impedance, and so are called the *open circuit* time constants.

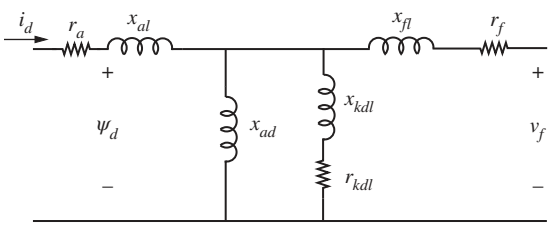

Figure 7.2 d-axis equivalent circuit.

Figure 7.3 Pole-zero plot of reactance of *d*-axis.

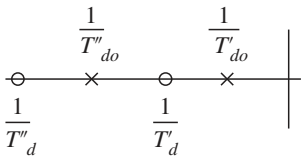

Figure 7.4 Frequency response of terminal impedance.

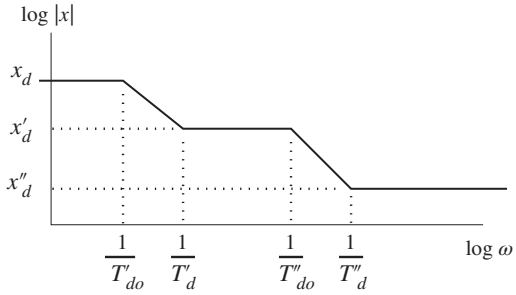

This description has been cast as if there are two sets of well-defined time constants. If the time constants are spaced far enough in time (or the reciprocal of time), the magnitude of machine reactance would, if plotted on a logarithmic chart, look like what is shown in Figure 7.4. In this case, it is possible to define what are called transient and subtransient reactances. That plus the synchronous reactance are, from the circuit model of Figure 7.2,

$$\begin{aligned} x_d &= x_{al} + x_{ad} \\ x'_d &= x_{al} + x_{ad} \| x_{fl} \\ x''_d &= x_{al} + x_{ad} \| x_{fl} \| x_{kdl} \end{aligned} \tag{7.38}$$

To illustrate, the impedance of a hypothetical synchronous generator with a synchronous reactance of 2 per-unit, a transient reactance of 0.5 per-unit and a subtransient reactance of 0.15 per-unit, a transient short-circuit time constant of 0.5 seconds and a subtransient short-circuit time constant of 0.005 seconds would have a reactance magnitude vs. frequency plot as shown in Figure 7.5.

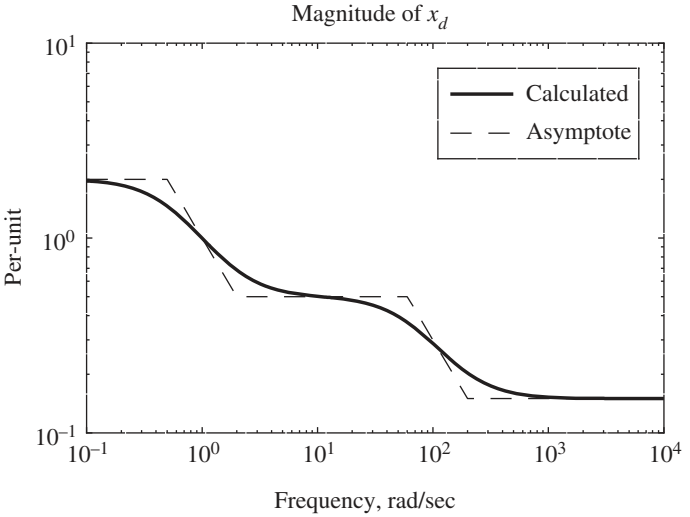

Figure 7.5 Calculated reactance.

7.9 Statement of Simulation Model

Now it is possible to write down the simulation model. Actually, more than one simulation model is necessary, since the machine can be driven by either voltages or currents. Further, the expressions for permanent magnet machines are a bit different. The first model is one in which the terminals are all constrained by voltage.

The state variables are the two *stator* fluxes ψ_d, ψ_q, two *damper fl*uxes ψ_{kd} and ψ_{kq}, field flux ψ_f, rotor speed ω, and torque angle δ. The most straightforward way of stating the model employs currents as auxiliary variables, and these are:

$$\begin{bmatrix} i_d \\ i_{kd} \\ i_f \end{bmatrix} = \begin{bmatrix} x_d & x_{ad} & x_{ad} \\ x_{ad} & x_{kd} & x_{ad} \\ x_{ad} & x_{ad} & x_f \end{bmatrix}^{-1} \begin{bmatrix} \psi_d \\ \psi_{kd} \\ \psi_f \end{bmatrix}$$
$$\begin{bmatrix} i_q \\ i_{kq} \end{bmatrix} = \begin{bmatrix} x_q & x_{aq} \\ x_{aq} & x_{kq} \end{bmatrix}^{-1} \begin{bmatrix} \psi_q \\ \psi_{kq} \end{bmatrix} \tag{7.39}$$

Then the state equations are:

$$\begin{aligned} \frac{d\psi_d}{dt} &= \omega_0 v_d + \omega \psi_q - \omega_0 r_a i_d \\ \frac{d\psi_q}{dt} &= \omega_0 v_q - \omega \psi_d - \omega_0 r_a i_q \\ \frac{d\psi_{kd}}{dt} &= -\omega_0 r_{kd} i_{kd} \\ \frac{d\psi_{kq}}{dt} &= -\omega_0 r_{kq} i_{kq} \\ \frac{d\psi_f}{dt} &= v_f - \omega_0 r_f i_f \\ \frac{d\omega}{dt} &= \frac{\omega_0}{2H}(T_e + T_m) \\ \frac{d\delta}{dt} &= \omega - \omega_0 \end{aligned} \tag{7.40}$$

And, of course,

$$T_e = \psi_d i_q - \psi_q i_d \tag{7.41}$$

For a machine connected to a "stiff" system (a constant frequency voltage source), as shown in Figure 7.6, d- and q-axis voltages are:

$$v_d = v \sin\delta \quad \text{and} \quad v_q = v \cos\delta \tag{7.42}$$

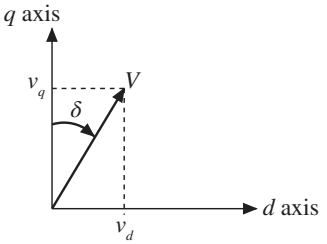

Figure 7.6 Voltage in d-q coordinates.

7.9.1 Statement of Parameters

Note that often data for a machine may be given in terms of the reactances x_d, x_q, x'_d, x'_q, x''_d and time constants T'_{do}, T''_{do}, rather than the elements of the equivalent circuit model. Note that there are four inductances in the equivalent circuit and they form a "cut set", so it is necessary to assume one. There is no loss in generality in doing so. Usually, a value for the stator leakage inductance x_{al} is assumed, and if this is done, the translation is straightforward. For the d-axis:

$$x_{ad} = x_d - x_{al} \qquad x_{fl} = \frac{x_{ad}\left(x'_d - x_{al}\right)}{x_{ad} - x'_d + x_{al}} \qquad x_{kdl} = \frac{1}{\frac{1}{x''_d - x_{al}} - \frac{1}{x_{ad}} - \frac{1}{x_{fl}}}$$

$$r_f = \frac{x_{fl} + x_{ad}}{\omega_0 T'_{do}} \qquad r_{kd} = \frac{x_{kdl} + x_{ad} \| x_{fl}}{\omega_0 T'_{do}} \tag{7.43}$$

And for the q-axis:

$$x_{aq} = x_q - x_{al} \quad x_{kql} = \frac{x_{aq}\left(x''_q - x_{al}\right)}{x_{aq} - x''_q + x_{al}} \quad r_{kq} = \frac{x_{aq} + x_{kql}}{\omega_0 T''_{q0}} \tag{7.44}$$

7.9.2 Example: Balanced Fault Simulation

Balanced short-circuits are very unusual, but mechanical design must be able to handle the forces involved: not only the shaft but also electromagnetic forces on busbars and other current handling parts. The simulation model described here and simulation code at the end of this chapter were used to simulate a sudden short circuit from open circuit with unity per-unit voltage and the following parameters: $x_d = 2$, $x'_d = 0.4$, $x''_d = x''_q = 0.2$, $T'_{do} = 5$, $T''_{do} = T''_{qo} = 0.03$, $T_a = 0.05$. Note T_a is the "armature time constant" and is approximated by $T_a = \frac{x''_d + x''_q}{2\,\omega_0 r_a}$. Armature leakage was taken, arbitrarily, to be 0.1 per-unit. The results are shown in Figure 7.7.

7.9.3 Linearized Model

Often, it becomes desirable to carry out a linearized analysis of machine operation to, for example, examine the damping of the swing mode at a particular operating point. What is done, then, is to assume a steady state operating point and examine the dynamics for deviations from that operating point that are "small". The definition of "small" is really "small enough" that everything important

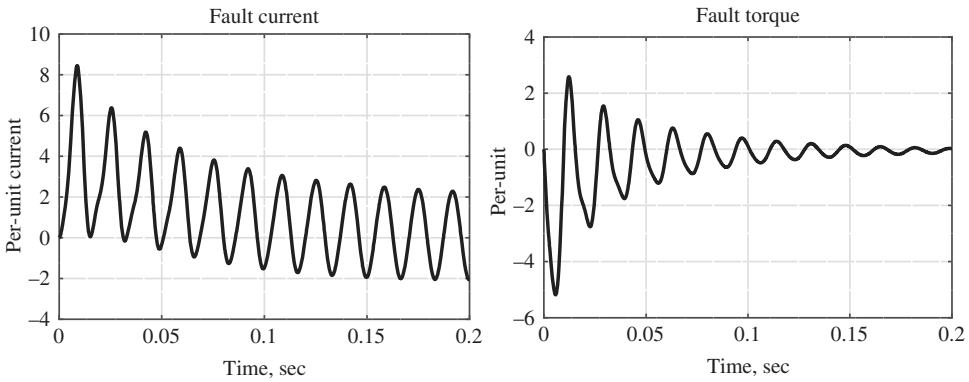

Figure 7.7 Results of fault simulation.

appears in the first-order term of a Taylor series about the steady operating point. Note that the expressions in the machine model are, for the most part, linear. There are, however, a few cases in which products of state variables require the expansion of the Taylor series. Assuming a steady state operating point $[\psi_{d0}, \psi_{q0}, \psi_{f0}, \psi_{kd0}, \psi_{kq0}, \omega_0, \delta_0]$, the first-order (small-signal) variations are described by the following set of equations. First, since the flux–current relationship is linear:

$$\begin{bmatrix} i_{d1} \\ i_{kd1} \\ i_{f1} \end{bmatrix} = \begin{bmatrix} x_d & x_{ad} & x_{ad} \\ x_{ad} & x_{kd} & x_{ad} \\ x_{ad} & x_{ad} & x_f \end{bmatrix}^{-1} \begin{bmatrix} \psi_{d1} \\ \psi_{kd1} \\ \psi_{f1} \end{bmatrix}$$

$$\begin{bmatrix} i_{q1} \\ i_{kq1} \end{bmatrix} = \begin{bmatrix} x_q & x_{aq} \\ x_{aq} & x_{kq} \end{bmatrix}^{-1} \begin{bmatrix} \psi_{q1} \\ \psi_{kq1} \end{bmatrix} \tag{7.45}$$

Then the differential equations governing the first-order variations are:

$$\begin{aligned}
\frac{d\psi_{d1}}{dt} &= (\omega_0 v \cos\delta_0)\delta_1 + \omega_0\psi_{q1} + \omega_1\psi_{q0} - \omega_0 r_a i_{d1} \\
\frac{d\psi_{d1}}{dt} &= -(\omega_0 v \sin\delta_0)\delta_1 - \omega_0\psi_{d1} - \omega_1\psi_{d0} - \omega_0 r_a i_{q1} \\
\frac{d\psi_{kd1}}{dt} &= -\omega_0 r_{kd} i_{kd1} \\
\frac{d\psi_{kq1}}{dt} &= -\omega_0 r_{kq} i_{kq1} \\
\frac{d\psi_{f1}}{dt} &= -\omega_0 r_f i_{f1} \\
\frac{d\omega_1}{dt} &= \frac{\omega}{2H}(T_{e1} + T_{m1}) \\
\frac{d\delta_1}{dt} &= \omega_1 \\
T_e &= \psi_{d0} i_{q1} + \psi_{d1} i_{q0} - \psi_{q0} i_{d1} + \psi_{q1} i_{d0}
\end{aligned} \tag{7.46}$$

7.9.4 Reduced Order Model for Electromechanical Transients

In many situations, the two armature variables contribute little to the dynamic response of the machine. Typically, the armature resistance is small enough that there is very little voltage drop across it and transients in the difference between armature flux and the flux that would exist in the "steady state" decay rapidly (or are not even excited). Further, the relatively short armature time constant makes for very short time steps required in simulation. For this reason, it is often convenient, particularly when studying the relatively slow electromechanical transients, to omit the first two differential equations and set:

$$\begin{aligned}
\psi_d &= v_q = v\cos\delta \\
\psi_q &= -v_d = -v\sin\delta
\end{aligned} \tag{7.47}$$

The set of differential equations changes only a little when this approximation is made. Note, however, that it can be simulated with far fewer "cycles" if the armature time constant is short.

7.9.5 Current Driven Model: Connection to a System

The simulation expressions developed so far are useful in a variety of circumstances. They are, however, difficult to tie to network simulation programs because they use terminal voltage as an

input. Generally, it is more convenient to use current as the input to the machine simulation and accept voltage as the output. Further, it is difficult to handle unbalanced situations with this set of equations.

An alternative to this set would be to employ the phase currents as state variables. Effectively, this replaces ψ_d, ψ_q, and ψ_0 with i_a, i_b, and i_c. The resulting model will interface nicely with network simulations.

To start, note that one could write an expression for terminal flux, on the d-axis:

$$\psi_d = x_d'' i_d + \psi_f \frac{x_{ad} \| x_{kdl}}{x_{ad} \| x_{kdl} + x_{fl}} + \psi_{kd} \frac{x_{ad} \| x_{fl}}{x_{ad} \| x_{fl} + x_{kdl}} \tag{7.48}$$

And here, of course,

$$x_d'' = x_{al} + x_{ad} \| x_{kdl} \| x_{fl} \tag{7.49}$$

This motivates the definition of a "flux behind subtransient reactance":

$$\psi_d'' = \frac{x_{ad}\, x_{kdl}\, \psi_f \;+\; x_{ad}\, x_{fl}\, \psi_{kd}}{x_{ad}\, x_{kdl} \;+\; x_{ad}\, x_{fl} \;+\; x_{kdl}\, x_{fl}} \tag{7.50}$$

So that $\psi_d = \psi''_d + x''_d\, i_d$

On the quadrature axis, the situation is essentially the same, but one step easier if there is only one quadrature axis rotor winding:

$$\psi_q = x_q''\, i_q + \psi_{kq} \frac{x_{aq}}{x_{aq} + x_{kql}} \qquad \text{where} \quad x_q'' = x_{al} + x_{aq} \| x_{kql} \tag{7.51}$$

Very often, these fluxes are referred to as *voltage behind subtransient reactance*, with

$$\psi_d'' = e_q'' \quad \text{and} \quad \psi_q'' = -e_d''$$

Then:

$$\begin{aligned} \psi_d &= x_d'' i_d \;+\; e_q'' \\ \psi_q &= x_q'' i_q \;-\; e_d'' \end{aligned} \tag{7.52}$$

Now, if i_d and i_q are determined, it is straightforward to find the other currents required in the simulation. Note:

$$\begin{bmatrix} \psi_{kd} \\ \psi_f \end{bmatrix} = \begin{bmatrix} x_{kd} & x_{ad} \\ x_{ad} & x_f \end{bmatrix} \begin{bmatrix} i_{kd} \\ i_f \end{bmatrix} + \begin{bmatrix} x_{ad} \\ x_{ad} \end{bmatrix} i_d \tag{7.53}$$

which is easily inverted:

$$\begin{bmatrix} i_{kd} \\ i_f \end{bmatrix} = \begin{bmatrix} x_{kd} & x_{ad} \\ x_{ad} & x_f \end{bmatrix}^{-1} \left(\begin{bmatrix} \psi_{kd} \\ \psi_f \end{bmatrix} - \begin{bmatrix} x_{ad} \\ x_{ad} \end{bmatrix} i_d \right) \tag{7.54}$$

The quadrature axis rotor current is simply $i_{kq} = \frac{\psi_{kq}}{x_{kq}} - \frac{x_{aq}}{x_{kq}} i_q$

The torque equation is the same, but since it is usually convenient to assemble the fluxes behind subtransient reactance, it is possible to use:

$$T_e = e''_q i_q + e''_d i_d + \left(x''_d - x''_q \right) i_d i_q \tag{7.55}$$

Now, it is necessary to consider terminal voltage. This is most conveniently cast in matrix notation. The vector of phase voltages is:

$$\underline{v}_{ph} = \begin{bmatrix} v_a \\ v_b \\ v_c \end{bmatrix}$$

Then, with similar notation for phase flux, terminal voltage is, ignoring armature resistance:

$$\underline{v}_{ph} = \frac{1}{\omega_0}\frac{d\underline{\psi}_{ph}}{dt} = \frac{1}{\omega_0}\frac{d}{dt}\{\underline{T}^{-1}\underline{\psi}_{dq}\} \tag{7.56}$$

The transformed vector of fluxes is defined to be $\underline{\psi}_{dq} = \underline{x}''\underline{i}_{dq} + \underline{e}''$ where the matrix of reactances is:

$$\underline{x}'' = \begin{bmatrix} x_d'' & 0 & 0 \\ 0 & x_q'' & 0 \\ 0 & 0 & x_0 \end{bmatrix} \tag{7.57}$$

And the vector of internal fluxes is:

$$\underline{e}'' = \begin{bmatrix} e_q'' \\ -e_d'' \\ 0 \end{bmatrix} \tag{7.58}$$

Since $\underline{i}_{dq} = \underline{T}\,\underline{I}_{ph'}$, the terminal voltage expression may be re-cast as:

$$\underline{v}_{ph} = \frac{1}{\omega_0}\frac{d}{dt}\{\underline{T}^{-1}\underline{x}''\underline{T}\,i_{ph} + \underline{T}^{-1}\underline{e}''\} \tag{7.59}$$

Now it is necessary to make one assumption and one definition. The assumption, which is only moderately restrictive, is that subtransient saliency may be ignored. That is, it is assumed that $x_d'' = x_q''$

The definition separates the "zero sequence" impedance into phase and neutral components: $x_0 = x''_d + 3x_g$.

Note that according to this definition, the reactance x_g accounts for any impedance in the neutral of the synchronous machine as well as mutual coupling between phases.

Then, the impedance matrix becomes:

$$\underline{x}'' = \begin{bmatrix} x_d'' & 0 & 0 \\ 0 & x_d'' & 0 \\ 0 & 0 & x_d'' \end{bmatrix} + \begin{bmatrix} 0 & 0 & 0 \\ 0 & 0 & 0 \\ 0 & 0 & 3x_g \end{bmatrix} = x_d''\underline{I} + \underline{x}_g \tag{7.60}$$

Now the vector of phase voltages is:

$$\underline{v}_{ph} = \frac{1}{\omega_0}\frac{d}{dt}\left\{x''_{dph} + \underline{T}^{-1}\underline{x}_g\underline{T}\,\underline{i}_{ph} + \underline{T}^{-1}\underline{e}''\right\} \tag{7.61}$$

The next step is to carry out the matrix multiplication in the second term of (119):

$$\underline{T}^{-1}\underline{x}_g\underline{T} = x_g\begin{bmatrix} 1 & 1 & 1 \\ 1 & 1 & 1 \\ 1 & 1 & 1 \end{bmatrix} \tag{7.62}$$

The third and final term in the voltage equation describes voltages induced by rotor fluxes:

$$\frac{1}{\omega_0}\frac{d}{dt}\{\underline{T}^{-1}\underline{e}''\} = \frac{1}{\omega_0}\frac{d}{dt}\{\underline{T}^{-1}\}\underline{e}'' + \frac{1}{\omega_0}\underline{T}^{-1}\frac{d\underline{e}''}{dt} \tag{7.63}$$

The time derivative of the inverse transform is:

$$\frac{1}{\omega_0}\frac{d}{dt}\underline{T}^{-1} = \frac{\omega}{\omega_0}\begin{bmatrix} -\sin\theta & -\cos\theta & 0 \\ -\sin\left(\theta - \frac{2\pi}{3}\right) & -\cos\left(\theta - \frac{2\pi}{3}\right) & 0 \\ -\sin\left(\theta + \frac{2\pi}{3}\right) & -\cos\left(\theta + \frac{2\pi}{3}\right) & 0 \end{bmatrix} \tag{7.64}$$

Now the three-phase voltages can be extracted from all of this matrix algebra:

$$
\begin{aligned}
v_a &= \frac{x''_d}{\omega_0}\frac{di_a}{dt} + \frac{x_g}{\omega_0}(i_a + i_b + i_c) + e''_a \\
v_b &= \frac{x''_d}{\omega_0}\frac{di_b}{dt} + \frac{x_g}{\omega_0}(i_a + i_b + i_c) + e''_b \\
v_c &= \frac{x''_d}{\omega_0}\frac{di_c}{dt} + \frac{x_g}{\omega_0}(i_a + i_b + i_c) + e''_c
\end{aligned}
\tag{7.65}
$$

where the internal voltages are:

$$
\begin{aligned}
e''_a &= -\frac{\omega}{\omega_0}\left(e''_q \sin\theta - e''_d \cos\theta\right) + \frac{1}{\omega_0}\cos\theta\,\frac{de''_q}{dt} + \frac{1}{\omega_0}\sin\theta\frac{de''_d}{dt} \\
e''_b &= -\frac{\omega}{\omega_0}\left(e''_q \sin\left(\theta - \frac{2\pi}{3}\right) - e''_d \cos\left(\theta - \frac{2\pi}{3}\right)\right) + \frac{1}{\omega_0}\cos\left(\theta - \frac{2\pi}{3}\right)\frac{de''_q}{dt} \\
&\quad + \frac{1}{\omega_0}\sin\left(\theta - \frac{2\pi}{3}\right)\frac{de''_d}{dt} \\
e''_c &= -\frac{\omega}{\omega_0}\left(e''_q \sin\left(\theta + \frac{2\pi}{3}\right) - e''_d \cos\left(\theta + \frac{2\pi}{3}\right)\right) + \frac{1}{\omega_0}\cos\left(\theta + \frac{2\pi}{3}\right)\frac{de''_q}{dt} \\
&\quad + \frac{1}{\omega_0}\sin\left(\theta + \frac{2\pi}{3}\right)\frac{de''_d}{dt}
\end{aligned}
\tag{7.66}
$$

This set of expressions describes the equivalent circuit of Figure 7.8.

7.9.6 Restatement of the Model

The synchronous machine model, which uses the three-phase currents as state variables may now be stated in the form of a set of differential and algebraic equations. Note the assumption that differences between subtransient reactances on the d- and q-axes are negligible:

$$
\begin{aligned}
\frac{d\psi_{kd}}{dt} &= -\omega_0 r_{kd} i_{kd} \\
\frac{d\psi_{kq}}{dt} &= -\omega_0 r_{kq} i_{kq} \\
\frac{d\psi_f}{dt} &= \omega_0 v_f - \omega_0\, r_f\, i_f \\
\frac{d\delta}{dt} &= \omega - \omega_0 \\
\frac{d\omega}{dt} &= \frac{\omega_0}{2H}\left(\, T_m + e''_q\, i_q + e''_d\, i_d\right)
\end{aligned}
\tag{7.67}
$$

Figure 7.8 Equivalent network model.

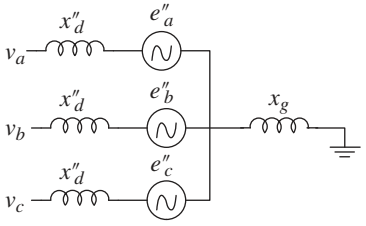

where:

$$\begin{bmatrix} i_{kd} \\ i_f \end{bmatrix} = \begin{bmatrix} x_{kd} & x_{ad} \\ x_{ad} & x_f \end{bmatrix}^{-1} \left(\begin{bmatrix} \psi_{kd} \\ \psi_f \end{bmatrix} - \begin{bmatrix} x_{ad} \\ x_{ad} \end{bmatrix} i_d \right) \tag{7.68}$$

and

$$i_{kq} = \frac{\psi_{kq}}{x_{kq}} - \frac{x_{aq}}{x_{kq}} i_q \tag{7.69}$$

The network interface equations are, from the network to the machine and back:

$$\begin{aligned}
i_d &= i_a \cos\theta + i_b \cos\left(\theta - \frac{2\pi}{3}\right) + i_c \cos\left(\theta + \frac{2\pi}{3}\right) \\
i_q &= -i_a \sin\theta - i_b \sin\left(\theta - \frac{2\pi}{3}\right) - i_c \sin\left(\theta + \frac{2\pi}{3}\right) \\
e''_a &= -\frac{\omega}{\omega_0}\left(e''_q \sin\theta - e''_d \cos\theta\right) + \frac{1}{\omega_0}\cos\theta \frac{de''_q}{dt} + \frac{1}{\omega_0}\sin\theta \frac{de''_d}{dt} \\
e''_b &= -\frac{\omega}{\omega_0}\left(e''_q \sin\left(\theta - \frac{2\pi}{3}\right) - e''_d \cos\left(\theta - \frac{2\pi}{3}\right)\right) + \frac{1}{\omega_0}\cos\left(\theta - \frac{2\pi}{3}\right)\frac{de''_q}{dt} \\
&\quad + \frac{1}{\omega_0}\sin\left(\theta - \frac{2\pi}{3}\right)\frac{de''_d}{dt} \\
e''_c &= -\frac{\omega}{\omega_0}\left(e''_q \sin\left(\theta + \frac{2\pi}{3}\right) - e''_d \cos\left(\theta + \frac{2\pi}{3}\right)\right) + \frac{1}{\omega_0}\cos\left(\theta + \frac{2\pi}{3}\right)\frac{de''_q}{dt} \\
&\quad + \frac{1}{\omega_0}\sin\left(\theta + \frac{2\pi}{3}\right)\frac{de''_d}{dt}
\end{aligned} \tag{7.70}$$

And

$$\begin{aligned}
\theta &= \omega_0 t + \delta \\
e''_q &= \psi''_d \\
e''_d &= -\psi''_q \\
\psi''_d &= \frac{x_{ad}\, x_{kdl}\, \psi_f + x_{ad}\, x_{fl}\, \psi_{kd}}{x_{ad}\, x_{kdl} + x_{ad}\, x_{fl} + x_{kdl}\, x_{fl}} \\
\psi''_q &= \frac{x_{aq}\, \psi_{kq}}{x_{aq} + x_{kql}}
\end{aligned} \tag{7.71}$$

7.9.7 Network Constraints

This model may be embedded in a number of networks. Different configurations will result in different constraints on currents. Consider, for example, the situation in which all of the terminal voltages are constrained, but perhaps by unbalanced (not entirely positive sequence) sources. In that case, the differential equations for the three-phase currents would be:

$$\begin{aligned}
\frac{x''_d}{\omega_0}\frac{di_a}{dt} &= \left(v_a - e''_a\right)\frac{x''_d + 2x_g}{x''_d + 3x_g} - \left(\left(v_b - e''_b\right) + \left(v_c - e''_c\right)\right)\frac{x_g}{x''_d + 3x_g} \\
\frac{x''_d}{\omega_0}\frac{di_b}{dt} &= \left(v_b - e''_b\right)\frac{x''_d + 2x_g}{x''_d + 3x_g} - \left(\left(v_a - e''_a\right) + \left(v_c - e''_c\right)\right)\frac{x_g}{x''_d + 3x_g} \\
\frac{x''_d}{\omega_0}\frac{di_c}{dt} &= \left(v_c - e''_c\right)\frac{x''_d + 2x_g}{x''_d + 3x_g} - \left(\left(v_a - e''_a\right) + \left(v_b - e''_b\right)\right)\frac{x_g}{x''_d + 3x_g}
\end{aligned} \tag{7.72}$$

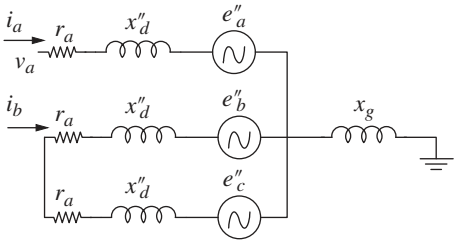

Figure 7.9 Line-line fault.

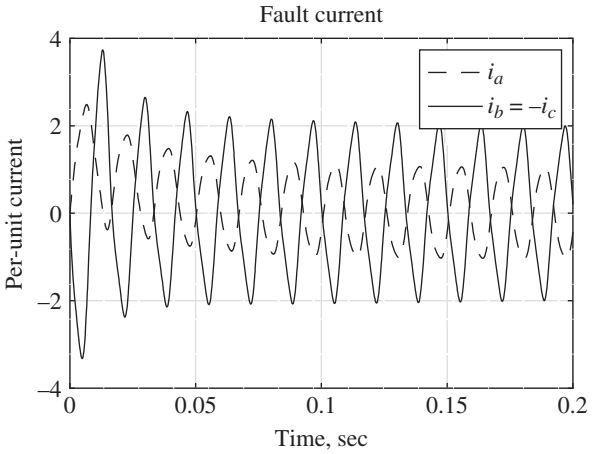

Figure 7.10 Line-line fault current.

7.9.8 Example: Line-Line Fault

This model is suitable for embedding into network analysis routines. It is also possible to handle many different situations directly. Consider, for example, the unbalanced fault represented by the network shown in Figure 7.9. This shows a line-line fault situation, with one phase still connected to the network.

In this situation, only two currents are involved, since $i_c = -i_b$, and the differential equations governing the two currents are:

$$\begin{aligned}\frac{di_b}{dt} &= \frac{\omega_0}{2x''_d}\left(e''_c - e''_b - 2r_a\, i_b\right)\\ \frac{di_a}{dt} &= \frac{\omega_0}{x''_d + x_g}\left(v_a - e''_a - r_a i_a\right)\end{aligned} \tag{7.73}$$

The simulated currents are shown in Figure 7.10.

7.10 Permanent Magnet Machines

Permanent Magnet machines are one state variable simpler than their wound-field counterparts. They may be accurately viewed as having a constant field current. Note that the internal (field) flux is the equivalent of $\psi_0 = x_{ad} i_{f0}$.

7.10.1 Model: Voltage-Driven Machine

In the case of a voltage-driven machine, a reasonably simple expression for the rotor currents is:

$$\begin{bmatrix} i_d \\ i_{kd} \end{bmatrix} = \begin{bmatrix} x_d & x_{ad} \\ x_{ad} & x_{kd} \end{bmatrix}^{-1} \begin{bmatrix} \psi_d - \psi_0 \\ \psi_{kd} - \psi_0 \end{bmatrix}$$
$$\begin{bmatrix} i_q \\ i_{kq} \end{bmatrix} = \begin{bmatrix} x_q & x_{aq} \\ x_{aq} & x_{kq} \end{bmatrix}^{-1} \begin{bmatrix} \psi_q \\ \psi_{kq} \end{bmatrix} \tag{7.74}$$

The simulation model has six states:

$$\begin{aligned} \frac{d\psi_d}{dt} &= \omega_0 \, v_d \; + \; \omega \, \psi_q \; - \; \omega_0 r_a \, i_d \\ \frac{d\psi_q}{dt} &= \omega_0 \, v_q \; - \; \omega \, \psi_d \; - \; \omega_0 r_a \, i_q \\ \frac{d\psi_{kd}}{dt} &= -\omega_0 \, r_{kd} \, i_{kd} \\ \frac{d\psi_{kq}}{dt} &= -\omega_0 \, r_{kq} \, i_{kq} \\ \frac{d\psi_f}{dt} &= v_f - \omega_0 \, r_f \, i_f \\ \frac{d\omega}{dt} &= \frac{\omega_0}{2H}(\psi_d i_q \; - \; \psi_q i_d \; + \; T_m) \\ \frac{d\delta}{dt} &= \omega - \omega_0 \end{aligned} \tag{7.75}$$

7.10.2 Current-Driven Machine

In the case of a current-driven machine, rotor currents required in the simulation are:

$$\begin{aligned} i_{kd} &= \frac{1}{x_{kd}}(\psi_{kd} - x_{ad} i_d - \psi_0) \\ i_{kq} &= \frac{1}{x_{kq}}(\psi_{kq} - x_{aq} i_q) \end{aligned} \tag{7.76}$$

Flux behind subtransient reactance is:

$$\begin{aligned} \psi_d'' &= \frac{x_{kdl}\,\psi_0 + x_{ad}\,\psi_{kd}}{x_{ad} + x_{kdl}} \qquad \psi_q'' = \frac{x_{aq}\,\psi_{kq}}{x_{aq} + x_{kql}} \\ x_d'' &= x_{al} + x_{ad} \| x_{kdl} \qquad x_q'' = x_{al} + x_{aq} \| x_{kql} \end{aligned} \tag{7.77}$$

In this case, there are only four state equations:

$$\begin{aligned} \frac{d\psi_{kd}}{dt} &= -\omega_0 r_{kd} i_{kd} \\ \frac{d\psi_{kq}}{dt} &= -\omega_0 r_{kq} i_{kq} \\ \frac{d\omega}{dt} &= \frac{\omega_0}{2H}(\psi_d i_q - \psi_q i_d + T_m) \\ \frac{d\delta}{dt} &= \omega - \omega_0 \end{aligned} \tag{7.78}$$

The interconnections to and from the network are the same as for the wound-field machine.

7.10.3 PM Machines with No Damper

The PM machines without much rotor conductivity may often behave as if they have no damper winding at all. In this case, the model simplifies even further. Armature currents are:

$$\begin{aligned} i_d &= \frac{\psi_d - \psi_0}{x_d} \\ i_q &= \frac{\psi_q}{x_q} \end{aligned} \tag{7.79}$$

The state equations are:

$$\begin{aligned} \frac{d\psi_d}{dt} &= \omega_0 v_d + \omega\psi_q - \omega_0 r_a i_d \\ \frac{d\psi_q}{dt} &= \omega_0 v_q - \omega\psi_d - \omega_0 r_a i_q \\ \frac{d\omega}{dt} &= \frac{\omega_0}{2H}(\psi_d i_q - \psi_q i_d + T_m) \\ \frac{d\delta}{dt} &= \omega - \omega_0 \end{aligned} \tag{7.80}$$

7.10.4 Current-Driven PM Machines with No Damper

In the case of no damper, the machine becomes quite simple. There is no "internal flux" on the quadrature axis. Further, there are no time derivatives of the internal flux on the d-axis. The only machine state equations are mechanical:

$$\begin{aligned} \frac{d\omega}{dt} &= \frac{\omega_0}{2H}(\psi_0 i_q - (x_d - x_q) i_d i_q + T_m) \\ \frac{d\delta}{dt} &= \omega - \omega_0 \end{aligned} \tag{7.81}$$

The network interface is simpler than before:

$$\begin{aligned} i_d &= i_a \cos\theta + i_b \cos\left(\theta - \frac{2\pi}{3}\right) + i_c \cos\left(\theta + \frac{2\pi}{3}\right) \\ i_q &= -i_a \sin\theta - i_b \sin\left(\theta - \frac{2\pi}{3}\right) - i_c \sin\left(\theta + \frac{2\pi}{3}\right) \\ e''_a &= -\frac{\omega}{\omega_0}\psi_0 \sin\theta \\ e''_b &= -\frac{\omega}{\omega_0}\psi_0 \sin\left(\theta - \frac{2\pi}{3}\right) \\ e''_c &= -\frac{\omega}{\omega_0}\psi_0 \sin\left(\theta + \frac{2\pi}{3}\right) \end{aligned} \tag{7.82}$$

7.11 Problems

7.1 This concerns an improbably large machine for this degree of saliency, or an implausibly large amount of saliency for a machine of this size, but since it is on paper, no damage will be done. The machine has a base (rating) of 1000 MVA and 26 kV (line-line, RMS), at 60 Hz. On that rating, $x_d = 2.2$, $x_q = 1.8$ and $x_0 = 0.2$. Find expressions for the three-phase inductances of this machine, in ordinary units: $L_a(\theta)$, $L_b(\theta)$, and $L_c(\theta)$.

7.2 This problem concerns a large two-pole synchronous generator that has the following parameters, expressed in per-unit:

Machine rating	800 MVA
Rated terminal voltage	24 kV (RMS, line-line)
Field current for rated no-load voltage	2000 A
Synchronous, d-axis reactance x_d	2.0 per-unit
Synchronous, q-axis reactance x_q	1.8

(a) What is field current required for operation of this machine at rated volt-amperes (800 MVA), and 85% lagging, power factor?
(b) What is the field current when the machine is operating at its under-excited stability limit, with 85% leading power factor and rated volt-amperes? (Hint: The power angle is not exactly 90° at the stability limit for a salient machine.)

Example machine: The next several problems are all about one machine, which has the following parameters:

Machine rating	P	600 MVA
Rated terminal voltage	$V_{l\text{-}l}$	22 kV RMS
Field current for rated voltage, no-load	I_{fnl}	2500 A
Synchronous, d-axis reactance	x_d	2.0 per-unit
Synchronous, q-axis reactance	x_q	1.8 per-unit
Transient, d-axis reactance	x'_d	0.4 per-unit
Subtransient, d-axis reactance	x''_d	0.2 per-unit
Subtransient, q-axis reactance	x''_q	0.2 per-unit
Transient, open-circuit time constant	T'_{do}	5.0 s
Subtransient, open-circuit time constant	T''_{do}	0.2 s
Subtransient, open-circuit time constant	T''_{qo}	0.5 s
Inertia constant	H	3.0 s
Armature time constant	T_a	0.1

7.3 Find equivalent *equal mutuals* circuit models for the d- and q-axes for this machine. Assume for this purpose that the stator leakage inductance is $x_{al} = 0.1$ per-unit.

7.4 What are the actual parameters (in ohms) of the reactive and resistive parameters for these models, on a machine base of 600 MVA, 24 kV, line-line, RMS?

7.5 The generator is operated initially unloaded, with terminal voltage equal to 1.0 per-unit. A sudden, symmetrical short circuit is imposed just at the instant when the flux is a maximum in Phase A. Classical methods would tell you that fault current is, in per-unit:

$$i_a = \frac{1}{x''_d} e^{\frac{t}{T_a}} + \left(\frac{1}{x_d} + \left(\frac{1}{x'_d} - \frac{1}{x_d} \right) e^{\frac{t}{T'_d}} + \left(\frac{1}{x''_d} - \frac{1}{x'_d} \right) e^{\frac{t}{T''_d}} \right) \cos \omega t$$

Using MATLAB, simulate this transient and compare with the "classical" result.

7.6 The machine is operated at rated current, unity power factor.

Draw the phasor diagram for this operation.

What are the internal fluxes for each of the elements of the circuit diagrams?

The armature terminals are suddenly open-circuited. Ignoring the initial voltage spikes and assuming no speed change, calculate terminal voltage as a function of time. Note both axes will have voltage transients.

7.7 Calculate and plot the *transient* torque angle curve for this machine, assuming that steady state operation is at rated load, unity power factor. Transient conditions mean that the field winding is assumed to have constant flux. Also, calculate a (fictional) torque-angle curve that assumes the *d*-axis transient reactance on both axes. Remember that this curve should match actual operation at the rating point, which means that the transient torque angle will be displaced somewhat from the actual, steady-state torque angle.

7.8 In preparation for doing a simulation of this machine, we need to set up initial conditions. Assume the machine is operating at rated volt-amperes at a power factor of 0.85, over-excited (meaning the machine is delivering reactive power to the system). Find initial conditions for each of the state variables. Show that these are correct by running a simulation for a short time (say, 0.01 seconds) and observing that the state variables are constant.

7.9 The machine is to be synchronized to a power system. Set up a simulation that assumes the machine is excited so that its terminal voltage is one per-unit at the point of synchronization. Consider two cases:

1) The machine has the correct speed but is synchronized (the switch to the power system) out of phase by 20°.
2) The machine is synchronized at the correct angle but is going too fast by, say 10 rad per second.

7.10 Consider the situation of Problem 7.9, but do the simulation ignoring armature transients and subtransient interactions. (That is, use a reduced state order model.)

8

Commutator Machines

8.1 Introduction

Virtually all electric machines, and all practical electric machines, employ some form of rotating field/current system to produce torque. While it is possible to produce a "true DC" machine (e.g. the "Faraday disk" introduced in Chapter 3), for practical reasons, such machines have not reached wide application and are not likely to do so. In the machines we have examined so far, they are operated from an alternating voltage source. Indeed, this is one of the principal reasons for employing AC in power systems.

Commutator machines are found in a very wide range of applications. The starting motor of the internal combustion engine in most automobiles is a series-connected commutator machine. Many of the other electric motors in automobiles, from the motors that position the outside rearview mirrors to the motors that drive the windshield wipers, are permanent magnet commutator machines. In older transportation systems, the large traction motors that drive subway trains and diesel/electric locomotives are DC commutator machines (although induction machines are making inroads here). And many common appliances and some machine tools use "universal" motors. Commutator machines are important to understand, not only because of their widespread application, but also because of important concepts, such as "base speed", that arise from their application.

The first electric machines employed a mechanical switch, in the form of a carbon brush/commutator system, to produce this rotating field. While the widespread use of power electronics is making "brushless" motors (which are really synchronous machines) more popular and common, commutator machines are still economically very important. They are relatively cheap to make, particularly in small sizes, and they tend to be rugged and simple, although their operational lifetime is limited by wear of the brushes.

8.2 Basic Geometry

A schematic ("cartoon view") of a commutator-type machine is shown in Figure 8.1. The armature of this machine is on the rotor (this is the part that handles the electric power), and current is fed to the armature through the brush/commutator system. The interaction magnetic field is provided (in this picture) by a field winding. In many commutator machines, the field winding is replaced by a permanent magnet or combination of permanent magnets.

Electromagnetic Analysis of Electric Machines: First Principles, Modeling, and Design, First Edition.
James L. Kirtley, Christopher H. T. Lee, and Sajjad Mohammadi.

Companion website: www.wiley.com/go/kirtleyelectric

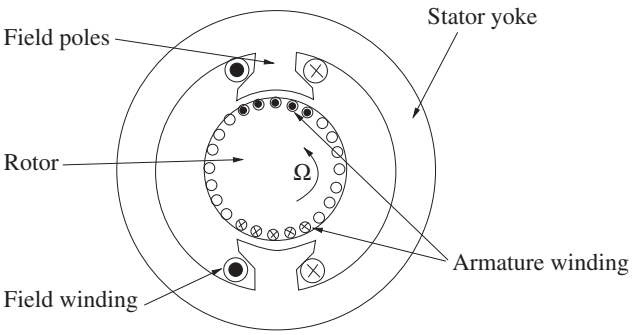

Figure 8.1 Wound field DC machine geometry.

8.3 Torque

To start, assume that the interaction magnetic flux density that crosses the relative rotation gap has an average value of B_r. There are C_a active conductors underneath the poles at any one time. Those conductors are divided into m parallel paths. Torque is estimated by using the Lorentz force law. Each conductor is carrying current I_a/m in the axial (z-)direction, and so produces an azimuthal (θ directed) force $F_\theta = \ell \frac{I_a}{m} B_r$. Noting that there will be C_a such interactions and that the rotor has moment arm R, torque is then:

$$T_e = \frac{C_a}{m} R \ell B_r I_a \tag{8.1}$$

where R and ℓ are rotor radius and length. Note that C_a is not necessarily the total number of conductors, but rather the total number of *active* conductors (that is, conductors underneath the pole and therefore subject to the interaction field).

If N_f is the number of field turns per pole, the radial interaction field is:

$$B_r = \mu_0 \frac{N_f I_f}{g} \tag{8.2}$$

Leading to a simple expression for torque in terms of the two currents:

$$T_e = G\, I_a\, I_f \tag{8.3}$$

where the motor coefficient G has units of $N.m$ per ampere squared:

$$G = \mu_0 \frac{C_a}{m} \frac{N_f R \ell}{g} \tag{8.4}$$

8.4 Voltage Induction

Now look at this machine from the point of view of electric field and voltage. It was shown in Chapter 3 that the electric field E' within an object moving with velocity v through a magnetic flux density B is:

$$\vec{E}' = \vec{E} + \vec{v} \times \vec{B}$$

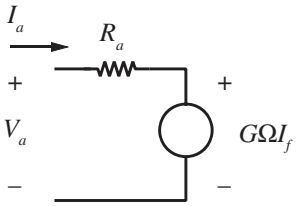

Figure 8.2 Simple circuit model of DC machine armature.
Note: Power into voltage source is mechanical power converted.

Note that the armature conductors are moving through the magnetic field produced by the stator (field) poles, and we can ascribe to them an axially directed electric field:

$$E_z = -R\Omega B_r \tag{8.5}$$

If the armature conductors are arranged as described above, with C_a conductors in m parallel paths underneath the poles and with a mean active radial magnetic field of B_r, voltage induced in the stator conductors is, in total:

$$E_b = \frac{C_a}{m}\ell R\Omega B_r$$

Note that this is only the voltage induced by motion of the armature conductors through the field and does not include brush or conductor resistance. Including the expression for effective magnetic field, the 'back voltage' is:

$$E_b = G\Omega I_f \tag{8.6}$$

which leads to the conclusion that newton-meters per ampere squared equals volt seconds per ampere. This stands to reason if electric power into the interaction and mechanical power out are compared:

$$P_{em} = E_b I_a = T_e\Omega$$

A more complete model of this machine would include the effects of armature, brush, and lead resistance, so that in steady state operation, as shown in Figure 8.2:

$$V_a = R_a I_a + G\Omega I_f \tag{8.7}$$

8.5 Voltage Driven Operation

Consider this machine with its armature connected to a voltage source and its field operating at steady current, so that:

$$I_a = \frac{V_a - G\,\Omega\, I_f}{R_a} \tag{8.8}$$

Then torque, electric power in, and mechanical power out are:

$$\begin{aligned} T_e &= G\, I_f \frac{V_a - G\,\Omega\, I_f}{R_a} \\ P_e &= V_a \frac{V_a - G\,\Omega\, I_f}{R_a} \\ P_m &= G\,\Omega\, I_f \frac{V_a - G\,\Omega\, I_f}{R_a} \end{aligned} \tag{8.9}$$

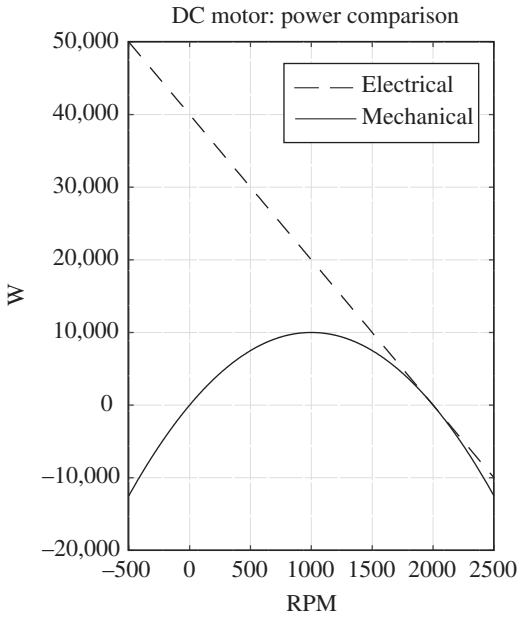

Figure 8.3 DC motor power in/out.

Note that these expressions define three regimes defined by rotational speed. The two "break points" are at zero speed and at the "zero torque" speed:

$$\Omega_0 = \frac{V_a}{G I_f} \tag{8.10}$$

Figure 8.3 shows power input and output for a DC motor with $G = 0.9549$, $R_a = 1$, $I_f = 1$, and $V_a = 200$. These parameters were picked to make the zero-torque speed equal to 2000 RPM (209.44 rad/sec). Note that for speeds above the zero-torque speed, both power in and mechanical power out are negative, implying that the machine is now a generator. For negative speed, electrical power in is positive and mechanical power out is negative. This is rarely done, but when it is, it is called "plugging" and results in rapid deceleration.

8.6 Connections and Capability: Separately Excited

The machines discussed so far have two electrical connections: the armature is generally on the rotor and supplied through a mechanical switch that maintains active conductors underneath the field poles. The field winding is on the stator and produces the flux density with which the armature conductors interact. The machine can be controlled through either or both of these electrical inputs.

In Figure 8.3, the armature of the motor is connected to a voltage source and the field winding is assumed to have constant current. In reality, both armature voltage and field current, by way of voltage, can be adjusted. Figure 8.4 illustrates speed control of a separately excited motor; actually, the same one as illustrated in Figure 8.3. For speeds below, in this case, about 2000 RPM, field current is at its maximum value, and armature voltage is adjusted. Maximum armature current is, in this case, limited to 10 A. The armature voltage is limited to 200 V, so for speeds above about 2000 RPM, field current must be reduced. Note that this can be done by reducing the voltage of the field supply or by inserting additional resistance. Note that this reduces both the maximum torque that can be achieved and the slope of the speed-torque curve.

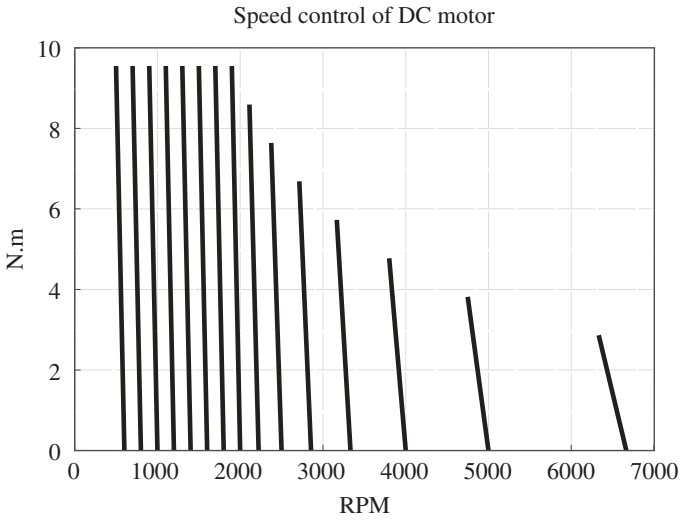

Figure 8.4 Speed control of separately excited motor.

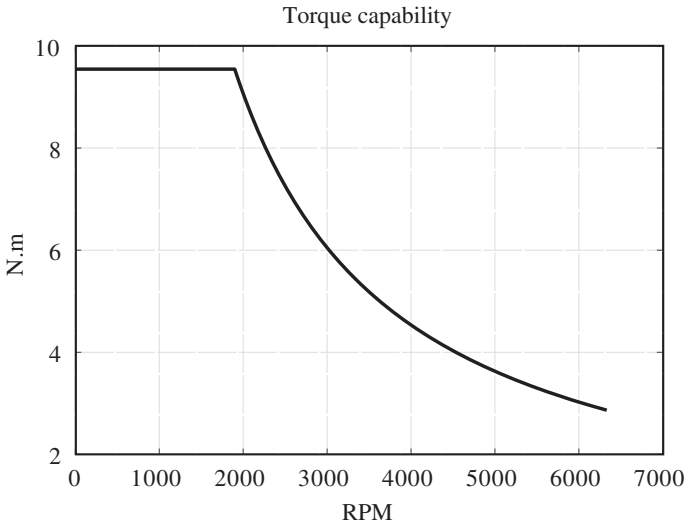

Figure 8.5 Torque capability vs. speed.

If maximum torque is plotted against speed, the result is shown, for the same motor, in Figure 8.5. The armature current is at its maximum permitted value, and armature voltage is varied. At some speed (in this case, just below 2000 RPM), the motor achieves its 'base' speed, which is the maximum speed for which the motor can achieve "base" torque. This is sometimes called the "rating point". That base speed is limited by, typically, the maximum voltage that can be applied to the commutator. Above base speed, field current is reduced, armature voltage is constant, and torque capability is approximately inversely proportional to speed. The maximum torque vs. speed curve is thus divided into *constant torque* and *constant power* regions.

In actual operation as, for example, a traction motor, the machine will be operating at a point below the maximum torque, and there will be some optimum mix of field and armature currents to

produce the required torque. For braking, one could (and this is often done) reconnect the armature of the machine to a resistor and turn the machine into a generator. Braking torque would then be controlled by field current.

A subset of the separately excited machine is the *shunt connection* in which armature and field are supplied, in parallel, by the same source. This connection is no longer widely used. It does not yield any meaningful ability to control speed, aside from field weakening, and doing that results in an oversized machine for most loads. The constant or nearly constant speed applications to which it was used are typically handled by induction machines.

8.7 Series Connection

Another connection which is still widely used is the series connection, in which the field winding is sized so that its normal operating current level is the same as normal armature current, and the two windings are connected in series. Then:

$$I_a = I_f = \frac{V}{R_a + R_f + G\,\Omega} \tag{8.11}$$

and torque is:

$$T_e = \frac{G\,V^2}{(R_a + R_f + G\,\Omega)^2} \tag{8.12}$$

It is important to note that this machine has no "zero-torque" speed, leading to the possibility that an unloaded machine might accelerate to dangerous speeds. This is particularly true because the commutator, made of pieces of relatively heavy material tied together with non-conductors, may not be capable of holding together at high speeds.

Speed control of series-connected machines can be achieved with voltage control, and many appliances using this type of machine use choppers or phase control. An older form of control used in traction applications was the series dropping resistor: obviously not a very efficient way of controlling the machine and not widely used. This kind of control is illustrated in Figure 8.6.

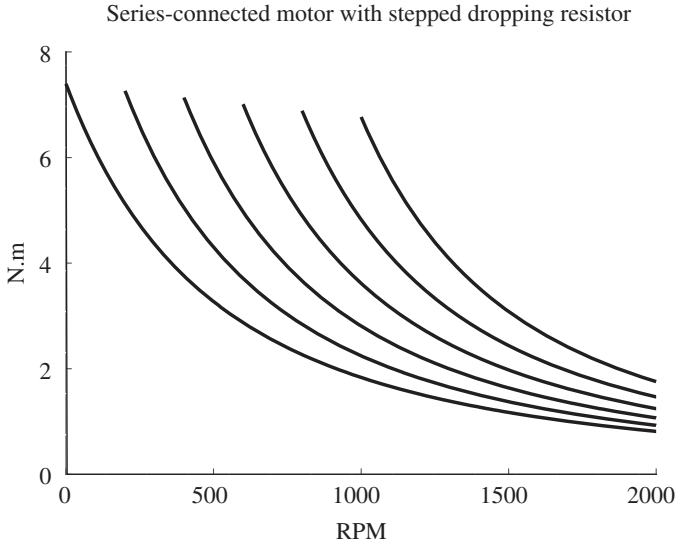

Figure 8.6 Torque vs. speed of series motor with dropping resistors.

8.8 Universal Motors

A variation on this class of machine is the very widely used "universal motor", in which the stator and rotor (field and armature) of the machine are both constructed to operate with alternating current. This means that both the field and armature must be made of laminated steel. Note that such a machine will operate just as it would have with direct current, with the only addition being the reactive impedance of the two windings. Working with RMS quantities:

$$\begin{aligned} \underline{I} &= \frac{\underline{V}}{R_a + R_f + G\Omega + j\omega(L_a + L_f)} \\ T_e &= \frac{G|V|^2}{(R_a + R_f + G\Omega)^2 + \omega^2(L_a + L_f)^2} \end{aligned} \tag{8.13}$$

where ω is the electrical supply frequency. Note that, unlike other AC machines, the universal motor is not limited in speed to the supply frequency. Appliance motors often turn substantially faster than the 3600 RPM limit of induction or synchronous motors, and this is one reason why they are so widely used. With the high rotational speeds, it is possible to produce more power per unit mass (and more power per dollar).

8.9 Commutator

The commutator is what makes this kind of machine work. The brush and commutator system of this class of motor involves much experience and experimentation, and there are still aspects of how they work that are poorly understood.

A drawing of an exemplar commutator is shown in Figure 8.7. Represented are a pair of poles (shaded) and a pair of brushes. Conductors make a group of closed paths. Current from one of the brushes takes two parallel paths. Those paths go around a closed loop, under each of the two poles (remember that the poles are of opposite polarity) to the opposite brush. Open commutator segments (most of them) do not carry current into or out of the machine.

8.9.1 Commutation Process

A commutation interval occurs when the current in one coil must be reversed (see Figure 8.8). In the simplest form, this involves a brush bridging between two commutator segments, shorting out that coil. The resistance of the brush causes the current to decay. When the brush leaves the leading segment, the current in the leading coil must reverse.

Several different mechanisms are used to assist the commutation process. *Resistive commutation* is the process relied upon in small machines. When the current in one coil must be reversed (because it has left one pole and is approaching the other), that coil is shorted by one of the brushes. The brush resistance causes the current in the coil to decay. Then the leading commutator segment leaves the brush, the current MUST reverse (the trailing coil has current in it), and there is often sparking.

In larger machines, the commutation process would involve too much sparking, which causes brush wear, dust from brush wear, and noxious gases (ozone) that promote corrosion.

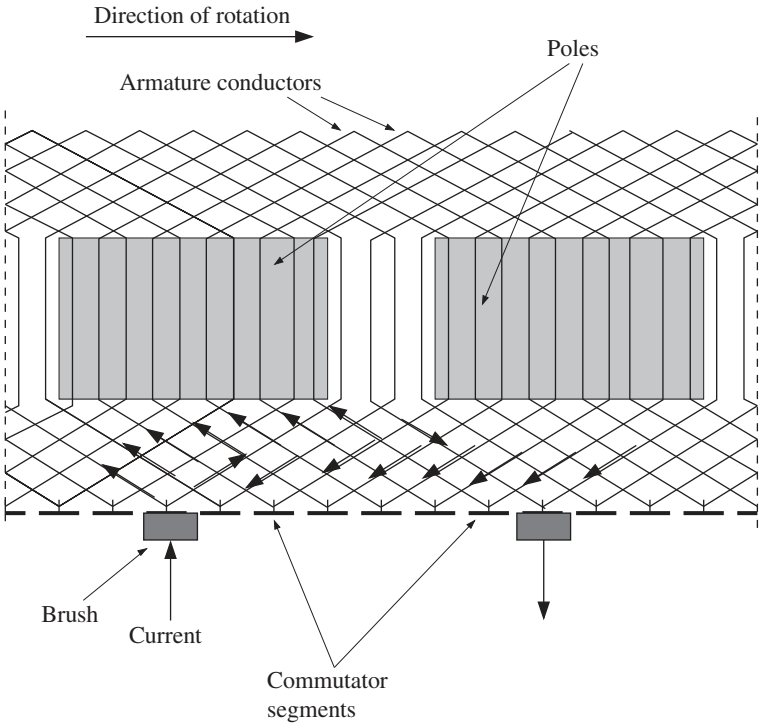

Figure 8.7 Commutator.

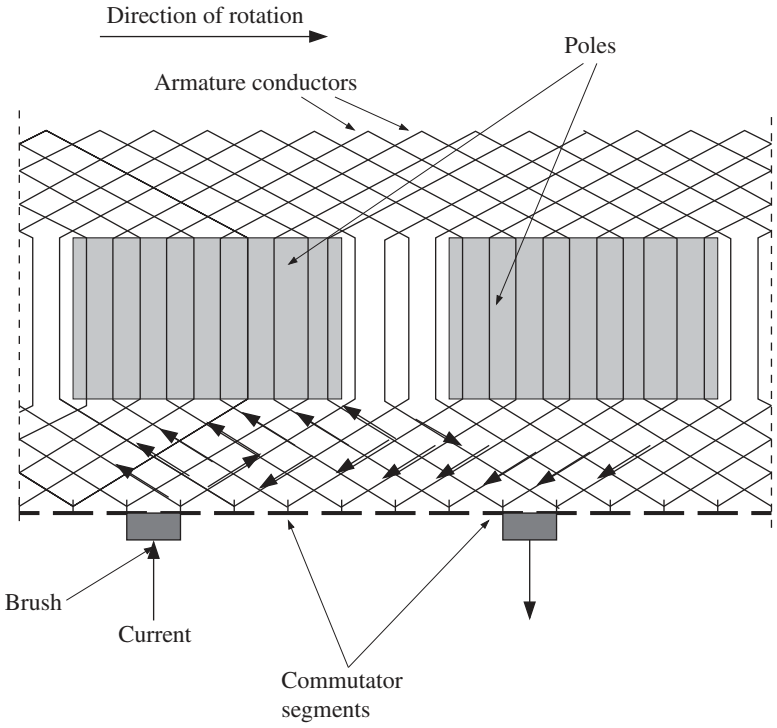

Figure 8.8 Commutator during commutation.

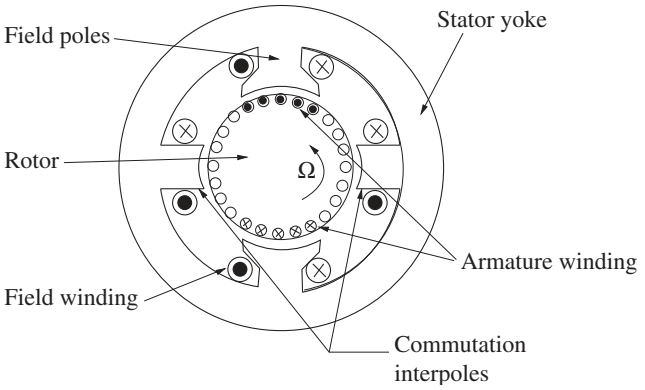

Figure 8.9 Commutation interpoles.

In these cases, it is common to use separate commutation interpoles. As shown schematically in Figure 8.9, these are separate, usually narrow pole pieces that are wired in series with the armature brushes, and so carry armature current. They are arranged in such a way that the flux from the interpole drives current in the commutated coil in the proper direction. The coil being commutated is located physically between the active poles and the interpole is therefore in the right spot to influence commutation. The interpole is wound with armature current (it is in series with the main brushes). It is easy to see that the interpole must have a flux density proportional to the current to be commutated. Since the speed with which the coil must be commutated is proportional to rotational velocity and so is the voltage induced by the interpole, if the right number of turns is put around the interpole, commutation can be made to be quite accurate.

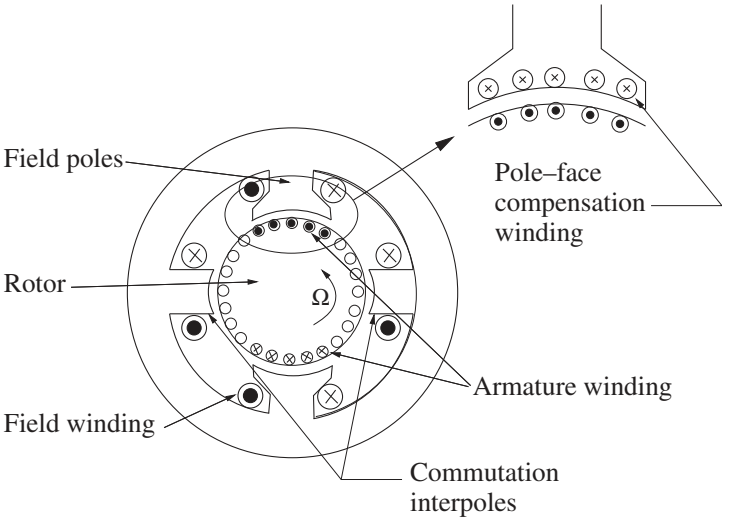

Figure 8.10 Pole face compensation winding.

8.9.2 Compensation

The analysis of commutator machines often ignores armature reaction flux. Obviously, these machines DO produce armature reaction flux, in quadrature with the main field. Normally, commutator machines are highly salient and the quadrature inductance is lower than direct-axis inductance, but there is still flux produced. This adds to the flux density on one side of the main poles (possibly leading to saturation). To make the flux distribution more uniform and therefore to avoid this saturation effect of quadrature axis flux, it is common in very highly rated machines to wind compensation coils: essentially mirror-images of the armature coils, but this time wound in slots in the surface of the field poles. Such coils will have the same number of ampere-turns as the armature. Normally, they have the same number of turns (but generally not the same number or spacing of armature slots) and are connected directly in series with the armature brushes. What they do is to almost exactly cancel the flux produced by the armature coils, leaving only the main flux produced by the field winding. One might think of these coils as providing a reaction torque, produced in exactly the same way as main torque is produced by the armature. A cartoon view of this is shown in Figure 8.10.

8.10 Compound Machines

It is possible to modify the torque-speed characteristics of commutator machines by using two field windings: one connected in shunt (that is, excited by the voltage of the power supply) and the other in series with the armature. One can look at this in two different ways: on the one hand, a series field winding contributes an increased "droop" to the torque-speed characteristic by reinforcing the flux and therefore reducing the armature current required for a given torque. On the other hand, adding a shunt field winding to a series-wound field produces a zero torque speed, helping to control low torque operation and preventing overspeed.

Consider the long-shunt connection of Figure 8.11. Since the shunt winding is directly across the terminals, current in it is simply $I_{shunt} = \frac{V_s}{R_{shunt}}$, and then armature current and torque are:

$$I_a = \frac{V_s - G_{shunt}\, I_{shunt}\Omega}{R_a + R_{shunt} + G_{series}\Omega}$$

$$T^e = G_{series}\, {I_a}^2 + G_{shunt}\, I_{shunt}\, I_a \tag{8.14}$$

Figure 8.12 illustrates the behavior of a compound motor: as torque increases, speed "droops", but current rises not as fast as in an uncompensated motor.

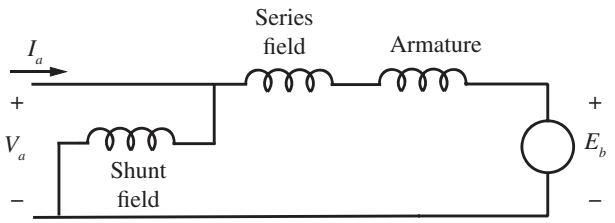

Figure 8.11 Long shunt compound machine connection.

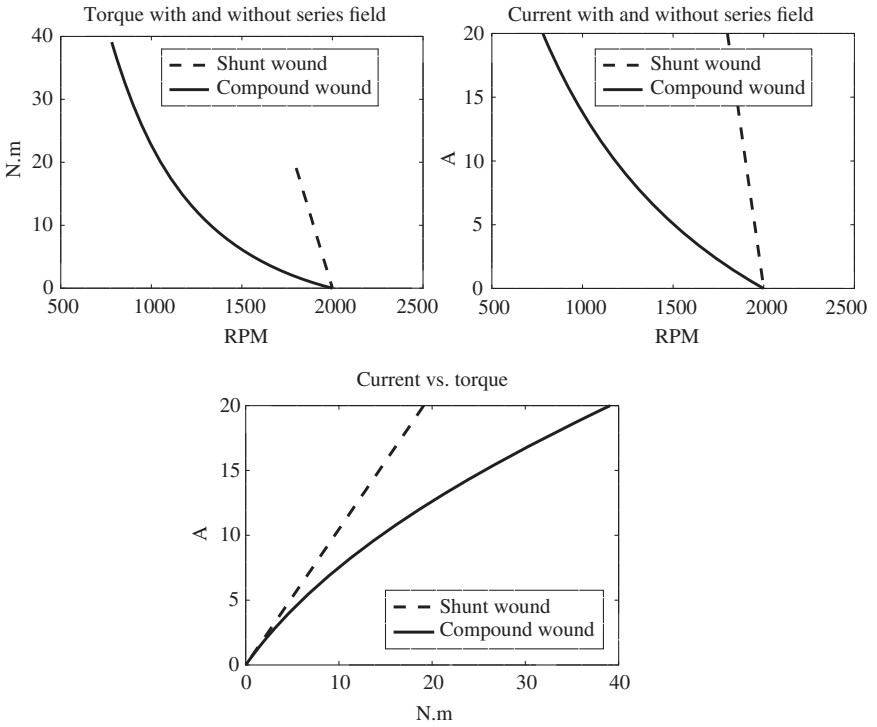

Figure 8.12 Compound wound DC motor.

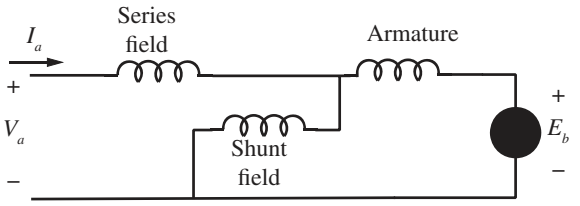

Figure 8.13 Short shunt compound machine connection.

The situation with a short shunt machine, as shown in Figure 8.13, is a bit more complex as neither field windings is directly across the terminals. To attack this problem, note that the voltage across the shunt field is found as the sum of two voltage dividers:

$$v_{shunt} = \frac{R_a \| R_{shunt}}{R_a \| R_{shunt} + R_{series}} V_a + \frac{R_{series} \| R_{shunt}}{R_{series} \| R_{shunt} + R_a} E_b \tag{8.15}$$

where

$$E_b = (G_{shunt} I_{shunt} + G_{series} I_a)\Omega \tag{8.16}$$

Figure 8.14 illustrates using a shunt field winding to modify the behavior of a series motor to have a zero torque speed.

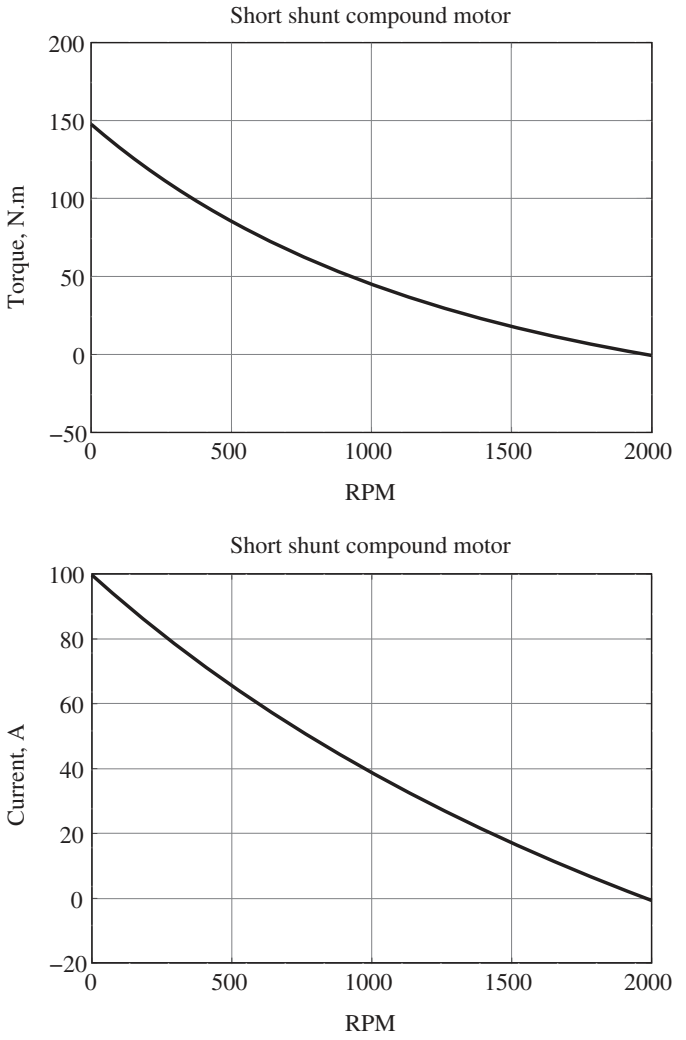

Figure 8.14 Short shunt motor behavior.

8.11 Problems

The next few problems are about a DC generator that has the following parameters:

Field resistance	R_f	249 Ω
Armature resistance	R_a	1 Ω
Field inductance	L_f	10 Hy
Motor constant	G	5 Hy (V/rad/sec—A)
Number of field turns		1000

8.1 What is the terminal voltage of this machine if, with the machine turning at 1000 RPM, the field current is set at 2 A and the armature is connected to a load of 10 Ω?

8.2 Find and plot the terminal voltage as a function of time if the machine is operating at 1000 RPM and the field is suddenly connected to a voltage source of 400 V. The armature is open circuited.

8.3 This generator is to serve as a brake for some rotational inertia. Mechanically, it is connected to a flywheel, and the inertia of the flywheel and machine together is $J = 5\,\text{kg.m}^2$. Electrically, the machine is connected through a switch to a resistor of 10 Ω. With a field current of 1 A, and an initial speed of 1000 RPM, what is speed, as a function of time, after the switch to the resistor is closed at time $t = 0$?

8.4 The generator is connected to a voltage source of 200 VDC. With a field current of 1 A, and with no load on the shaft, what speed does the machine operate at (it is a motor for now)?

The shaft of the generator is driven by an engine that produces torque between zero and 25 N.m. For that range of torque, calculate and sketch speed of the shaft. And calculate power delivered to the 200 VDC voltage source.

8.5 Now the machine is to be used as a motor. It is connected to a voltage source of 200 V and is connected in "shunt" configuration. Compute and sketch or plot the torque-speed curve.

8.6 The motor is to be made into a compound motor with a series field winding of 200 turns. The series field will have a resistance of 50 Ω, and is wired as a "short shunt" configuration. With a terminal voltage of 200 V, calculate speed vs. torque and armature current vs. torque.

Now we take a little more detailed look at the motor. As it turns out, it's magnetic circuit saturates for currents above about one ampere, so it's excitation curve is as shown in Figure 8.15. This curve can be modeled to be:

$$E_{af} = 5\,I_f + 245\ \tanh\left(\frac{I_f}{I_{f0}}\right)$$

where I_{f0} is 1 A.

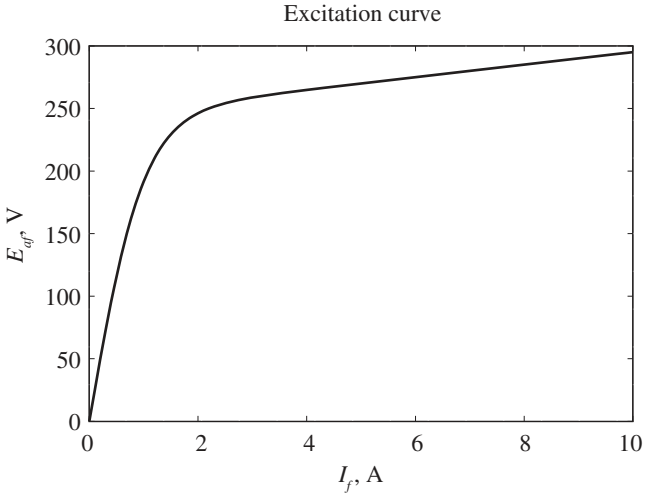

Figure 8.15 DC generator excitation curve at 500 RPM.

The machine is set up to be a dynamo (a self-excited generator), with the field winding connected directly to the terminals of the armature.

8.7 Above what speed will this machine self-excite?

8.8 Operating at 750 RPM, what is the steady-state voltage if the machine is otherwise unloaded?

8.9 For a speed range of 750–2000 RPM, estimate and plot the terminal voltage, assuming the machine is not otherwise loaded. HINT: This is an excellent application for MATLAB's fzero function or the equivalent non-linear equation solvers of other mathematical assistants.

8.10 Calculate the output voltage as a function of load current, with the machine turning at a steady 750 RPM.

8.11 Now, the machine is to be compounded by use of a series field winding to make it a "stiffer" voltage source. To estimate how many turns should be there to make it "flat" compounded (Zero apparent output impedance), calculate the derivative of internal voltage with field current, and give the series field enough turns to make the increase in internal voltage with load current match the decrease in terminal voltage because of armature resistance. Plot the output voltage with the uncompounded machine and with the compounded machine for load currents from zero to 25 A.

8.12 Without this series (compound) field, the machine is operating at 750 RPM when the field winding is suddenly connected to the armature terminals. We expect it to self-excite. Simulate this buildup, plotting voltage as a function of time. Assume the field current starts at 0.1 A.

9

Induction Machines

9.1 Introduction

Induction machines are perhaps the most widely used of all electric motors. They are generally simple to build and rugged, and offer reasonable asynchronous performance: a manageable torque-speed curve, stable operation under load, and generally satisfactory efficiency. Because they are so widely used, they are worth understanding in depth.

In addition to their current economic importance, induction motors and generators may find application in some new applications with designs that are not similar to motors currently in commerce. An example is very high-speed motors for gas compressors. Because it is possible that future, high-performance induction machines will be required to have characteristics different from those of existing machines, it is necessary to understand them from first principles, and that is the objective of this chapter. It starts with a circuit theoretical view of the induction machine. This analysis is strictly appropriate only for wound-rotor machines, but leads to an understanding of more complex machines. This model will be used to explain the basic operation of induction machines. Then a model for squirrel-cage machines will be derived.

9.2 Transformer Model

The induction machine has two electrically active elements: a rotor and a stator. In normal operation, the stator is excited by alternating voltage. The stator excitation creates a magnetic field in the form of a rotating or traveling wave, which induces currents in the circuits of the rotor. Those currents, in turn, interact with the traveling wave to produce torque. Figure 9.1 is a representation of an axial cross-section of an induction machine. The "stator" winding is in slots in the surface of the outer magnetic "core." The rotor also has slots, and to start assume that there is a polyphase winding in those slots. As its name implies, the rotor can turn with respect to the stator. The stator and rotor windings are mutually coupled and so form a kind of transformer. Shown in Figure 9.2 is a suggestion of that transformer coupling, in which there are three polyphase windings, one on the stator and one on the rotor.

Electromagnetic Analysis of Electric Machines: First Principles, Modeling, and Design, First Edition.
James L. Kirtley, Christopher H. T. Lee, and Sajjad Mohammadi.

Companion website: www.wiley.com/go/kirtleyelectric

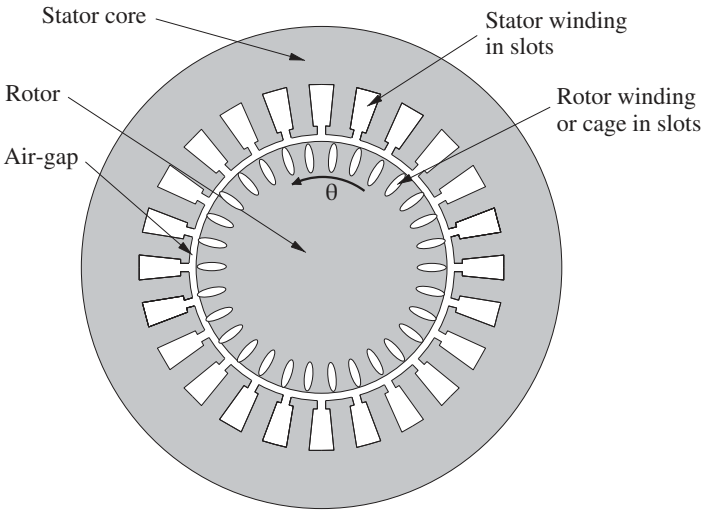

Figure 9.1 Axial cross-section of an induction machine.

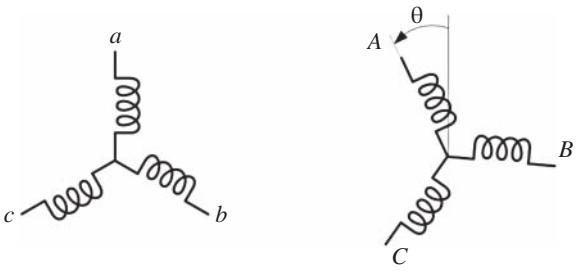

Figure 9.2 Schematic of transformer model.

Stator fluxes are λ_a λ_b and λ_c and rotor fluxes are λ_A λ_B and λ_C. The rotor and stator are actually closely coupled, and the coupling is modified by rotor position. The flux vs. current relationship is given by:

$$\begin{bmatrix} \lambda_a \\ \lambda_b \\ \lambda_c \\ \lambda_A \\ \lambda_B \\ \lambda_C \end{bmatrix} = \begin{bmatrix} \underline{L}_S & \underline{M}_{SR} \\ \underline{M}_{SR}^T & \underline{L}_R \end{bmatrix} \begin{bmatrix} i_a \\ i_b \\ i_c \\ i_A \\ i_B \\ i_C \end{bmatrix} \tag{9.1}$$

where the component submatrices are:

$$\underline{L}_S = \begin{bmatrix} L_a & L_{ab} & L_{ab} \\ L_{ab} & L_a & L_{ab} \\ L_{ab} & L_{ab} & L_a \end{bmatrix} \quad \underline{L}_R = \begin{bmatrix} L_A & L_{AB} & L_{AB} \\ L_{AB} & L_A & L_{AB} \\ L_{AB} & L_{AB} & L_A \end{bmatrix}$$

$$\underline{M}_{SR} = \begin{bmatrix} M\cos p\theta & M\cos\left(p\theta + \frac{2\pi}{3}\right) & M\cos\left(p\theta - \frac{2\pi}{3}\right) \\ M\cos\left(p\theta - \frac{2\pi}{3}\right) & M\cos p\theta & M\cos\left(p\theta + \frac{2\pi}{3}\right) \\ M\cos\left(p\theta + \frac{2\pi}{3}\right) & M\cos\left(p\theta - \frac{2\pi}{3}\right) & M\cos p\theta \end{bmatrix} \tag{9.2}$$

Note that the mutual inductance submatrices are circulant, and the submatrices at the upper right and lower left must be transposes of each other because of reciprocity. To carry the analysis further, it is necessary to make some assumptions regarding operation. To start, assume balanced currents in both the stator and rotor:

$$\begin{aligned} i_a &= I_S \cos \omega t & i_A &= I_R \cos(\omega_R t + \zeta_R) \\ i_b &= I_S \cos\left(\omega t - \frac{2\pi}{3}\right) & i_B &= I_R \cos\left(\omega_R t + \zeta_R - \frac{2\pi}{3}\right) \\ i_c &= I_S \cos\left(\omega t + \frac{2\pi}{3}\right) & i_C &= I_R \cos\left(\omega_R t + \zeta_R + \frac{2\pi}{3}\right) \end{aligned} \tag{9.3}$$

The rotor position θ can be described by $\theta = \omega_m t + \theta_0$.

Under these assumptions, we may calculate the form of stator fluxes. As it turns out, we need only write out the expressions for λ_a and λ_A to see what is going on:

$$\begin{aligned} \lambda_a = {} & (L_a - L_{ab}) I_S \cos \omega t + M \ I_R(\cos(\omega_R t + \zeta_R) \ \cos p(\omega_m t + \theta_0)) \\ & + M \ I_R \left(\cos\left(\omega_R t + \zeta_R + \frac{2\pi}{3}\right) \ \cos p\left(\omega_m t + \theta_0 - \frac{2\pi}{3}\right)\right) \\ & + M \ I_R \left(\cos\left(\omega_R t + \zeta_R - \frac{2\pi}{3}\right) \ \cos p\left(\omega_m t + \theta_0 + \frac{2\pi}{3}\right)\right) \end{aligned} \tag{9.4}$$

$$\begin{aligned} \lambda_A = {} & M I_S(\cos(p\omega_m t + \theta_0) \cos \omega t) \\ & + M I_S \left(\cos\left(p\omega_m t + \theta_0 - \frac{2\pi}{3}\right) \cos\left(\omega t + \frac{2\pi}{3}\right)\right) \\ & + M I_S \left(\cos\left(p\omega_m t + \theta_0 + \frac{2\pi}{3}\right) \cos\left(\omega t - \frac{2\pi}{3}\right)\right) + (L_A - L_{AB}) I_R \cos(\omega_R t + \zeta_R) \end{aligned} \tag{9.5}$$

After reducing the trig expressions, these become:

$$\begin{aligned} \lambda_a &= (L_a - L_{ab}) I_S \cos \omega t + \frac{3}{2} M I_R \cos((p\omega_m + \omega_R)t + \zeta_R + p\theta_0) \\ \lambda_A &= \frac{3}{2} M I_S(\cos(\omega - p\omega_m)\, t - p\theta_0) + (L_A - L_{AB}) I_R \cos(\omega_R t + \zeta_R) \end{aligned} \tag{9.6}$$

These last two expressions give fluxes in the armature and rotor windings in terms of currents in the same two windings, assuming that both current distributions are sinusoidal in time and space and represent balanced distributions. The next step is to make another assumption, that the stator and rotor frequencies match through rotor rotation. That is that $\omega - p\omega_m = \omega_R$. It is important to keep straight the different frequencies:

ω is stator *electrical* frequency
ω_R is rotor *electrical* frequency
ω_m is *mechanical* rotation speed, so that
$p\omega_m$ is *electrical* rotation speed

To refer rotor quantities to the stator frame (i.e. non-rotating), and to work in complex amplitudes, the following definitions are made:

$$\begin{aligned} i_a &= Re\{\underline{I}_a e^{j\omega t}\} \quad i_A = Re\left\{\underline{I}_A e^{j\omega_R t}\right\} \\ \lambda_a &= Re\{\Lambda_a e^{j\omega t}\} \quad \lambda_A = Re\left\{\Lambda_A e^{j\omega_R t}\right\} \end{aligned} \tag{9.7}$$

With these definitions, the complex amplitudes become:

$$\underline{\Lambda}_a = L_S \underline{I}_a + \frac{3}{2} M \underline{I}_A e^{j(\zeta_R + p\theta_0)}$$
$$\underline{\Lambda}_A = \frac{3}{2} M \underline{I}_a e^{jp\theta_0} + L_R e^{j\zeta_R} \tag{9.8}$$

where $L_S = L_a - L_{ab}$ and $L_R = L_A - L_{AB}$ are the synchronous inductances of stator and rotor, respectively.

There are two phase angles embedded in these expressions: θ_0, which describes the rotor physical phase angle with respect to stator current, and ζ_R, which describes the phase angle of rotor currents with respect to stator currents. It is appropriate to invent two new rotor variables, which are simple rotations of the variables already derived:

$$\underline{\Lambda}_{AR} = \underline{\Lambda}_A e^{jp\theta_0} \quad \underline{I}_{AR} = \underline{I}_A e^{j(p\theta_0 + \zeta_R)} \tag{9.9}$$

These are rotor flux and current referred to armature phase angle. Note that Λ_{AR} and I_{AR} have the same phase relationship to each other as do Λ_A and I_A. The basic flux/current relationship for the induction machine becomes:

$$\begin{bmatrix} \underline{\Lambda}_a \\ \underline{\Lambda}_{AR} \end{bmatrix} = \begin{bmatrix} L_s & \frac{3}{2}M \\ \frac{3}{2}M & L_R \end{bmatrix} \begin{bmatrix} \underline{I}_a \\ \underline{I}_{AR} \end{bmatrix} \tag{9.10}$$

This is an equivalent single-phase statement, describing the flux/current relationship in phase a, assuming balanced operation. The same expression will describe phases b and c.

Voltage at the terminals of the stator and rotor (possibly equivalent) windings is then:

$$\underline{V}_a = j\omega \underline{\Lambda}_a + R_a I_a = j\omega L_S \underline{I}_a + j\omega \frac{3}{2} M \underline{I}_{AR} + R_a I_a$$
$$\underline{V}_{AR} = j\omega_R \underline{\Lambda}_{AR} + R_A \underline{I}_{AR} = j\omega_R \frac{3}{2} M \underline{I}_a + j\omega_R L_R \underline{I}_{AR} + R_A \underline{I}_{AR} \tag{9.11}$$

To carry this further, it is necessary to go a little deeper into the machine's parameters. Note synchronous inductances for the stator and rotor may be separated into space fundamental and "leakage" components as follows:

$$L_S = L_a - L_{ab} = \frac{3}{2} \frac{4}{\pi} \frac{\mu_0 R \ell N_S^2 k_S^2}{p^2 g} + L_{s\ell}$$
$$L_R = L_A - L_{AB} = \frac{3}{2} \frac{4}{\pi} \frac{\mu_0 R \ell N_R^2 k_R^2}{p^2 g} + L_{R\ell} \tag{9.12}$$

where the normal set of machine parameters holds:

R is rotor radius
ℓ is active length
g is the *effective* air-gap
p is the number of pole pairs
N represents the number of turns
k represents the winding factor
S as a subscript refers to the stator
R as a subscript refers to the rotor
L_ℓ is "leakage" inductance

The two "leakage" terms $L_{S\ell}$ and $L_{R\ell}$ contain higher-order harmonic stator and rotor inductances, slot inductances, end-winding inductances, and, if necessary, a provision for rotor skew. Essentially, they are used to represent all flux in the rotor and stator that is not mutually coupled. In the same terms, the stator-to-rotor mutual inductance, which is taken to comprise only a space fundamental term, is:

$$M = \frac{4}{\pi}\frac{\mu_0 R\ell N_S N_R k_S k_R}{p^2 g} \tag{9.13}$$

Note that there are, of course, space harmonic mutual flux linkages. These are unimportant in properly designed wound rotor machines but are of substantial impact in squirrel cage machines. These will be considered later.

Air-gap permeance is common to all of these inductance expressions:

$$\wp_{ag} = \frac{4}{\pi}\frac{\mu_0 R\ell}{p^2 g} \tag{9.14}$$

so the inductances are:

$$\begin{aligned} L_S &= \frac{3}{2}\wp_{ag}k_S^2 N_S^2 + L_{S\ell} \\ L_R &= \frac{3}{2}\wp_{ag}k_R^2 N_R^2 + L_{R\ell} \\ M &= \wp_{ag}N_S N_R k_S k_R \end{aligned} \tag{9.15}$$

"Slip" s is the rotor frequency relative to the stator frequency. As the name implies, it is a measure of how the rotor is slipping with respect to the synchronously rotating flux wave from stator excitation:

$$\omega_R = s\omega$$

or

$$s = 1 - \frac{p\omega_m}{\omega} \tag{9.16}$$

Using these definitions, the two voltage balance equations become:

$$\begin{aligned} \underline{V}_a &= j\omega\left(\frac{3}{2}\wp_{ag}k_S^2 N_S^2 + L_{S\ell}\right)\underline{I}_a + j\omega\frac{3}{2}\wp_{ag}N_S N_R k_S k_R \underline{I}_{AR} + R_a\underline{I}_a \\ \underline{V}_{AR} &= js\omega\frac{3}{2}\wp_{ag}N_S N_R k_S k_R \underline{I}_a + js\omega\left(\frac{3}{2}\wp_{ag}k_R^2 N_R^2 + L_{R\ell}\right)\underline{I}_{AR} + R_A\underline{I}_{AR} \end{aligned} \tag{9.17}$$

If it is assumed that the rotor is shorted so that $\underline{V}_{AR} = 0$ and if the rotor voltage expression is divided by slip s, and if the rotor expressions are referred across the "transformer ratio" to the stator, the two voltage expressions become:

$$\begin{aligned} \underline{V}_a &= j(X_M + X_1)\underline{I}_a + jX_M\underline{I}_2 + R_a\underline{I}_a \\ 0 &= jX_M\underline{I}_a + j(X_M + X_2)\underline{I}_2 + \frac{R_2}{s}\underline{I}_2 \end{aligned} \tag{9.18}$$

where the following definitions have been made:

$$\begin{aligned} X_M &= \frac{3}{2}\omega\wp_{ag}N_S^2 k_S^2 & X_1 &= \omega L_{S\ell} \\ X_2 &= \omega L_{R\ell}\left(\frac{N_S k_S}{N_R k_R}\right)^2 & R_2 &= R_A\left(\frac{N_S k_S}{N_R k_R}\right)^2 \end{aligned} \tag{9.19}$$

These expressions describe a simple equivalent circuit for the induction motor shown in Figure 9.3.

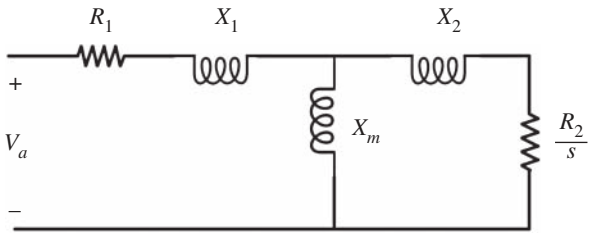

Figure 9.3 Induction motor equivalent circuit.

9.3 Operation: Energy Balance

Assume for the moment that Figure 9.3 represents one phase of a polyphase system and that the machine is operated under balanced conditions and that speed is constant or varying only slowly. "Balanced conditions" means that each phase has the same terminal voltage magnitude and that the phase difference between phases is uniform. Under those conditions, each phase can be analyzed separately. Assume an RMS voltage magnitude of V_t across each phase. The "gap impedance," or the impedance looking to the right from the right-most terminal of X_1 is:

$$\underline{Z}_g = jX_m \Big\| \left(jX_2 + \frac{R_2}{s} \right)$$

Terminal impedance is then:

$$\underline{Z}_t = jX_1 + R_1 + \underline{Z}_g$$

Terminal current is: $\underline{I}_t = \underline{V}_t / \underline{Z}_t$. Rotor current is found using a current divider:

$$\underline{I}_2 = \underline{I}_t \frac{jX_m}{jX_2 + \frac{R_2}{s} + jX_m} \tag{9.20}$$

"Air-gap" power is calculated, assuming a three-phase machine:

$$P_{ag} = 3\,|\underline{I}_2|^2 \frac{R_2}{s} \tag{9.21}$$

This is *real* (time-average) power crossing the air-gap of the machine. Positive slip implies rotor speed less than synchronous and positive air-gap power (motor operation). Negative slip means rotor speed is higher than synchronous, negative air-gap power (from the rotor to the stator), and generator operation. Note that this equivalent circuit represents a real physical structure, so it should be possible to calculate power dissipated in the physical rotor resistance, and that is:

$$P_s = sP_{ag} = 3|I_2|^2 R_2$$

(Since both P_{ag} and s will always have the same sign, dissipated power is positive.)

The rest of this discussion is framed in terms of motor operation, but the conversion to generator operation is simple. The difference between power crossing the air-gap and power dissipated in the rotor resistance must be converted from electrical to mechanical:

$$P_m = P_{ag} - P_s = (1-s)P_{ag} = 3|\underline{I}_2|^2 \frac{R_2}{s}(1-s) \tag{9.22}$$

It should be emphasized that P_m is converted, not necessarily output power. There are a number of parasitic losses that subtract from this: losses due to space harmonics (more on that later),

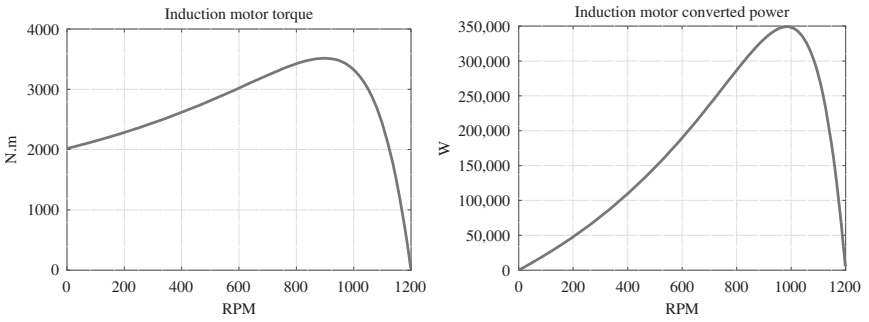

Figure 9.4 Torque and power of the exemplar motor.

windage, and bearing friction. Because mechanical power is torque multiplied by physical rotor speed, torque becomes:

$$T = \frac{P_m}{\frac{\omega(1-s)}{p}} = 3\frac{p}{\omega}|\underline{I}_2|^2\frac{R_2}{s} \tag{9.23}$$

9.3.1 Example

An example motor with a rating of about 250 hp (186.5 kW) might have the following parameters:

Pole number p	3
Voltage	440 V (line-line) or 254 V (line-neutral) RMS
Frequency	60 Hz
Stator resistance R_1	0.073 Ω
Rotor Resistance R_2	0.035 Ω
Stator Reactance X_1	0.06 Ω
Rotor Reactance X_2	0.06 Ω
Magnetizing Reactance X_m	2.5 Ω

Solving for currents in the circuit model of Figure 9.3 and then using (9.22) and (9.23) yields the torque and power shown in Figure 9.4.

9.4 Squirrel Cage Machine Model

The most common induction machines in application are actually what are called *squirrel cage* machines. The name arises from the fact that in such machines, the rotor conductors are not windings as was assumed earlier in this chapter, but are simply bars of conducting material (usually aluminum or copper) that are all shorted together by conductive rings at each end of the rotor. If one ignores the ferromagnetic material that constitutes most of the rotor, the conductor bars and associated end rings would resemble the sort of 'cage' that a small animal might run around in.

A circuit model for the squirrel-cage motor can be derived using field analytical techniques. The model consists of two major parts. The first of these is a description of stator flux in terms of stator and rotor currents. The second is a description of rotor current in terms of air-gap flux. The result of all of this is a set of expressions for the elements of the circuit model for the induction machine.

To start, assume that the rotor is symmetrical enough to carry a surface current, the fundamental of which is:

$$\vec{K}_r = \vec{i}_z Re\{\underline{K}_r e^{j(\omega t - p\phi)}\} = \vec{i}_z Re\{\underline{K}_r e^{j(s\omega t - p\phi')}\} \tag{9.24}$$

Note the transformation from stator to rotor coordinates:

$$\begin{aligned} \phi' &= \phi - \omega_m t \\ p\omega_m &= \omega - \omega_r = \omega(1-s) \end{aligned} \tag{9.25}$$

The rotor current sheet described will produce an air-gap flux density of the form:

$$\begin{aligned} B_r &= Re\{\underline{B}_r e^{j(\omega t - p\phi)}\} \\ \underline{B}_r &= -j\mu_0 \frac{R}{pg}\underline{K}_r \end{aligned} \tag{9.26}$$

Note that this describes only radial magnetic flux density produced by the space fundamental of rotor current. Flux linked by the armature winding due to this flux density is:

$$\lambda_{AR} = \ell N_s k_S \int_{-\frac{\pi}{p}}^{0} B_r(\phi)\, d\phi$$

This yields a complex amplitude for the flux linked by the armature winding due to the rotor surface current:

$$\begin{aligned} \lambda_{AR} &= Re\,\{\underline{\Lambda}_{AR} e^{j\omega t}\} \\ \underline{\Lambda}_{AR} &= \frac{2\ell\mu_0 R^2 N_s k_S}{p^2 g}\underline{K}_r \end{aligned} \tag{9.27}$$

Adding this to flux produced by the stator currents, total stator flux is:

$$\underline{\Lambda}_a = \left(\frac{3}{2}\frac{4}{\pi}\frac{\mu_0 R\ell N_S^2 k_s^2}{p^2 g} + L_{s\ell}\right)\underline{I}_a + \frac{2\ell\mu_0 R^2 N_S k_S}{p^2 g}\underline{K}_r \tag{9.28}$$

This motivates a definition of an equivalent rotor current I_2 in terms of the space fundamental of rotor surface current density:

$$\underline{I}_2 = \frac{\pi}{3}\frac{R}{N_S k_S}\underline{K}_z \tag{9.29}$$

Then an expression for stator flux in terms of stator and secondary current is:

$$\underline{\Lambda}_a = \left(L_{ad} + L_{S\ell}\right)\underline{I}_a + L_{ad}\underline{I}_2 \tag{9.30}$$

where Lad is the fundamental space harmonic component of stator inductance:

$$L_{ad} = \frac{3}{2}\frac{4}{\pi}\frac{\mu_0 R\ell N_S^2 k_S^2}{p^2 g} \tag{9.31}$$

9.4.1 Squirrel Cage Currents

The second part of this derivation is the equivalent of finding a relationship between rotor flux and effective rotor current I_2. However, since this machine has no discrete windings, it is necessary to focus on the individual rotor bars.

Assume that there are N_R slots in the rotor. Each of these slots is carrying some current. If the machine is symmetrical and operating with balanced currents, each bar is carrying current of the same magnitude and a phase angle that decreases progressively slot by slot. An expression for current in the k^{th} slot is:

$$i_k = Re\,\{\underline{I}_k e^{js\omega t}\} \qquad \underline{I}_k = \underline{I} e^{-jk\frac{2\pi p}{N_R}} \tag{9.32}$$

And $\underline{I}$ is the complex amplitude of current in slot number zero. This expression shows a uniform progression of rotor current phase about the rotor. All rotor slots carry the same current, but that current is phase retarded (delayed) from slot to slot because of relative rotation of the current wave at slip frequency.

The rotor current density can then be expressed as a sum of impulses in space:

$$K_z = Re\left\{\sum_{k=0}^{N_R-1}\frac{1}{R}\underline{I}e^{j\left(s\omega t-k\frac{2\pi p}{N_R}\right)}\delta\left(\phi'-\frac{2\pi k}{N_R}\right)\right\} \tag{9.33}$$

The unit impulse function $\delta()$ is an approximation of the rotor current as being a series of current impulses, one for each of the rotor bars. This is actually not a bad approximation as the rotor slot openings tend to be quite small and the results will be integrated.

The rotor surface current may also be expressed as a Fourier series of traveling waves:

$$K_z = Re\left\{\sum_{n=-\infty}^{\infty}\underline{K}_n e^{j(s\omega t-np\phi')}\right\} \tag{9.34}$$

Note that this Fourier series has both positive and negative values of the space harmonic index n to allow for both forward-going and reverse-rotating waves. This is really part of an expansion in both time and space, although only the time fundamental part is considered. The *n*th space harmonic component is found by employing the following formula:

$$\underline{K}_n = \left\langle\frac{1}{\pi}\int_0^{2\pi}K_z(\phi',\ t)\,e^{-j(s\omega t-np\phi')}\,d\phi'\right\rangle$$

Here, the brackets <> denote time average and are here because of the two-dimensional nature of the expansion. To carry this out, first expand into its complex conjugate parts:

$$K_z = \sum_{k=0}^{N_R-1}\left\{\frac{\underline{I}}{R}e^{j\left(s\omega t-k\frac{2\pi p}{N_R}\right)}+\frac{\underline{I}^*}{R}e^{-j\left(s\omega t-k\frac{2\pi p}{N_R}\right)}\right\}\delta\left(\phi'-\frac{2\pi k}{N_R}\right) \tag{9.35}$$

The second half of this expression results in a sum of terms that time averages to zero. The first half of the expression results in:

$$\underline{K}_n = \frac{\underline{I}}{2\pi R}\int_0^{2\pi}\sum_{k=0}^{N_R-1}e^{-j\frac{2\pi pk}{N_R}}e^{jnp\phi'}\delta\left(\phi'-\frac{2\pi k}{N_R}\right)d\phi'$$

The impulse function turns the integral into an evaluation of the rest of the integrand at the impulse. What remains is the sum:

$$\underline{K}_n = \frac{\underline{I}}{2\pi R}\sum_{k=0}^{N_R-1}e^{j(n-1)\frac{2\pi pk}{N_R}} \tag{9.36}$$

When this sum is evaluated, it is:

$$\sum_{k=0}^{N_R-1}e^{j(n-1)\frac{2\pi pk}{N_R}} = \begin{cases} N_R \ \textit{if}\ (n-1)\ \frac{p}{N_R}\ \textit{is an integer} \\ 0 \quad \textit{otherwise}\end{cases} \tag{9.37}$$

The integer in this expression may be positive, negative, or zero. As it turns out, only the first three of these components (zero, plus, and minus one) are important, because they produce the

largest magnetic fields and therefore fluxes. These are:

$$\begin{aligned}(n-1)\frac{p}{N_R} &= -1 \quad or \;\; n = -\frac{N_R - p}{p} \\ &= 0 \quad or \;\; n = 1 \\ &= 1 \quad or \;\; n = \frac{N_R + p}{p}\end{aligned} \tag{9.38}$$

This appears to produce space harmonic orders that may be of non-integer order. This is not really true: it is necessary that np be an integer, and this will always satisfy that condition. So, the harmonic orders of interest to us are one and $n_+ = N_R/p + 1$ and $n_- = -N_R/p + 1$. That latter represents a flux wave rotating backward.

Each of the space harmonics of the squirrel cage current will produce radial flux density. A surface current of the form:

$$K_n = Re\left\{\frac{N_R \underline{I}}{2\pi R} e^{j(s\omega t - np\phi')}\right\} \tag{9.39}$$

produces a radial magnetic flux density:

$$\begin{aligned}B_{rn} &= Re\left\{\underline{B}_{rn} e^{j(s\omega t - np\phi')}\right\} \\ \underline{B}_{rn} &= -j\frac{\mu_0 N_R \underline{I}}{2\pi npg}\end{aligned} \tag{9.40}$$

In turn, each of the components of radial flux density will produce a component of induced voltage. Faraday's law is, in this case:

$$\nabla \times E = -\frac{\partial B}{\partial t} \Rightarrow \frac{1}{R}\frac{\partial E_z}{\partial \phi} = -\frac{\partial B_r}{\partial t} \tag{9.41}$$

Assuming an electric field component of the form:

$$\begin{aligned}E_{zn} &= Re\left\{\underline{E}_n e^{j(s\omega t - np\phi')}\right\} \\ \underline{E}_n &= \frac{s\omega R}{np}\underline{B}_n = -j\frac{\mu_0 N_R s\omega R}{2\pi g(np)^2}\underline{I}\end{aligned} \tag{9.42}$$

The total voltage induced in a slot pushes current through the conductors in that slot. Taking the lowest order (that is, the most consequential) harmonics:

$$\underline{E}_1 + \underline{E}_{n-} + \underline{E}_{n+} = \underline{Z}_{slot}\underline{I} \tag{9.43}$$

There are three components of air-gap field. $\underline{E}_1$ is the space fundamental field, produced by the space fundamental of rotor current as well as by the space fundamental of stator current. The other two components on the left of (9.43) are produced only by rotor currents and actually represent additional reactive impedance to the rotor. This is often called zigzag leakage inductance. The parameter $\underline{Z}_{slot}$ represents impedance of the slot itself: resistance and reactance associated with cross-slot magnetic fields. The voltage expression can be rewritten as:

$$\underline{E}_1 = \underline{Z}_{slot}\underline{I} + j\frac{\mu_0 N_R s\omega R}{2\pi g}\left(\frac{1}{(n_+ p)^2} + \frac{1}{(n_- p)^2}\right)\underline{I} \tag{9.44}$$

Noting that secondary current is directly proportional to bar current:

$$\underline{I}_2 = \frac{N_R}{N_S k_S}\underline{I}$$

Now, the fundamental axial electric field is:

$$\underline{E}_1 = \left[\frac{6N_S k_S}{N_R}\underline{Z}_{slot} + js\omega\frac{3}{\pi}\frac{\mu_0 N_S k_S R}{g}\left(\frac{1}{(n_+ p)^2} + \frac{1}{(n_- p)^2}\right)\right]\underline{I}_2 \tag{9.45}$$

This must be translated into an equivalent stator voltage. To do so, first find the fundamental of magnetic flux density:

$$\underline{B}_r = \frac{p\underline{E}_1}{\omega_r R} = \left[\frac{6pN_S k_S}{N_R R}\left(\frac{R_{slot}}{\omega_r} + jL_{slot}\right) + j\frac{3}{\pi}\frac{\mu_0 pN_S k_S R}{g}\left(\frac{1}{(n_+ p)^2} + \frac{1}{(n_- p)^2}\right)\right]\underline{I}_2 \tag{9.46}$$

Flux linking the armature winding is:

$$\lambda_{ag} = N_S k_S \ell R\int_{-\frac{x}{p}}^{0} Re\left\{\underline{B}_r e^{j(\omega t - p\phi)}\right\} = Re\left\{\underline{\Lambda}_{ag} e^{j\omega t}\right\}$$

$$\underline{\Lambda}_{ag} = j\frac{2N_S k_S \ell R}{p}\underline{B}_r$$

Air-gap voltage is:

$$\begin{aligned}\underline{V}_{ag} &= j\omega\underline{\Lambda}_{ag} = -\frac{2\omega N_S k_S \ell R}{p}\underline{B}_r \\ &= -\underline{I}_2\left[\frac{12\ell N_S^2 k_S^2}{N_R}\left(j\omega L_{slot} + \frac{R_{slot}}{s}\right) + j\omega\frac{6}{\pi}\frac{\mu_0 R\ell N_S^2 k_S^2}{g}\left(\frac{1}{(n_+ p)^2} + \frac{1}{(n_- p)^2}\right)\right]\end{aligned} \tag{9.47}$$

9.4.2 Squirrel Cage Impedance Elements

This describes the relationship between the space fundamental air-gap voltage $\underline{V}_{ag}$ and rotor current $\underline{I}_2$. This expression fits the equivalent circuit of Figure 9.5 if the definitions made below hold:

$$X_2 = \omega\frac{12\ell N_S^2 k_S^2}{N_R}L_{slot} + \omega\frac{6}{\pi}\frac{\mu_0 R\ell N_S^2 k_S^2}{g}\left(\frac{1}{(N_R + p)^2}\frac{1}{(N_R - p)^2}\right)$$

$$R_2 = \frac{12\ell N_S^2 k_S^2}{N_R}R_{slot} \tag{9.48}$$

The first term in the expression above expresses slot leakage inductance for the rotor. Similarly, the second expression expresses rotor resistance in terms of slot resistance. Note that L_{slot} and R_{slot} are both expressed per unit length. The second term in the expression above expresses the "zigzag" leakage inductance resulting from harmonics on the order of rotor slot pitch.

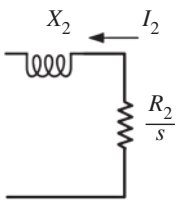

Figure 9.5 Fundamental circuit of squirrel cage.

As can readily be seen from considering the magnetic flux produced by the armature winding, there are a number of space harmonic flux components. In a wound rotor machine, those harmonic components can usually be ignored or treated as leakage. But in a squirrel cage machine, those space harmonics can, in many cases, link with the rotor. And when space harmonic fluxes link with the rotor, they can cause parasitic torques and what are sometimes called "stray" load loss. It is important to recognize that the characteristic harmonic numbers in a three-phase winding are the fundamental, of order one, then five, seven, eleven, and thirteen, and so forth. That is, the characteristic harmonics are of order $n = 6k \pm 1$, where k is an integer. The components of order $6k + 1$ rotate forward at a velocity inversely proportional to the harmonic number; the components of order $6k - 1$ rotate in the inverse direction.

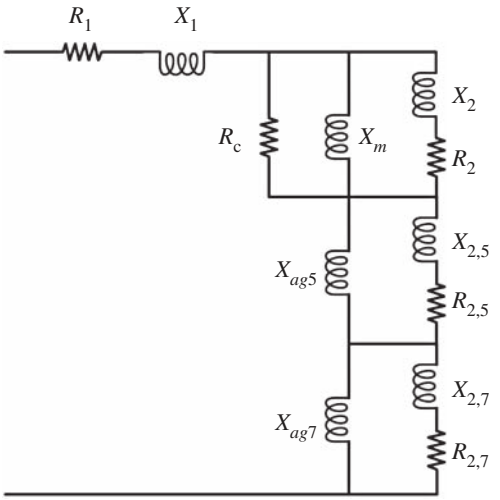

Figure 9.6 Equivalent circuit, including belt harmonics.

There are a number of components of stator "leakage," representing flux paths that do not directly involve the rotor. These include stator slot leakage inductance and end winding leakage inductance. Space harmonics of the stator MMF constitute what might be, in some cases, referred to as "leakage," but are actually more actively involved in the interaction of the machine. The most prominent components of these space harmonics are referred to as "belt" and "zigzag". Each of these will be discussed in the following paragraphs.

It is important to note that all of the space harmonic components are excited by the same armature current, and that fluxes produced by those currents all link the same winding. So, those harmonic components are all in series in a machine. Thus, an equivalent circuit that can represent both fundamental and harmonic interactions is in the form shown by Figure 9.6.

9.4.3 Belt Leakage

Belt and zigzag leakage components are due to air-gap space harmonics of order $n = 5$ and $n = 7$. If there were no rotor coupling, the belt harmonic leakage terms would be:

$$X_{ag\,5} = \frac{3}{2}\frac{4}{\pi}\omega\frac{\mu_0 N_S^2 k_5^2 R\ell}{5^2 p^2 g}$$

$$X_{ag\,7} = \frac{3}{2}\frac{4}{\pi}\omega\frac{\mu_0 N_S^2 k_7^2 R\ell}{7^2 p^2 g} \tag{9.49}$$

The belt harmonics link to the rotor, however, and actually appear to be in parallel with components of rotor impedance appropriate to $5p$ and $7p$ pole-pair machines. Those components are:

$$X_{2,5} = \omega\frac{12\ell N_S^2 k_5^2}{N_R}L_{slot} + \omega\frac{6}{\pi}\frac{\mu_0 R\ell N_S^2 k_5^2}{g}\left(\frac{1}{(N_R+5p)^2} + \frac{1}{(N_R-5p)^2}\right)$$

$$X_{2,7} = \omega\frac{12\ell N_S^2 k_7^2}{N_R}L_{slot} + \omega\frac{6}{\pi}\frac{\mu_0 R\ell N_S^2 k_7^2}{g}\left(\frac{1}{(N_R+7p)^2} + \frac{1}{(N_R-7p)^2}\right)$$

$$R_{2,5} = \frac{12\ell N_S^2 k_5^2}{N_R}R_{slot}$$

$$R_{2,7} = \frac{12\ell N_S^2 k_7^2}{N_R}R_{slot} \tag{9.50}$$

9.4.4 Zigzag Leakage

Stator zigzag leakage is from those harmonics of the orders $p_{ns} = N_{slots} \pm p$, where N_{slots} is the total number of stator slots. Harmonics of these orders can be handled in the same way as the belt harmonics (substitute the appropriate order for the expressions above); or, since coupling from the rotor to these harmonics can be sharply reduced by skew, they can be accounted for by:

$$X_z = \frac{3}{2}\frac{4}{\pi}\omega\frac{\mu_0 N_S^2 R\ell}{g}\left(\frac{k_{ns+}^2}{(N_{slots}+p)^2} + \frac{k_{ns-}^2}{(N_{slots}-p)^2}\right) \tag{9.51}$$

where k_{ns+} and k_{ns-} are the winding factors for the appropriate harmonic orders.

9.4.5 Operation: Harmonics Interactions

Because the space harmonics of stator MMF can interact with the rotor, they do have some impact on motor operation. If operation of an induction machine is estimated from the equivalent circuit of Figure 9.3, typically the losses are underestimated and sometimes simply characterized (or dismissed) as "stray" load loss. These losses can be understood, however. The belt and higher-order harmonics will have relative frequencies (slips) that are:

$$s_n = 1 \mp n\,(1-s)\begin{Bmatrix} n = 6k+1 \\ n = 6k-1 \end{Bmatrix} \qquad k \text{ is an integer} \tag{9.52}$$

Referring to Figure 9.6, note that the terminal flux of the machine is the sum of all of the harmonic fluxes, and each space harmonic is excited by the same current, so the individual harmonic components are in series. Each of the space harmonics will have an electromagnetic interaction similar to the fundamental. Power transferred across the air-gap is:

$$P_{em,n} = 3|\underline{I}_{2,n}|^2\frac{R_{2,n}}{s_n}$$

Dissipation in each circuit is:

$$P_{d,n} = 3|\underline{I}_{2,n}|^2 R_{2,n}$$

Leaving power converted by this harmonic:

$$P_{m,n} = 3|\underline{I}_{2,n}|^2\frac{R_{2,n}}{s_n}(1-s_n) \tag{9.53}$$

Note that, when an induction machine is operating under normal conditions, fundamental slip is generally fairly small, so harmonic slips are large or negative, and net power from each space harmonic is negative, but generally fairly small. For starting and spin-up from low speed, individual space harmonics may have a non-trivial impact on torque.

9.4.6 Rotor Skew

In order to reduce saliency effects that occur because the rotor teeth will tend to try to align with the stator teeth, induction motor designers always use a different number of slots in the rotor and stator. There still may be some tendency to align, and this produces "cogging" torques, which in turn produce vibration and noise and, in severe cases, can retard or even prevent starting. To reduce this tendency to "cog," rotors are often built with a little *skew*, or twist of the slots from one end to the other. Thus, when one tooth is aligned at one end of the machine, it is unaligned at the other end. Skewing the rotor also reduces coupling of slot order space harmonics. A side effect of skew

is to reduce the stator and rotor coupling by just a little for the space fundamental but possibly by a lot for the space harmonics. Consider a flux density $B_r = B_1 \cos p\theta$, linking a (possibly) skewed full-pitch current path:

$$\lambda = \int_{-\frac{\ell}{2}}^{\frac{\ell}{2}} \int_{-\frac{\pi}{2p}+\frac{\xi}{p}\frac{x}{\ell}}^{\frac{\pi}{2p}+\frac{\xi}{p}\frac{x}{\ell}} B_1 \cos p\theta \, R d\theta \, dx = \frac{2B_1 R\ell}{p} \frac{\sin\frac{\xi}{2}}{\frac{\xi}{2}}$$

The skew in the rotor is ξ electrical radians from one end of the machine to the other. Note that the electrical skew angle for harmonic number n is $\xi_n = n\xi$, the air-gap mutual reactance is modified by skew as follows:

$$X_{m,n} = X_{ag,n} k_{\sigma,n} \tag{9.54}$$

where $X_{ag,n}$ is the un-skewed mutual reactance and the skew factor for the nth harmonic is:

$$k_{\sigma,n} = \frac{\sin\frac{n\xi}{2}}{\frac{n\xi}{2}} \tag{9.55}$$

Illustrated in Figure 9.7 is what is going on. The impact of skew is not only to introduce an equivalent transformer with a ratio of $1 : k_\sigma$ but also to impose leakage reactance. The magnetizing reactance is described above. The leakage reactance is $X_1 = X_{ag}(1 - k_\sigma)$. Transformed across the transformer ratio, the elements in Figure 9.7b are:

$$X' = X_{ag}\left(\frac{1}{k_\sigma^2} - 1\right) \qquad Z'_r = \frac{Z_r}{k_\sigma^2} \tag{9.56}$$

For the higher-order harmonics, in which the skew factor is small, the equivalent rotor impedances can be quite high, reflecting the reduced coupling caused by rotor skew.

9.4.7 Stator Leakage Inductances

The behavior of induction machines is strongly affected by what are called "leakage" inductances. Principal among those are inductances arising from energy stored in space harmonic fields, dealt with in the sections above, stator slot leakage, dealt with in Section 6.5 of Chapter 6, and, to a somewhat lesser extent, end winding leakage.

Stator end winding leakage is perhaps the most difficult of the machine parameters to estimate, being essentially three-dimensional in nature. There are a number of ways of estimating this parameter, but Alger [1] suggests a simplified parameter:

$$L_e = \frac{3}{2}\frac{14}{4\pi^2}\frac{\mu_0 R N_a^2}{p^2}(p - 0.3) \tag{9.57}$$

As with all such formulae, extreme care is required here, since we can give little guidance as to when this expression is correct or even close.

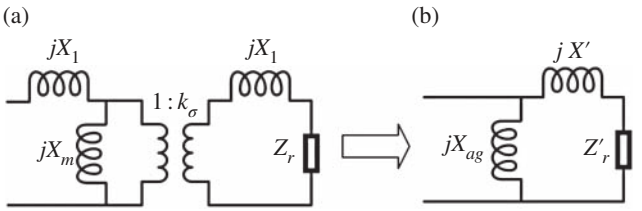

Figure 9.7 Illustration of skew effect.

9.4.8 Stator Winding Resistance

Estimating stator winding resistance is fairly straightforward once end winding geometry is known. Total length of the armature winding is, per phase:

$$\ell_w = 2N_a(\ell + \ell_e) \tag{9.58}$$

Estimating ℓ_e, the length of one end winding, requires knowing how the winding is laid out and that is beyond the scope of this discussion. Once the winding is laid out, that length is determined. If the winding consists of single or multiple strands of round wire, the area of the winding may be estimated by knowing the wire diameter and how many strands are in parallel:

$$A_w = \frac{\pi}{4} N_{inh} d_w^2 \tag{9.59}$$

where d_w is wire diameter and N_{inh} is the number of conductors in parallel, or "in hand." For rectangular or square wire, a similar estimate can be easily derived.

The area of the winding is related to slot area by a winding factor: $\lambda_a = \frac{2N_c A_w}{A_{slot}}$, assuming a two-layer winding with N_c conductors or conductor bundles in each turn.

Winding resistance, per phase, is:

$$R_a = \frac{\ell_w}{\sigma A_w} \tag{9.60}$$

where σ is wire conductivity. Note that conductivity of the materials used in induction machines is a function of temperature and so will be winding resistance (and rotor resistance for that matter). Fitzgerald, Kingsley, and Umans [2] give the following correction for resistance of copper:

$$\rho_T = \rho_t \frac{T_0 + T}{T_0 + t} \tag{9.61}$$

where ρ_T and ρ_t are resistivities ($\rho = 1/\sigma$) at temperatures T and t. $T_0 = 234.5$ for copper with basic conductivity of IACS (International Annealed Copper Standard $= 5.81 \times 10^7$ S/m). For aluminum with conductivity of 63% of IACS, $T_0 \approx 212.9$. Temperatures are given in Celsius.

9.4.9 Rotor End Ring Effects

It is necessary to correct for "end ring" resistance in the rotor. To do this, note that the magnitude of surface current density in the rotor is related to the magnitude of individual bar current by:

$$I_z = K_z \frac{2\pi R}{N_R}$$

Current in the end ring is:

$$I_R = K_z \frac{R}{p}$$

Then it is straightforward to calculate the ratio between power dissipated in the end rings and to power dissipated in the conductor bars themselves, considering the ratio of current densities and volumes.

Assuming that the bars and end rings have the same radial extent, the ratio of current densities is:

$$\frac{J_R}{J_z} = \frac{N_R}{2\pi p} \frac{w_r}{\ell_r}$$

where w_r is the average width of a conductor bar and ℓ_r is the axial end ring length. The ratio of losses (and hence the ratio of resistances) is found by multiplying the square of current density ratio by the ratio of volumes. This is approximately:

$$\frac{R_{end}}{R_{slot}} = \left(\frac{N_R}{2\pi p}\frac{w_r}{\ell_r}\right)^2 \times 2 \times \frac{2\pi R}{N_R \ell}\frac{\ell_r}{w_r} = \frac{N_R R w_r}{\pi \ell \ell_r p^2} \tag{9.62}$$

9.4.10 Deep Rotor Slots

In many cases, rotor slot depth is not small enough that diffusion effects can be ignored. The slot becomes "deep" to the extent that its depth is less than (or even comparable to) the skin depth for conduction at slip frequency. Conduction in this case may be represented by using the Diffusion Equation:

$$\nabla^2 \vec{H} = \mu_0 \sigma \vec{H}$$

In the steady state, and assuming that only cross-slot flux (in the y direction) is important, and the only variation that is important is in the radial (x) direction:

$$\frac{\partial^2 H_y}{\partial x^2} = j\omega_s \mu_0 \sigma H_y$$

This is solved by solutions of the form $H_y = H_{\pm} e^{\pm(1+j)\frac{x}{\delta}}$, where the skin depth δ is:

$$\delta = \sqrt{\frac{2}{\omega_s \mu_0 \sigma}}$$

where σ is conductivity of material in the slot. Since H_y must vanish at the bottom of the slot, it must take the form:

$$\underline{H}_y = \underline{H}_{top} \frac{\sinh\left((1+j)\frac{x}{\delta}\right)}{\sinh\left((1+j)\frac{h_s}{\delta}\right)} \tag{9.63}$$

Since current is the curl of magnetic field:

$$\underline{J}_z = \sigma \underline{E}_z = \frac{\partial H_y}{\partial x} = \underline{H}_{top} \frac{1+j}{\delta} \frac{\cosh\left((1+j)\frac{h_s}{\delta}\right)}{\sinh\left((1+j)\frac{h_s}{\delta}\right)}$$

and since $\underline{H}_{top}\, w_s$ is slot current, impedance per unit length is:

$$\underline{Z}_{slot} = \frac{\underline{E}_z}{\underline{I}_{slot}} = \frac{1}{w_s}\frac{1+j}{\sigma\delta} coth\left((1+j)\frac{h_s}{\delta}\right) \tag{9.64}$$

To the imaginary part of this (reactance) must be added the inductance of the slot depression.

9.4.11 Arbitrary Slot Shape Model

It is possible to obtain a better model of the behavior of rotor conductor slots by using simple numerical methods. In many cases, rotor slots are shaped with the following objectives in mind:

1) A substantial part of the periphery of the rotor should be devoted to active conductor, for good running performance.

2) The magnetic iron of the rotor must occupy a certain fraction of the periphery to avoid saturation.
3) For good starting performance, some means of forcing current to flow only in the top part of the rotor bar should be devised.

Generally, the rotor teeth, which make up part of the machine's magnetic circuit, are of roughly constant width to avoid flux concentration. The rotor conductor bars are therefore tapered, with their narrow ends toward the center of the rotor. To provide for current concentration on starting, they often have a "starting bar" at the outer periphery of the rotor with a much narrower region which has high inductance just below. The bulk of the rotor bar occupies the tapered region allowed between the teeth.

This geometry is quite a bit more complicated than that described in the previous section. Note that, if we can describe the slot impedance per unit length as a function of frequency $\underline{Z}_s(\omega) = R_s(\omega) + jX_s(\omega)$, the analysis of the machine can be carried out as described previously. Thus, the analysis is directed toward frequency response modeling of the rotor slot. Focusing then on a single slot, use the notation as described in Figure 9.8.

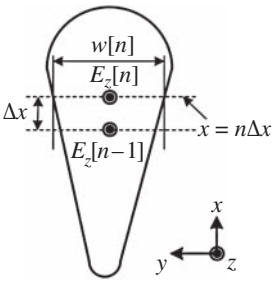

Figure 9.8 Rotor slot geometry.

The impedance per unit length is the ratio between slot current and axial electric field: $\underline{Z}_s = \frac{\underline{E}_z}{\underline{I}}$

For the purpose of this analysis, x is the radial distance from the bottom of the slot. Assume the slot can be divided radially into a number of regions or "slices," each with radial height Δx. We further assume that currents are axially (z) directed and that magnetic field crosses the slot in the y direction. Under these assumptions, the electric field at the top of one of the slices is related to the electric field at the bottom of the slice by magnetic field crossing through the slice. Using the trapezoidal rule for integration:

$$\underline{E}_z(x) - \underline{E}_z(x - \Delta x) = j\omega\mu_0 \frac{\Delta x}{2}(\underline{H}_y(x) + \underline{H}_y(x - \Delta x))$$

From Ampere's law, magnetic flux crossing the gap is:

$$\underline{H}_y(x) = \frac{1}{w(x)} \int_0^x \sigma w(x)\, \underline{E}_z(x)\, dx = \frac{1}{w_n} \sum_{i=0}^{n-1} \underline{I}_i$$

where I_i is the total current flowing in slice i. Note that this can be reformulated into a ladder network by again using the trapezoidal rule for integration: current flowing in slice number n would be:

$$\underline{I}_n = \sigma \frac{\Delta x}{2}(w_n \underline{E}_n + w_{n-1} \underline{E}_{n-1})$$

Now the slot may be described as shown in the ladder network of Figure 9.9. The incremental reactance and resistance of one slice are:

$$X_n = \omega\mu_0 \Delta x \frac{2}{w_n + w_{n-1}}$$
$$R_n = \frac{1}{\sigma \Delta x} \frac{2}{w_n + w_{n-1}} \tag{9.65}$$

The procedure is to start at the bottom of the slot, corresponding to the right-hand end of the ladder (the inductance at the bottom of the slot is infinite, so the first slice has only the resistance), and building toward the top of the slot.

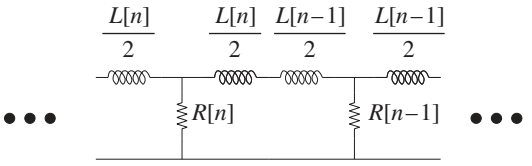

Figure 9.9 Slot impedance ladder network.

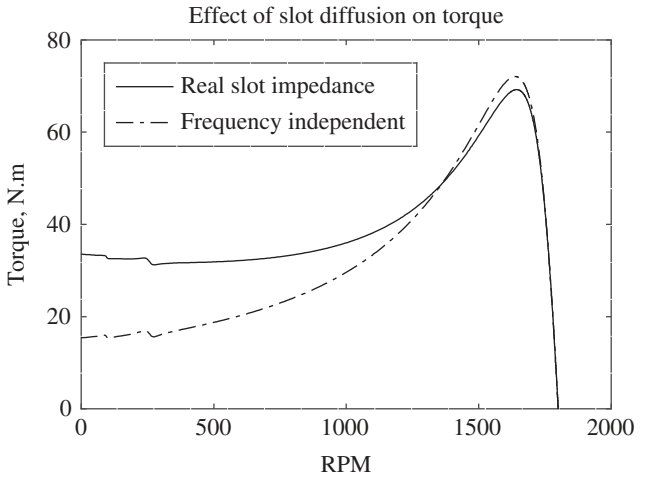

Figure 9.10 Impact of diffusion in deep slot on torque.

The impact of diffusion effects on motor operation can be substantial. Figure 9.10 shows a torque-speed curve for a 5.5 kW motor for which the slot depth is about 13 mm. As can be seen, diffusion increases slot resistance the most at low speed and is therefore used to improve starting performance. The "frequency independent" curve is calculated for how the motor would behave if the rotor slot inductance and resistance were to be at their low-frequency limits for the full speed range.

9.4.12 Magnetic Circuit Loss and Excitation

There will be some loss in the stator magnetic circuit due to eddy current and hysteresis effects in the core iron. In addition, particularly if the rotor and stator teeth are saturated, there will be MMF expended to push flux through those regions. These effects are very difficult to estimate from first principles, so we resort to a simple model.

Assume that the loss in the core iron follows a law such as was developed in Chapter 3:

$$P_d = P_B \left(\frac{\omega}{\omega_B} \right)^{\varepsilon_f} \left(\frac{B}{B_B} \right)^{\varepsilon_b} \tag{9.66}$$

Typically, ε_f is typically a bit less than two (between about 1.3 and 1.6) and ε_b is typically a bit more than two (between about 2.1 and 2.4). Of course, this model is good only for a fairly restricted range of flux density. Base dissipation is usually expressed in *watts per kilogram*, so we first compute flux density and then mass of the two principal components of the stator iron, the teeth, and the back iron. In a similar way, we can model the exciting volt-amperes consumed by core iron can be modeled by something like:

$$VA_c = \left(VA_1 \left(\frac{B}{B_B} \right)^{\varepsilon_{V1}} + VA_2 \left(\frac{B}{B_B} \right)^{\varepsilon_{V2}} \right) \frac{\omega}{\omega_B} \tag{9.67}$$

This, too, is a form that appears to be valid for some steels. Quite obviously, it may be necessary to develop different forms of curve "fits" for different materials.

And then, reactive power is:

$$Q_c = \sqrt{VA_c^2 - P_c^2} \tag{9.68}$$

Flux density (RMS) in the air-gap is:

$$B_r = \frac{pV_a}{2R\ell N_a k_1 \omega} \tag{9.69}$$

Flux density in the stator teeth is:

$$B_t = B_r \frac{w_t + w_s}{w_t} \tag{9.70}$$

where w_t is tooth width and w_s is slot top width.

Flux in the back-iron of the core is:

$$B_c = B_r \frac{R}{p\ d_c} \tag{9.71}$$

where d_c is the radial depth of the core.

One approximate way of handling this loss is to assume that the core handles flux corresponding to terminal voltage, and compute an equivalent resistance and reactance:

$$\begin{aligned} r_c &= \frac{3|V_a|^2}{P_{core}} \\ x_c &= \frac{3|V_a|^2}{Q_{core}} \end{aligned} \tag{9.72}$$

Note that the overall loss and excitation are the quantities per unit mass times the mass of the core and teeth. Then these equivalent resistance and reactance are placed in parallel with the air-gap reactance element in the equivalent circuit.

9.4.13 Effective Air-Gap: Carter's Coefficient

In induction motors, where the air-gap is usually quite small, it is often necessary to correct the air-gap permeance for the effect of slot openings. These make the permeance of the air-gap slightly smaller than calculated from the physical gap, effectively making the gap a bit bigger. The effective air-gap is: $g_{eff} = gc_s$. There are many approximations to the permeance correction. One such approximation is [3]:

$$c_s = \frac{w_{ss} + w_{st}}{w_{ss} + \frac{4}{\pi} g \ln\left(1 + \frac{\pi}{4}\frac{w_{ss}}{g}\right)} \tag{9.73}$$

where

w_{ss} is slot opening width

w_{st} is tooth top width

g is the physical air-gap

9.5 Single-Phase Induction Motors

This is a very important class of motor, because there are many places where polyphase power is unavailable. Single-phase motors are typically limited in power range to several horsepower, but

there are many applications for motors in this size range. Note that a single winding that produces an approximately sinusoidally distributed magnetic flux density and is driven by alternating current will produce an air-gap field that can be viewed as the superposition of two rotating fields, going in opposite directions. A rotor that is turning in one direction will have the effect of making the flux density component rotating in the same direction stronger than the component rotating in the other direction. Thus, single-phase motors will run stably, but the principal issue with them is starting. And starting is accomplished in a variety of fashions.

The single-phase machine contemplated here usually has two windings, usually referred to as the "main" or "run" winding and the "auxiliary" or "start" winding. The two windings are typically geometrically in quadrature but they need not have the same number of turns nor the same distribution. The typical arrangement is to have the current in the 'auxiliary' winding have a phase advance with respect to the 'main' winding: this is often done by putting a capacitor in series with that winding, although it is possible to have that phase advance caused by having a higher resistance in the starting winding. In fact, some smaller induction motors accomplish the phase advance using what are called "shading" coils that produce a component of flux that is advanced in phase and therefore causes rotation. Capacitor windings can be either *starting* windings, in which case they are switched off once the motor has started and is rotating, or they can be *run* windings in which the capacitor is left in the circuit. Or in some cases, there may be two capacitors: one for starting and one for running.

With the geometry shown in Figure 9.11, radial magnetic flux density in the air-gap is:

$$B_r = \sum_{n\ odd} \mu_0 \frac{4}{n\pi} \left(\frac{N_a i_a}{2pg} k_{wna} \sin np\theta + \frac{N_b i_b}{2pg} k_{wnb} \sin n\frac{\pi}{2} \cos np\theta \right) \tag{9.74}$$

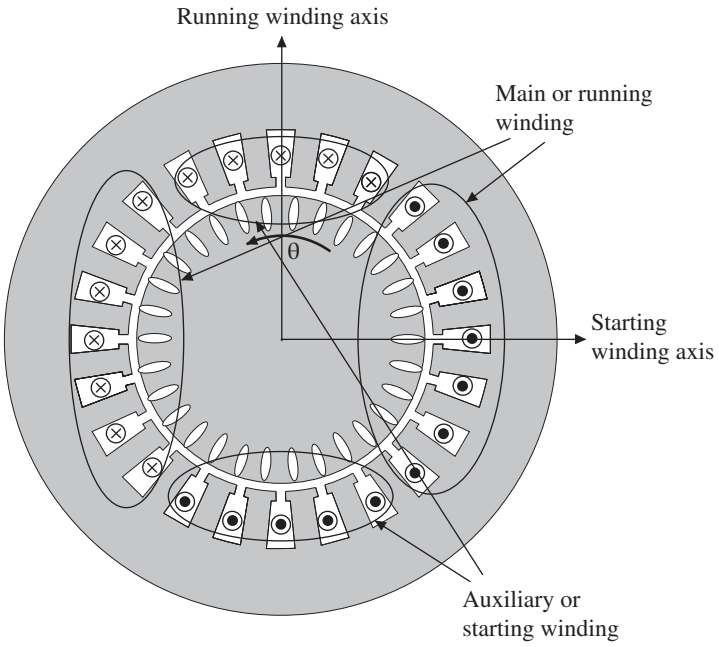

Figure 9.11 Single-phase induction motor.

where N_a is the number of turns in the main winding, N_b is the number of turns in the auxiliary winding, p is the number of pole pairs, g is the effective air-gap, and k_{wna} and k_{wnb} are the winding factors for the n^{th} harmonic fields of the two windings, respectively.

To estimate inductance, first it is necessary to compute flux linkages of the two windings. The flux linkages for the n^{th} harmonic fields are:

$$\lambda_{an} = \ell \int_{-\frac{\pi}{p}}^{0} N_a k_{wna} B_{rn}(\theta)\ R\, d\theta$$

$$\lambda_{bn} = \ell \int_{-\frac{\pi}{2p}}^{\frac{\pi}{2p}} N_b k_{wnb} B_{rn}(\theta)\ R\, d\theta$$

To estimate winding self-inductance, the nth space harmonic flux linkages are (no surprise here):

$$\lambda_{an} = \mu_0 \frac{4}{\pi} \frac{N_a^2 k_{wna}^2 R\ell}{n^2 p^2 g} i_a$$

$$\lambda_{bn} = \mu_0 \frac{4}{\pi} \frac{N_b^2 k_{wnb}^2 R\ell}{n^2 p^2 g} i_b \tag{9.75}$$

Define the effective turns ratio: $\alpha_n = \sin\left(n\frac{\pi}{2}\right) \frac{N_b k_{wnb}}{N_a k_{wna}}$ so that the nth harmonic inductances of the windings are:

$$L_{an} = \mu_0 \frac{4}{\pi} \frac{N_a^2 k_{wna}^2 R\ell}{n^2 p^2 g}$$

$$L_{bn} = \mu_0 \frac{4}{\pi} \frac{N_b^2 k_{wnb}^2 R\ell}{n^2 p^2 g} = \alpha_n^2 L_{an} \tag{9.76}$$

The sign of the effective turns ratio does not affect the self-inductances but does affect the direction of rotation of the various magnetic field components. Harmonics number 3 and 7 (and one of the zigzag components) rotate in the reverse direction than would be indicated by the sequence order of currents in the stator windings.

9.5.1 Squirrel Cage Model

The derivation of the elements of the equivalent circuit model for the squirrel cage follows that for the polyphase machine, except for the fact that there is no phase circuit coupling. The circuit elements that arise from this derivation are:

$$L_{agn} = \frac{4}{\pi} \frac{\mu_0 N_a^2 k_{wan}^2 R\ell}{n^2 p^2 g}$$

$$x_{2,n} = \frac{8\ell N_a^2 k_{wan}^2}{N_R} \omega L_{slot} + \omega \frac{4}{\pi} \frac{\mu_0 N_a^2 k_{wan}^2 R\ell}{g} \left(\frac{1}{(N_R + np)^2} + \frac{1}{(N_R - np)^2} \right)$$

$$R_{2,n} = \frac{8\ell N_a^2 k_{wan}^2}{N_R} R_{slot} \tag{9.77}$$

Note too that rotor resistance must be corrected for end ring effects as described above.

9.5.2 Winding Factor

In the single-phase machines, the windings can be described as *concentric*, or as a collection of some number of coils, all with the same axis, with different coil throws and perhaps a different number of turns. If we denote $N_s(k)$ as the number of turns in coil k and $N_c(k)$ as the coil throw,

then the total number of turns is just the sum of all of the N_s's and the electrical span angle for coil k is $\varphi_k = \frac{2\pi p N_c(k)}{S}$, where S is the total number of slots in the stator (this assumes the slots have equal spacing). The winding factor is then the weighted sum of the winding factors of all of the coils:

$$k_{wna} = \sum_k \frac{N_{s(k)}}{N_a} \sin\left(\frac{n}{2}\phi_k\right) N_a \tag{9.78}$$

9.5.3 Operation

Assume that the two stator phases are noted as a and b and two equivalent rotor phases are A and B, flux linkages are

$$\begin{aligned} \lambda_a &= L_a i_a + L_\phi i_A \qquad & \lambda_A &= L_\phi i_a + L_A i_A \\ \lambda_b &= L_b i_b + \alpha L_\varphi i_B \qquad & \lambda_B &= \alpha L_\phi i_b + L_A i_B \end{aligned} \tag{9.79}$$

where it is assumed that the rotor equivalent winding has the same number of turns and winding factor as the run winding of the stator.

This is not a convenient set to use because the interaction of the rotor makes the equivalent phases A and B difficult to use. So, a coordinate transformation is used. Working in complex amplitudes, assume that the equivalent quantities in the rotor coordinates are the sum of components rotating forward and backward as shown in Figure 9.12:

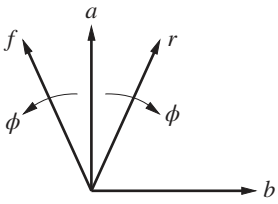

Figure 9.12 Single-phase induction motor coordinates.

$$\begin{bmatrix} \underline{I}_A \\ \underline{I}_B \end{bmatrix} = \frac{1}{2}\begin{bmatrix} 1 & 1 \\ j & -j \end{bmatrix}\begin{bmatrix} \underline{I}_F \\ \underline{I}_R \end{bmatrix} \tag{9.80}$$

The inverse transformation is:

$$\begin{bmatrix} \underline{I}_F \\ \underline{I}_R \end{bmatrix} = \begin{bmatrix} 1 & -j \\ 1 & j \end{bmatrix}\begin{bmatrix} \underline{I}_A \\ \underline{I}_B \end{bmatrix} \tag{9.81}$$

The complex amplitudes of flux linkages are:

$$\begin{aligned} \underline{\Lambda}_a &= L_a \underline{I}_a + \frac{L_\phi}{2}\underline{I}_F + \frac{L_\phi}{2}\underline{I}_R \\ \underline{\Lambda}_b &= L_b \underline{I}_b + \frac{j\alpha L_\phi}{2}\underline{I}_F - \frac{j\alpha L_\phi}{2}\underline{I}_R \\ \underline{\Lambda}_F &= L_\phi \underline{I}_a - j\alpha L_\phi \underline{I}_b + L_A \underline{I}_F \\ \underline{\Lambda}_R &= L_\phi \underline{I}_a + j\alpha L_\phi \underline{I}_b + L_A \underline{I}_F \end{aligned} \tag{9.82}$$

Voltage equations are, in the stator coordinate system:

$$\begin{aligned} \underline{V}_a &= (jX_a + R_a)\underline{I}_a + \frac{jX_\phi}{2}\underline{I}_F + \frac{jX_\phi}{2}\underline{I}_R \\ \underline{V}_b &= (jX_b + R_b + \underline{Z}_e)\underline{I}_b + \frac{\alpha X_\phi}{2}\underline{I}_F - \frac{\alpha X_\phi}{2}\underline{I}_R \\ 0 &= \frac{jX_\phi}{2}\underline{I}_a - \frac{\alpha X_\phi}{2}\underline{I}_b + \left(\frac{jX_A}{2} + \frac{R_2}{2s}\right)\underline{I}_F \\ 0 &= \frac{jX_\phi}{2}\underline{I}_a + \frac{\alpha X_\phi}{2}\underline{I}_b + \left(\frac{jX_A}{2} + \frac{R_2}{2(2-s)}\right)\underline{I}_R \end{aligned} \tag{9.83}$$

This set of four linear equations is readily solved for the four currents I_a I_b I_F, and I_R. To find mechanical energy converted, see that air-gap power and power dissipated on the rotor are (working in RMS):

$$P_{ag} = |I_F|^2 \frac{R_2}{2s} + |I_R|^2 \frac{R_2}{2(2-s)}$$
$$P_d = |I_F|^2 \frac{R_2}{2} + |I_R|^2 \frac{R_2}{2} \tag{9.84}$$

Mechanical energy converted is the difference:

$$P_m = |I_F|^2 \frac{R_2}{2s}(1-s) - |I_R|^2 \frac{R_2}{2(2-s)}(1-s) \tag{9.85}$$

Torque is:

$$T_m = \frac{p}{\omega(1-s)} P_m = \frac{p}{w} \left\{ |I_F|^2 \frac{R_2}{2s} - |I_R|^2 \frac{R_2}{2(2-s)} \right\} \tag{9.86}$$

9.5.4 Operation as Affected by Space Harmonics

The space harmonics couple together only in the stator winding, which produces the space harmonic fields in response to armature currents. They are independent of each other in the rotor, however. The coupling is reflected in the addition of all of the harmonic components in the production of voltage in the stator. Each rotating component (forward and backward at each harmonic order) will have its own voltage balance equation. Considering only one of the harmonics, of order n, the voltage equations become:

$$\underline{V}_A = (jX_a + R_a)\underline{I}_a + \frac{jX_\phi}{2}\underline{I}_F + \frac{jX_\phi}{2}\underline{I}_R + \frac{jX_{\phi n}}{2}\underline{I}_{Fn} + \frac{jX_{\phi n}}{2}\underline{I}_{Rn}$$
$$\underline{V}_B = (jX_b + R_b + \underline{Z}_e)\underline{I}_b - \frac{\alpha X_\phi}{2}\underline{I}_F + \frac{\alpha X_\phi}{2}\underline{I}_R - \frac{\alpha_n X_{\phi n}}{2}\underline{I}_{Fn} + \frac{\alpha_n X_{\phi n}}{2}\underline{I}_R$$
$$0 = \frac{jX_\phi}{2}\underline{I}_a + \frac{\alpha X_\phi}{2} I_b + \left(\frac{jX_A}{2} + \frac{R_2}{2s}\right)\underline{I}_F$$
$$0 = \frac{jX_\phi}{2}\underline{I}_a - \frac{\alpha X_\phi}{2} I_b + \left(\frac{jX_A}{2} + \frac{R_2}{2(2-s)}\right)\underline{I}_F$$
$$0 = \frac{jX_{\phi n}}{2}\underline{I}_a + \frac{\alpha_n X_{\phi n}}{2}\underline{I}_b + \left(\frac{jX_{An}}{2} + \frac{R_{2n}}{2s_{n+}}\right)\underline{I}_{Fn}$$
$$0 = \frac{jX_{\phi n}}{2}\underline{I}_a - \frac{\alpha X_\phi}{2} I_b + \left(\frac{jX_{An}}{2} + \frac{R_2}{2s_{n-}}\right)\underline{I}_{Fn} \tag{9.87}$$

Harmonic slips are the ratio between rotor frequency and stator frequency and are:

$$s_{n+} = n\,s - (n-1)$$
$$s_{n-} = (n+1) - n\,s \tag{9.88}$$

Torques from space harmonics are estimated in the same way as for the fundamental, so that the torque resulting from the nth space harmonic interaction is:

$$T_{mn} = \frac{np}{\omega}\left(|I_{Fn}|^2 \frac{R_{2n}}{2s_{n+}} - |I_{Rn}|^2 \frac{R_{2n}}{2s_{n-}}\right) \tag{9.89}$$

Adding harmonic terms is straightforward. If there are a lot of space harmonics considered, a relatively large coupling matrix results. The resulting linear equation set is straightforward to solve.

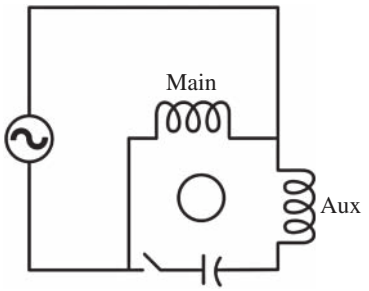

Figure 9.13 Single-phase motor with start capacitor and switch.

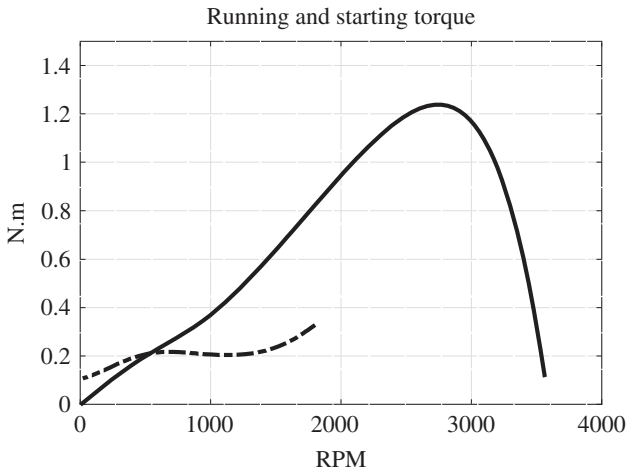

Figure 9.14 Single-phase motor operation.

Generally, in a single-phase motor, the auxiliary circuit is connected to an external impedance (e.g. a capacitor or parallel combination of a capacitor and a resistor) and then to the same voltage source as the main winding, as shown in Figure 9.13. The value of the external element is Z_e in the voltage equation for the auxiliary winding (B). With a starting switch, there will be two separate torque vs. speed curves, as shown in Figure 9.14, which shows operation for a small motor for a home refrigerator. This one employs a physical switch, operated by a centrifugal mechanism on the rotor. There are several other schemes for starting control, including timers and thermal resistors.

9.6 Problems

Here is a description of a 350 kW induction motor:

Voltage	V	480	Line-line, RMS
Frequency	f	60	Hz
Number of pole pairs	p	6	
Stator leakage reactance	X_1	37.5	mΩ
Stator resistance	R_1	17	mΩ
Rotor leakage reactance	X_2	114	mΩ
Rotor resistance	R_2	10	mΩ
Magnetizing reactance	X_m	3.5	Ω

For this motor, assume core loss at rated frequency and voltage is 12 kW, and that this core loss is proportional to flux density to the power of 2.2 and to frequency to the power of 1.8. That is:

$$P_c = P_0 \left(\frac{f}{f_0} \right)^{1.8} \left(\frac{B}{B_0} \right)^{2.2}$$

Assume also that friction and windage loss is proportional to the cube of rotor speed and is 10 kW at rated speed.

Finally, assume that "stray" loss is 2.5% of output power (8750 W at rated power) and is directly proportional to output power.

9.1 Ignoring all of those added loss elements (Core, Friction, Windage, and Stray, generate and plot a torque-speed curve for this motor, at rated terminal voltage and frequency.

9.2 Accounting for the added loss elements, estimate and plot motor efficiency and terminal power factor, while the motor is operated at rated terminal voltage and frequency for mechanical loads between 100 kW and 400 kW. (Yes, we are overloading the machine.)

9.3 The motor is to be used in an adjustable speed drive application. For lower speeds, the motor is to be driven by a balanced voltage that is proportional to frequency ("constant volts per Hz"). For drive frequency greater than 60 Hz, the terminal voltage is fixed at 600 V, RMS, line-line. Plot torque-speed curves for this motor and drive combination, for frequencies of 20, 40, 60, 80, 100, and 120 Hz.

9.4 Find and plot the machine efficiency and power factor for this motor when it is delivering 3000 N/m, under V/Hz control, between electrical frequencies of 30 Hz and 60 Hz.
A "squirrel cage" induction motor has an equivalent circuit model as shown in the figure below. This is a four-pole motor, with an applied terminal voltage of 346 V across each phase (so that line-line voltage is 600 V, RMS, with a frequency of 150 Hz. The impedance parameters are, at 150 Hz:

Stator resistance	R_1	8.481	mΩ
Stator leakage reactance	X_1	31.16	mΩ
Core resistance	R_c	235	Ω
Fundamental	X_m	2.884	Ω
	X_2	41.87	mΩ
	R_2	13	mΩ
Fifth harmonic	$X_{m,5}$	19.79	mΩ
	$X_{2,5}$	4.126	mΩ
	$R_{2,5}$	4.3	mΩ
Seventh harmonic	$X_{m,7}$	58.85	mΩ
	$X_{2,7}$	24.4	mΩ
	$R_{2,7}$	4.2	mΩ
Negative sequence harmonic (23)	$X_{m,m}$	5.451	mΩ
	$X_{2,m}$	41.4	mΩ
	$R_{2,m}$	55	mΩ
Positive sequence harmonic (25)	$X_{m,p}$	4.614	mΩ
	$X_{2,p}$	53.01	mΩ
	$R_{2,p}$	55	mΩ

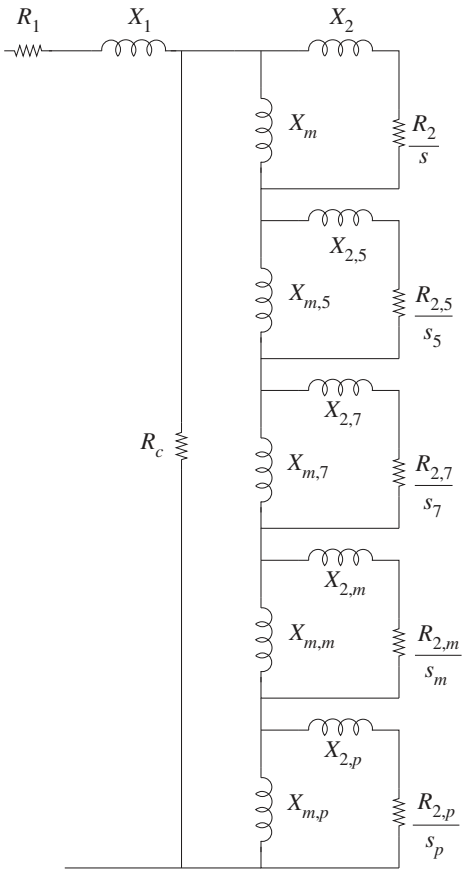

Equivalent circuit of induction motor

Note that this model accounts for core loss with a simple, linear resistor across the core. For the purpose of these problems, neglect friction and windage loss.

9.5 Using your favorite numerical assistant (solutions will be in MATLAB), generate and plot a torque-speed curve for this motor operating against a fixed frequency (150 Hz) supply. Don't worry about the abnormality of this curve: we will be running it with an inverter.

9.6 The motor is to be operated at an electrical frequency of 150 Hz, producing 500 kW. Find the required slip (and so speed) and estimate the efficiency and power factor. What are the principal elements of loss, including armature winding loss, fundamental slip loss, core loss, and "stray" loss in the harmonic elements?

9.7 Here is a physical description of a relatively small (1 kW) induction motor. The motor has a "concentric" winding.

Rotor radius	45	mm
Active length	100	mm
Relative rotation gap	0.35	mm
Number of pole pairs	2	
Number of stator slots	36	
Stator winding:		
Turns per coil	60	
Coil throw	7, 9, 11	
Coils in series	6	
Stator slot depth	14.5	mm
Stator slot width	3.51	mm
Stator slot depression width	2.2	mm
Stator slot depression height	0.7	mm
Stator wire diameter	0.53	mm
Stator winding wires "in hand"	2	
Rotor:		
Number of rotor slots	28	
Rotor slot width	3	mm
Rotor slot depth	24	mm
Rotor slot depression width	0.25	mm
Rotor slot depression height	1	mm
Rotor end ring height	24	mm
Rotor end ring length	10	mm

The stator winding is copper, with a conductivity of $\sigma = 5.81 \times 10^7$ S/m. The rotor cage is made of Aluminum with a conductivity of $\sigma = 2 \times 10^7$ S/m.
Make the assumption about winding shape: that the end turns of the stator are roughly circular on the surface of a cylinder at the air-gap radius. Also, ignore any diffusion effects that might occur in the rotor conductors (no "deep bar" effects).
Find the parameters of the simple equivalent circuit for the motor: R_1, X_1, X_m, X_2, and R_2.

Single-Phase Motor
Assume, somewhat unrealistically, that a single-phase motor has identical running and starting windings, oriented perpendicular to each other. This is a two-pole motor to be operated with a terminal voltage of 120 V, RMS, 60 Hz.

Magnetizing reactance	x_m	169	Ω
Stator leakage	X_1	2.94	Ω
Rotor leakage	X_2	0.428	Ω
Stator resistance	R_1	4.13	Ω
Rotor resistance	R_2	2.07	Ω

9.8 Calculate and plot the running torque vs. speed curve for this motor over the speed range of zero to 3600 RPM.

9.9 Assuming the starting winding is put in series with a 50 μF capacitor, calculate and plot the torque speed curve from zero to 3600 RPM.

9.10 A picture of the cross-section of a slot is shown in Figure 9.2. While it is unlikely this slot would be used in an actual induction motor, its geometry is at least tractable. The slot is in material that is perfectly permeable but non-conducting, an approximation to laminated iron. The slot is filled with a conductor with the conductivity of copper (IASC = 5.81×10^7 S/m).

1) Find and plot the impedance per unit length for current carried by the slot in the axial direction (into the paper). That is, V/m per ampere. Do this over the frequency range of $1 < f < 1000$ Hz. Plot resistance $R(f)$, reactance $X(f)$, impedance magnitude and angle: $|Z|(f)$ and $Z(f)$. Use log–log coordinates for R, X, and $|Z|$ and log-linear coordinates for the angle. You will probably want to use a mathematical assistant to do the heavy lifting and plotting here. The solutions will be done using MATLAB.
2) Now we are going to look into the impact of "deep bars" on large induction motors. Assume that the bars of the induction motor of Problem 2 are shaped like the bar you just analyzed. Assume that all of the rotor resistance (R_2) and 80% of rotor leakage (X_2) are due to the rotor slots. The resistance stated in the table specifying the machine of Problem 2 is the low-frequency limit of the resistance of the squirrel cage made up of the bars you just analyzed. Re-plot the torque-speed curve of the induction motor that begins these problems.

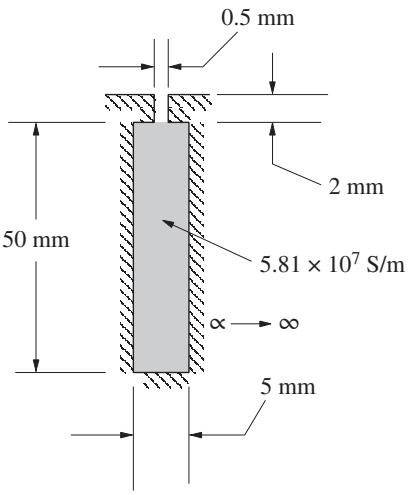

References

1 Alger, P.L. (1969). *Induction Machines*. Gordon and Breach.
2 Fitzgerald, A.E., Kingsley, C. Jr., and Umans, S.D. (2003). *Electric Machinery*, 6e. McGraw Hill.
3 Krause, P., Wasynczuk, O., Sudhoff, S., and Pekarek, S. (2013). *Analysis of Electric Machinery and Drive Systems*, 3e. Wiley.

10

Switched Reluctance Motors

This class of electric machines works a bit like the solenoid that was described in Chapter 3, in which force might be described by a change in magnetic stored energy. It is not widely used, but there has been a lot of development of this type of machine and there are a number of arguments in favor.

10.1 Fundamentals and Operating Principles

A cross-section of one version of a switched reluctance machine (SRM) is shown in Figure 10.1. The rotor of this machine is very simple: It is made of ferromagnetic material and has no windings. Typically, both the rotor and stator are made of thin laminations of steel because both the rotor and stator have time-varying flux. The rotor and stator both have projections (poles), but with different numbers. What is shown in the figure has six stator poles and four rotor poles. Each of the poles of the stator has a winding around it. Shown in the figure is one *phase*: Both opposing poles are wound in the same fashion. This machine would have three-phase windings, and as shown, opposite poles are wound alike, so that, with the rotor in the position shown and with the current as pictured, flux would enter the rotor through the gap on the left and leave the rotor through the gap on the right. It should be intuitive that, with the current as shown, the rotor would be attracted to be in the position shown, aligned with the Phase A poles. Rotating in the positive θ direction, it would be attracted to the poles marked "Phase B", and then "Phase C".

The simplest description of operation yields a basic understanding of how this machine works, but to get a quantitative understanding, consider the simple black box of Figure 10.2. Power into the terminals of this thing is $p_{in} = vi = i\frac{d\lambda}{dt}$. Over a time interval, energy into the electrical terminals is $w_{12} = \int_{t_1}^{t_2} i\frac{d\lambda}{dt}dt = \int_{\lambda_1}^{\lambda_2} id\lambda$. If the voltage and current are periodic, or even if they just repeat so that the path in the λ–I plane is closed, energy over one cycle is:

$$w_{cycle} = \oint id\lambda \tag{10.1}$$

Illustrated in Figure 10.3 is a path in which net energy flows through the terminals into the box. (Going around the other way would indicate power flowing out of the box.) Now, consider the interaction of one rotor pole with one of the stator poles, as shown in Figure 10.4. The rotor (the lower element) is moving to the left, so the rotor angle is increasing in that direction, similar to what is shown in Figure 10.1. The inductance of a winding wound around the stator (upper) pole would have a form similar to what is shown in Figure 10.5.

Electromagnetic Analysis of Electric Machines: First Principles, Modeling, and Design, First Edition.
James L. Kirtley, Christopher H. T. Lee, and Sajjad Mohammadi.

Companion website: www.wiley.com/go/kirtleyelectric

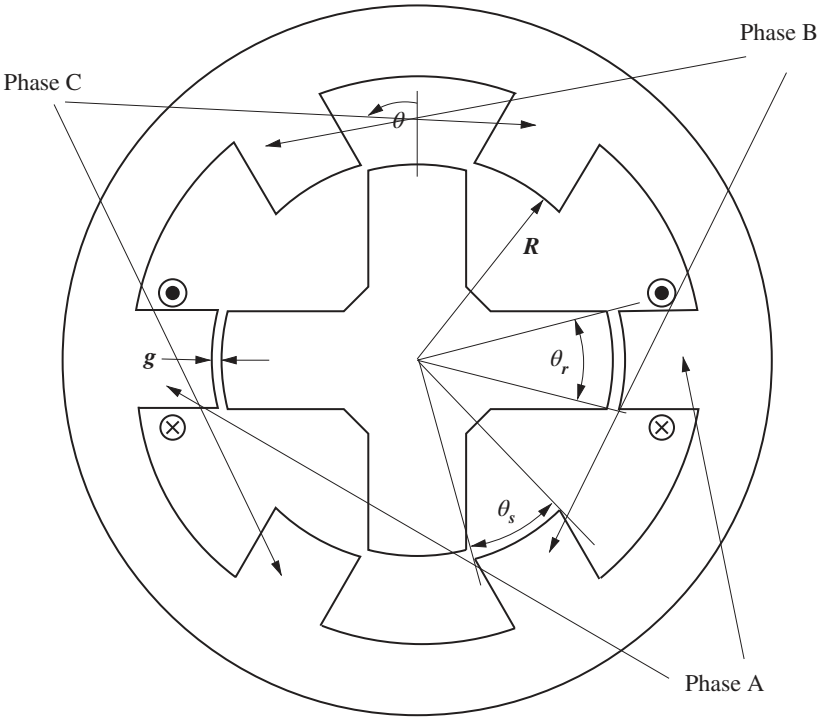

Figure 10.1 Axial cut view of a 6/4 switched reluctance machine.

If there is current in that coil, the rotor pole will be attracted to the stator pole, and thus there will be positive torque if the two poles are engaging. That may be further described by finding the magnetic co-energy:

$$W'_m = \int_0^i \lambda(i')di' = \int_0^i L(\theta)i'\,di' = \frac{1}{2}i^2L(\theta) \tag{10.2}$$

Then torque is

$$T^e = \frac{\partial W'_m}{\partial \theta} = \frac{i^2}{2}\frac{dL}{d\theta} \tag{10.3}$$

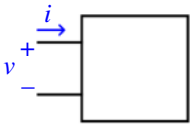

Figure 10.2 Magnetic storage element with a single terminal pair.

As expected, torque is positive for angles when inductance is increasing. Now, consider a different look at potential operation as shown in Figure 10.6. When the rotor is in alignment with the stator, the inductance is "big" and when it is out of alignment, it is "small". One could hypothesize an operation around a loop in the flux-current plane as shown in Figure 10.7. One would "charge" the coil when the inductance is small, hold the current constant as the rotor turns toward maximum inductance and then discharge the coil at maximum inductance. Let the rotor turn to a minimum inductance and repeat.

Where this mode of operation is possible, energy converted per cycle would be:

$$W_{ideal} = \frac{i^2}{2}(L_{big} - L_{small}) \tag{10.4}$$

This mode of operation is not likely to work because of rotor inertia and the effect of inductance, so a more realistic path in the λ–I plane would be roughly like what is shown in Figure 10.8, noting

Figure 10.3 Path in the flux-current plane.

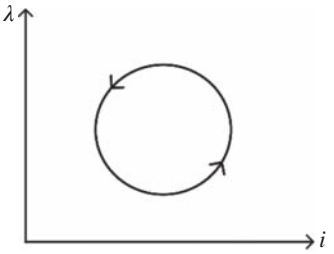

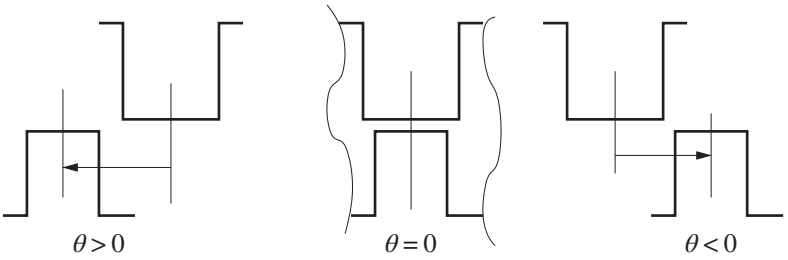

Figure 10.4 Pole alignment with rotor position.

Figure 10.5 Phase inductance vs. rotor position.

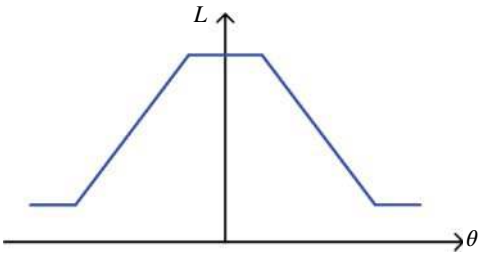

Figure 10.6 Flux vs. current for different angles.

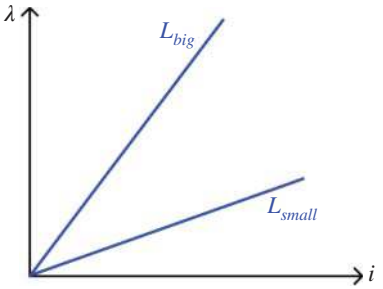

Figure 10.7 Idealized flux vs. current loop.

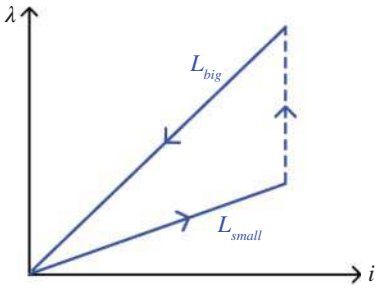

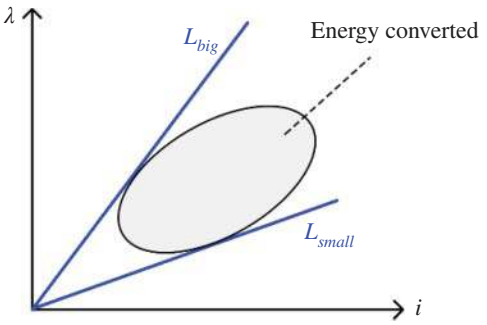

Figure 10.8 More realistic flux vs. current loop.

that the rotor would be turning continuously at a nearly constant rate of speed. However, the basic features hold: positive power conversion from electrical to mechanical form occurs when current is increased as inductance increases with angle, while current is discharged as inductance decreases with angle. That is, when the flux vs. current path makes a counterclockwise loop.

In practical SRMs, operation can be made well into saturation, at least in the vicinity of maximum inductance, as shown in Figure 10.9. If the shaded area in this figure has area W_ϕ, torque can be calculated as:

$$T_e = \frac{W_{tot}}{2\pi} = \frac{N_S N_R W_\phi}{2\pi} \tag{10.5}$$

where N_S and N_R are the total numbers of stator and rotor poles, respectively, so the product of their numbers is the total number of interactions per revolution.

10.2 Drive Circuitry

The variable reluctance machine has one feature that makes its drive problematic: It is necessary to remove quite a lot of energy from the stator coils each cycle. Were that energy to be simply abandoned, the efficiency would be very poor. One solution is the use of a bifilar coil, as shown in Figure 10.10. This circuit uses a single switch to energize the coil, and when that switch turns off, the closely coupled second winding drives current back into the power supply. Note the direction noting dots next to the two windings.

There are a few disadvantages to this drive circuit. For one thing, the recovery winding takes up space and this leads to poorer efficiency. A second issue is that the voltage across the winding

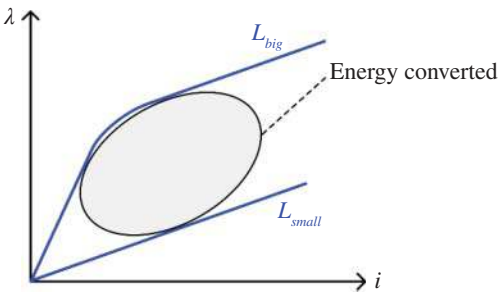

Figure 10.9 Flux vs. current loop considering saturation.

is either positive or negative but not zero (unless the coil is completely discharged). And, even if the two coils are wound together (that is what "bifilar" means), there will still be some energy abandoned each cycle.

To make for a better, more efficient drive, the circuit of Figure 10.11 is more commonly used. This requires two switches but only a single winding for each phase. To energize the coil, both switches are turned on. To discharge the coil, both switches are turned off and current in the coil circulates through the two diodes. One can readily see that the power supply is reversed in this case, so until the current in the coil is driven to zero, power flows back into the supply. If pulse width modulation is to be used, one switch can be left on and the second switch cycled in the PWM pattern. If Q_2 is left on and Q_1 does the PWM, current can circulate through the left-hand diode.

Design Considerations: Lawrenson's Triangle

There are a number of things to be considered in designing an SRM; in particular, picking the angles of the stator and rotor pole pieces. It is necessary, for example, that there be *some* overlap of poles somewhere in the machine so that the machine can always be started. On the other hand, so that there will be a low minimum inductance, there should not be any overlap of a given stator pole when the inductance is at a minimum. The graphic shown in Figure 10.12 is attributed to Peter Lawrenson, a Professor at Leeds University and an early developer of variable reluctance motors.

If N_S is the total number of stator poles, and is an even number, the number of phases would be:

$$q = \frac{N_s}{2} \tag{10.6}$$

Figure 10.10 Drive circuit using bifilar winding.

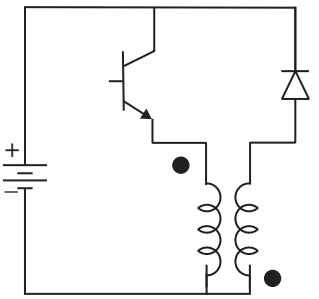

Figure 10.11 Drive circuit.

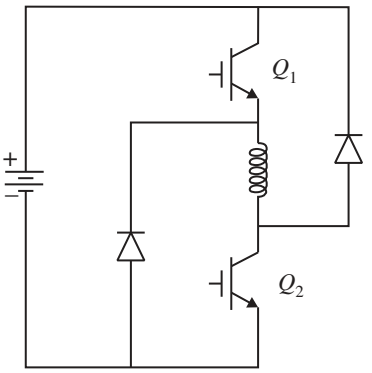

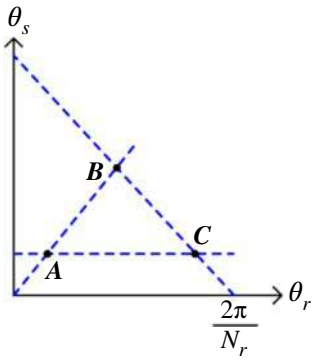

Figure 10.12 Lawrenson's feasible triangle.

Then the "stroke" angle is the angular distance between maximum engagement of any pole combination:

$$\varepsilon = \frac{2\pi}{qN_R} \tag{10.7}$$

To ensure that there is some engagement at all angles, stator pole angular width must be greater than the stroke: $\theta_S > \varepsilon$. To ensure that there is some range of angles for which there is no overlap of a stator pole, $\theta_S + \theta_R < \frac{2\pi}{N_R}$. And finally, $\theta_S < \theta_R$. This is a relatively weak requirement, but ensures that there is sufficient area for rotor flux.

10.3 Magnetic Equivalent Circuits Using Flux Tubes

This section focuses on the development of a flux tube-based magnetic equivalent circuit (MEC) for a four-phase SRM. However, the strategy outlined in Figure 10.13 can be generalized to other motors and even other magnetic systems. Due to symmetry, it is sufficient to develop the MEC for the excitation period of a single phase from unaligned to aligned positions.

Initially, flux lines (equipotential lines of the z-component of the magnetic vector potential A_z) are obtained using numerical techniques such as the finite element method (FEM) or estimated by other means. Here, the process is illustrated for the case when phase A of the SRM is excited. Based on the flux lines, the flux paths within the device are determined. The next step involves developing the MEC. For the case study SRM, it can be observed that there are two magneto-motive forces (MMFs) corresponding to the two windings of the excited phase as follows:

$$F = N\, i_c \tag{10.8}$$

where i_c is the coil current and N is the number of turns per coil. Along the flux path, reluctances for iron parts, including stator yoke R_{sy}, rotor yoke R_{ry}, stator teeth R_{st}, and rotor teeth R_{rt} can be considered, yet they are ignored here by assuming infinite permeability for the cores. The gap reluctance R_g is modeled accurately by representing it as multiple parallel paths corresponding to parallel permeances P_1–P_N as:

$$R_g(\theta) = \Bigg(\underbrace{\sum_{i=1}^{N} P_i(\theta)}_{P_g(\theta)} \Bigg)^{-1} \tag{10.9}$$

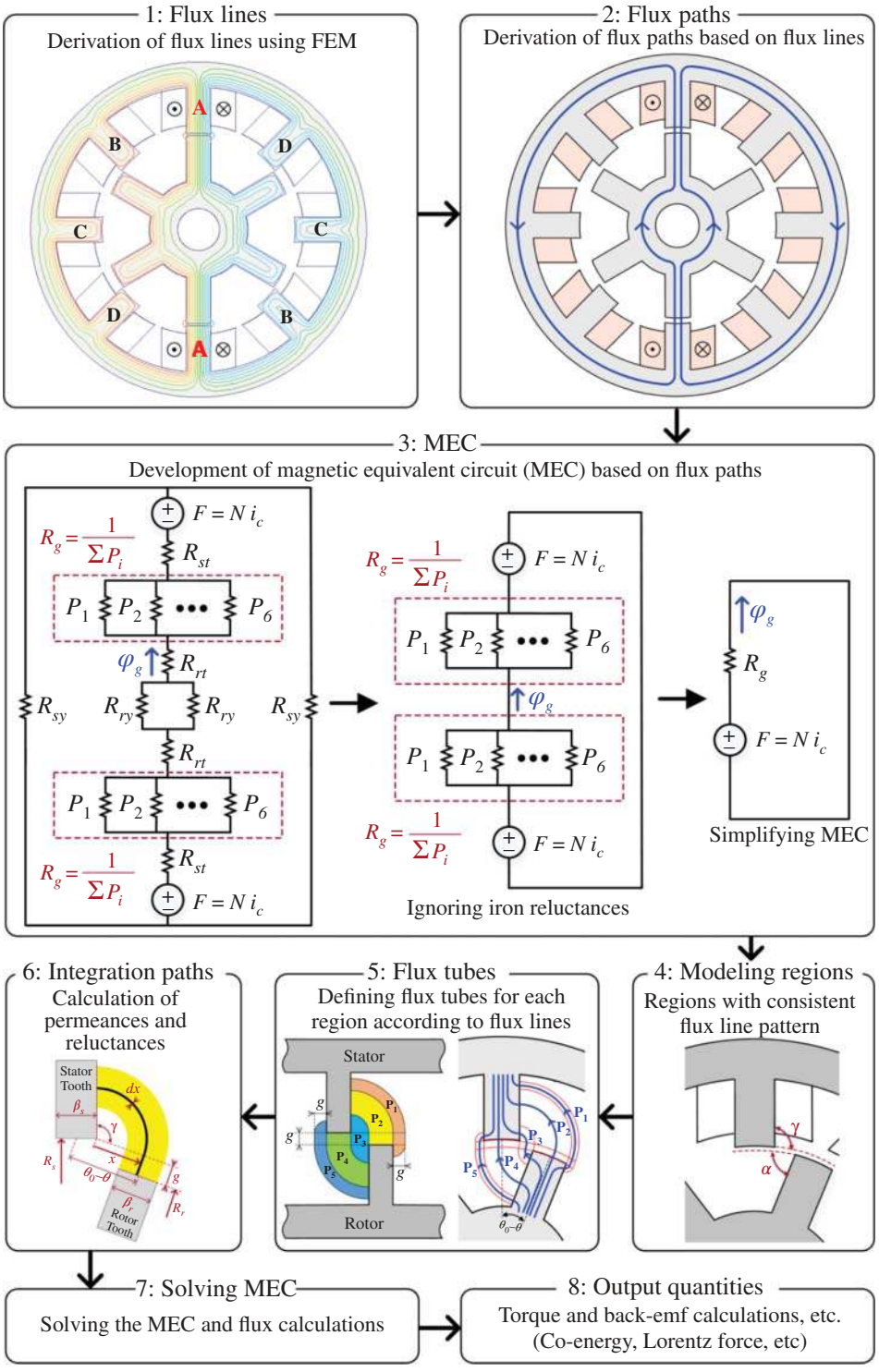

Figure 10.13 Strategy for the development of flux tube-based MEC.

Table 10.1 Modeling regions.

	Region	Rotor Position
1	Non-overlapping	From unaligned position ($\theta = 0$) to overlapping edge position ($\theta = \theta_0 - \beta_r/2 - \beta_s/2$)
2	Overlapping edge	Overlapping edge of rotor and stator poles ($\theta = \theta_0 - \beta_r/2 - \beta_s/2$)
3	Overlapping	From overlapping edge ($\theta = \theta_0 - \beta_r/2 - \beta_s/2$) to aligned position ($\theta = \theta_0$)
4	Fully aligned	Rotor and stator poles aligned after half of rotor pole pitch rotation ($\theta = \theta_0$)

Due to symmetry, the flux tube model is developed for half of the rotor pole pitch $\theta_{rp} = 2\pi/N_r$ from unaligned position ($\theta = 0$) to aligned position ($\theta = \theta_0 = \theta_{rp}/2$). The angular distance between the centers of rotor and stator teeth is given by $\theta_0 - \theta$.

Based on the rotor's angular displacement θ from the unaligned position, four distinct regions can be defined, where the flux line patterns remain nearly constant. Accordingly, the corresponding flux tubes can be developed. These four regions are described in Table 10.1.

Figure 10.14 illustrates the flux lines and the associated flux tubes for the four operating regions [1]. Figure 10.15 depicts the integration paths for the flux tubes corresponding to permeances P_1–P_6 across the four operating regions. The angles α and γ can be approximated to 90° for motors with a large radius. However, for smaller machines, their accurate values should be employed for higher precision.

For the regions 1, 2, and 3, the flux path from the bottom side of the stator tooth to the upper side of the rotor tooth can be represented by a flux tube corresponding to the permeance P_1, with a width of g, as follows:

$$P_1(\theta) = \int_0^g \frac{\mu_0 \, l \, dx}{\frac{\pi}{2}x + g + \gamma \left[x + R_s \left(\theta_0 - \frac{\beta_s}{2} + \frac{\beta_r}{2} - \theta \right) \right]} \tag{10.10}$$

Hence,

$$P_1(\theta) = \frac{\mu_0 \, l}{\frac{\pi}{2} + \gamma} \ln \left[1 + \frac{g\left(\frac{\pi}{2} + \gamma\right)}{g + \gamma R_s \left(\theta_0 - \frac{\beta_s}{2} + \frac{\beta_r}{2} - \theta \right)} \right] \tag{10.11}$$

For the region 1, the flux path from the middle side of the stator tooth to the tip of the rotor tooth can be represented by a flux tube corresponding to the permeance P_2, with a width of roughly rotor pole thickness $R_s\beta_r$, as follows:

$$P_2(\theta) = \int_{R_s\left(\theta_0 - \frac{\beta_s}{2} - \frac{\beta_r}{2} - \theta\right)}^{R_s\left(\theta_0 - \frac{\beta_s}{2} + \frac{\beta_r}{2} - \theta\right)} \frac{\mu_0 \, l \, dx}{g + \gamma x} \tag{10.12}$$

Hence,

$$P_2(\theta) = \frac{\mu_0 l}{\gamma} \ln \left[1 + \frac{\gamma \, \beta_r R_s}{\gamma \, R_s \left(\theta_0 - \frac{\beta_s}{2} - \frac{\beta_r}{2} - \theta \right) + g} \right] \tag{10.13}$$

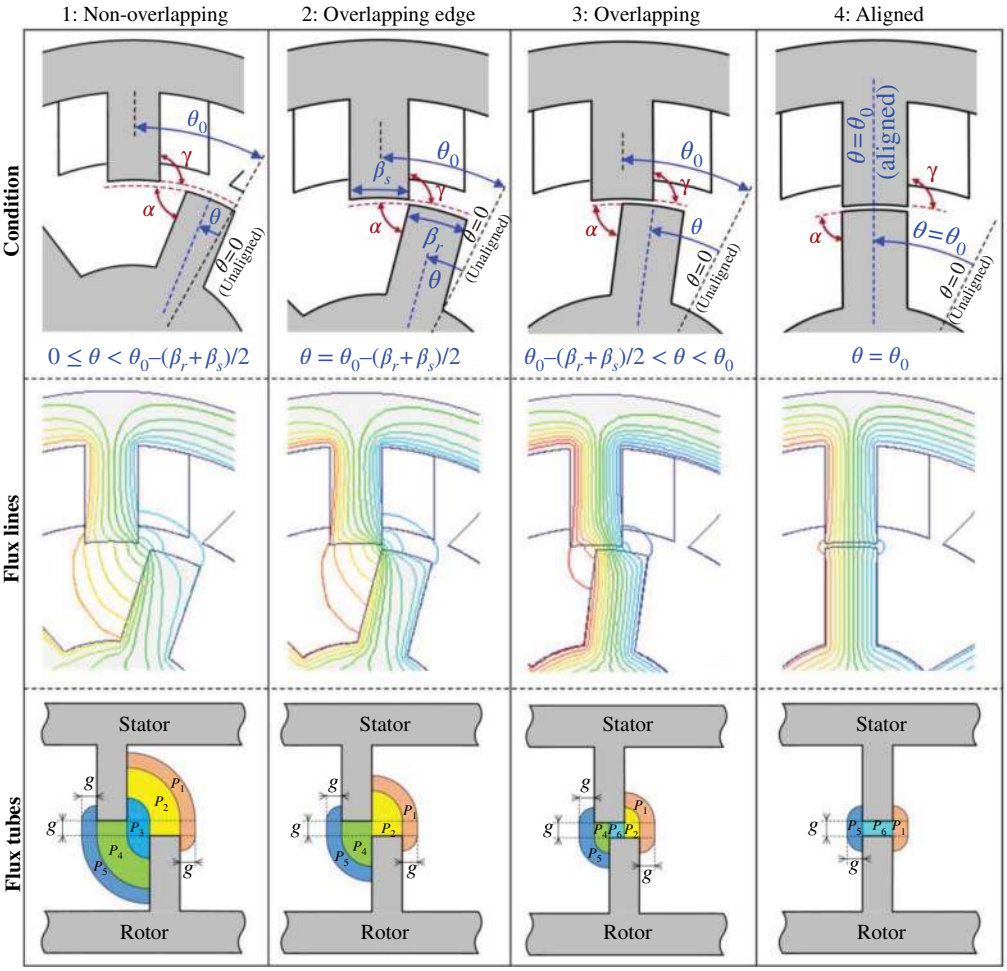

Figure 10.14 The flux lines and the corresponding flux tubes for the four operating regions 1–4.

For the regions 2 and 3, the permeance P_2 can be obtained as below:

$$P_2(\theta) = \int_0^{R_s\left(\theta_0-\frac{\beta_s}{2}+\frac{\beta_r}{2}-\theta\right)} \frac{\mu_0 l\, dx}{g+\gamma x} \tag{10.14}$$

Hence,

$$P_2(\theta) = \frac{\mu_0 l}{\gamma} \ln\left[1+\frac{\gamma R_s\left(\theta_0-\frac{\beta_s}{2}+\frac{\beta_r}{2}-\theta\right)}{g}\right] \tag{10.15}$$

For the region 1, the flux path from the top side of the stator tooth to the top side of the rotor tooth can be represented by a flux tube corresponding to the permeance P_3, with a width of roughly rotor pole thickness $(R_s - g/2)(\theta_0-\theta-\beta_s/2-\beta_s/2)$, as follows:

$$P_3(\theta) = \int_0^{\left(R_s-\frac{g}{2}\right)\left(\theta_0-\frac{\beta_s}{2}-\frac{\beta_r}{2}-\theta\right)} \frac{\mu_0 l\, dx}{\alpha x+g+\gamma x} \tag{10.16}$$

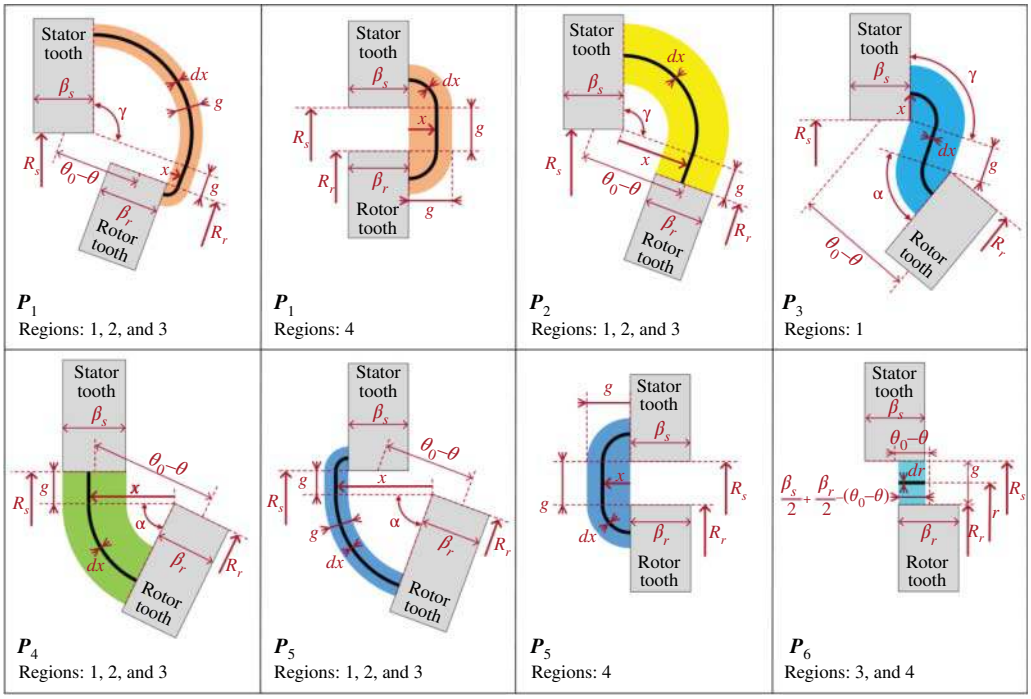

Figure 10.15 Integration paths for the flux tubes of permeances P_1–P_6 in operating regions 1–4.

Hence,

$$P_3(\theta) = \frac{\mu_0 l}{\alpha + \gamma} \ln\left[1 + \frac{(\alpha+\gamma)\left(R_s - \frac{g}{2}\right)\left(\theta_0 - \frac{\beta_s}{2} - \frac{\beta_r}{2} - \theta\right)}{g}\right] \tag{10.17}$$

For the region 1, the flux path from the tip of the stator tooth to the upper side of the rotor tooth can be represented by a flux tube corresponding to the permeance P_4, with a width of roughly stator pole thickness $(R_s - g)\,\beta_s$, as follows:

$$P_4(\theta) = \int_{(R_s-g)\left(\theta_0 - \frac{\beta_r}{2} - \frac{\beta_s}{2} - \theta\right)}^{(R_s-g)\left(\theta_0 - \frac{\beta_r}{2} + \frac{\beta_s}{2} - \theta\right)} \frac{\mu_0\, l\, dx}{g + \alpha x} \tag{10.18}$$

Hence,

$$P_4(\theta) = \frac{\mu_0 l}{\alpha} \ln\left[1 + \frac{\alpha\,\beta_s(R_s - g)}{\alpha(R_s - g)\left(\theta_0 - \frac{\beta_s}{2} - \frac{\beta_r}{2} - \theta\right) + g}\right] \tag{10.19}$$

For the regions 2 and 3, the permeance P_4 can be obtained as below:

$$P_4(\theta) = \int_{0}^{(R_s-g)\left(\theta_0 - \frac{\beta_r}{2} + \frac{\beta_s}{2} - \theta\right)} \frac{\mu_0\, l\, dx}{g + \alpha x} \tag{10.20}$$

Hence,

$$P_4(\theta) = \frac{\mu_0 l}{\alpha} \ln\left[1 + \frac{\alpha(R_s - g)\left(\theta_0 - \frac{\beta_r}{2} + \frac{\beta_s}{2} - \theta\right)}{g}\right] \tag{10.21}$$

For the regions 1, 2, and 3, the flux path from the bottom side of the rotor tooth to the upper side of the stator tooth can be represented by a flux tube corresponding to the permeance P_5, with a width of g, as follows:

$$P_5(\theta) = \int_0^g \frac{\mu_0\, l\, dx}{\frac{\pi}{2}x + g + \alpha\left[x + (R_s - g)\left(\theta_0 - \frac{\beta_r}{2} + \frac{\beta_s}{2} - \theta\right)\right]} \tag{10.22}$$

Hence,

$$P_5(\theta) = \frac{\mu_0 l}{\frac{\pi}{2} + \alpha}\ \ln\left[1 + \frac{g\left(\frac{\pi}{2} + \alpha\right)}{g + \alpha(R_s - g)\left(\theta_0 - \frac{\beta_r}{2} + \frac{\beta_s}{2} - \theta\right)}\right] \tag{10.23}$$

For the regions 3 and 4, the flux path from the tip of the rotor tooth to the tip of the stator tooth can be represented by a flux tube corresponding to the permeance P_6 with an overlapping angle of $\beta_s + \beta_r - (\theta_0 - \theta)$. It is easier to calculate the reluctance R_6 as follows:

$$R_6(\theta) = \frac{1}{P_6(\theta)} = \int_{R_s - g}^{R_s} \frac{dr}{\mu_0 l\left[\frac{\beta_r}{2} + \frac{\beta_s}{2} - (\theta_0 - \theta)\right] r} \tag{10.24}$$

Hence,

$$R_6(\theta) = \frac{1}{P_6(\theta)} = \frac{1}{\mu_0 l\left[\frac{\beta_r}{2} + \frac{\beta_s}{2} - (\theta_0 - \theta)\right]} \ln\left[1 + \frac{g}{R_s - g}\right] \tag{10.25}$$

For the region 4 ($\theta = \theta_0$), the permeances P_1 and P_5 are calculated for $\alpha = \gamma = 90°$ as in below:

$$P_1(\theta = \theta_0) = P_5(\theta = \theta_0) = \int_0^g \frac{\mu_0\, l\, dx}{\frac{\pi}{2}x + g + \frac{\pi}{2}x} \tag{10.26}$$

Hence,

$$P_1(\theta = \theta_0) = P_5(\theta = \theta_0) = \frac{\mu_0 l}{\pi}\ \ln(1 + \pi) \tag{10.27}$$

Finally, the air-gap flux can be obtained as:

$$\varphi_g = \frac{N\, i_c}{R_g} \tag{10.28}$$

The flux linkage can be obtained as follows:

$$\lambda(\theta, i_c) = L(\theta)\, i_c = N\, \varphi_g \tag{10.29}$$

If iron saturation is also considered, the inductance L is a function of rotor angle θ and coil current i_c. The inductance is also obtained as:

$$L(\theta) = \frac{N^2}{R_g(\theta)} \tag{10.30}$$

At the end, co-energy and thus electromagnetic torque are calculated as follows:

$$W_c(\theta, i_c) = \frac{1}{2} L(\theta)\, {i_c}^2 \tag{10.31}$$

$$T_e(\theta, i_c) = \left.\frac{\partial W_c(\theta, i_c)}{\partial \theta}\right|_{i_c = const} = \frac{1}{2} {i_c}^2 \frac{\partial L(\theta)}{\partial \theta} \tag{10.32}$$

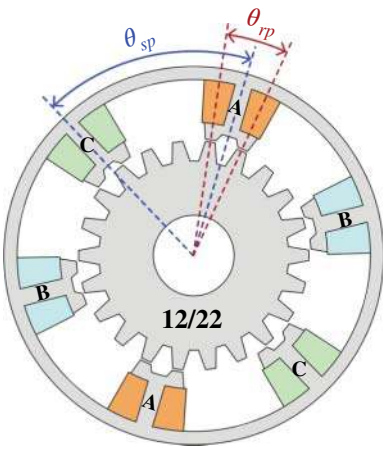

Figure 10.16 Three-phase SRM with 12/22 multi-tooth topology ($m = 2$).

10.4 Multi-Tooth SRMs

As shown in Figure 10.16, there can be multiple teeth on each stator pole, leading to an increased number of rotor teeth [2]. This configuration can result in a higher average torque by increasing the number of energy conversion strokes. To ensure proper alignment, the angle between the teeth added to the stator poles should be equal to the rotor pole pitch θ_{rp}.

However, there is an optimal number of teeth per stator pole m, as an excessive number may negatively affect dynamic torque and increase losses. An increased number of rotor teeth results in narrower rotor teeth, reducing the commutation angle, which may fall below the time constant of the stator coils. In other words, at high rotor speeds, the coil current may not have sufficient time to reach the steady-state value at the desired nominal hysteresis current setpoint during the ON period. Additionally, the extra flux path introduced by the added teeth may increase the inductance and thus the time constant of the coil. Consequently, the dynamic torque capability is reduced due to the lower average current, and the motor's maximum operating speed is limited by the increased coil time constant.

Furthermore, when a phase is turned off at the aligned position, the phase current takes longer to decay to zero, generating negative torque and further reducing dynamic torque performance. Narrower teeth can also lead to saturation and core loss problems. Moreover, an increased number of rotor teeth necessitates a higher switching frequency, which increases switching and core losses, as well as the cost of the drive circuit. It has been observed that a value of $m = 2$ or 3 provides satisfactory performance.

10.5 Connected and Modular C-Core SRMs

Instead of placing the two poles of a phase on opposite sides of the stator with a diametrical flux path, an SRM can be designed with c-core topologies for the stator featuring local flux loops. In this configuration, the two coils are placed on adjacent poles of the c-core. A key advantage of this topology is the shortened flux path, which significantly reduces reluctance along the flux path, particularly in motors with a large diameter. In other words, less MMF and thus less current is required to achieve the same flux density in the air-gap, leading to reduced copper loss in the stator coils. Additionally, core losses, including both eddy current and hysteresis losses, occur in a smaller

volume of the laminations. With a more localized flux path, the negative torques caused by the flux of an excited phase passing through unexcited phases are either eliminated or significantly reduced. Overall, the efficiency, power density, and torque density of c-core SRMs can be higher than those of traditional topologies. Figure 10.17 shows the flux lines for both unaligned and aligned conditions in conventional, c-core, and multi-tooth c-core SRMs.

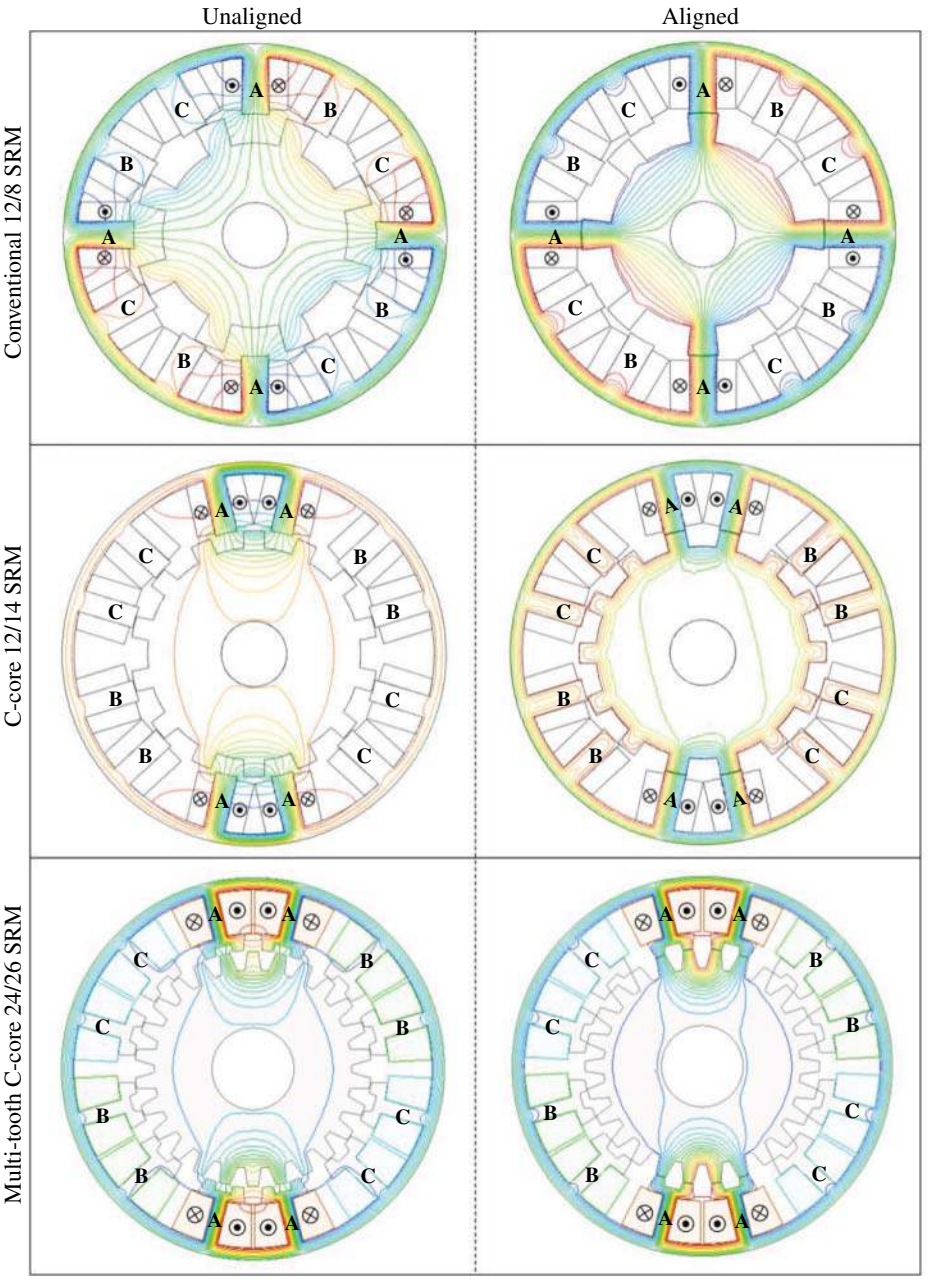

Figure 10.17 Flux lines within conventional, c-core and multi-tooth c-core SRMs in unaligned and aligned conditions.

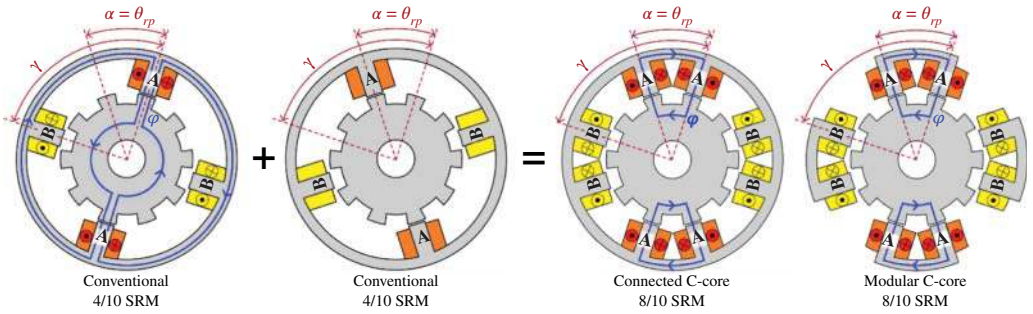

Figure 10.18 Development of connected and modular two-phase 8/10 c-core SRMs ($q = 2$, $n_{cp} = 2$, $m = 1$) from conventional 4/10 SRMs.

Figure 10.18 illustrates the strategy for obtaining two-phase single-tooth SRMs ($m = 1$) with connected and modular c-core topologies [3]. To develop a connected c-core topology for the stator, the c-core arc angle α should match the rotor pole pitch θ_{rp} for proper alignment. Thus, merging the stator of a conventional SRM with another stator rotated by an angle of α results in a c-core SRM. A modular topology can be obtained by eliminating the connecting yoke path between the adjacent c-cores. Modular topologies offer enhanced redundancy, reliability, and fault tolerance. For example, stator modules with independent drive and control systems that are galvanically, magnetically, and thermally decoupled ensure continued motor operation even if one module fails, preventing damage propagation to other modules.

Rotor pole pitch of SRMs is obtained as follows:

$$\theta_{rp} = 360^\circ / N_r \tag{10.33}$$

where N_r is the number of rotor teeth. The c-core pitch angle, defined as the angular span between the center or the corresponding poles of adjacent c-cores, can be obtained as follows:

$$\gamma = \frac{360^\circ}{q\, n_{cp}} \tag{10.34}$$

where q and n_{cp} are the number of phases and the number of c-cores per phase, respectively. As shown in Figure 10.18, for the case-study two-phase SRM ($q = 2$, $n_{cp} = 2$), we obtain $\gamma = 90^\circ$.

Figure 10.19 illustrates the development of single-tooth and multi-tooth three-phase SRMs. For multi-tooth topologies, the angle between the two poles of a c-core (c-core arc angle) is obtained as below:

$$\alpha = m\, \theta_{rp} \tag{10.35}$$

For the case-study three-phase SRM with two c-cores per phase ($q = 3$, $n_{cp} = 2$), we obtain $\gamma = 60^\circ$. For the single-tooth c-core SRM ($m = 1$) shown in Figure 10.19a, we obtain $\alpha = \theta_{rp} = 360^\circ/10 = 36^\circ$, and for the multi-tooth c-core SRM ($m = 2$) shown in Figure 10.19b, $\alpha = 2\theta_{rp} = 2^*(360^\circ/22) = 32.7^\circ$. An even number of c-cores per phase is advantageous compared to odd values of n_{cp}, as having c-cores of the same phase on opposite sides of the rotor helps eliminate radial forces, which reduces issues such as vibration, acoustic noise, bearing damage, eccentricity, and a shortened motor lifetime.

In general, the number of stator poles in a q-phase SRM with n_{cp} c-cores per phase and m teeth per c-core pole is given by:

$$N_s = 2q\, n_{cp} m \tag{10.36}$$

Not every value of N_r works for the development of c-core SRMs. Let's consider the three-phase SRM shown in Figure 10.19b with $N_s = 2^*3^*2^*2 = 24$. Since a c-core has two poles, odd numbers

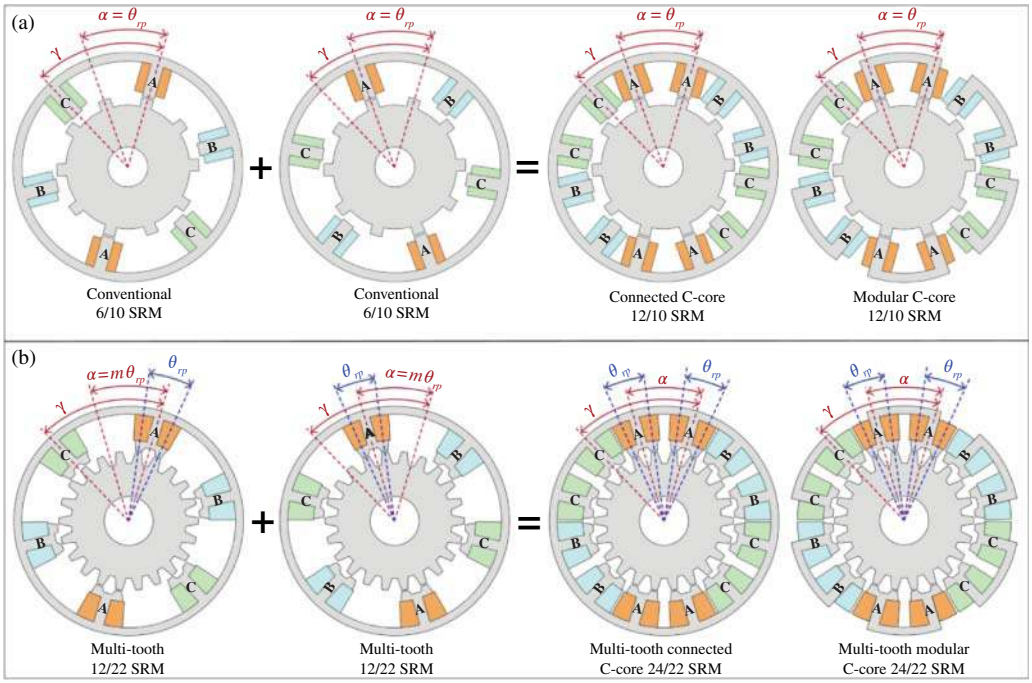

Figure 10.19 Development of connected and modular three-phase c-core SRMs ($q = 2$, $n_{cp} = 2$) with (a) single-tooth ($m = 1$) and (b) multi-tooth ($m = 2$) topologies.

of N_r are not feasible. Also, $N_r < 22$ does not work because the poles of adjacent c-cores overlap. Multiples of the number of c-cores ($q\ n_{cp}$, herein 6) are unfeasible for N_r because all phases would be aligned simultaneously. For example, $N_r = 24$, 30, and 36 do not work. Overall, the possible values for N_r include 22, 26, 28, 32, 34, 38, and so on.

Another advantage of c-core SRMs over conventional SRMs is the reduced occurrence of flux reversals within the c-cores and some other regions of the laminations. Minimizing regions with flux reversals significantly reduces core losses. Figure 10.20 illustrates the flux paths in

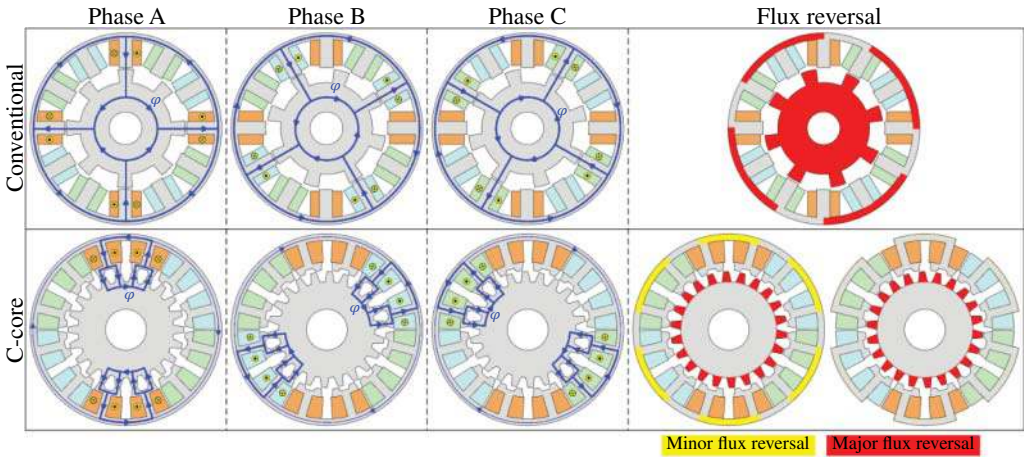

Figure 10.20 Regions with flux reversal within conventional 12/8 SRMs and 24/22 multi-tooth c-core SRMs.

a conventional 12/8 SRM and a multi-tooth c-core 24/22 SRM when each phase is excited, highlighting the regions where flux direction changes. It is evident that the conventional SRM experiences flux reversals throughout the entire rotor core and a large portion of the stator back iron. In contrast, flux reversals in c-core SRMs are limited to the rotor teeth. For connected SRMs with c-cores, there are minor flux reversals on the backside of the c-cores caused by minor flux paths outside the excited c-cores.

10.6 SRMs with Embedded Permanent Magnets

Achieving higher torque is critical to improving the overall performance of SRMs. Embedding permanent magnets (PMs) into SRMs is an approach to enhance torque density, which is crucial

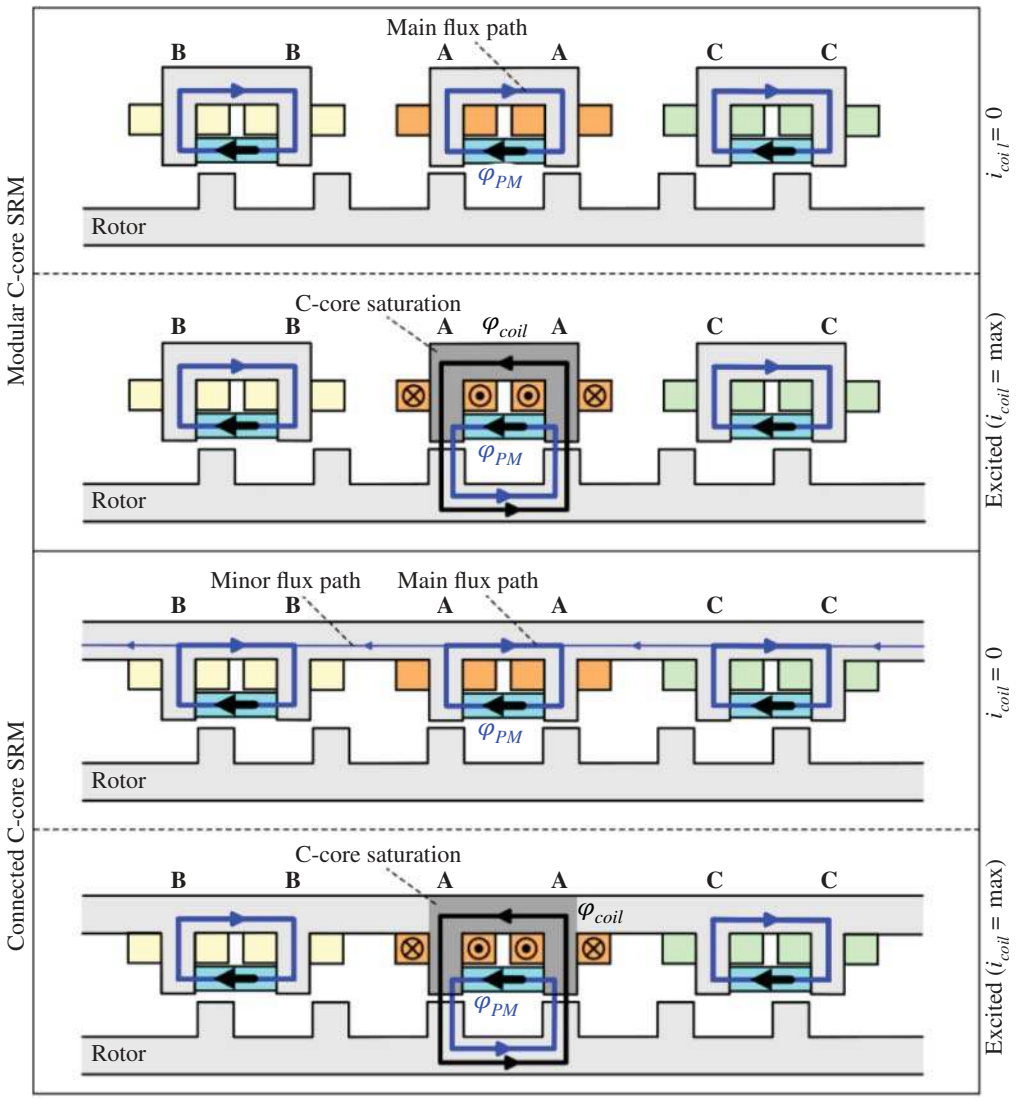

Figure 10.21 Modular and connected c-core SRM with PMs placed within the c-cores.

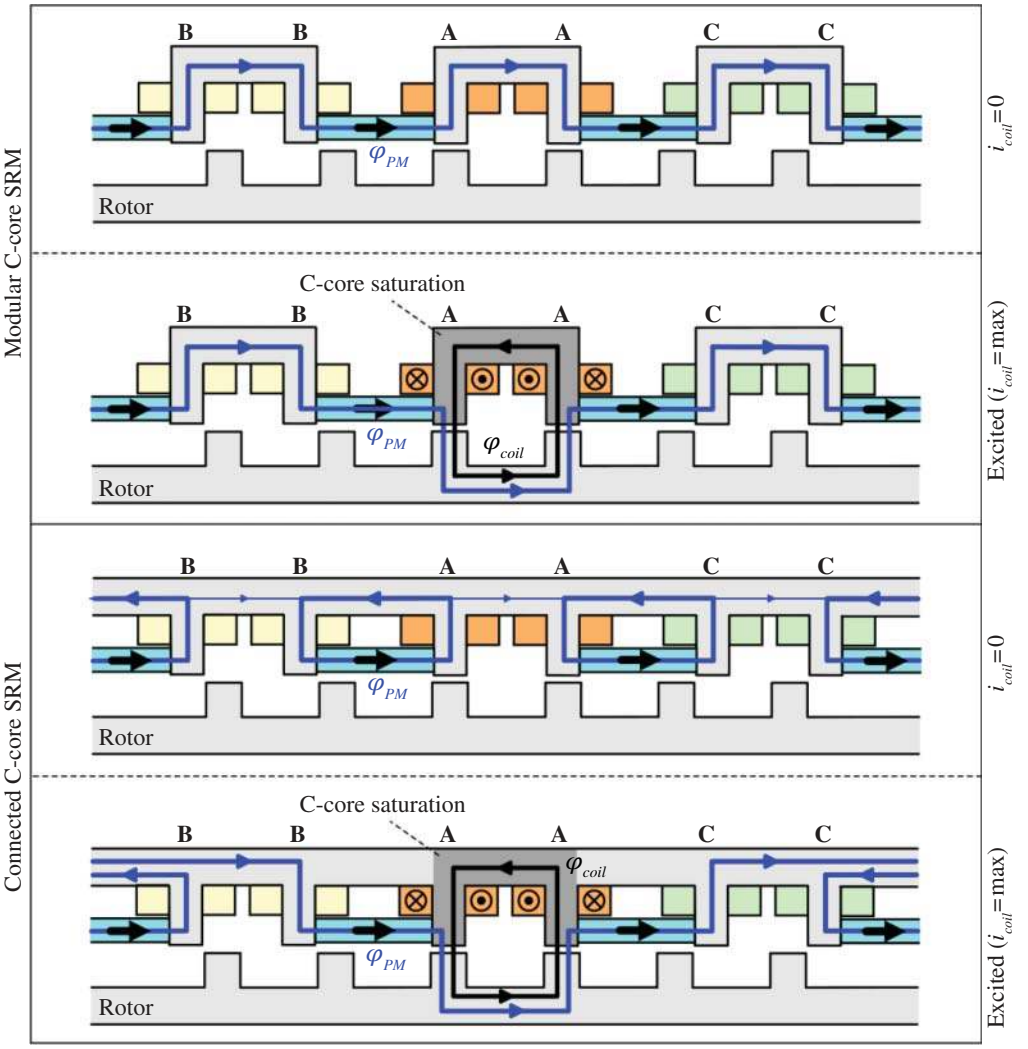

Figure 10.22 Modular and connected c-core SRM with PMs placed between the c-cores of adjacent phases.

in various applications, such as electrified transportation. Figures 10.21 and 10.22 illustrate two topologies for connected and modular c-core SRMs with embedded PMs [4–8].

In the topology shown in Figure 10.21, the PMs are placed inside the c-cores, at the tip of the c-core poles, near the air-gap. The operating principles of such topologies rely on the saturation of the c-cores during excitation. At zero or very low currents, the flux generated by the PMs closes its loop through the c-cores without crossing the air-gap, thereby not contributing to torque production. At higher stator currents during phase excitation, the c-cores approach saturation levels, increasing their reluctance. This forces the PM flux to cross the air-gap instead of closing its path through the c-cores, contributing to energy conversion and resulting in higher torque. The higher the current, the greater the saturation of the c-cores, which leads to an increased contribution of the PMs to energy conversion and torque production. A critical design consideration here is ensuring the stator reaches its saturation knee point at the nominal current. In the connected c-core topology, there is an additional minor flux path through the stator yoke connecting the

c-cores. This parallel path may reduce the total reluctance, increasing the air-gap flux density and torque production. Moreover, the connected c-core topology may be preferred for structural strength.

In the second topology with modular c-cores, as shown in Figure 10.22, the PMs are placed between adjacent c-cores. Under no-excitation conditions, the PM flux closes its path through the c-cores around the stator in a series magnetic circuit. When a c-core is excited, its saturation forces the PM flux to cross the air-gap, contributing to energy conversion. In the first topology with connected or modular c-cores, the PM flux path is localized along the c-cores, which is a shorter path with lower reluctance, which is an advantage. In the second topology with modular c-cores, PMs take a longer path around the stator, but all PMs are in series and contribute to the torque production of the excited phase, while in the first topology, only the PM within the excited phase contributes to energy conversion. In the second topology with connected c-cores, the flux paths are different slightly. When the stator is not excited, the PMs have localized flux paths. However, under phase excitation, the flux paths extend around the stator. Unlike the second topology with modular c-cores, not all PMs contribute effectively to torque production in a series magnetic circuit.

Generally, the most effective strategy is to place the PMs as close to the air-gap as possible, where energy conversion occurs. This approach can be referred to as point-of-conversion (PoC) magnet placement, which minimizes MMF drops across the iron path and injects more flux into the air-gap. The concept is analogous to point-of-load (PoL) power electronics converters, which recommend placing the converter close to the load to reduce conductive losses across high-current PCB tracks.

A third topology, shown in Figure 10.23, involves placing PMs on the back of the stator yokes between adjacent c-cores. This arrangement is much less effective and is not recommended. In this case, under phase excitation, the PM flux must pass through the saturated poles of the c-cores,

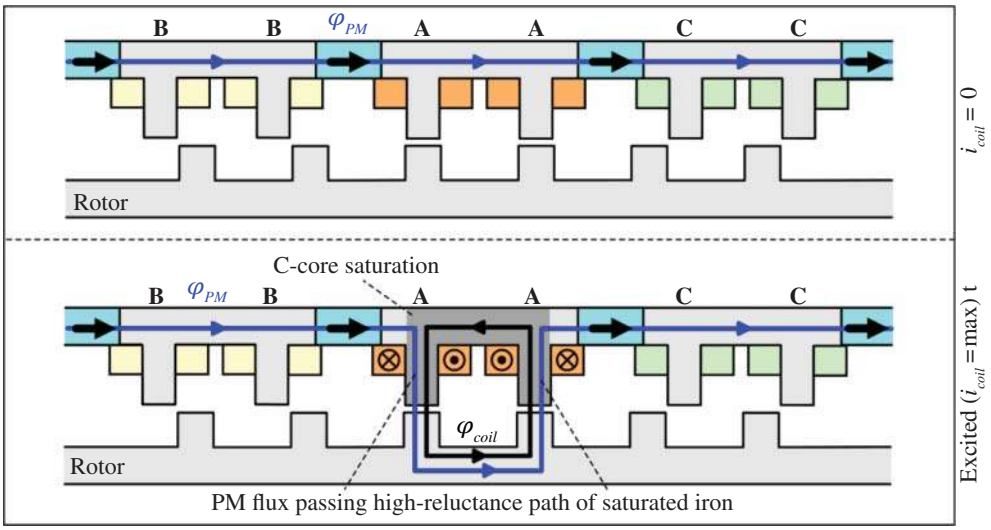

Figure 10.23 Modular and connected c-core SRM with PMs placed within the stator yoke connecting the adjacent c-cores.

encountering significantly higher reluctance. Additionally, the PM flux aligns with the coil flux, intensifying saturation and increasing the reluctance of the flux path for the coil MMF, which negatively impacts torque production. As a result, c-core poles may require increased thickness to mitigate excessive saturation along the coil flux path. This, however, reduces the space available for windings, limiting the motor's electrical loading and torque production. Conversely, placing PMs near the air-gap, like the first two topologies, ensures nearly independent flux paths for the PMs and the coils within the stator, which is an added advantage for improving torque density and overall performance.

10.7 Self-Starting Torque in Two-Phase SRMs

Two-phase SRMs, with fewer components in the power electronics drive, offer reduced cost and lower electronic losses, making them an appealing choice for various industrial applications, including fans, pumps, traction, and industrial tools. However, a major drawback of two-phase SRMs is the lack of starting torque. If one phase is fully aligned, the other phase, which is about to be excited, is fully unaligned. As a result, there is no starting torque at these positions, leading to a random direction of rotation. As shown in Figure 10.24, one approach to eliminate this symmetry in two-phase SRMs is to cut small portions from one tip of the rotor teeth or create small holes in one corner of the teeth [9]. This creates an imbalance in the air-gap reluctances at the two corners of the rotor teeth. The corner without the cut has a lower air-gap reluctance, so it will be attracted to the excited stator teeth in the unaligned position, which is how a predetermined direction of rotation is obtained.

Figure 10.25 illustrates a self-starting technique for two-phase c-core SRMs [10]. It can be observed that, in the unaligned condition, the topology does not inherently enforce a specific direction of rotation. To introduce the required asymmetry to the topology, the thickness of one pole of each c-core is slightly extended. This results in a smaller reluctance between the extended side of the stator pole of the excited phase and the rotor teeth in unaligned position, generating an attraction force (starting torque). As shown in the torque-angle characteristics, for example, when phase 1 is aligned at the end of its excitation period ($\theta = 180°$) and phase 2 is about to be excited, phase 2 develops a non-zero torque. There is an optimal value for the extension width, which should not be too small or too large. To reverse the enforced direction of rotation, the extension can be applied to the other c-core pole.

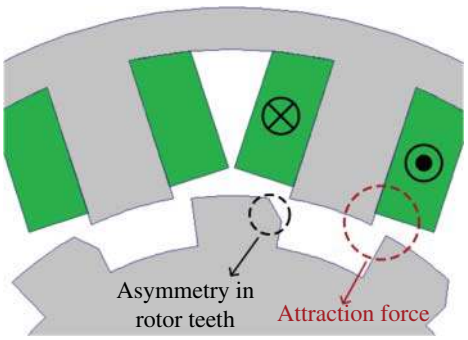

Figure 10.24 Two-phase SRM with self-starting torque due to asymmetry in rotor teeth.

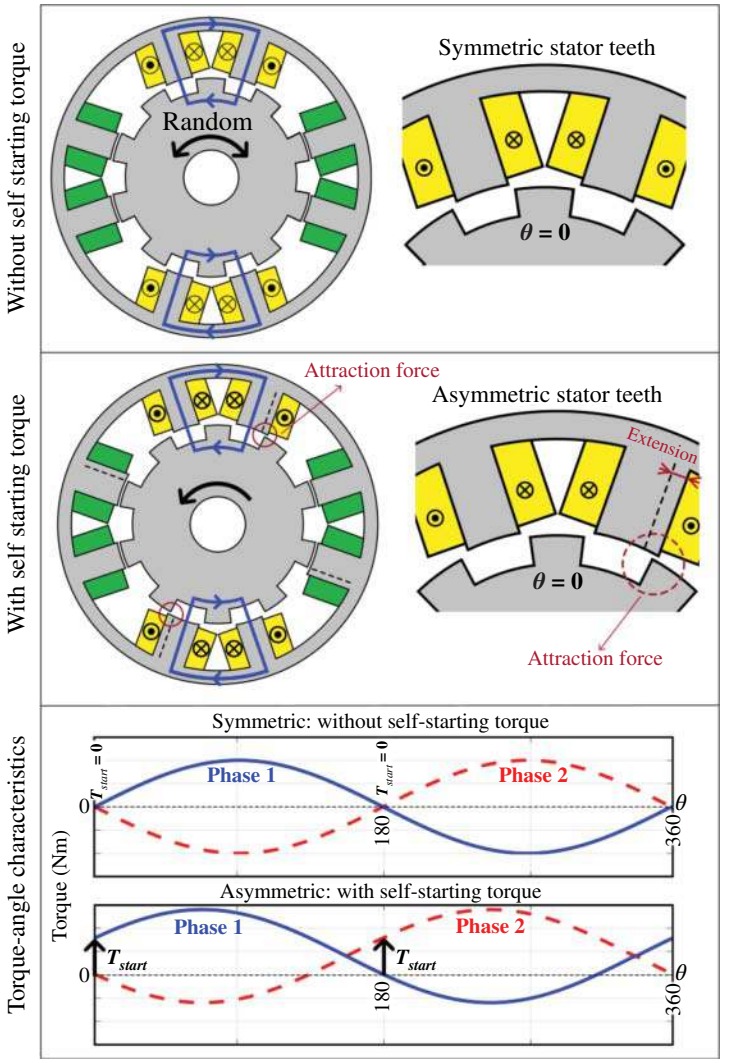

Figure 10.25 Two-phase c-core SRM without and with self-starting torque.

10.8 Current Hysteresis Control of SRMs

Figure 10.26 shows the block diagram of current hysteresis control for a three-phase SRM, including three half-bridge circuits with free-wheeling diodes and a processor containing control algorithms. It can be seen that the phase currents i_A, i_B, and i_C are measured by three current sensors and fed back to the processor through analog inputs (AIs) to be processed within the hysteresis controllers, which generate S_A, S_B, and S_C pulses by comparing them with a current setpoint of i^*. Also, the rotor position θ, measured by an encoder or another type of position sensor, is fed back through a digital input (DI) to be processed within the commutation algorithm. Finally, the gate signals G_A, G_B, and G_C are generated at the digital outputs to drive the six switches.

In a nutshell, the current hysteresis controllers generate gate pulses to apply $\pm V_{dc}$ to the stator coils, keeping the current within a band of δ around the setpoint i^*. However, before these pulses

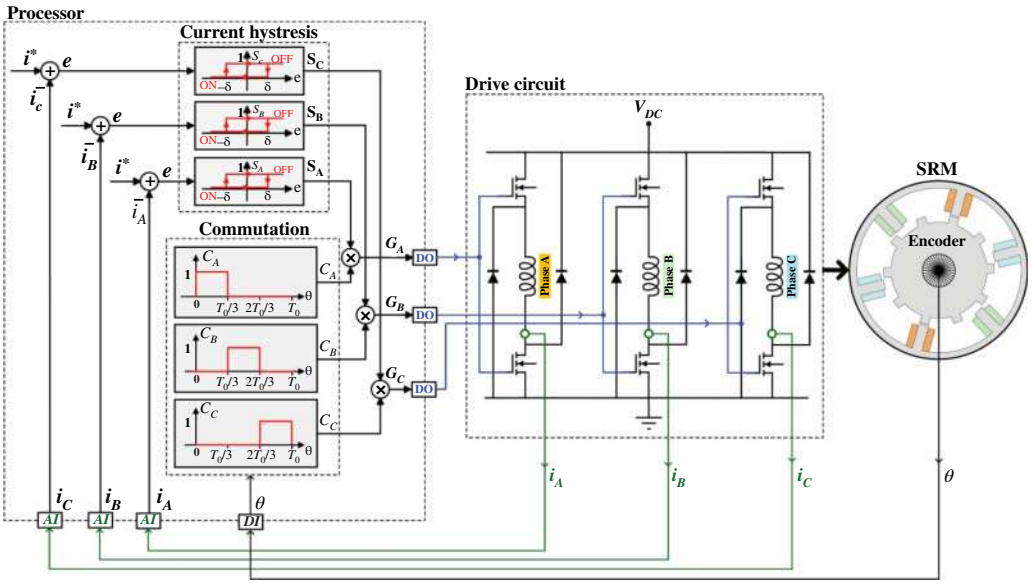

Figure 10.26 Block diagram of current hysteresis control of three-phase SRMs.

are applied to the gates of the switches, they need to pass through the commutation algorithm to ensure that only the switches of the half-bridge for the phase requiring excitation receive those pulses. Based on the rotor position θ, the commutation pulses C_A, C_B, and C_c determine whether a phase needs to be excited. The resulting logic for gate signals is obtained as follows:

$$G_A = S_A \cdot C_A \tag{10.37}$$

$$G_B = S_B \cdot C_B \tag{10.38}$$

$$G_C = S_C \cdot C_C \tag{10.39}$$

These control pulses, along with phase voltages, phase currents, and dynamic torque profiles for the non-overlapping control technique, are shown in Figure 10.27. The period T_0 is defined as the time taken for the rotor to rotate by one pole pitch θ_{rp} if all phases are excited once. The turn-on position for a phase occurs when the previous phase has reached its aligned position. For a three-phase SRM, this position is not the unaligned position of the phase but is offset by one-third of the period from the unaligned to aligned position, i.e. one-third of $\theta_{rp}/2$. The excitation period for each phase is $T_0/3$, corresponding to two-thirds of $\theta_{rp}/2$, until it reaches the aligned position.

During the hysteresis period, the voltage across each phase alternates between $\pm V_{dc}$. When the switches of the half-bridge for a phase are turned on ($G_i = 1$), the applied voltage is $+V_{dc}$. When the switches are turned off, the coil current passes through the free-wheeling diodes, resulting in a phase voltage of $-V_{dc}$. At the end of the commutation period ($T_0/3$), when the phase is turned off, the voltage remains at $-V_{dc}$ until the current decays through the diodes and eventually reaches zero.

At the beginning of the commutation period, when a phase is turned on, the coil time constant causes the current to take time to rise and reach the current setpoint i^*. Torque also starts to develop during this period. As detailed in Figure 10.28, after the current reaches i^*, the dynamic torque follows the corresponding torque-angle characteristics of the SRM at i^*. Also, when a phase is turned off at the end of the excitation period ($T_0/3$) at its aligned position, it still carries the current i^*,

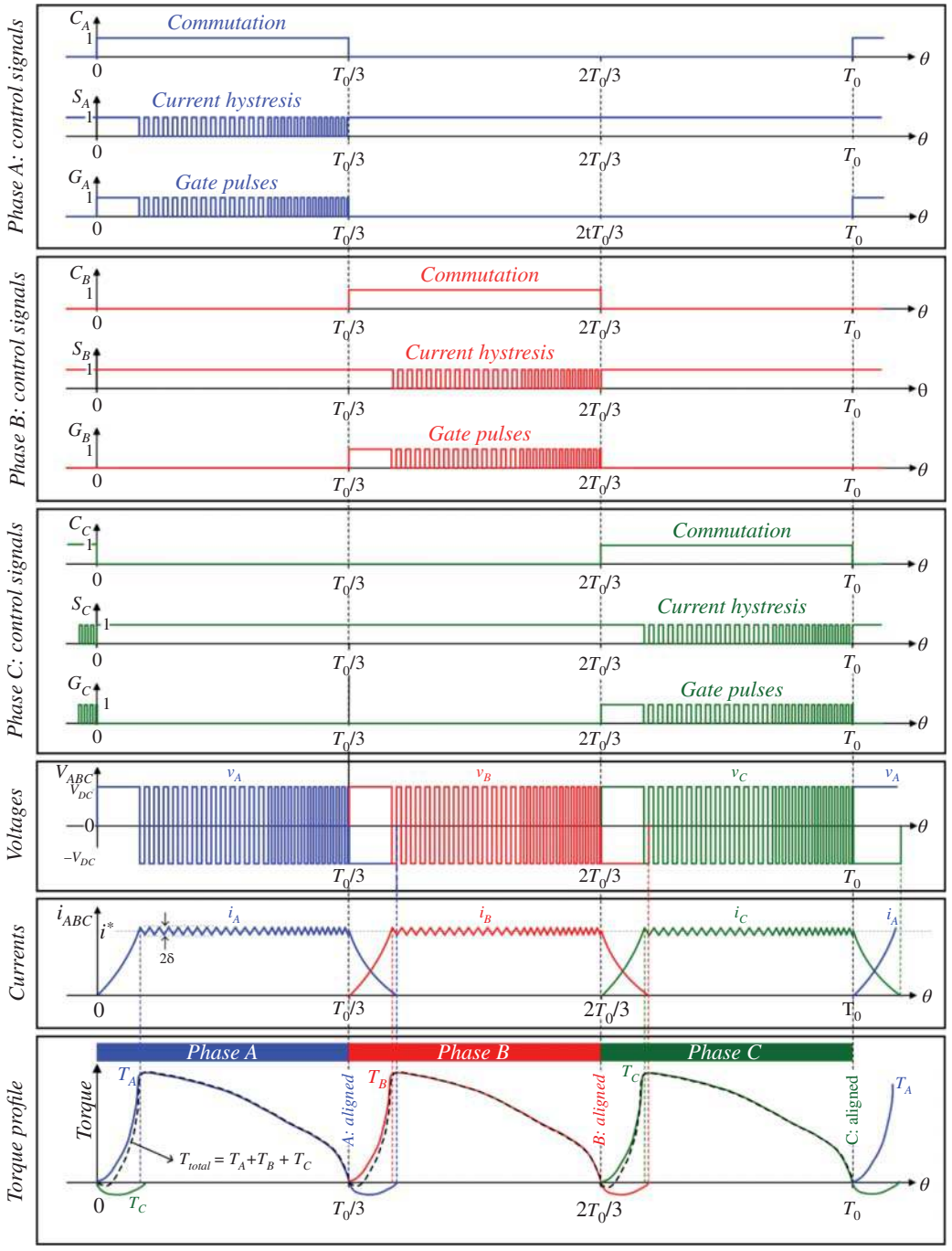

Figure 10.27 Control signals, gate pulses, waveforms of phase current, phase voltage, and developed torques for phase non-overlapping control of three-phase SRMs.

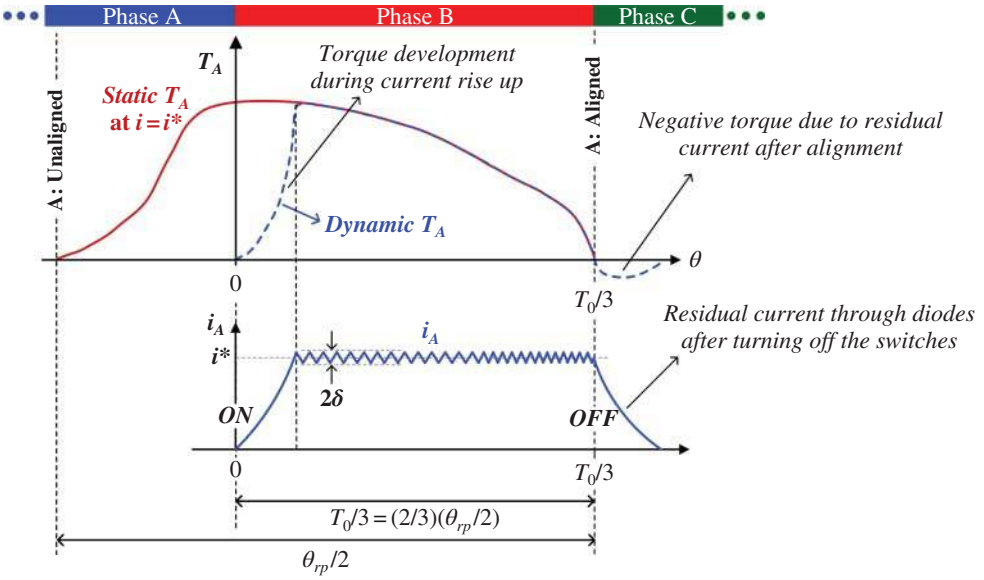

Figure 10.28 Static torque-angle characteristics and dynamic torque for phase non-overlapping excitation of three-phase SRMs.

which begins to decay through the free-wheeling diodes. As the rotor continues to rotate due to the excitation of the next phase and its moment of inertia, this decaying current generates a small negative torque, tending to pull the rotor back toward the aligned position of the previously excited phase.

10.9 Problems

10.1 Below is a two-phase multi-tooth c-core SRM with asymmetrical teeth on each c-core pole to generate self-starting torque. It also includes permanent magnets embedded between c-cores of different phases to increase torque density, along with its magnetic equivalent circuit (MEC). The stator coils of the excited phase are represented as magneto-motive forces $F = Ni_c$, and the magnets are represented as reluctances in series with a magneto-motive force $F_m = l_m H_c$, where H_c is the coercivity of the magnets.

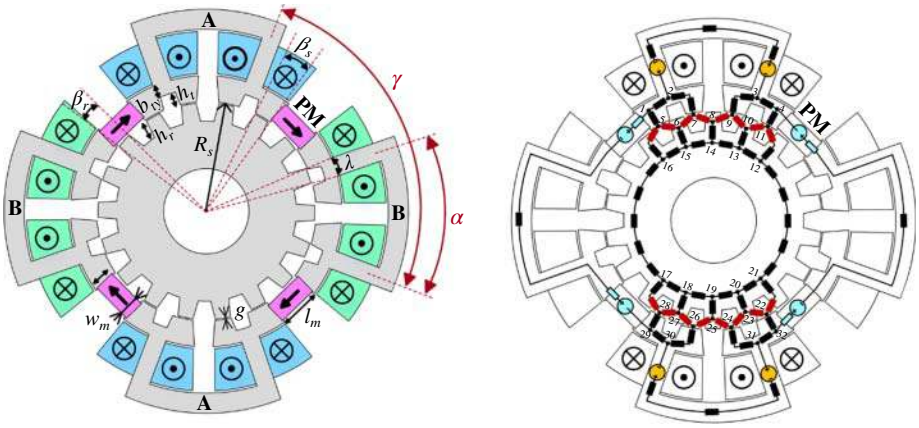

(a) For the flux tubes in unaligned condition, as shown below, determine the corresponding permeances of the air-gap region and the magnets.

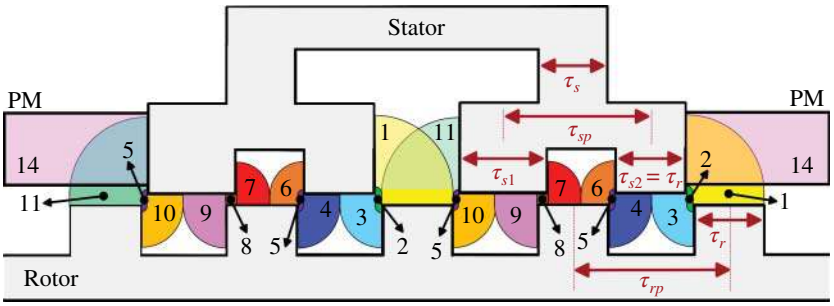

(b) The fluxes within the motor due to the coil-only, PM-only, and both under excitation are shown below. Explain the operating principles of the device according to its magnetic equivalent circuit. Hint: under stator excitation, the iron reluctances go up due to saturation.

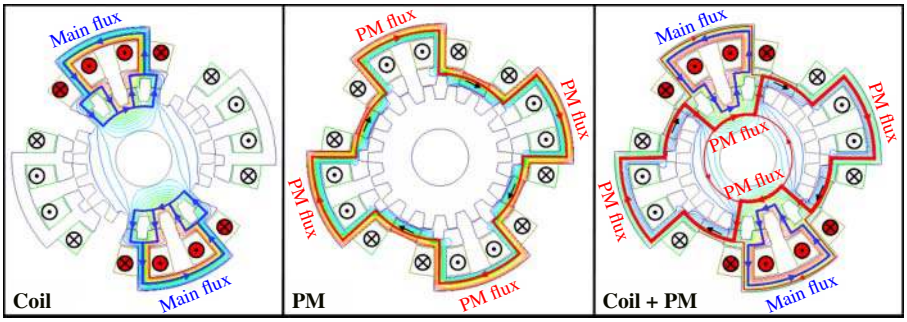

10.2 We discussed placing magnets inside the c-core as well as between the c-cores of adjacent phases. For SRMs with connected and modular c-core topologies having both of these magnet arrangements, draw the flux paths for the two cases of no excitation and nominal current excitation.

10.3 Similar to Figure 10.27 for three-phase SRMs, draw the control signals and waveforms of phase voltages, phase currents, and electromagnetic torque for two-phase SRMs with and without self-starting torque.

10.4 SRMs can be controlled such that there are periods when more than one phase is turned on simultaneously. This method, called phase overlapping control, reduces torque ripple and improves average torque. The torque-angle characteristics and the dynamic torque profile of one phase of a three-phase SRM, excited from a fully unaligned position to a fully aligned position, are shown below. This leads to overlap with the excitation of other phases.

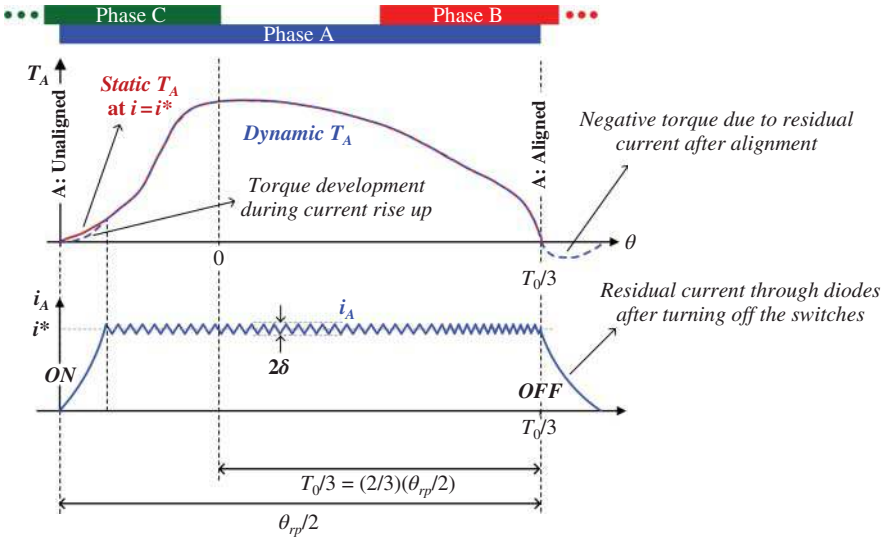

(a) Draw the hysteresis current waveforms and dynamic torque profiles for all three phases and calculate the total motor torque. Compare it to the non-overlapping control technique.

(b) As we know, when the excited phase reaches the aligned position (the moment it needs to be turned off), if it is still carrying current, a negative torque is generated during the excitation of the next phase. Can optimizing turn-on and turn-off times eliminate this negative torque and consequently increase the torque density of the motor? For example, would turning off the phases before reaching the fully aligned position help? How is this timing related to the time constant of the stator coils?

10.5 As shown below, single-pulse control is another technique to drive SRMs. In this method, there is no hysteresis control for the currents, and the motor is excited by applying the DC link voltage to the phases only through commutation. Although it is less effective than hysteresis control because the current is not maintained at the nominal level, it is simple and cost-effective, making it suitable for many applications. For this control technique, draw the gate pulses along with the phase voltages, phase currents, and developed torques.

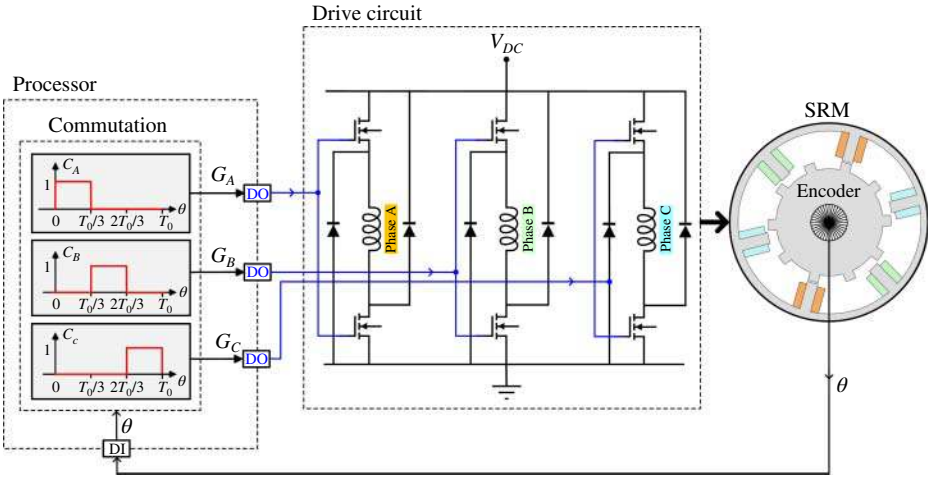

References

1 Davarpanah, G., Mohammadi, S., and Kirtley, J.L. (2020). Modelling of switched reluctance machines. *IET Elect. Power Application* 14 (11): 1997–2006.

2 Zhu, J., Cheng, K.W.E., Xue, X., and Zou, Y. (2017). Design of a new enhanced torque in-wheel switched reluctance motor with divided teeth for electric vehicles. *IEEE Transactions on Magnetics* 53 (11).

3 Davarpanah, G., Mohammadi, S., and Kirtley, J.L. (2019). A Novel 8/10 TwoPhase Switched Reluctance Motor with Enhanced Performance: Analysis and Experimental Study. *IEEE Transactions on Industrial Application* 55 (4): 3402–3410.

4 Afinowi, I.A.A., Zhu, Z.Q., Guan, Y., Mipo, J.C., and Farah, P. (2015). Hybrid-excited doubly salient synchronous machine with permanent magnets between adjacent salient stator poles. *IEEE Transactions on Magnetics* 51 (10).

5 Ding, W., Yang, S., Hu, Y., Li, S., Wang, T., and Yin, Z. (2017). Design consideration and evaluation of a 12/8 high-torque modular-stator hybrid excitation switched reluctance machine for EV applications. *IEEE Transactions on Industrial Electronics* 64 (12): 9221–9232.

6 Zhu, J., Cheng, K.W.E., and Xue, X. (2018). Design and analysis of a new enhanced torque hybrid switched reluctance motor. *IEEE Transactions on Energy Conversion* 33 (4): 1965–1977.

7 Davarpanah, G., Mohammadi, S., Lang, J. H., and Kirtley, J. L. (2023). "Two-phase switched reluctance motor with hybrid excitation: modeling and evaluation," IET Electric Power Applications 17 (7): 939–951.

8 Davarpanah, G. and Mohammadi, S. (2024). "A New Switched Reluctance Motor with Embedded Permanent Magnets for Transportation Electrification," *IECON* 2024 - *50th Annual Conference of the IEEE Industrial Electronics Society*, Chicago, IL, USA.

9 Lee, C., Krishnan, R., and Lobo, N.S. (2009). Novel two-Phase switched reluctance machine using common-pole E-Core structure: Concept, analysis, and experimental verification. *IEEE Transactions on Industrial Applications* 45 (2): 703–711.

10 Davarpanah, G., Faiz, J., Mohammadi, S., and Kirtley, J.L. (2022). A self-starting technique for two-phase switched reluctance motors. *IEEE Transactions on Energy Conversion* 37 (2): 1314–1323.

11

Power Electronics Drives

11.1 Introduction

Power electronics is a diverse field that combines concepts from electrical, electronic, and control engineering to explore and enhance the conversion, regulation, and management of electrical power. Its main goal is to design efficient, compact, and cost-effective solutions for transforming and controlling electrical energy in a wide range of applications. The field has gained increasing prominence with the rapid advancements in renewable energy systems, electric vehicles, and smart grid technologies. Power electronic systems are utilized across various domains, including power generation, transmission, distribution, and control. Power electronics in control of electric machines is commonly referred to as "drives".

In these applications, power semiconductor devices play a critical role in regulating input voltages and currents to produce the desired electrical outputs. Fundamental semiconductor components, such as diodes, field-effect transistors (FETs), and bipolar junction transistors (BJTs), have been developed to handle high voltages and currents. Other types of semiconductor devices that have been developed specifically for power applications include silicon-controlled rectifiers (SCRs), gate turn-off thyristors (GTOs), and insulated gate bipolar transistors (IGBTs). The selection of a specific device depends on factors such as power levels, switching frequency requirements, efficiency, and the characteristics of the input and output.

Figure 11.1 presents a block diagram of a typical power electronic system. Modern power electronic systems are capable of handling power levels ranging from a few watts to several megawatts, offering efficient and reliable interfaces for converting raw power into regulated outputs. This versatility has driven the widespread replacement of hydraulic and mechanical actuators with electric motors, which can be precisely controlled through power electronic interfaces. As advancements in power electronics technology continue, its applications are expanding across industries such as transportation, energy, telecommunications, and consumer electronics. By enabling efficient and dependable electrical power conversion and control, power electronics are driving innovation, fostering progress, and accelerating technological advancements in these diverse sectors.

This chapter is focused on the types of power electronic circuits that are used in drives for electric machinery. Direct current to direct current (DC/DC) converters, characterized as "buck" and "boost" converters or "choppers", are employed to drive commutator machines. Inverters, used to convert DC to alternating current (DC/AC), are employed in drives for synchronous and induction motors. And rectifier circuits that convert AC to DC are often employed in generator systems.

Electromagnetic Analysis of Electric Machines: First Principles, Modeling, and Design, First Edition.
James L. Kirtley, Christopher H. T. Lee, and Sajjad Mohammadi.

Companion website: www.wiley.com/go/kirtleyelectric

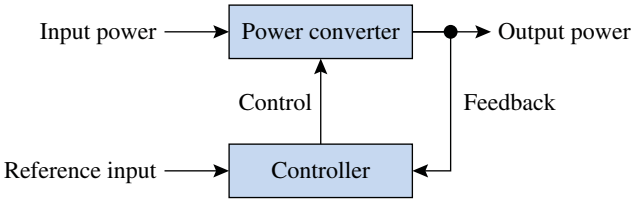

Figure 11.1 Block diagram of a typical power electronic system.

11.2 DC Converters

DC-DC converters are essential components in contemporary power management systems, specifically designed to modulate the voltage of a DC source from one level to another. This modulation is critical for ensuring consistent and efficient power delivery across a broad array of electronic devices and systems. In scenarios where input voltage levels fluctuate due to factors such as battery depletion or varying load conditions, DC-DC converters play a pivotal role in stabilizing the output voltage, thereby ensuring a reliable power supply to system components.

11.2.1 Buck Converter (Step-Down)

The buck converter, commonly known as a step-down converter, is a fundamental topology in power electronics used to lower a higher input voltage to a desired lower output voltage. It plays a vital role in various applications, such as portable electronics and automotive systems, where specific components or subsystems require reduced voltage levels for optimal functionality. A key advantage of the buck converter is its straightforward design, enabling efficient voltage regulation with relatively few components. Typically integrated into a closed-loop control system, it utilizes a feedback mechanism to continuously compare the output voltage to a reference voltage. This feedback ensures stable and regulated output, even in the face of input voltage variations or changes in load conditions, making it a reliable solution for modern power management needs.

Figure 11.2 depicts the circuit diagram of a buck converter, which includes a DC power supply E, a switch S (typically implemented using a MOSFET or IGBT), a diode D, an LC low-pass filter, and a load resistor R. The switch is represented by a symbol S featuring a small arrow to indicate the allowable direction of current flow.

When the switch S is turned on, the current flowing through the inductor will increase, rising from its minimum to maximum value. Meanwhile, the diode D becomes reverse biased due to the supply voltage E, causing the voltage across the inductor u_L to equal the difference between the supply voltage and the load voltage (as shown in Figure 11.3), i.e.

$$u_L = E - U \tag{11.1}$$

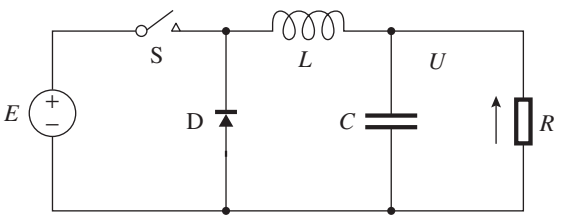

Figure 11.2 Buck converter.

Figure 11.3 Buck converter—interval t_{on}.

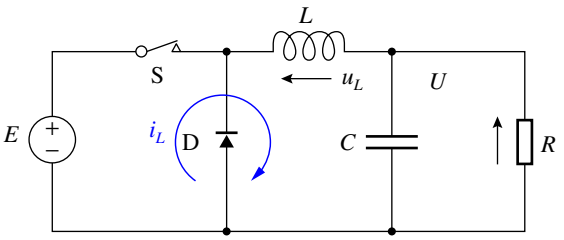

Figure 11.4 Buck converter—interval t_{off}.

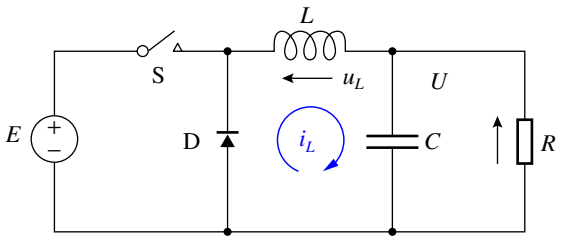

When S is turned off, the commutation process occurs as illustrated in Figure 11.4, allowing the current from the inductor, previously supplied by the source E, to flow through the diode D until it reaches the minimum value. As a result, the voltage across the inductor becomes equal to the load voltage, i.e.

$$u_L = -U \tag{11.2}$$

The current and voltage waveforms passing through the inductor during the switching on and off periods are shown in Figure 11.5. In steady-state operation, over one full switching cycle, the net change in the inductor current is zero:

$$\Delta I_L = \frac{1}{L}\int_0^T u_L dt = 0 \Longrightarrow \int_0^T u_L dt = 0 \tag{11.3}$$

This implies that the total area under the voltage waveform across the inductor over a full cycle is also zero, which can be expressed as:

$$S_+ = S_- \Rightarrow (E-U)\cdot t_{ON} = U \cdot t_{OFF} \tag{11.4}$$

Thus, the average load voltage during one complete cycle T can be calculated as:

$$U = E \cdot \frac{t_{ON}}{t_{ON}+t_{OFF}} = E \cdot \frac{t_{ON}}{T} = E \cdot d \tag{11.5}$$

where d is the duty cycle of the switch.

Figure 11.5 Voltage and current across the inductor in a buck converter.

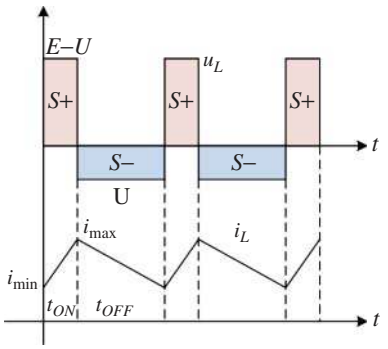

The inductor is crucial in a buck converter, as it stores and releases energy during each switching cycle. Moreover, the average output voltage is determined by the duty cycle as $V_{out} = dV_{in}$.

11.2.2 Boost Converter (Step-Up)

The boost converter is a DC-DC switching converter designed to increase (step-up) the input voltage to a higher output voltage. This conversion process involves storing energy in an inductor while the switch is on, and then transferring that energy to the load when the switch is off. Similar to the buck converter, the operation of a boost converter can be understood by analyzing its switch-on and switch-off intervals. During the switch-on phase, energy is stored in the inductor, while in the switch-off phase, the stored energy is released and combined with the input voltage to produce a higher output voltage for the load.

When the switch S is closed, the inductor is connected to the DC power supply E, as shown in Figure 11.6. During this phase, the diode D is reverse biased due to the output voltage, and the load is powered by energy supplied from the capacitor. The input voltage E causes the current through the inductor to increase linearly from its minimum to maximum value.

When S is turned off, the inductor's current, which carries stored magnetic energy, flows through the diode to the load, transferring energy from both the DC source and the inductor to the load (as shown in Figure 11.7). During this phase, the voltage across the inductor reverses direction and becomes equal to the difference between the load voltage and the DC supply voltage. Simultaneously, the current in the inductor decreases from its maximum value to its minimum value.

The waveforms showing the current and voltage through the inductor during the switch-on and switch-off periods are depicted in Figure 11.8.

In steady state, the average voltage across the inductor is zero:

$$\begin{aligned} & E \cdot t_{ON} = (U - E) \cdot t_{OFF} \\ & \Rightarrow U = E \cdot \frac{1}{\frac{t_{OFF}}{t_{ON} + t_{OFF}}} = E \cdot \frac{1}{\frac{T - t_{ON}}{T}} = E \cdot \frac{1}{1 - d} \end{aligned} \tag{11.6}$$

From (6), it is evident that the voltage at the load equals the voltage of the DC source when $d = 0$. As the active portion t_{ON} increases, the load voltage increases, verifying that this is a

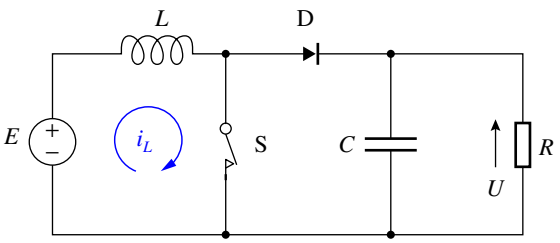

Figure 11.6 Boost converter circuit—interval t_{on}.

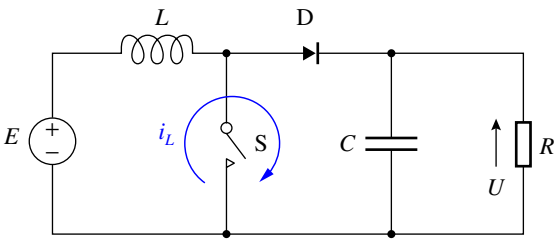

Figure 11.7 Boost converter circuit—interval t_{off}.

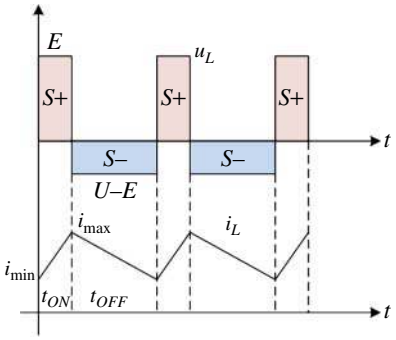

Figure 11.8 Voltage and current across the inductor in a boost converter.

voltage-boosting chopper. This equation also indicates that if $d = 1$, the load voltage would theoretically become infinitely large. However, a duty cycle of 1 implies that $t_{ON} = T$, meaning the switch remains continuously on state, preventing any energy transfer from the DC source to the load.

11.2.3 Buck-Boost Converters

The buck-boost converter is a flexible power conversion device that can produce an output voltage either higher (boost mode) or lower (buck mode) than the input voltage. This versatility makes it well-suited for various power electronics applications that demand precise input voltage regulation and adjustable output voltage levels. Its ability to smoothly switch between buck and boost modes enables efficient power management in systems with fluctuating input voltages, ensuring stable and reliable performance in a wide range of situations.

When S is turned on, the inductor is connected to the DC power source E, as shown in Figure 11.9. This causes the inductor current to increase linearly from its minimum to maximum value. During this phase, the diode is reverse biased due to the combined voltage of the load U and the DC power source E, preventing it from conducting.

When the switch is turned off, the inductor current flows through the diode, as shown in Figure 11.10, transferring the magnetic energy stored in the inductor to the load. During this phase, the inductor current decreases from its maximum to minimum value, governed by the load voltage.

During the periods of switching on and off, the waveforms depicting current and voltage passing through the inductor are illustrated in Figure 11.11.

In steady state, the average voltage across the inductor is zero:

$$S_+ = E \cdot t_{ON} = S_- = U \cdot t_{OFF} \Rightarrow U = E \cdot \frac{t_{ON}}{t_{OFF}} = E \cdot \frac{d}{1-d} \tag{11.7}$$

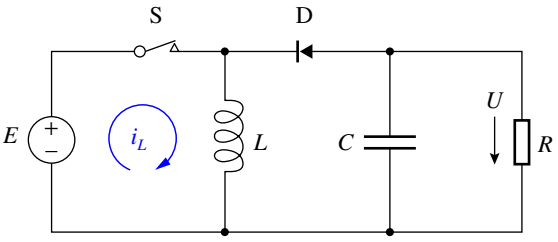

Figure 11.9 Buck-boost converter circuit—interval t_{on}.

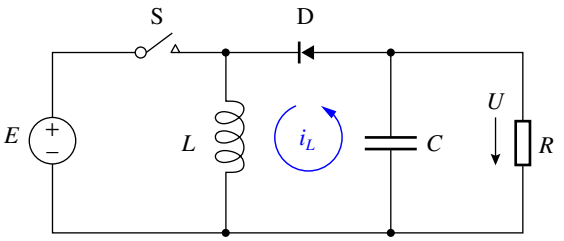

Figure 11.10 Buck-boost converter circuit—interval t_{off}.

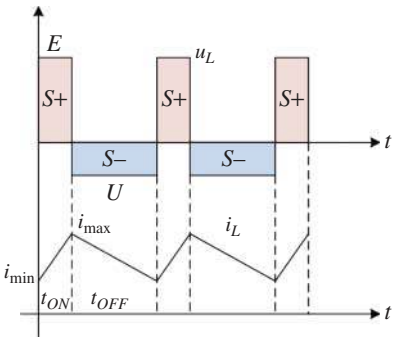

Figure 11.11 Voltage and current across the inductor in a buck-boost converter.

Therefore, this converter is capable of functioning as either a step-down or step-up converter (with t_{ON}/t_{OFF} ranging from 0 to infinity). However, it is important to recognize that, similar to the boost converter, the voltage boosting capability is limited by circuit losses.

11.2.4 Applications of DC Converters in Motor Drives

DC-DC converters are extensively employed across a wide range of applications due to their versatility and efficiency. They can be designed as independent units, incorporated into large power management systems, or embedded within individual components such as microprocessors or microcontrollers. In DC (commutator) machines, buck converters are used in both the field and armature circuits to control speed. In these applications, the filter capacitor is often not needed because the inductance of the windings does the filtering required.

11.3 Voltage Source Inverter

As another commonly used power electronics circuit, the primary function of DC-to-AC inverters is to convert a DC power source into an AC output waveform. Inverters are typically classified based on the nature of the power supply into voltage-source inverters (VSIs) and current-source inverters (CSIs). A VSI operates with a DC voltage supply, where the Thévenin equivalent resistance of the voltage source is ideally zero. The DC input voltage for a VSI typically originates from a rectifier, battery, or photovoltaic array, and the AC outputs generated by these inverters can be either single-phase or multiphase. Recent advancements have even led to the development of DC-to-AC inverters capable of producing more than three-phase outputs, driven by the need to enhance the reliability of AC motors in critical applications.

Inverters produce various output waveforms, including square wave, sinusoidal wave, and modified sinusoidal wave. Pulse-width modulation (PWM) techniques are commonly employed to

adjust the output AC voltage to desired amplitudes and frequencies while minimizing harmonics through multiple switching operations with a constant DC input voltage. VSIs have diverse practical applications, including AC motor drives, uninterruptible power supplies (UPS), active power filters, AC batteries, induction heating, and high-voltage direct current (HVDC) power transmission systems [1].

11.3.1 Single-Phase Half-Bridge Inverter

First, we explore the operating principles of the single-phase inverter with two switches. As shown in Figure 11.12, the half-bridge inverter is a basic single-phase inverter design. This configuration consists of two switching devices—typically transistors, IGBTs, or MOSFETs—arranged in series with a DC voltage source. It also includes two feedback diodes and two capacitors that connect the source to the load (in this case, an RL load). The load is placed between the midpoint of the capacitors (node A) and the midpoint of the diodes and switches (node B). In this setup, the complementary operation of the switches produces an AC output voltage across the load. The role of the capacitors is to maintain the voltage at Node A at a constant level of half of the DC supply voltage. The diodes are used to "freewheel" current that would have nowhere else to go when a switch turns off. This is particularly important when the load is inductive.

The half-bridge inverter functions in four distinct modes when powering a resistive-inductive load.

Figure 11.12 depicts Mode 1 for an R-L load in a half H-bridge inverter configuration. In this mode, the upper switch S_1 is turned on (activated), while the lower switch S_2 remains off (deactivated). Consequently, the output voltage across the load is half of the DC source voltage. During this phase, the current flows through the load and increases gradually from zero to its maximum value. As the current and voltage polarities are aligned, the inductor in the load stores energy.

Figure 11.13 illustrates Mode 2 operation of the half H-bridge inverter. In this mode, when D_2 is activated, the output voltage becomes the negative half of the DC source voltage. Although the output voltage is reversed, the current continues to flow through the load in the same direction as in Mode 1. This is because the inductor resists sudden changes in current. As the inductor releases its stored energy, the current through the load gradually decreases. It would eventually reach zero, but for further switching operation.

Figure 11.14 demonstrates the operation of Mode 3 in the half-bridge inverter. In this mode, the lower switch S_2 is turned on. This causes current to flow through both the load and S_2, resulting in the output voltage being equal to the negative half of the DC source voltage. Unlike Mode 1 and Mode 2, Mode 3 reverses the current direction through the load. As the lower switch is activated,

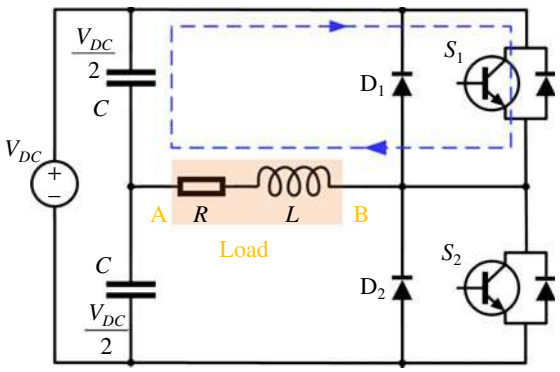

Figure 11.12 Mode 1 for RL-Load in half H-bridge inverter.

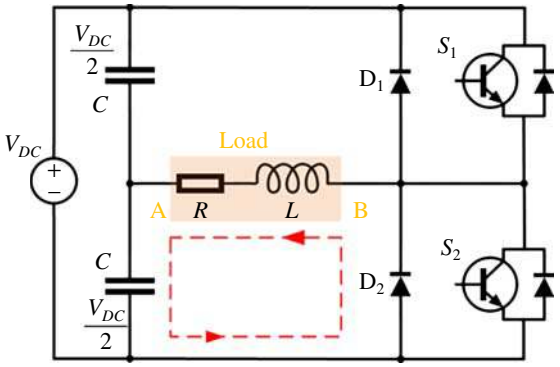

Figure 11.13 Mode 2 for half H-bridge inverter.

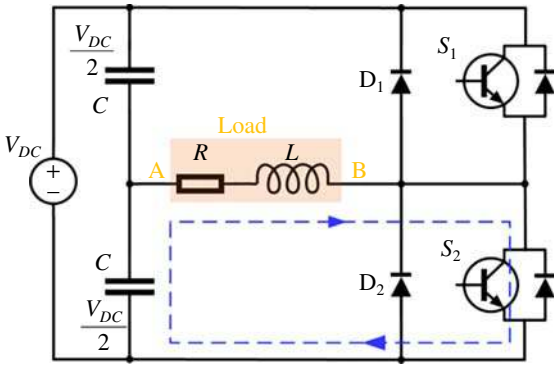

Figure 11.14 Mode 3 of half H-bridge inverter.

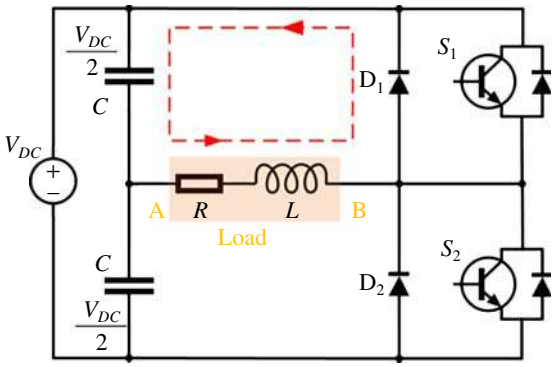

Figure 11.15 Mode 4 of half H-bridge inverter.

the current begins to increase in the reverse direction and eventually reaches a negative peak, at which point the inductor begins to store energy again.

In Mode 4, as shown in Figure 11.15, the diode D_1 is activated, causing the output voltage to be half of the DC source voltage. The current through the load continues in the same direction as in Mode 3, due to the inductor's resistance to abrupt changes in current. As the inductor discharges, the current gradually decreases until the load current drops to zero.

In conclusion, Figure 11.16 shows the waveforms of the output voltage and current, along with the currents through the switches and diodes, for a half-bridge inverter with an RL load. The figure also illustrates the operation modes M1 to M4, as well as the states of the diodes and switches.

The single-phase half-bridge inverter has a straightforward circuit design, making its operational principles easy to understand. More complex inverter types, like the single-phase full-bridge

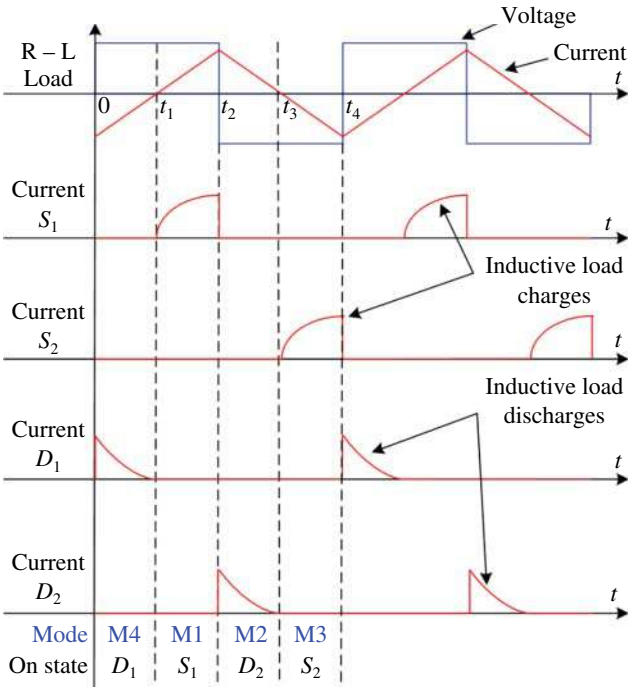

Figure 11.16 Voltage and current Waveforms of half H-bridge inverter with R-L load.

inverter and three-phase inverters, can be considered as combinations of multiple single-phase half-bridge inverters.

11.3.2 Three-Phase Voltage Source Inverters

Three-phase bridge VSIs are widely used in AC electric drives and general-purpose AC power supplies. On the DC side, a capacitor or a series-connected set of capacitors is typically placed in parallel with the DC source. Specifically, Figure 11.17a shows configurations with one capacitor and two capacitors connected to the DC supply, respectively. In Figure 11.17b, the two capacitors have equal values, and the point N' represents the auxiliary middle-central point (or neutral point) of the DC supply voltage. As a result, the voltages across the capacitors C_1 and C_2 are both $0.5\,V_d$.

In Figure 11.17, six switches (Q1–Q6) are configured into three bridge arms: the left bridge arm (Q1 and Q4), the middle bridge arm (Q3 and Q6), and the right bridge arm (Q5 and Q2). Within

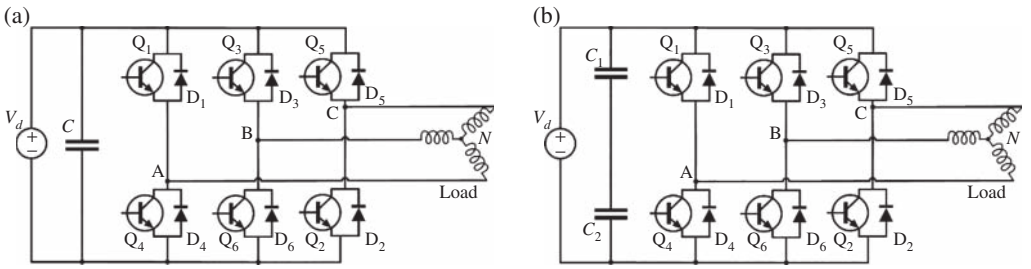

Figure 11.17 Three-phase voltage source inverter.

each bridge arm (or phase), the switches are turned ON to either the upper or lower rails. But both switches are never ON at the same time (which would short the power supply!). One mode of operation is to switch each of the two switches in a duty cycle of ½, alternating between the upper and lower power supply rails. To avoid shorting the power supply, a very short delay is built in between turning one switch OFF and the other switch ON. The conduction times of the switches in the three bridge arms (or phases) are shifted by 120°. Specifically, Q3's conduction period is delayed by 120° compared to Q1, and Q5's conduction period is delayed by 120° relative to Q3. This staggered pattern is also followed by Q4, Q6, and Q2.

When Q1 and Q4 are alternately activated, the voltage of phase A ($V_{AN'}$) alternates between $0.5\,V_d$ and $-0.5\,V_d$, resulting in a square wave with a period of 360°. Similarly, when Q3 and Q6 are alternately activated, the voltage of phase B ($V_{BN'}$) exhibits the same waveform as $V_{AN'}$, but with a phase delay of 120°. Additionally, when Q5 and Q2 are alternately activated, the voltage of phase C ($V_{CN'}$) displays a waveform delayed by 120° relative to $V_{BN'}$. In Figure 11.17, it is evident that

$$\begin{aligned} V_{AB} &= V_{AN'} - V_{BN'} \\ V_{BC} &= V_{BN'} - V_{CN'} \\ V_{CA} &= V_{CN'} - V_{AN'} \end{aligned} \tag{11.8}$$

Thus, the waveforms of the line voltages V_{AB}, V_{BC}, and V_{CA} can be directly derived from the waveforms of $V_{AN'}$, $V_{BN'}$, and $V_{CN'}$ which are all illustrated in Figure 11.18.

When the neutral point N of the load is connected to the neutral point N' of the DC supply, the three-phase load voltages are denoted as $V_{AN'}$, $V_{BN'}$, and $V_{CN'}$, respectively. Nevertheless, if the neutral points N and N' are isolated, such as when motor loads provide the isolation, the equivalent circuit is represented as shown in Figure 11.19. In this configuration, the *triplen* harmonics, i.e. the zero-sequence component of the supply, manifest across the points N and N'. Therefore, the following equations can be derived:

$$\begin{aligned} V_{AN'} &= V_{AN} + V_{NN'} \\ V_{BN'} &= V_{BN} + V_{NN'} \\ V_{CN'} &= V_{CN} + V_{NN'} \end{aligned} \tag{11.9}$$

For three-phase balance loads, it is noted that

$$V_{AN} + V_{BN} + V_{CN} = 0 \tag{11.10}$$

Then, adding the three equations given in (9), one can obtain:

$$V_{NN'} = \frac{1}{3}\left(V_{AN'} + V_{BN'} + V_{CN'}\right) \tag{11.11}$$

Substituting (11) into (9) yields

$$\begin{aligned} V_{AN} &= \frac{2}{3}V_{AN'} - \frac{1}{3}V_{BN'} - \frac{1}{3}V_{CN'} \\ V_{BN} &= \frac{2}{3}V_{BN'} - \frac{1}{3}V_{AN'} - \frac{1}{3}V_{CN'} \\ V_{CN} &= \frac{2}{3}V_{CN'} - \frac{1}{3}V_{AN'} - \frac{1}{3}V_{BN'} \end{aligned} \tag{11.12}$$

Based on equation (11.12), the waveform of V_{AN} is depicted in Figure 11.18g, which exhibits a six-step pattern. Additionally, a typical current waveform with an inductive load is also presented.

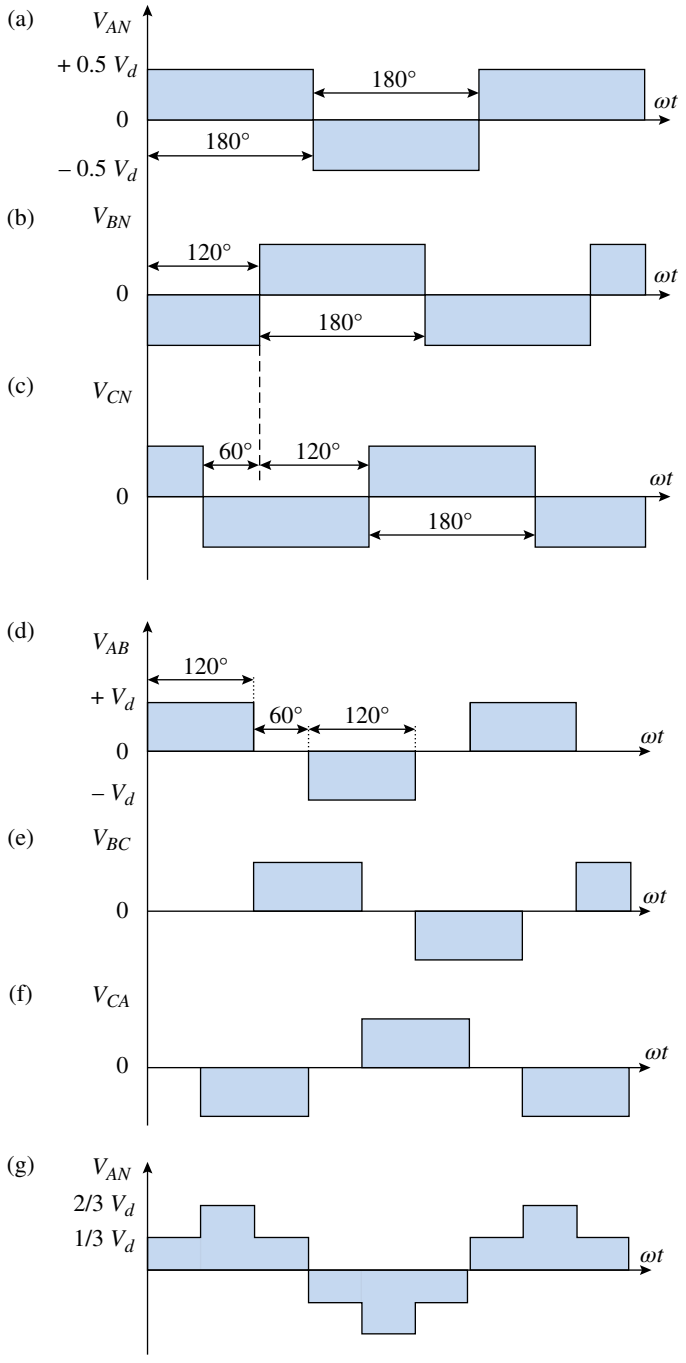

Figure 11.18 Voltage waveforms in square wave mode.

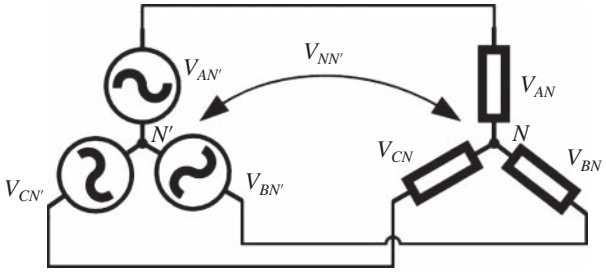

Figure 11.19 Neutral point voltage.

11.4 Current-Source Inverter

In an ideal scenario, the DC supplies for CSIs would be constant current sources with infinite Thévenin impedances. However, such ideal sources are not practically achievable. Instead, a near-ideal DC current source is typically realized using a controlled rectifier with a DC link that includes a sufficiently large inductance. When using a constant current supply, the AC output waveforms remain relatively stable despite changes in load conditions. A typical CSI configuration is shown in Figure 11.20.

In CSIs, the power semiconductor devices must be designed to handle reverse voltages. To fulfill this need, various standard asymmetric voltage-blocking devices are commonly used. These include power bipolar junction transistors (BJTs), power metal-oxide-semiconductor field-effect transistors (MOSFETs), insulated-gate bipolar transistors (IGBTs), MOS-controlled thyristors (MCTs), and integrated gate-commutated thyristors (IGCTs), often in combination with supplementary power diodes. Furthermore, symmetric voltage-blocking power semiconductor devices, which possess strong reverse-blocking capabilities, such as gate turn-off thyristors (GTOs) and silicon-controlled rectifiers (SCRs) (also known as thyristors), can be directly employed in CSIs.

In the following contents of this section, the structure and operating principles of both single-phase and three-phase CSI inverters will be introduced.

11.4.1 Single-Phase Current-Source Inverter

A single-phase CSI, as shown in Figure 11.21, comprises a DC source and is connected in series with a DC link inductor, while an RL load is connected in parallel with a capacitor. The capacitor serves to ensure that the load current leads the voltage, thereby facilitating the load commutation

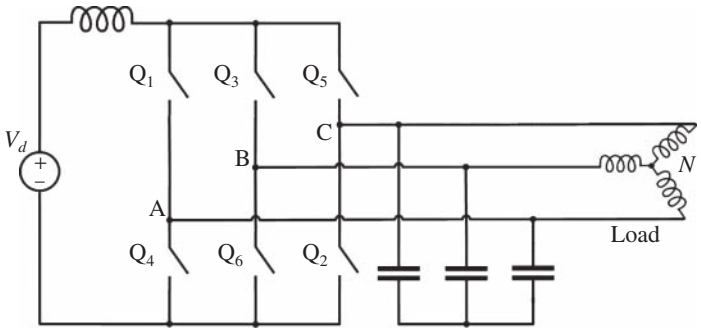

Figure 11.20 Current-source inverter.

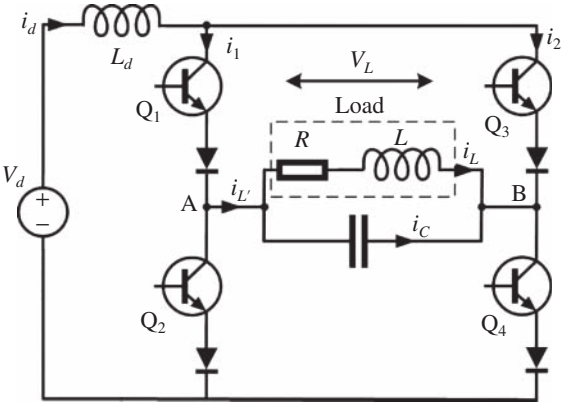

Figure 11.21 Single-phase current-source inverter.

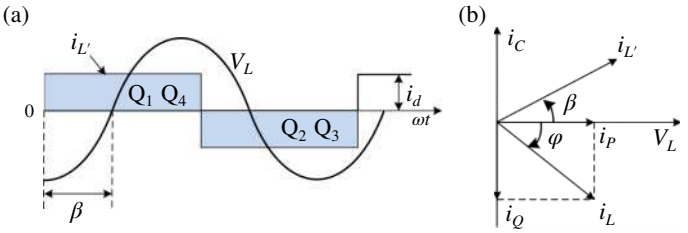

Figure 11.22 Load voltage and current waveforms.

of the thyristors. This configuration is commonly employed in high-frequency induction heating applications [2]. It is assumed that the DC link inductance is sufficiently large to smooth out ripples in the DC current, while the capacitor effectively filters harmonic currents.

The load voltage and current waveforms are shown in Figure 11.22a. The switch pairs (Q1, Q4) and (Q2, Q3) are alternately activated for 180°, generating a square-wave current at the output. The fundamental component of the load current leads the nearly sinusoidal output waveform by an angle β°. When the pair (Q1, Q4) is turned on, the pair (Q2, Q3) experiences a negative voltage for a period β°, which helps facilitate load commutation. Given that $\beta = \omega t_q$, the minimum value of β must be sufficient to ensure the thyristors are completely turned off during the interval t_q.

The phasor diagram illustrating the relationship between load voltage and current is shown in Figure 11.22 (b). For an RL load, the current I_L lags the load voltage V_L by an angle φ. The load current can be separated into its active component I_P and reactive component I_Q. The capacitor current I_C opposes the reactive current I_Q, causing the overall effective load current I_L' to lead the load voltage V_L by an angle β. In conclusion, the AC output current waveform is square and does not depend on the load angle, while both the waveform and phase of the AC output voltage are affected by the load angle.

To achieve a desired phase angle β, adjustments can be made either by varying the capacitance C of the capacitor or by altering the inverter's frequency ω, with the latter being more straightforward to implement. When the inverter frequency ω is adjusted to be just above the resonant frequency ω_r of the circuit, causing the effective load to act as a parallel resonant circuit, the power factor cos β of the load becomes leading. This inverter frequency can be regulated through a phase-locked loop (PLL) control system. As shown in Figure 11.23, the phase angle β, as a function of the inverter frequency, forms a feedback loop that compares with the target β (β*), enabling the actual β to track β*.

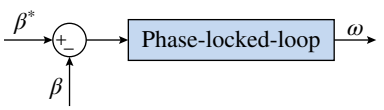

Figure 11.23 Phase-locked-loop control.

11.4.2 Three-Phase Current-Source Inverter

The three-phase CSI and three-phase VSI can be considered as mutually dual circuit structures, exhibiting certain differences in power device configuration, converter models, and operating characteristics. The conventional three-phase CSI, often referred to as the H6-CSI, consists of six bridge arms corresponding to the three phases, as illustrated in Figure 11.24. Theoretically, each bridge arm should incorporate a self-commutating power switch with reverse-blocking capability. When using insulated IGBTs or MOSFETs as the switching devices, a power diode is typically added in series with the bridge arm to enhance the reverse-blocking capability of the switch. In contrast to the VSI, which does not require reverse-blocking capability, the CSI circuit imposes stricter performance requirements on power semiconductor devices, generally necessitating a greater number of such devices compared to VSI circuits. Consequently, the H6-CSI experiences relatively higher conduction losses.

In the DC side of the H6-CSI, a stable DC current source is theoretically required. In practical applications, this is typically achieved by connecting a large inductor in series with a voltage source to maintain an approximately constant DC current. The inductance value is generally substantial to ensure smooth and stable DC current. However, the significant size of the inductor necessitates a larger hardware space to accommodate the H6-CSI.

During operation, the H6-CSI performs chopper output of the constant DC current through the inverter bridge, resulting in a PWM-form current pulse at the AC side output of the inverter. Therefore, unlike the inductor filter design used in VSI, the output of the CSI is directly connected to a capacitor filter.

The commutation models of CSI and VSI exhibit a dual relationship due to the differing nature of their DC power sources. In a VSI, the modulation rules emphasize avoiding the simultaneous conduction of the upper and lower bridge arm switches to prevent short circuits, which could damage the devices. In VSI modulation, the zero vector is represented by an open-circuit state, and switching typically occurs between vertical switches, characterizing vertical commutation. At any given moment during operation, a VSI maintains three power switches in the conducting state. In contrast, in a CSI, the circuit maintains two power switches in the conducting state, with

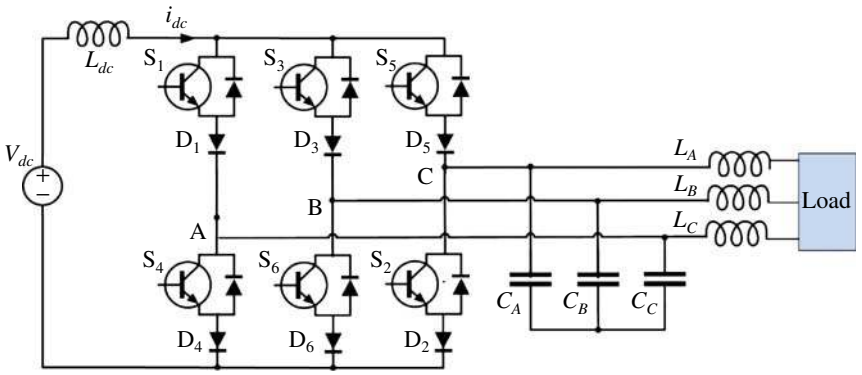

Figure 11.24 Configuration of current-source inverter.

Table 11.1 Switching states and corresponding output currents of the CSI.

Vector States		Switch-ON Combination	Output Currents		
			Phase-A	Phase-B	Phase-C
Non-zero vectors	I_1	{12}	I_{dc}	0	$-I_{dc}$
	I_2	{23}	0	I_{dc}	$-I_{dc}$
	I_3	{34}	$-I_{dc}$	I_{dc}	0
	I_4	{45}	$-I_{dc}$	0	I_{dc}
	I_5	{56}	0	$-I_{dc}$	I_{dc}
	I_6	{16}	I_{dc}	$-I_{dc}$	0
Zero vectors	I_7	{14}	0	0	0
	I_8	{36}	0	0	0
	I_9	{52}	0	0	0

commutation characterized by the switching of DC current between horizontal switches, known as horizontal commutation. Due to the presence of a large inductor on the DC side, the bridge arms in a CSI can safely operate in a short-circuit state for a brief period, during which the circuit presents a zero vector state externally.

The traditional H6-CSI operates with six non-zero vector states and three zero vector states. The output current associated with each switching combination is detailed in Table 11.1. Here, {xy} (where x, y = 1, 2, 3, 4, 5, or 6) denotes the combination of switch numbers in the upper and lower bridge arms that are in the conducting state during operation. For example, {16} represents the non-zero vector state I6, corresponding to the conduction of the upper bridge power switch S_1 and the lower bridge power switch S_6.

According to Figure 11.25, the system model of the CSI is expressed by

$$\begin{cases} i_a = S_{11} \cdot I_{dc} - S_{12} \cdot I_{dc} = m_a I_{dc} \\ i_b = S_{21} \cdot I_{dc} - S_{22} \cdot I_{dc} = m_b I_{dc} \\ i_c = S_{31} \cdot I_{dc} - S_{32} \cdot I_{dc} = m_c I_{dc} \end{cases} \tag{11.13}$$

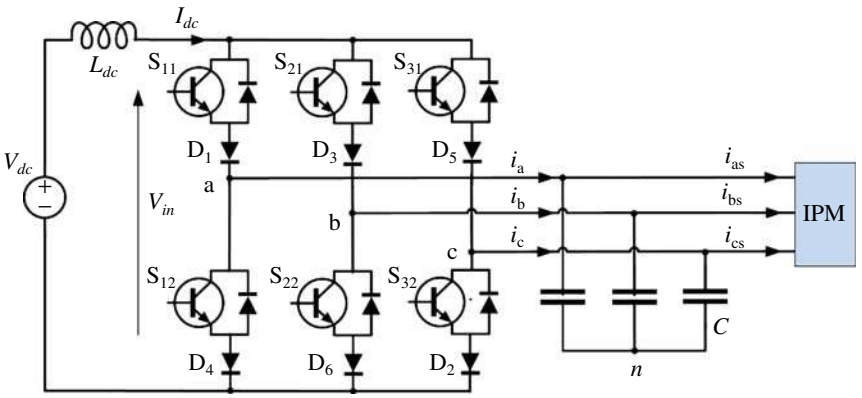

Figure 11.25 Load driven by a current-source inverter.

where i_a, i_b, and i_c are the three-phase currents, m_a, m_b, and m_c are the modulation signals of each phase, and I_{dc} is the *dc* link current.

Then the state equations of each capacitor voltage and inductor current can be written as

$$\begin{cases} \dot{v}_{an} = \frac{i_a - i_{as}}{C} \\ \dot{v}_{bn} = \frac{i_b - i_{bs}}{C} \\ \dot{v}_{cn} = \frac{i_c - i_{cs}}{C} \end{cases} \tag{11.14}$$

$$\dot{I}_{dc} = \frac{V_{dc} - V_{in}}{L_{dc}} \tag{11.15}$$

where i_{as}, i_{bs}, and i_{cs} are the three-phase currents of the loading, v_{an}, v_{bn}, and v_{cn} are the ac voltages of three capacitors. Thus, the input voltage of the CSI can be expressed by using the switching functions and the capacitor voltages as:

$$\begin{aligned} V_{in} &= v_{an}(S_{11} - S_{12}) + v_{bn}(S_{21} - S_{22}) + v_{cn}(S_{31} - S_{32}) \\ &= \frac{3}{2}(m_q \cdot v_{Cq} + m_d \cdot v_{Cd}) \end{aligned} \tag{11.16}$$

where m_d and m_q are the modulation signals, v_{Cd} and v_{Cq} are the capacitor voltages of d and q axes, respectively. It should be noted that the capacitor voltage equals to the loading terminal voltage.

In summary, compared to VSI, CSI has the following advantages:

1) Boost topology: The CSI employs a boost-type topology, where the bus inductor can work together with the DC power source to supply energy to the load, effectively extending the constant power operating range of the motor.
2) High-quality output current: The AC side of the CSI is connected in parallel with three-phase filter capacitors, forming a second-order LC filter with the load inductance. This arrangement efficiently filters out high-order harmonics from the output voltage and current, resulting in a superior quality output current waveform.
3) Inherent short-circuit protection: The direct conduction of the upper and lower bridge arms in a CSI corresponds to its zero vector state, providing built-in short-circuit protection. In the event of a short-circuit fault in the load, the bus inductor on the DC side helps to suppress abrupt current changes, thereby enhancing the system's fault tolerance and reliability.

11.5 Pulse Width Modulation

Pulse-width modulation (PWM) has emerged as a predominant control technique in power electronics for regulating the output voltage of converters. PWM operates by adjusting the duration of individual pulses to control the average output voltage. Using this technique, a steady DC input voltage can be converted into a good approximation of a sinusoidal output with adjustable frequency and amplitude. In VSIs, PWM allows for fine-tuned control of the output waveform, ensuring precise regulation of both voltage and current. This precision is essential in applications where careful voltage management is necessary for optimal operation, such as in motor drives, renewable energy systems, and UPS. Moreover, PWM enables the management of harmonic distortions in the output waveform, thereby improving power quality and reducing system losses. Compared to basic square-wave modulation methods, PWM provides superior control over output voltage, frequency, and harmonic content. Various PWM techniques, including sinusoidal

PWM (SPWM), hysteresis band current control PWM, random PWM, and space-vector PWM, are available. This section will focus on the sinusoidal PWM technique due to its widespread application and popularity in industrial inverters.

11.5.1 Fundamentals of SPWM Technique

It is widely recognized that the primary function of most DC/AC inverters is to generate a smooth sinusoidal voltage output, either at a fixed or variable frequency, which is typically much lower than the switching frequency. The sinusoidal pulse width modulation (SPWM) technique effectively addresses this requirement. The process for generating the SPWM signal is depicted in Figure 11.26.

Unlike traditional PWM technique, where the modulation signal is a constant DC value, SPWM utilizes a sinusoidal modulation signal, denoted as v_m. This sinusoidal modulation signal v_m and a high-frequency sawtooth carrier signal v_{cr} are fed into a comparator. The points of intersection between these signals determine the switching frequency of the power inverter. When v_m is smaller than v_{cr}, the comparator outputs a low constant DC voltage, whereas it produces a high constant DC voltage when v_m is larger than v_{cr}. This results in a square-wave pulse signal, where the width and notches of the pulses vary sinusoidally. Consequently, the fundamental frequency of the pulse signal aligns with the frequency of the modulation waveform. Thus, by adjusting the modulation waveform, both the amplitude and frequency of the output can be controlled.

The modulation index is defined as:

$$M = \frac{V_m}{V_{cr}} \tag{11.17}$$

where V_m and V_{cr} represent the peak voltages of the modulation and carrier waveforms, respectively. The modulation index M, ranging from 0 to 1, establishes a linear relationship between these waveforms. For values of the modulation index, this relationship is expressed as

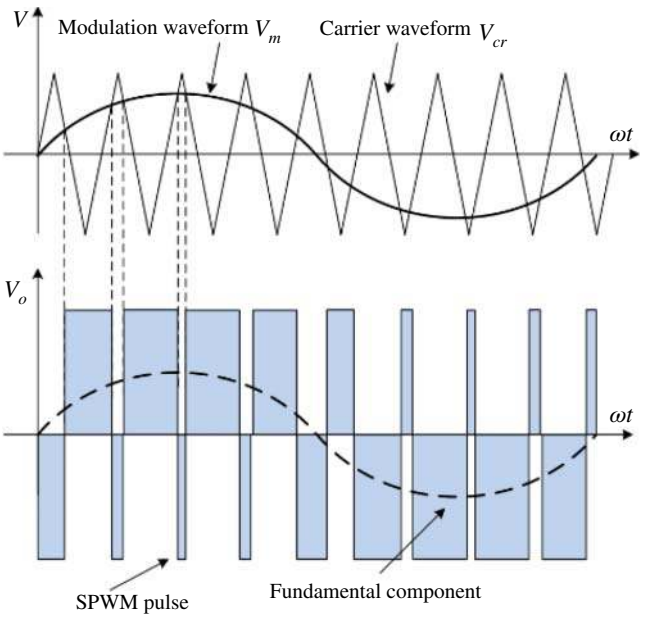

Figure 11.26 Sinusoidal PWM pulses.

$V_{m1} = MV_{DIN}$, where V_{m1} denotes the fundamental component of the output voltage and V_{DIN} represents the DC supply voltage. As the modulation index increases, the fundamental output voltage (which follows a sinusoidal waveform) also increases. Additionally, the modulation ratio is defined as:

$$p = \frac{f_{cr}}{f_m} \tag{11.18}$$

where f_{cr} and f_m represent the frequencies of the carrier and modulation waveforms, respectively. In SPWM, the output harmonics generally appear at multiples of the carrier frequency, as shown by

$$f = kf_{cr} = kpf_m \tag{11.19}$$

where f is the frequency of output harmonic and $k > 0$ is an integer.

11.5.2 Bipolar SPWM Inverter

Consider a single-phase inverter with an RL load, controlled by bipolar SPWM pulse signals as shown in Figure 11.27. When the modulation voltage v_m exceeds the carrier voltage v_{cr}, positive pulse signals are generated, triggering transistors Q1 and Q2 to turn on while the transistors Q3 and Q4 are turned off. During this phase, if the load current i_o is positive, Q1 and Q2 will conduct. Otherwise, diodes D1 and D2 will conduct. In both scenarios, the output voltage v_o equals to V_d. Conversely, when v_{cr} is larger than v_m, negative pulse signals activate Q3 and Q4, turning on these transistors while Q1 and Q2 are turned off. In this case, if the load current is in negative direction, Q3 and Q4 will conduct; otherwise, diodes D3 and D4 will conduct. The output voltage v_o will then be equal to $-V_d$. The resultant output voltage waveform is illustrated in Figure 11.28.

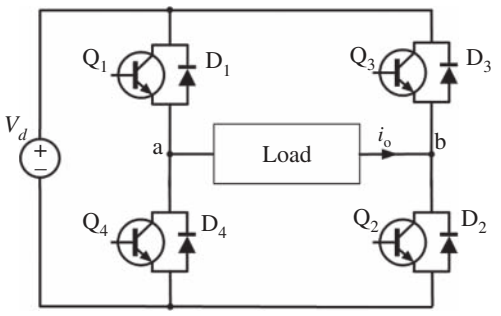

Figure 11.27 SPWM single-phase inverter.

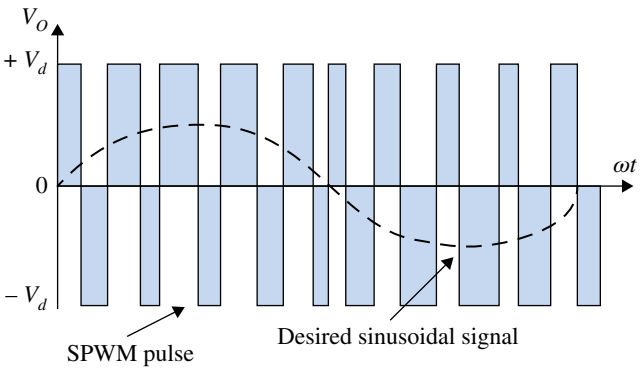

Figure 11.28 Output voltage of PWM inverter.

11.5.3 Unipolar SPWM Inverter

Unlike the bipolar SPWM, unipolar SPWM generates impulse signals with different polarities for the positive and negative half-cycles, as illustrated in Figure 11.29. In this modulation scheme, v_m represents the sinusoidal modulation signal, while v_{cr} is the sawtooth carrier signal, which has a positive amplitude during the positive half-cycle of the modulation signal and a negative amplitude during the negative half-cycle. During the positive half-cycle, if v_m is larger than v_{cr}, positive DC voltages are produced; otherwise, the output is zero. Conversely, during the negative half-cycle, when v_m is larger than v_{cr}, the output is zero; otherwise, a negative DC constant voltage is provided. The fundamental frequency of the resulting pulse signal matches the frequency of the modulation signal.

Figure 11.29 demonstrates the application of unipolar SPWM for controlling the single-phase inverter depicted in Figure 11.27. The switches Q1 and Q4 in the left-hand arm are controlled by a square wave synchronized with the modulation signal v_m, while switches Q2 and Q3 in the opposite arm are governed by the unipolar SPWM signal. During the positive half-cycle, Q1 remains on while Q4 is off, and Q2 and Q3 are alternately activated based on the SPWM impulses. Specifically, when $v_m > v_{cr}$, Q2 is turned on and Q3 is turned off, resulting in the load voltage v_o being equal to V_d. Conversely, when $v_m < v_{cr}$, Q2 is off and Q3 is on, leading to $v_o = 0V$. During the negative half-cycle, Q4 is kept on and Q1 off, with Q2 and Q3 switching alternately. When $v_m < v_{cr}$, Q3 is turned on and Q2 off, causing v_o equal to $-V_d$. When $v_m > v_{cr}$, Q3 is turned off and Q2 is on, resulting in $v_o = 0V$.

11.5.4 Three-phase SPWM Inverter

Figure 11.30 illustrates that the bipolar SPWM control techniques are applied in a three-phase inverter. This inverter utilizes three sinusoidal modulation waveforms, denoted as v_{mA}, v_{mB}, and

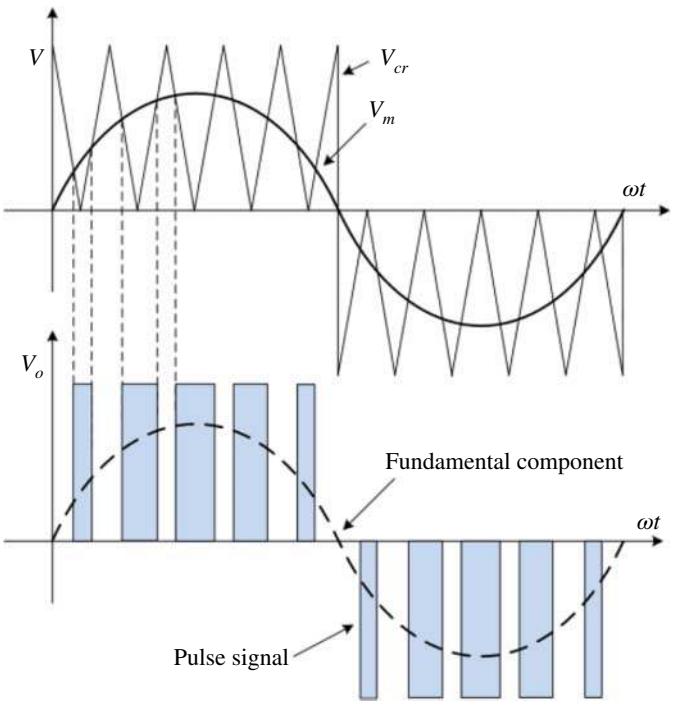

Figure 11.29 Unipolar SPWM pulse signals.

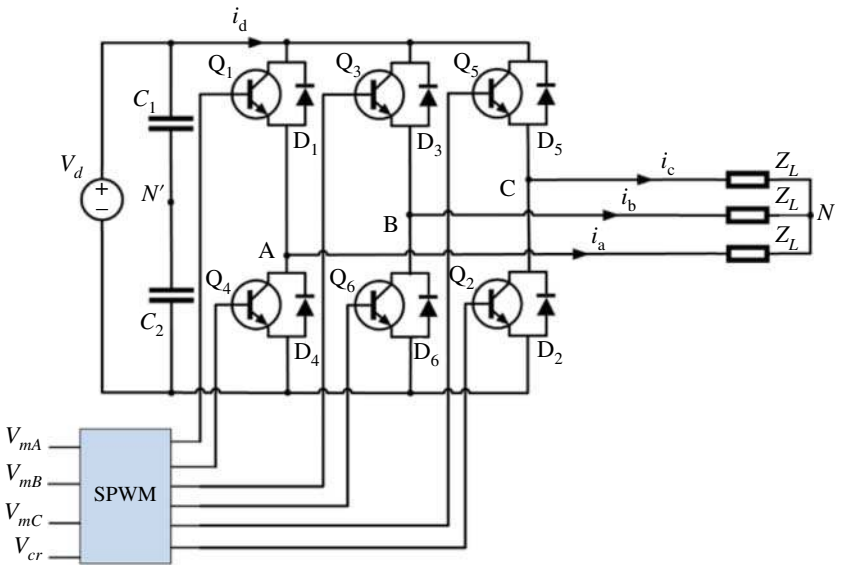

Figure 11.30 SPWM three-phase inverter.

v_{mC}, which are phase-shifted by 120° relative to one another. The common carrier waveform is a sawtooth signal, represented as v_{cr}. The triggering mechanism for each arm of the inverter is consistent. To elucidate the operation principle, consider phase A as an example. When $v_{mA} > v_{cr}$, transistor Q4 is turned off, and transistor Q1 is triggered on. If the load current is negative, diode D1 conducts; otherwise, Q1 conducts. In both scenarios, the resulting voltage $v_{AN'} = V_d/2$. Conversely, when $v_{mA} < v_{cr}$, Q1 is turned off, and Q4 (or D4) is activated, resulting in $v_{AN'} = -V_d/2$.

Consequently, the output waveforms $v_{AN'}$, $v_{BN'}$, and $v_{CN'}$ can be obtained, as depicted in Figure 11.31. In terms of $v_{AB} = v_{AN'} - v_{BN'}$ and $v_{AN} = v_{AN'} - \left(v_{AN'} + v_{BN'} + v_{CN'}\right)/3$, it can be calculated that the phase voltage v_{AN} exhibits five distinct voltage levels: $0, \pm V_d/3, \pm 2V_d/3$, while the line voltage v_{AB} displays three voltage levels $0, \pm V_d$.

11.6 Conduction and Switching Losses

In the previous sections, both converter and inverter switches were modeled as ideal components. However, in practical applications, these components inevitably incur power losses, presenting a significant challenge for power supply designers: identifying and mitigating these losses in switching power supplies.

Given that MOSFETs are the most widely utilized switches in contemporary high-frequency designs, this analysis focuses on the power losses associated with MOSFET-based switches. These losses can be categorized into three primary types:

1) Conduction losses: These occur due to the product of voltage and current when a MOSFET or rectifier conducts current. The magnitude of these losses is influenced by the duty cycle.
2) Switching losses: These arise during the transition between the ON and OFF states of the power switch or rectifier. The frequency dependence of these losses is notable, as higher frequencies lead to an increased number of transitions, thereby exacerbating losses.
3) Gate drive losses: These losses occur when some of the conduction loss in the MOSFET driver's output stage results in current returning through the input stage instead of being delivered as output power.

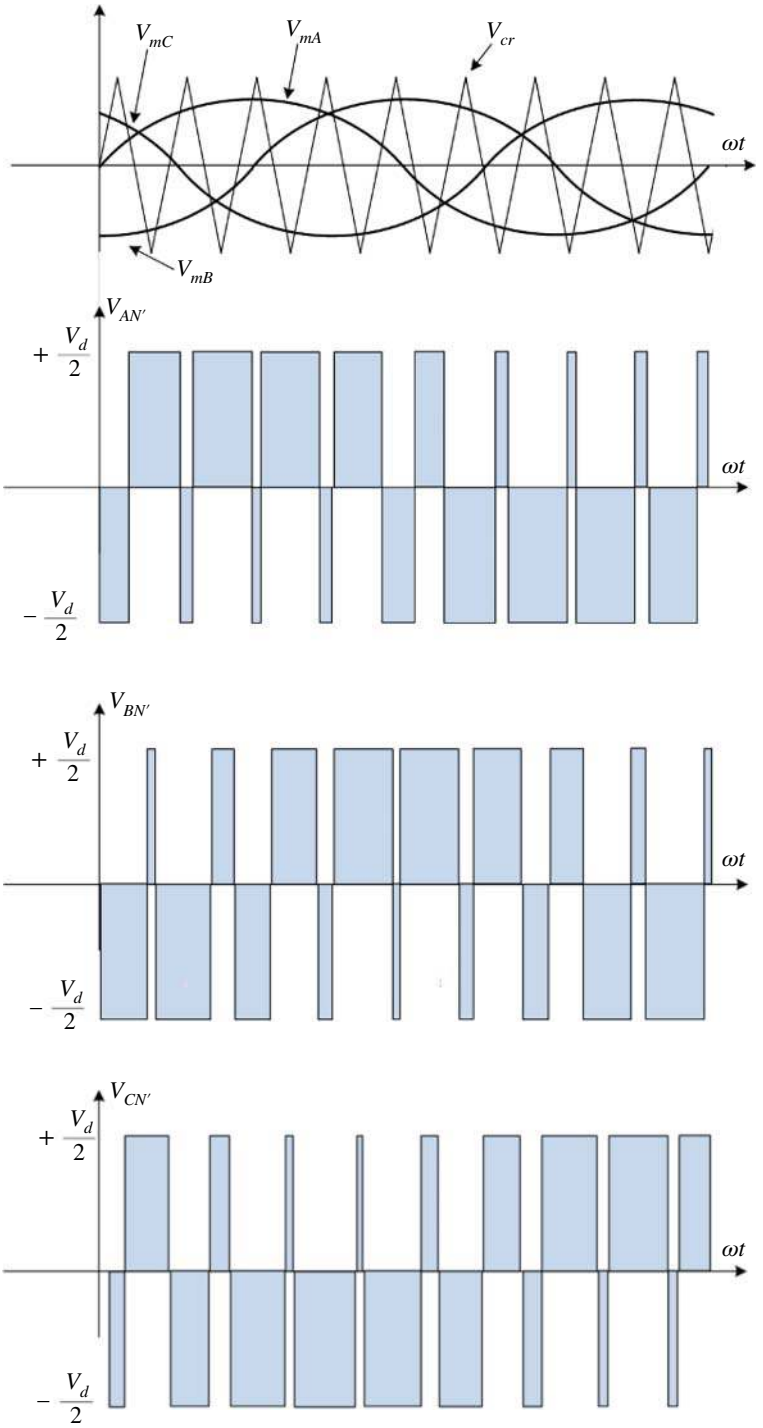

Figure 11.31 Waveforms of the SPWM three-phase inverter.

Beyond the inherent characteristics of the switching elements, power loss is also induced by the dead-time effect, a predefined interval intended to prevent the simultaneous conduction of the upper and lower bridge arms in the circuit.

11.6.1 Conduction Loss

An equivalent circuit of the MOSFET is illustrated in Figure 11.32. When the MOSFET is in the on-state, the path between the drain and source exhibits a resistance known as R_{ds}. Consequently, conduction losses can be calculated similarly to power dissipation in a resistor. The formula for determining power dissipation in a resistor is given by

$$P_{cond} = I_{drms}^2 R_{ds} \tag{11.20}$$

But since

$$I_{drms} = I_{d(on)} \sqrt{D} \tag{11.21}$$

where $I_{d(on)}$ is the current flowing through the device when it is on and D is the duty cycle. Thus, the conduction losses can be calculated using the following equation

$$P_{cond} = I_{d(on)}^2 R_{ds} D \tag{11.22}$$

where P_{cond} is the conduction power losses.

Since the current flowing through the MOSFET is dictated by application requirements, the primary method to decrease conduction loss is by minimizing the R_{ds}. This can be accomplished through careful component selection. Advanced FETs, such as those fabricated from silicon carbide (SiC) and gallium nitride (GaN), offer exceptionally low R_{ds} values, making them ideal for high-efficiency applications.

11.6.2 MOSFET Switching Power Loss

Each time a MOSFET is switched on, energy dissipation occurs, and similar process occurs when the device is switched off, thus causing switching losses. During the turn-on process, the drain current I_d begins to increase. Until the current has reached its final value, the drain-source voltage V_{ds} starts to decrease and finally approaches nearly zero, indicating that the MOSFET is fully on.

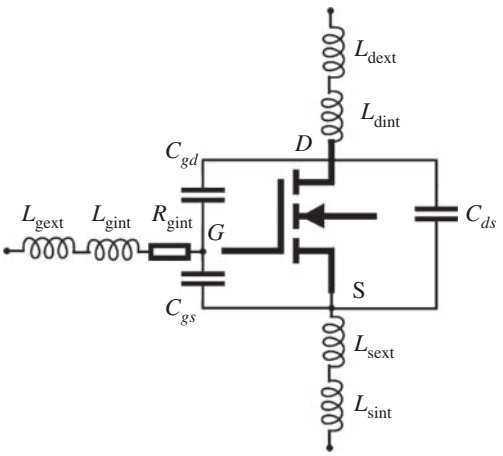

Figure 11.32 Equivalent circuit of a MOSFET.

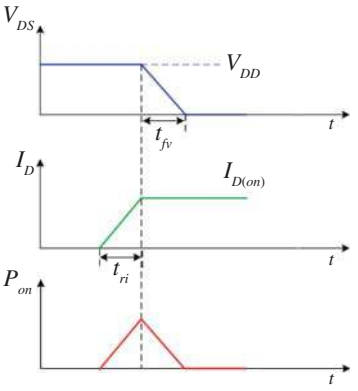

Figure 11.33 Waveforms of turn-on switching power loss.

The instantaneous power during this transition forms a triangular spike, and the area under this spike represents the energy dissipated during the turn-on process, as depicted in Figure 11.33.

The energy dissipated can be calculated as follows:

$$E_{on} = \frac{1}{2} I_{d(on)} V_{ds} t_{on} \tag{11.23}$$

where $I_{d(on)}$ represents the current flowing through the drain when the MOSFET is in the on state. V_{ds} is the voltage applied to the drain, and t_{on} encompasses both the time required for the current to increase and the time for the voltage to decrease. This relationship can be expressed as

$$t_{on} = t_{ri} + t_{fv} \tag{11.24}$$

where t_{ri} represents the time required for the current to rise, and t_{fv} denotes the time for the voltage to fall.

The turn-on energy dissipation of the MOSFET can be used to calculate the power losses associated with its activation. These losses are computed by multiplying the turn-on energy by the switching frequency, which dictates the number of turn-on events per second, and hence, the power losses can be expressed using the following formulas:

$$P_{on} = E_{on} f_{sw} \tag{11.25}$$

Where P_{on} represents the turn-on power losses, E_{on} denotes the energy dissipated during turn-on, and f_{sw} is the switching frequency.

Turn-off losses are similar to turn-on losses. When the MOSFET is on, V_{ds} is very small and approaching zero, while current flows through the MOSFET's drain. As the device turns off, V_{ds} begins to increase while the current $I_{d(on)}$ continues to flow through the device. As V_{ds} reaches its final value V_{dd}, the current decreases until it eventually becomes zero. The energy dissipated during the turn-off process is represented by the area beneath the triangular spike formed by the current and voltage, as illustrated in Figure 11.34.

The energy dissipated during the turn-off process can be calculated using the following formula:

$$E_{off} = \frac{1}{2} I_{d(on)} V_{dd} t_{off} \tag{11.26}$$

where E_{off} represents the energy dissipated during the turn-off process, $I_{d(on)}$ denotes the current flowing between the drain and source, V_{dd} is the peak voltage across the drain and source, and t_{off} is the duration of the turn-off transition. The total duration of the off transition is described by

$$t_{off} = t_{rv} + t_{fi} \tag{11.27}$$

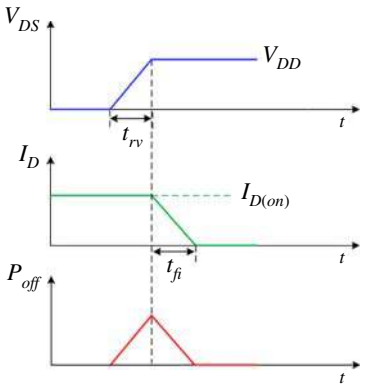

Figure 11.34 Waveform of turn-off switching power loss.

where t_{rv} represents the time required for the voltage to increase, and t_{fi} denotes the time required for the current to decrease. The power losses associated with turn-off can be calculated using the following formula.

$$P_{off} = E_{off} f_{sw} \tag{11.28}$$

where E_{off} represents the energy dissipation during turn-off, and f_{sw} denotes the switching frequency.

By applying the formulas for both turn-on and turn-off power losses, one can calculate the total switching power loss in the MOSFET, expressed as follows:

$$P_{switch} = P_{on} + P_{off} \tag{11.29}$$

And the waveform of the total switching power loss can be illustrated in Figure 11.35.

The above analysis indicates that the switching loss P_{switch} is influenced by several factors:

- The voltage applied to drive the switched current through the FET
- The drain current of the FET
- The rise and fall periods of the switching waveform
- The switching frequency

11.6.3 Gate Charge Loss

All MOSFETs are equipped with an insulating layer that prevents current from flowing through the gate terminal, distinguishing them from other types of FETs [3]. However, this insulation only blocks steady-state current. The gate of a MOSFET behaves as a capacitive structure. As a result,

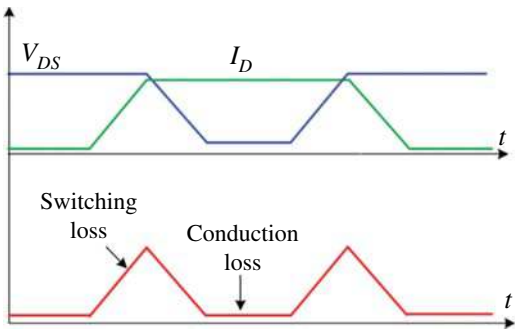

Figure 11.35 The waveform of the switching power loss.

transient currents will flow in the gate-drive circuit until the gate capacitor is fully charged or discharged.

This introduces an additional source of dissipative loss in switch-mode MOSFETs. The process of turning the FET on and off requires changes in the gate voltage. Power dissipation occurs as transient currents flow through parasitic resistances during these voltage transitions.

The formula for gate-charge loss (P_{gc}) is given as:

$$P_{gc} = Q_g \cdot V_{gs} \cdot f_{sw} \tag{11.30}$$

Where Q_g represents the total gate charge necessary for the FET, V_{gs} denotes the voltage applied between the gate and source terminals.

This underscores why reducing the on-state resistance alone is not always a panacea when dealing with switching MOSFETs. A lower on-state resistance necessitates a larger physical channel, which in turn results in increased total gate capacitance. As a result, the reduction in conduction loss may be offset by increased gate drive circuit losses, caused by the resistances within the drive circuit channel itself.

11.6.4 Deadtime Power Loss

Dead time loss arises from the forward voltage drop across the diode of the low-side MOSFET and the load current during the dead time interval. In synchronous rectification, high-side and low-side switches are alternately activated and deactivated. Ideally, switching should be coordinated to avoid any period when both switches on either side are simultaneously fully on or fully off. However, achieving this ideal condition is challenging in practice. To ensure safe operation, a dead time interval is introduced during which both switches are turned off. This precaution is essential to prevent "shoot-through"—a condition where both switches on either side are turned on simultaneously, causing high current to flow from the input voltage through both switches to ground, potentially resulting in a short circuit. Such a scenario could lead to excessive current flow and severe damage to the MOSFETs. To mitigate this risk, synchronous rectifying converter integrated circuits (ICs) incorporate control circuits that prevent the simultaneous activation of both switches, ensuring that both switches are turned off before a new switch is turned on. During the dead time shown as Figure 11.36, both switches are turned off, and ideally, no current should flow through either switch. However, in practice, the switches used are MOSFETs, which include a parasitic diode known as the body diode. In Figure 11.36, this diode is shown as being connected between the source and drain of the MOSFET.

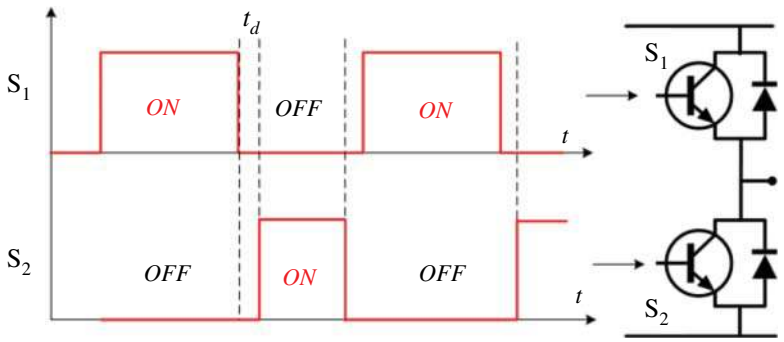

Figure 11.36 Dead-time effect.

Thus, the power loss during dead time can be calculated as:

$$P_D = V_D I_{out}(t_{dr} + t_{df}) \cdot f_{sw} \tag{11.31}$$

where P_D represents the power loss associated with dead time, V_D denotes the forward voltage of the body diode of the low-side MOSFET, I_{out} indicates the output current, t_{dr} refers to the dead time during the rising transition, t_{df} denotes the dead time during the falling transition, and f_{sw} represents the switching frequency.

11.7 Problems

11.1 A buck converter has the following specifications: input voltage $V_{in} = 24$ V, output voltage $V_{out} = 12$ V, and switching frequency $f_{sw} = 100$ kHz. Assume continuous conduction mode (CCM), (a) Determine the duty cycle D of the converter. b) If the load resistance is $R_{load} = 10\ \Omega$, calculate the output current I_{out} and power P_{out}. (c) Assuming an ideal converter, calculate the input current I_{in}.

11.2 The same buck converter as Q1 operates with the following inductor parameters: (a) If the inductor value is $L = 100$ μH, calculate the peak-to-peak ripple current ΔI_L in the inductor. (b) If the minimum output current is 1 A, verify whether the converter operates in CCM.

11.3 A DC-DC Boost converter is designed with the following parameters: input voltage $V_{in} = 20$ V, output voltage $V_o = 50$ V, switching frequency $f_s = 100$ kHz, and rated output power $P_o = 100$ W with 20% peak-to-peak inductor current ripple. (a) Determine the duty ratio D of the converter. (b) Determine the peak current and peak voltage of the switch. (c) determine the inductance L.

11.4 A DC-DC Buck-boost converter is designed with the following parameters to operate at the continuous conduction mode: input voltage $V_{in} = 24$ V, duty ratio $D = 0.5$, switching frequency $f_s = 20$ kHz, inductance $L = 180$ μH, and load resistance $R = 10\ \Omega$. (a) Determine the output voltage V_o of the converter. (b) Determine the inductor current ripple ΔI_L and the peak current of the switch.

11.5 You are designing a three-phase CSI with the following specifications: input DC voltage of $V_{DC} = 200$ V, input DC current $I_{DC} = 20$ A, load impedance per phase: $Z_{load} = 10\ \Omega$, switching frequency: $f_s = 10$ kHz. Determine the required DC link inductor value to minimize current ripple to less than 5% at the switching frequency.

11.6 A DC-DC Buck-boost converter is designed with the following parameters to operate at the continuous conduction mode: input voltage $V_{in} = 24$ V, duty ratio $D = 0.5$, switching frequency $f_s = 20$ kHz, inductance $L = 180$ μH, and load resistance $R = 10\ \Omega$. Determine the critical load resistance R_B.

11.7 A three-phase VSI uses SPWM to control the output. The DC input voltage is $V_{dc} = 600$ V, and the modulation index $m_a = 0.8$. (a) Determine the fundamental line-to-line RMS voltage of the inverter output. (b) If the carrier frequency is $f_c = 3$ kHz and the modulating frequency is $f_m = 50$ Hz, calculate the frequency modulation ratio f_r.

11.8 A three-phase VSI is used to drive an RL load with $R = 10\ \Omega$ and $L = 50$ mH. The inverter is operating in sinusoidal PWM mode with a fundamental line-to-line RMS voltage of $V_{LL} = 230$ V at 50 Hz. (a) Calculate the line current I_L. (b) Determine the real power delivered to the load.

11.9 A single-phase full-bridge VSI switches at $f_s = 10$ kHz with a DC voltage of $V_{dc} = 300$ V. The inverter uses MOSFETs with the following parameters: $V_{DS,on} = 1$ V (on-state voltage drop), $I_{aug} = 5$ A (average current), $E_{sw} = 10$ μJ switching energy loss per cycle, and duty cycle $D = 50\%$. (a) Calculate the conduction losses in the inverter. (b) Calculate the total switching losses for all switches.

11.10 A single-phase VSI operates with an input voltage of $V_{dc} = 300$ V and supplies an output current of $I_o = 10$ A at an RMS voltage of $V_{o,rms} = 220$ V. The inverter has a total loss (switching + conduction) of 100 W. (a) Calculate the efficiency of the inverter. (b) If the switching frequency is doubled, increasing the losses by 20%, what is the new efficiency?

11.11 Write a program that calculates the minimum inductance value for a Buck converter. The inductance can be estimated using the following formula:

$$L_{\min} = \frac{(V_{in} - V_{out}) \times V_{out} \times D}{f \times \Delta I_L}$$

Program input:
$V_{in} = 12\,V$ is the input voltage, $V_{out} = 5\,V$ is the output voltage, $D = 0.4$ is the duty cycle, $f = 100\,kHz$ is the switching frequency, $\Delta I_L = 0.2\,A$ is the ripple current in the inductor.

11.12 Write a program to calculate the ripple current in the inductor of a Buck converter. The ripple current can be estimated using:

$$\Delta I_L = \frac{V_{in} - V_{out}}{L} \times D \times T_s$$

Program input:
$V_{in} = 12V$ is the input voltage, $V_{out} = 5V$ is the output voltage, $D = 0.4$ is the duty cycle, $T_s = 1 \times 10^{-5}$s is the switching period, $L = 47\mu H$ is the inductance.

11.13 Write a function that calculates the efficiency of a boost converter based on input and output powers. The efficiency is given by:

$$\eta = \frac{P_{out}}{P_{in}} \times 100\%$$

Program input:
$P_{in} = 10\,W$ is the input power, $P_{out} = 8.5\,W$ is the output power.

11.14 Write a program to calculate the ripple voltage across the capacitor of a buck converter. The ripple voltage is given by:

$$\Delta V_C = \frac{\Delta I_L}{8 \times f \times C}$$

Program input:
$\Delta I_L = 0.2A$ is the ripple current in the inductor, $f = 100\,kHz$ is the switching frequency, $C = 220\,\mu F$ is the capacitance.

11.15 Write a program to calculate the efficiency of a Buck converter, considering conduction losses in the inductor and switch. The efficiency is:

$$\eta = \frac{P_{out}}{P_{in}} \times 100\%$$

$$P_{in} = V_{in} \times I_{in},\ P_{out} = V_{out} \times I_{out}$$

$$P_{loss} = I_{load}^2 \times R_{indactor} + V_{switch} \times I_{load}$$

Program input:
$V_{in} = 12\,V$ is the input voltage, $V_{out} = 5\,V$ is the output voltage, $I_{load} = 2\,A$ is the load current, $R_{inductor} = 0.2\,\Omega$ is the inductor resistance, $V_{switch} = 0.5\,V$ is the switch voltage.

References

1 Hart, D. (1997). *Introduction to Power Electronics*. New York: Prentice Hall.

2 Haitham Abu-Rub; Mariusz Malinowski; Kamal Al-Haddad, Multilevel converter/inverter topologies and applications, in power electronics for renewable energy systems, transportation and industrial applications, *IEEE*, 2014, pp. 422–462, doi: https://doi.org/10.1002/9781118755525.ch14.

3 Trzynadloswski, A. (2010). *Introduction to Modern Power Electronics.* New York: Wiley.

12

Basics of Machine Control

12.1 Introduction

Control of electric machines ranges from essentially no control to very sophisticated speed and/or position servomechanisms. This chapter will delve into the fundamental control techniques, covering aspects such as signal feedback, motor control algorithms, performance evaluation, and stability analysis. The simplest form of control, simply connecting the motor to a constant frequency source, relies on the inherent stability characteristic of the motor. Start with induction motors.

12.2 Adjustable Frequency Drive in Induction Motors

The torque-speed characteristic for an induction motor is shown in Figure 12.2. Typically, an induction motor is driving a load that will have some increase in torque with speed. If the load torque intercepts the motor characteristic to the right of the peak of the torque-speed curve, the motor/load combination will settle to and operate stably at a speed that is at the intersection of the two characteristics. One method of motor control is to operate at adjustable speed, and that may be done by simply adjusting drive frequency.

12.2.1 Idealized Model: No Stator Resistance

If the stator resistance can be neglected, the equivalent circuit is presented on the left side of Figure 12.1. It can be readily demonstrated that, when viewed from the rotor, an equivalent circuit, as illustrated on the right side, is capable of representing the combination of the voltage source, armature leakage, and magnetizing branch with

$$V' = V\frac{X_m}{X_1 + X_m}$$

$$X_1' = \frac{X_1 X_m}{X_1 + X_m} \tag{12.1}$$

When machine operates at a changing frequency ω, but the reactance is defined under a fixed frequency ω_B, the current will be:

$$I = \frac{V'}{j\left(X_1' + X_2\right)\dfrac{\omega}{\omega_B} + \dfrac{R_2}{s}} \tag{12.2}$$

Electromagnetic Analysis of Electric Machines: First Principles, Modeling, and Design, First Edition.
James L. Kirtley, Christopher H. T. Lee, and Sajjad Mohammadi.

Companion website: www.wiley.com/go/kirtleyelectric

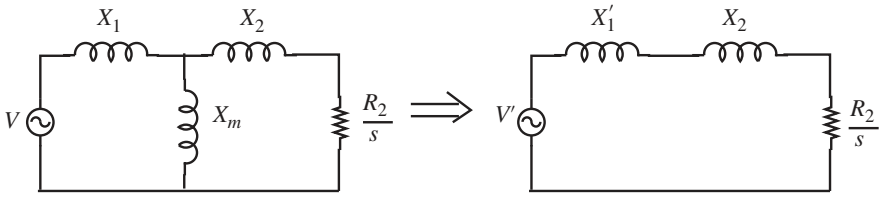

Figure 12.1 Simplified induction motor equivalent circuit.

Since the absolute slip of the rotor is the key factor, it is specified relative to the base frequency as:

$$s = \frac{\omega_r}{\omega} = \frac{\omega_r}{\omega_B}\frac{\omega_B}{\omega} = s_B\frac{\omega_B}{\omega} \tag{12.3}$$

Assume that the voltage is applied in proportion to the frequency, so that flux is constant:

$$V = V_0\frac{\omega}{\omega_B} \tag{12.4}$$

Torque becomes:

$$T_e = \frac{3p}{\omega_B}\frac{\left|V_0'\right|^2\frac{R_2}{s_B}}{\left(X_1' + X_2\right)^2 + \left(\frac{R_2}{s_B}\right)^2} \tag{12.5}$$

This suggests that when the voltage varies in proportion to the frequency, leading to a uniform applied flux, the torque relies entirely on the absolute slip. As a result, the torque-speed characteristic remains fixed, defined solely by the gap between the synchronous speed and the rotor's actual speed.

One more thing: Note that the peak torque is reached when $\frac{R_2}{s_B} = X_1' + X_2$, and that peak torque is $T_e = \frac{3p}{2\omega_B}\frac{\left|V_0'\right|^2}{(X_1' + X_2)}$.

12.2.2 Correction for Stator Resistance

While this approach works up to a point, the concept of "Volts per Hz" eventually reaches its limit, as there will be a maximum voltage available. This maximum voltage corresponds to the "base" speed of the drive. At speeds beyond this threshold, voltage amplitude is independent of speed and the peak torque becomes inversely proportion to the square of the speed. This is illustrated in Figure 12.2.

The idealization of zero stator resistance is clearly not right, as shown in Figure 12.3, which depicts the impact of stator resistance on the torque-speed characteristic. Note that the impact on torque is highest at low speed because the stator resistance is about constant, while the inductances are proportional to frequency. This effect can, of course, be countered by increasing voltage above the V/Hz level; and at very low frequencies there is voltage available.

12.3 Control and Simulation Models

In preparation for describing control methods for induction and synchronous machines, it is necessary to develop models for behavior of such machines. These models generally require some simplification from the complete models described in earlier chapters. Start with the induction machine.

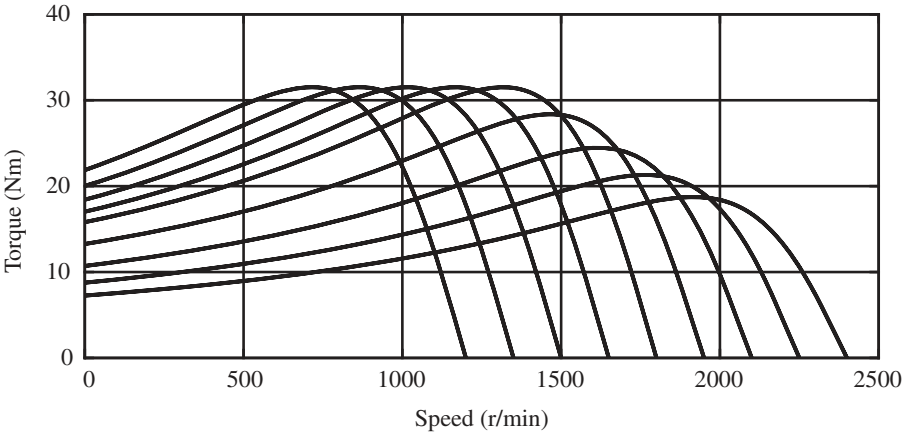

Figure 12.2 Idealized torque-speed curves with V/Hz control, assuming zero stator resistance.

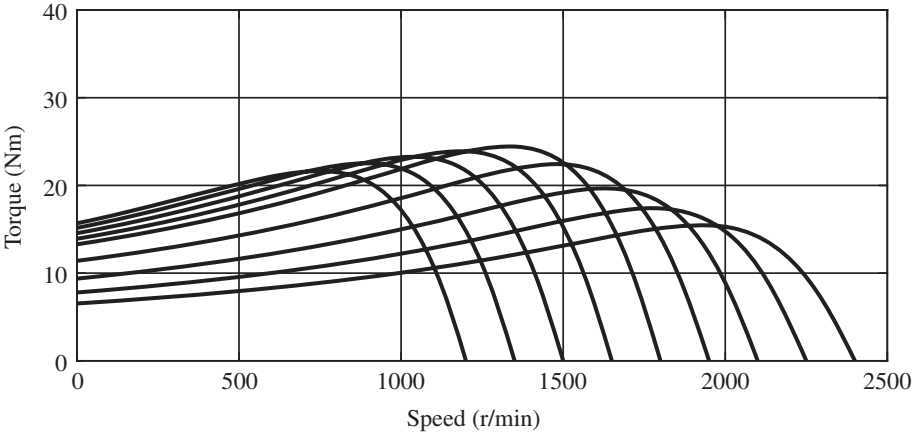

Figure 12.3 V/Hz drive accounting for stator resistance.

12.3.1 Induction Machine Model

In standard variables referenced to the stator, the behavior of an induction motor is characterized by flux-current equations under d–q reference frame:

$$\begin{bmatrix}\lambda_{dS}\\ \lambda_{dR}\end{bmatrix} = \begin{bmatrix}L_S & M\\ M & L_R\end{bmatrix}\begin{bmatrix}i_{dS}\\ i_{dR}\end{bmatrix}$$
$$\begin{bmatrix}\lambda_{qS}\\ \lambda_{qR}\end{bmatrix} = \begin{bmatrix}L_S & M\\ M & L_R\end{bmatrix}\begin{bmatrix}i_{qS}\\ i_{qR}\end{bmatrix} \tag{12.6}$$

The induction machine has no saliency, and there are leakage components in both the stator and rotor self-inductances:

$$L_S = M + L_{S\ell}$$
$$L_R = M + L_{R\ell} \tag{12.7}$$

The voltage equations are:

$$\begin{aligned} v_{dS} &= \frac{d\lambda_{dS}}{dt} - \omega\lambda_{qS} + R_S i_{dS} \\ v_{qS} &= \frac{d\lambda_{qS}}{dt} + \omega_{dS} + R_S i_{qS} \\ 0 &= \frac{d\lambda_{dR}}{dt} - \omega_s\lambda_{qR} + R_R i_{dR} \\ 0 &= \frac{d\lambda_{qR}}{dt} - \omega_s\lambda_{dR} + R_R i_{qR} \end{aligned} \tag{12.8}$$

Both the rotor and stator have voltage terms associated with their rotational speed, relative to the rotating coordinate system. The coordinate system itself rotates at a speed ω relative to the stator, while its speed relative to the rotor is $\omega - \omega_m$, where ω_m represents the rotor's mechanical angular frequency. It's important to note that this analysis does not assume the rotational speed of the reference frame, ω, to be constant. Therefore, the torque is expressed as:

$$T_e = \frac{3}{2}\, p(\lambda_{dS} i_{qS} - \lambda_{qS} i_{dS}) \tag{12.9}$$

Using these relationships, the overall state equations are as follows:

$$\begin{aligned} \frac{d\lambda_{dS}}{dt} &= v_{dS} + \omega\lambda_{qS} - R_S i_{dS} \\ \frac{d\lambda_{qS}}{dt} &= v_{qS} - \omega\lambda_{dS} - R_S i_{qS} \\ \frac{d\lambda_{dR}}{dt} &= \omega_s\lambda_{qR} - R_R i_{dR} \\ \frac{d\lambda_{qR}}{dt} &= \omega_s\lambda_{dR} - R_R i_{qR} \\ \frac{d\Omega_m}{dt} &= \frac{1}{J}(T_e - T_m) \end{aligned} \tag{12.10}$$

where the rotor frequency, also known as the slip frequency, is given by $\omega_s = \omega - p\,\Omega_m$.

For basic simulations with a constant excitation frequency, it is flexible to select the coordinate system, allowing for a convenient selection. For instance, the coordinate system can be aligned to a synchronous frame with stator frequency $\omega = \omega_0$. Under such a setup, the stator voltage may align with one of the axes, for example: $V_d = 0$ and $V_q = V$.

12.3.2 Idealized Model of Permanent Magnet Synchronous Machine

There are generally two types of Permanent Magnet Synchronous Machine classified according to rotor structure, namely surface-mounted type (SPMSM) and interior type (IPMSM). Both types leverage the benefits of permanent magnets but differ in their design, performance characteristics, and suitability for various applications. Their configurations are shown in Figure 12.4.

Surface Mount Motors, as the name implies, have permanent magnets mounted directly on their rotor surface, by bonding or using a retaining structure (not shown). This design does not have pronounced magnetic saliency. Surface mount machines are known for their simplicity and low manufacturing costs, as well as their lower moment of inertia, which allows for quick acceleration and deceleration. These attributes make SPMSM highly suitable for applications that require rapid response and precise control, such as in servomotors and other high-precision industrial equipment.

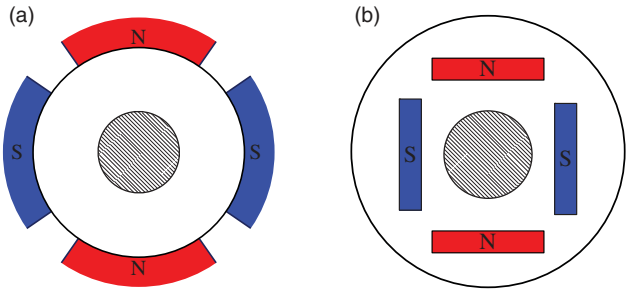

Figure 12.4 Rotor configurations of permanent magnet synchronous machine: (a) Surface mount; (b) Internal magnet.

In contrast, Interior Permanent Magnet Machines incorporate permanent magnets that are embedded within the rotor. This results in a salient pole structure, where the rotor's magnetic characteristics are more distinct. The embedded design of IPMSMs not only provides better mechanical protection for the magnets but also allows for higher torque production, particularly at lower speeds. This makes IPMSMs ideal for applications requiring high torque density and robust performance under demanding conditions, such as in automotive and heavy industrial applications.

To develop a general mathematical model applicable to both surface and interior magnet machines, assume that the three-phase permanent magnet machine operates under these conditions:

1) Motor core saturation is disregarded.
2) Eddy current and hysteresis losses in the motor are ignored.
3) The motor operates with symmetrical three-phase sinusoidal currents.

Under these assumptions, the three-phase voltage expressions of the PMSM are given by:

$$\boldsymbol{u}_{3s} = \boldsymbol{R}\boldsymbol{i}_{3s} + \frac{d}{dt}\boldsymbol{\psi}_{3s} \tag{12.11}$$

And the flux equation is:

$$\boldsymbol{\psi}_{3s} = \boldsymbol{L}_{3s}\boldsymbol{i}_{3s} + \psi_f \cdot \boldsymbol{F}_{3s}(\theta_e) \tag{12.12}$$

where $\boldsymbol{\psi}_{3s}$, $\boldsymbol{u}_{3s}$, $\boldsymbol{R}$, $\boldsymbol{i}_{3s}$, and $\boldsymbol{L}_{3s}$ are the magnetic flux linkage, phase voltage, resistance, current, and inductance of the three-phase windings, respectively; $\boldsymbol{F}_{3s}(\theta_e)$ is the position transformation matrix. They satisfy these equations:

$$\boldsymbol{i}_{3s} = \begin{bmatrix} i_A \\ i_B \\ i_C \end{bmatrix}, \quad \boldsymbol{R}_{3s} = \begin{bmatrix} R & 0 & 0 \\ 0 & R & 0 \\ 0 & 0 & R \end{bmatrix}, \quad \boldsymbol{\psi}_{3s} = \begin{bmatrix} \psi_A \\ \psi_B \\ \psi_C \end{bmatrix} \tag{12.13}$$

$$\boldsymbol{u}_{3s} = \begin{bmatrix} u_A \\ u_B \\ u_C \end{bmatrix}, \quad \boldsymbol{F}_{3s}(\theta_e) = \begin{bmatrix} \sin\theta_e \\ \sin(\theta_e - 2\pi/3) \\ \sin(\theta_e + 2\pi/3) \end{bmatrix} \tag{12.14}$$

$$\boldsymbol{L}_{3s} = L_{m3}\begin{bmatrix} 1 & \cos 2\pi/3 & \cos 4\pi/3 \\ \cos 2\pi/3 & 1 & \cos 2\pi/3 \\ \cos 4\pi/3 & \cos 2\pi/3 & 1 \end{bmatrix} + L_{l3}\begin{bmatrix} 1 & 0 & 0 \\ 0 & 1 & 0 \\ 0 & 0 & 1 \end{bmatrix} \tag{12.15}$$

where L_{m3} represents the stator mutual inductance, and L_{l3} represents the stator leakage inductance.

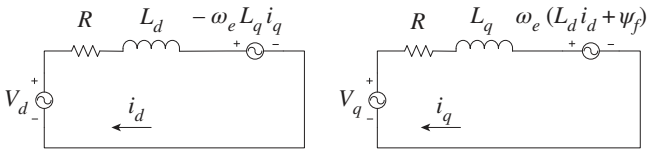

Figure 12.5 Simplified permanent magnet machine model.

Additionally, the equation of mechanical motion for the motor is:

$$J\frac{d\omega_m}{dt} = T_e - T_L - B\omega_m \tag{12.16}$$

where ω_m is the rotor mechanical angular speed, J is the moment of inertia, B is the damping coefficient, T_L is the load torque.

After coordinate transform, the PMSM mathematical expression under two-phase rotating reference frame is:

$$\begin{cases} u_d = Ri_d + \dot{\psi}_d - \omega_e \psi_q \\ u_q = Ri_q + \dot{\psi}_q + \omega_e \psi_d \end{cases} \tag{12.17}$$

where the stator magnetic flux linkage equation is:

$$\begin{cases} \psi_d = L_d i_d + \psi_f \\ \psi_q = L_q i_q \end{cases} \tag{12.18}$$

Substituting into previous equation, the stator voltage equation is derived as:

$$\begin{cases} u_d = L_d \dot{i}_d + Ri_d - \omega_e L_q i_q \\ u_q = L_q \dot{i}_q + Ri_q + \omega_e L_d i_d + \omega_e \psi_f \end{cases} \tag{12.19}$$

where u_d, u_q and i_d, i_q are the stator voltages and stator currents in the dq frame, R is the stator resistance, ψ_d, ψ_d and L_d, L_q are the d- and q-axis components of the stator magnetic flux linkage and inductance, ω_e is the electrical angular velocity, ψ_f represents the permanent magnet flux linkage. The equivalent circuit of the voltage expression is shown in Figure 12.5.

Torque is

$$T_e = \frac{3}{2}\, p_n\, i_q [i_d (L_d - L_q) + \psi_f] \tag{12.20}$$

Additionally, it is important to note the following key relationships:

$$\begin{cases} \omega_e = p_n \omega_m \\ \theta_e = p_n \theta_m \\ n_r = \dfrac{30}{\pi}\omega_e \end{cases} \tag{12.21}$$

12.4 Position Sensors

Control loops are fundamental to modern motor control systems, playing a crucial role in ensuring precise and reliable operation of electric motors. These loops are designed to monitor and adjust the motor's performance dynamically, allowing for the accurate control of various parameters such as position, speed, and current.

12.4.1 Position and Speed Feedback

At the core of a control loop is the concept of feedback, which is enabled by sensors. Feedback allows the system to continuously measure the motor's actual output and compare it with the desired or reference value. When any deviation or error is detected, the control loop adjusts the motor's input to realign the output with the target. This continuous process of monitoring and correction is crucial for maintaining stable and accurate operation. In this section, several commonly used sensors for position and current estimation are introduced.

12.4.2 Encoder

Encoders can be categorized based on their working principles into magnetic encoders and optical encoders. Additionally, according to the type of output they provide, encoders can be classified into incremental encoders and absolute encoders.

12.4.2.1 Incremental Encoder

A common type of incremental encoder is illustrated in Figure 12.6.

Its core component is a rotating disk attached to the shaft whose position is being measured. This disk has a series of alternating opaque and transparent segments arranged in a radial pattern. On its one side, there is a stationary light source, and on the opposite side, there are photodetectors aligned with the light source. As the disk rotates, the opaque and transparent segments alternately block and allow the passage of light from the LED to the photodetectors. This results in the photodetectors generating a series of pulses (digital signals) corresponding to the segments of the disk.

To determine the rotating direction and improve resolution, incremental encoders typically use two detectors positioned 90° out of phase. This setup produces two square wave signals (A and B), which are 90° out of phase with each other. By comparing the phase difference between these two signals, the direction of rotation can be determined. In addition, many incremental encoders include an additional photodetector aligned with a single reference mark on the disk, known as the index or Z pulse. This pulse occurs once per revolution, which provides the "clear" signal.

12.4.2.2 Absolute Encoder

Unlike the incremental type, the disk of absolute encoders which is shown in Figure 12.7 has a pattern of opaque and transparent segments arranged in an asymmetric pattern. Each track represents a binary bit, with the combination of bits across the tracks forming a unique binary code. As the disk rotates, each track produces a binary signal (1 for transparent, 0 for opaque). The combination of binary signals from all tracks forms a unique binary code representing the specific position of the shaft.

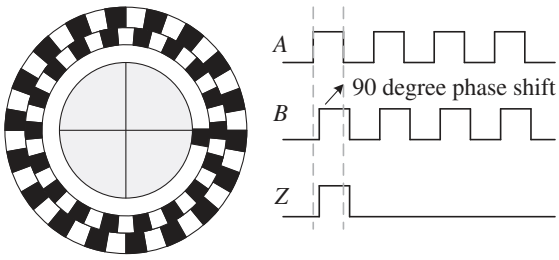

Figure 12.6 Illustration of an incremental encoder.

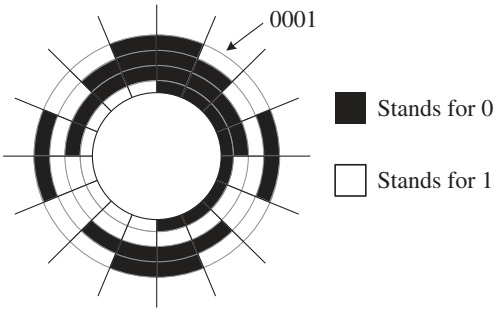

Figure 12.7 Illustration of an absolute encoder.

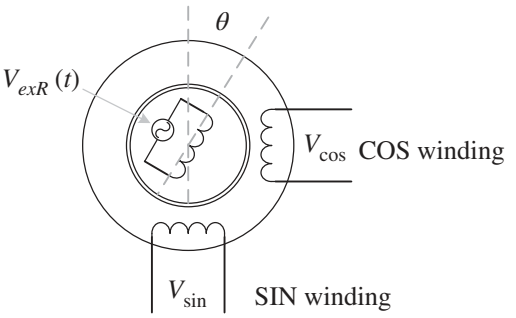

Figure 12.8 Illustration of a resolver.

12.4.3 Resolver

Another kind of position sensors commonly used in motor control is the resolver, which is illustrated in Figure 12.8. Similarly, it consists of a stator and a rotor. And there are two windings placed 90° apart on the rotor, typically called the sine (SIN) winding and cosine (COS) winding. The rotor has a single winding or, in some cases, two windings placed 90° apart.

An AC voltage, as the reference signal, is applied to the rotor winding. This reference signal is typically a sinusoidal waveform. As the rotor rotates, it induces voltages in the stator windings due to the transformer action. The induced voltages are sinusoidal and their magnitudes are determined by rotor position. The voltage induced in the SIN winding is proportional to the sine function of rotor angle θ while the voltage in the COS winding is proportional to the cosine function.

$$\begin{cases} V_{\sin} = V_{ref}\sin\theta \\ V_{\cos} = V_{ref}\cos\theta \end{cases} \tag{12.22}$$

By measuring the amplitudes and signs ($\mp$) of the SIN and COS signals, the angular position of the rotor can be calculated. The angle θ can be determined using the arctangent function:

$$\theta = \tan^{-1}\left(\frac{V_{\sin}}{V_{\cos}}\right) \tag{12.23}$$

12.5 Field-Oriented Control

One of the key breakthroughs made possible by advances in power electronics and control systems is the ability to convert induction motors into high-performance servomotors. The primary goal is to mimic a DC motor whose torque is directly proportional to its applied current. Taking a DC motor as an example, its torque can be expressed as: $T = GI_fI_a$

This simplicity in control makes DC machines highly appealing for applications such as servomotors. Once the desired torque is determined, it can be directly translated into a current command. However, DC motors have several drawbacks, especially in larger sizes. They are costly, less efficient, and require frequent maintenance due to the wear and tear of the brush-commutator interface. Additionally, they pose environmental challenges such as sparking and carbon dust generation. Consequently, AC motors, including induction motors and permanent magnet synchronous motors, are often more practical and reliable alternatives.

Currently, the two main high-performance AC motor control techniques are field-oriented control (FOC) and direct torque control (DTC). These two methods are based on controlling the rotor magnetic field and the stator magnetic field, respectively, to achieve high-performance closed-loop control. They are going to be introduced as follows.

12.5.1 Control Strategy for the Induction Motor

In FOC, the goal is to align the rotor flux to a known position, typically called the d-axis. Once this flux is established, a current is applied to the orthogonal q-axis, where it can most effectively generate torque. Mathematically, the objective is to set:

$$\begin{aligned} \lambda_{dR} &= \Lambda_0 \\ \lambda_{qR} &= 0 \end{aligned} \tag{12.24}$$

Torque is then generated by applying current along the quadrature (q) axis:

$$T_e = \frac{3}{2}\, p \frac{M}{L_R}\, \Lambda_0 i_{qS} \tag{12.25}$$

The process is nearly as straightforward as it seems, but there are some details to consider, such as determining the correct position for q-axis and how much to drive the d-axis magnetizing current. Assume that the flux is oriented along the d-axis, such that $\lambda_{qR} = 0$. For this case, the expression for two rotor voltage is:

$$\begin{aligned} 0 &= \frac{d\lambda_{dR}}{dt} + R_R \left(\frac{\lambda_{dR}}{L_R} - \frac{M}{L_R} i_{dS} \right) \\ 0 &= \omega_s \lambda_{dR} - R_R \frac{M}{L_R} i_{qS} \end{aligned} \tag{12.26}$$

Noting the rotor time constant is:

$$T_R = \frac{L_R}{R_R} \tag{12.27}$$

The pertinent expressions are:

$$\begin{aligned} T_R \frac{d\lambda_{dR}}{dt} + \lambda_{dR} &= M i_{dS} \\ \omega_s &= \frac{M}{T_R} \frac{i_{qS}}{\lambda_{dR}} \end{aligned} \tag{12.28}$$

The first equation characterizes the flux and current on d-axis, has a straightforward first-order relationship. The second equation, then connects slip to q-axis current and d-axis flux, essentially determines the rate at which rotating coordinate system needs to be adjusted in order to keep the flux aligned with the d-axis.

In an actual machine application, currents i_{dS} and i_{qS} are obtained from motor phase currents i_a, i_b, and i_c. This is accomplished through a coordinate transformation with angle θ determined based on the rotor mechanical speed and the slip:

$$\theta = \int (p\omega_m + \omega_s)dt \tag{12.29}$$

After obtaining the d–q axis currents, a good estimate of the d-axis flux is obtained by processing it through a first-order filter. The more challenging task is calculating slip by dividing the q-axis current by the d-axis flux, which is now easily handled numerically, along with the rotating coordinate transformation.

The block diagram for the process mentioned above is shown in Figure 12.9. In this diagram, we begin with the commanded values for the d- and q-axis currents, which correspond to flux and torque, respectively. These values are then converted into commanded phase currents through a rotating coordinate transformation, specifically the inverse Park's transform. The commanded currents i_a^*, i_b^*, and i_c^*, are shown as inputs to the "Amplifier." This could be implemented as a PWM current source, and with a tightly controlled loop, this setup leads to a high-performance servo system.

12.5.2 Control Strategy for a Synchronous Machine

A notional block diagram for FOC of a permanent magnet synchronous machine is shown in Figure 12.10.

The system includes an outer speed loop, in which the automatic speed regulator (ASR) provides the reference value for i_q by a PI controller whose transfer function is shown in equation (12.30).

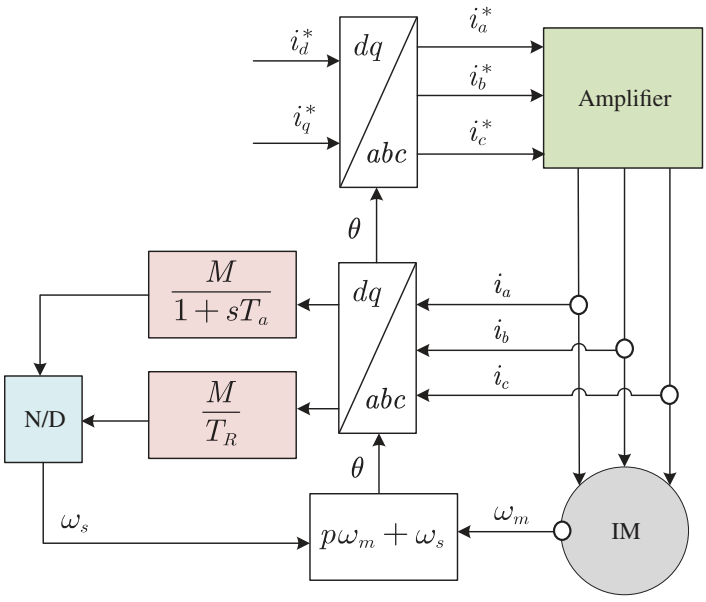

Figure 12.9 Block diagram of a field-oriented controller for an induction motor drive.

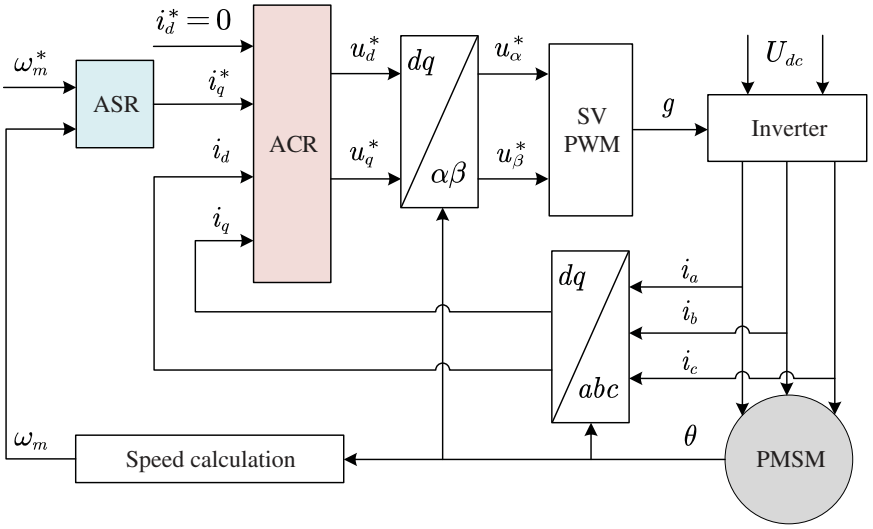

Figure 12.10 Block diagram of a field-oriented controller for a permanent magnet synchronous machine drive.

While the reference value for i_d supplied through other methods such as maximum torque per ampere (MTPA) and the degree of motor flux weakening.

$$G_{PI} = K_P + \frac{K_I}{s} \tag{12.30}$$

Similarly, the two current reference values are used by classic PI regulators to obtain the control voltages u_d and u_q for the dq axes. Subsequently, these voltages are converted into the $\alpha\beta$ stationary coordinate system, then transformed to a Pulse Width Modulated switching signal for the inverter.

12.5.3 Principle of Common Parts

12.5.3.1 Current Controller

After adding the PI controller into the current control loop, the system block diagram becomes as shown in Figure 12.11.

The open-loop transfer function regarding to speed is:

$$\begin{aligned} G_I(s) &= G_{plant}(s)G_{PI}(s) \\ &= \frac{k_{pdq}s + k_{idq}}{L_{dq}s^2 + Rs} \end{aligned} \tag{12.31}$$

And its closed-loop transfer function with unit feedback can be expressed as:

$$\begin{aligned} \boldsymbol{\Phi}_I(s) &= \frac{G_I(s)}{1 + G_I(s)H_I(s)} \\ &= \frac{k_{pdq}s + k_{idq}}{L_{dq}s^2 + (R + k_{pdq})s + k_{idq}} \end{aligned} \tag{12.32}$$

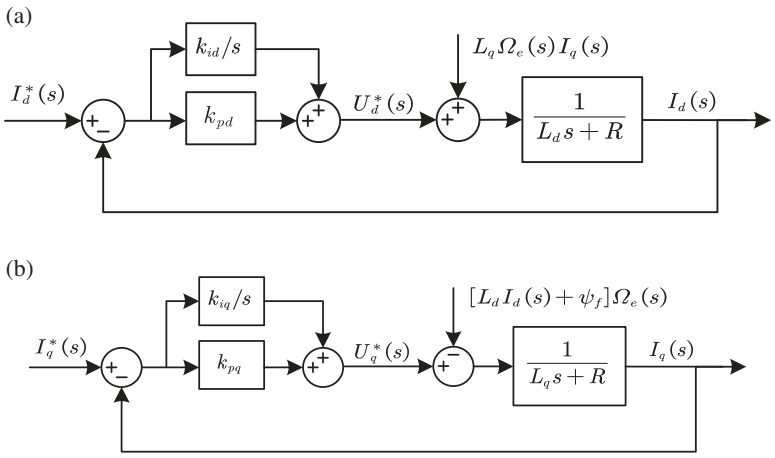

Figure 12.11 Control block diagram of current loops: (a) *d*-axis, (b) *q*-axis.

The control gains can be tuned to make it a typical second-order system whose transfer function is:

$$\Phi_{II} = \frac{\omega_n^2}{s^2 + 2\zeta\omega_n s + \omega_n^2} \tag{12.33}$$

where ω_n is the natural frequency, ζ is the damping ratio. If that is set to 0.707,

$$\begin{cases} k_{pdq} = 2L_{dq}\zeta\omega_n - R \\ k_{idq} = L_{dq}\omega_n^2 \end{cases} \tag{12.34}$$

12.5.3.2 Speed Controller

After adding the PI controller into the speed control loop, the block diagram is as shown in Figure 12.12.

The open-loop transfer function regarding to speed is:

$$\begin{aligned} G_\Omega(s) &= G_{plant}(s)G_{PI}(s) \\ &= \frac{k_p s + k_i}{Js^2 + Bs} \end{aligned} \tag{12.35}$$

And its closed-loop transfer function with unit feedback can be expressed as:

$$\begin{aligned} \Phi_\Omega(s) &= \frac{G_\Omega(s)}{1 + G_\Omega(s)H_\Omega(s)} \\ &= \frac{k_p s + k_i}{Js^2 + (B + k_p)s + k_i} \end{aligned} \tag{12.36}$$

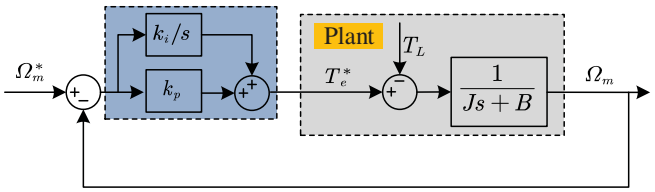

Figure 12.12 Block diagram of speed control loop.

Hence, similar as the way tuning the control gains in current control loop, the gains in speed control loop can be determined by:

$$\begin{cases} k_p = 2J\zeta\omega_n - B \\ k_i = J\omega_n^2 \end{cases} \tag{12.37}$$

12.5.3.3 Coordinate Transform

In FOC, coordinate transformation is a key technique used to simplify the control of three-phase motors by converting the complex, time-varying three-phase system into a more manageable two-dimensional coordinate system. This transformation involves mapping the three-phase system into a two-phase rotating frame aligned with the rotor's magnetic field. Specifically, the Clarke transformation first converts the three-phase currents into a stationary two-axis system ($\alpha\beta$ axis). The process is illustrated in Figure 12.13a, b.

$$\begin{bmatrix} \alpha \\ \beta \\ 0 \end{bmatrix} = \frac{2}{3} \begin{bmatrix} 1 & -\frac{1}{2} & -\frac{1}{2} \\ 0 & \frac{\sqrt{3}}{2} & -\frac{\sqrt{3}}{2} \\ \frac{1}{2} & \frac{1}{2} & \frac{1}{2} \end{bmatrix} \begin{bmatrix} a \\ b \\ c \end{bmatrix} \tag{12.38}$$

And then the Park transformation rotates these coordinates into a synchronous reference frame (d–q axis) that moves with the rotor. The process is illustrated in Figure 12.13b, c.

$$\begin{bmatrix} d \\ q \end{bmatrix} = \begin{bmatrix} \cos(\theta_e) & \sin(\theta_e) \\ -\sin(\theta_e) & \cos(\theta_e) \end{bmatrix} \begin{bmatrix} \alpha \\ \beta \end{bmatrix} \tag{12.39}$$

In the dq frame, the d-axis aligns with the rotor's magnetic field, and the q-axis is orthogonal to it. This coordinate system simplifies the control of motor currents by decoupling the torque and flux control, allowing them to be managed independently. By aligning the control axes with the rotor field, FOC enables precise regulation of torque and flux, leading to improved motor performance, efficiency, and dynamic response. The use of coordinate transformation not only streamlines the control process but also facilitates advanced control strategies that enhance the overall operation of electric motors.

12.5.4 Space Vector Pulse Width Modulation (SVPWM)

Space vector pulse width modulation (SVPWM) works by representing the three-phase voltage system as a single complex vector in a two-dimensional plane, known as the space vector. This vector

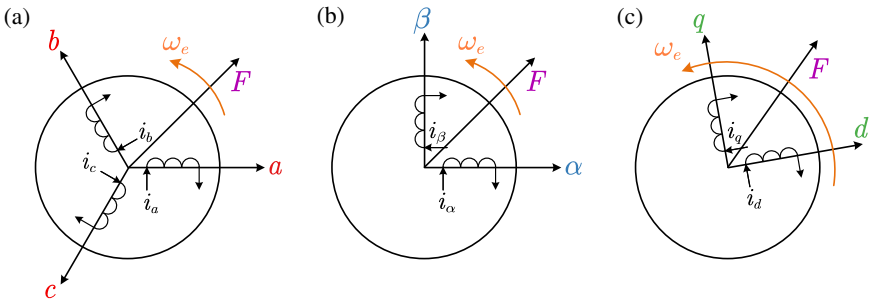

Figure 12.13 Illustration of coordinate transform: (a) three phase, stationary frame, (b) two phase stationary frame, (c) rotating frame.

is derived from the reference voltage computed by the FOC algorithm and is used to determine the most suitable switching states of the inverter to approximate the desired voltage vector. The process begins with the decomposition of the reference voltage into a combination of the six basic voltage vectors. SVPWM then calculates the duty cycles for these switching states to create a synthesized voltage vector that closely matches the reference vector over each switching period. By using this technique, SVPWM minimizes harmonic distortion and optimizes the utilization of DC bus voltage, leading to smoother and more efficient motor operation. The detailed illustration is as follows:

Define a switching function to represent the state of each switch of the inverter shown in Figure 12.14

$$S_x = \begin{cases} 0, & switch\ is\ off \\ 1, & switch\ is\ on \end{cases} \tag{12.40}$$

where x represents the switch of each phase.

And with these three-switching function S_a, S_b and S_c can be represented using one vector, for example, (100) represents VT_1, VT_4, and VT_6, conduct, while VT_2, VT_3, and VT_5 are off. And in total, there are $2^3 = 8$ states. The SVPWM algorithm inputs synthesized voltage vector V_δ shown in Figure 12.15. By controlling the states of those six switches in three-phase inverter, it synthesizes the equivalent PWM-form motor phase voltages. In other words, it reproduces V_δ in PWM form.

Voltage vector V_δ can be positioned anywhere and its magnitude can also vary. However, there are only six non-zero vectors and two zero vectors, and their magnitudes are fixed. Next, we will examine how to use these six non-zero vectors and two zero vectors to reproduce V_δ. During each switching period T_s, the SVPWM algorithm can use the eight vectors to synthesize V_δ once.

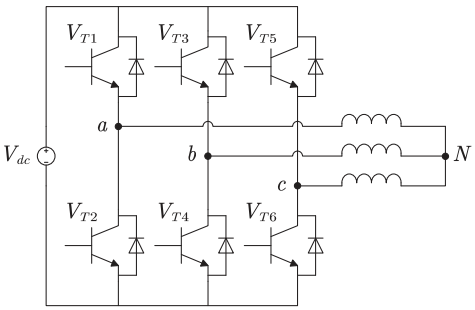

Figure 12.14 Illustration of an inverter.

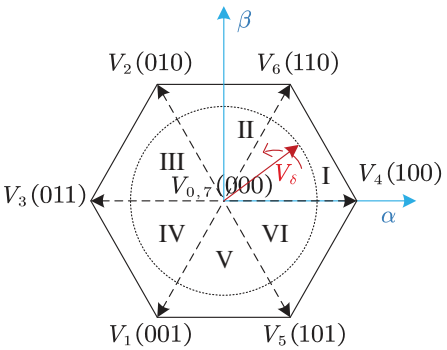

Figure 12.15 Illustration of voltage vectors on two-phase stationary reference frame.

Figure 12.16 Illustration of voltage vectors synthesized in sector 1.

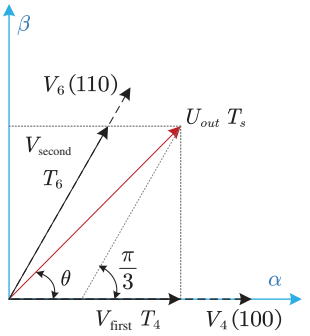

The shorter T_s is, the more times V_{out} can be synthesized within one rotation of V_δ, resulting in a smoother trajectory for the vertex of V_{out} and a path that more closely approximates the trajectory of V_δ.

Assuming that V_δ has rotated to Sector I, we can use the two adjacent non-zero voltage vectors in Sector I, V_4 and V_6, along with the two zero vectors V_0 and V_7, to synthesize V_δ. The resulting synthesized voltage vector is V_{out}. T_4 represents the duration within one PWM switching period during which the voltage vector V_4 is active. Similarly, T_6 is the duration during which the voltage vector V_6 is active. V_{first} is aligned with the first vector in the counterclockwise direction within each sector (in this case, it is aligned with V_4). V_{second} is aligned with the second vector in the counterclockwise direction within each sector (in this case, it is aligned with V_6). This process is illustrated in Figure 12.16.

Based on the volt-second balance principle, we have the following relationship:

$$\begin{cases} V_{\text{out}} = \dfrac{T_4}{T_s}V_4 + \dfrac{T_6}{T_s}V_6 + \dfrac{T_0}{T_s}V_0 \left(\text{or } \dfrac{T_0}{T_s}V_7\right) \\ V_{\text{first}} = \dfrac{T_4}{T_s}V_4 \\ V_{\text{second}} = \dfrac{T_6}{T_s}V_6 \end{cases} \tag{12.41}$$

Also, in Figure 12.16, the conclusion of equation (12.42) can be obtained:

$$\begin{aligned} |V_{\text{out}}|\sin(\theta) &= |V_{\text{second}}|\sin\left(\frac{1}{3}\pi\right) \\ |V_{\text{first}}|\sin(\theta) &= |V_{\text{second}}|\sin\left(\frac{\pi}{3}-\theta\right) \end{aligned} \tag{12.42}$$

Since

$$|V_4| = |V_6| = \frac{2}{3}V_{DC} \tag{12.43}$$

Substituting equations (12.42) and (12.43) into equation (12.41) yields:

$$\begin{cases} T_4 = \dfrac{\sqrt{3}\ T_s\ V_{out}}{V_{DC}}\sin\left(\dfrac{\pi}{3}-\theta\right) \\ T_6 = \dfrac{\sqrt{3}\ T_s\ V_{out}}{V_{DC}}\sin(\theta) \\ T_0 = T_7 = \dfrac{1}{2}\left(T_s - T_4 - T_6\right) \end{cases} \tag{12.44}$$

However, merely knowing this duration is not sufficient; we also need to understand how this duration T_4 is distributed within the switching period T_s.

The goal is to minimize the number of switch operations within a switching period T_s during the synthesis of the reference voltage vector. This minimization reduces the switching losses in the inverter. Therefore, when switching voltage vectors, we aim to change only one switching function, meaning we alter the switch state of only one phase of the inverter (each phase has two switches). By introducing zero vectors V_0 and V_7, we can easily achieve this objective.

The sequence in which the four voltage vectors appear can be arranged as follows: the two zero vectors are evenly distributed at the beginning, in the middle and at the ends, resulting in the sequence V_0, V_4, V_6, V_7, V_7, V_6, V_4, V_0. When switching from V_0 to V_4, the switching function

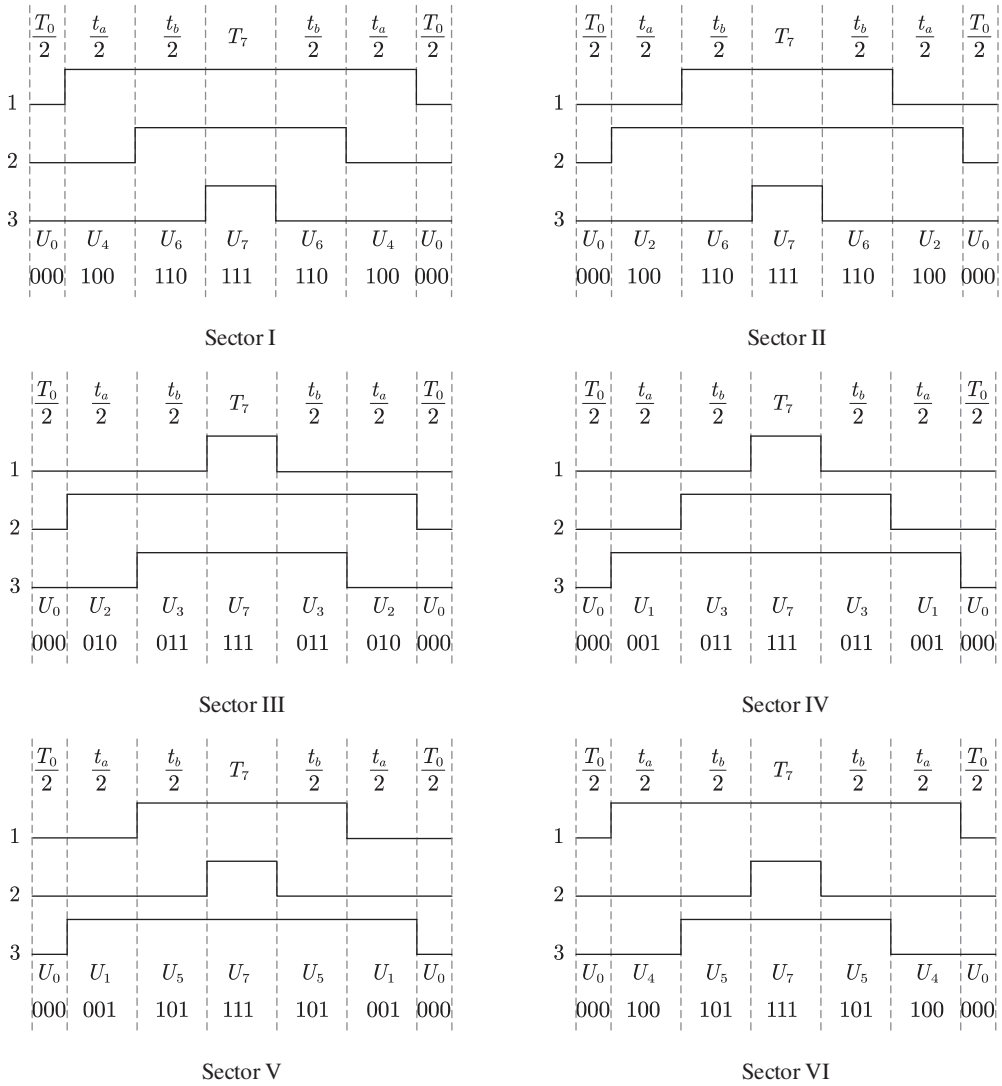

Figure 12.17 Switching sequence for SVPWM in all six sectors.

changes from (0 0 0) to (1 0 0), meaning that only the switch state of phase A in the inverter changes—the upper switch, which was previously off and the lower switch was on, now changes to the upper switch being on and the lower switch off. Similarly, in the above switching sequence, each switch transition only involves a change in the switch state of one phase in the inverter.

It also makes sure that, after synthesizing a reference voltage vector, the switching state always returns to the zero-vector position V_0 and V_7. And if the reference voltage vector moves from one sector to the next in the following switching period, the synthesis process always begins with a zero vector, ensuring the continuity of synthesizing reference voltage vector.

Figure 12.17 lists the switching sequence for compositing the reference voltage vector in all sectors.

12.6 Direct Torque Control

Unlike FOC that relies on complex coordinate transformations and pulse width modulation, DTC simplifies the control process by utilizing a predefined switching table, making real-time decisions based on the discrepancy between the reference and actual values of torque and flux. This approach allows for faster dynamic responses and greater efficiency in controlling motor behavior, making DTC particularly suitable for applications where rapid and accurate torque adjustments are critical. Figure 12.18 shows its overall working principle and it will be introduced in detail in the following subsectors.

DTC employs an estimate of stator flux magnitude and direction to establish the current that must be injected to produce commanded torque. From that required current, the controller must apply the correct voltage to the stator.

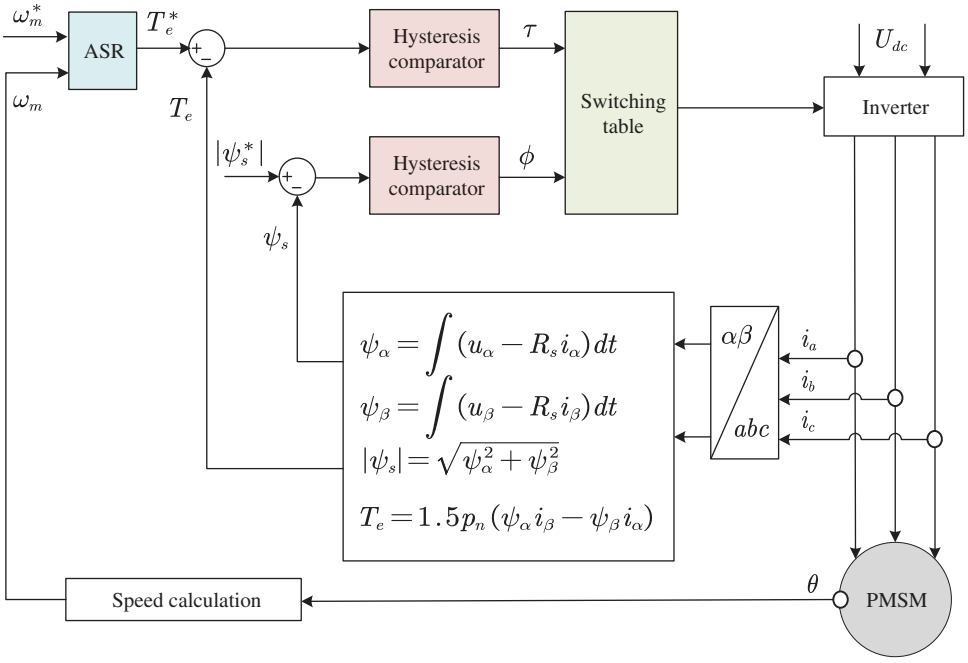

Figure 12.18 Block diagram of direct torque control.

12.6.1 Torque and Flux Estimator

From the PMSM mathematical model, stator flux can be directly calculated as:

$$\begin{cases} \psi_\alpha = \int (u_\alpha - R_s i_\alpha)\, dt \\ \psi_\beta = \int (u_\beta - R_s i_\beta)\, dt \end{cases} \tag{12.45}$$

However, the voltage may be affected by dead time and direct integrator may bring a DC offset. Hence, usually a flux observer is built as shown in Figure 12.19, based on both (12.45) and current model (12.46).

$$\begin{cases} \psi_d = L_d i_d + \psi_f \\ \psi_q = L_q i_q \end{cases} \tag{12.46}$$

With the obtained flux, torque is calculated by:

$$T_e = \psi_\alpha i_\beta - \psi_\beta i_\alpha \tag{12.47}$$

12.6.2 Bang-Bang Controller

The working principle is controlling the difference of the reference and actual value within a tolerance. If the difference is within the tolerance, the output remains. If the actual value is larger than its reference, then output "0" which means the output needs to be reduced. Otherwise, if the actual value is less than reference, then output "1" which means the output needs to be increased.

In general, it can be expressed as:

$$\phi = \begin{cases} 1, \ \ if\ \left(|\psi_s^*| - |\psi_s| > \varepsilon_\psi\right) \\ unchanged, if\ \left(||\psi_s^*| - |\psi_s|| \leqslant \varepsilon_\psi\right) \\ 0, if\ \left(|\psi_s^*| - |\psi_s| < -\varepsilon_\psi\right) \end{cases} \tag{12.48}$$

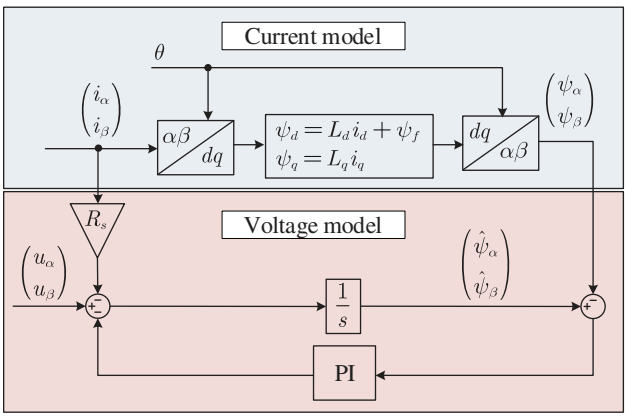

Figure 12.19 Block diagram of flux estimator.

$$\tau = \begin{cases} 1, if \left(T_e^* - T_e > \varepsilon_{T_e}\right) \\ unchanged, if \left(|T_e^* - T_e| \leqslant \varepsilon_{T_e}\right) \\ 0, if \left(T_e^* - T_e < -\varepsilon_{T_e}\right) \end{cases} \tag{12.49}$$

12.6.3 Voltage Vector Lookup Table

It is then necessary to select appropriate voltage vectors to achieve the desired changes in torque and flux. To facilitate this, the voltage vector plane is segmented into six sectors, as illustrated in Figure 12.20. Taking the example of stator flux lies in the first sector, the analysis proceeds as follows

First, the influence of voltage vectors on the magnitude of the stator flux can be intuitively determined by the angle between them. Specifically, voltage vectors V_6, V_4 and V_5 increase the amplitude due to its acute angle with the stator flux. V_2, V_3 and V_1 decreases it because of its obtuse angle. Zero voltage vectors V_0 and V_7 have no impact on the flux amplitude and are therefore excluded from consideration.

If the component of the voltage vectors perpendicular to the stator flux is positive, it will increase the rotation speed of the flux. Consequently, the torque increases to ensure that the rotor maintains rotating at the same speed. Hence, in the case of sector I, V_6 and V_2 will enlarge the torque while V_5 and V_1 will decrease the torque.

In summary, the influence of voltage vectors on stator flux of Sector I is listed in Table 12.1:

Therefore, in Sector I, V_6 should be applied to simultaneously increase both torque and flux. To increase torque while reducing flux, V_2 is recommended. Conversely, V_5 should

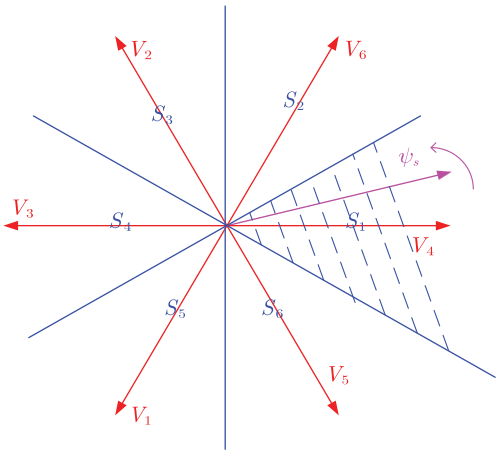

Figure 12.20 Sector division for direct torque control.

Table 12.1 Influence of voltage vectors on stator flux in sector.

Voltage Vectors	V_1	V_2	V_3	V_4	V_5	V_6
Effect on Flux	↓	↓	↓	↑	↑	↑
Effect on Torque	↓	↑	–	–	↓	↑

Table 12.2 DTC lookup table.

ϕ	τ	s_1	s_2	s_3	s_4	s_5	s_6
1	1	V_6 (110)	V_2 (010)	V_3 (011)	V_1 (001)	V_5 (101)	V_4 (100)
	0	V_5 (101)	V_4 (100)	V_6 (110)	V_2 (010)	V_3 (011)	V_1 (001)
0	1	V_2 (010)	V_3 (011)	V_1 (001)	V_5 (101)	V_4 (100)	V_6 (110)
	0	V_1 (001)	V_5 (101)	V_4 (100)	V_6 (110)	V_2 (010)	V_3 (011)

be used to reduce torque while increasing flux, and V_1 is appropriate for reducing both torque and flux.

With the same deduction on the other five sectors, the lookup table for implementing DTC can be obtained as Table 12.2.

12.7 Control System Design

As introduced in the previous sections, the ASR plays a vital role in both FOC and DTC. Previously, only PI control was introduced as an example. In this section, a more detailed discussion on controller design will be presented, covering various control strategies and their impact on system performance.

12.7.1 Fundamentals of Control Systems

Consider the control system illustrated in Figure 12.21, where P is the plant to be controlled, C is the unified compensator and drive system, H is the feedback path, which may include sensors and parts of the compensator, and F represents a pre-filter or pre-adjustment. The main inputs to the system are the reference R, disturbance D, and output noise N. The outputs of interest are the control and drive signal u, the physical output of the plant x, and the measured output y.

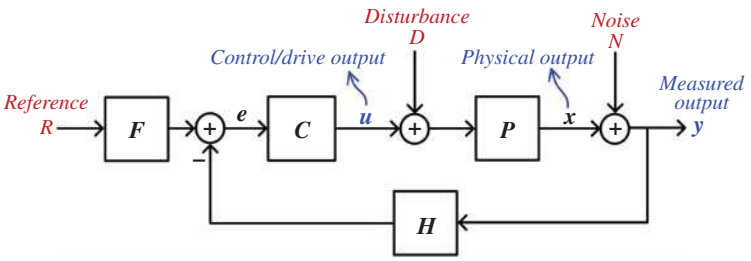

Figure 12.21 Block diagram of a typical control system.

We will analyze the relationship between the mentioned inputs and outputs later, focusing on the trade-offs in control system design. For now, let's examine the transfer function of the closed-loop system, which can be derived as follows:

$$E = FR - HY$$
$$Y = PCE \tag{12.50}$$

Hence

$$\frac{Y}{R} = F\frac{\overbrace{PC}^{Forward}}{1+\underbrace{PCH}_{Loop}} = F\frac{[Forward\ Path]}{[Loop\ Transmission]} \tag{12.51}$$

The stability criterion requires that the poles of the closed-loop transfer function, i.e. the roots of the denominator $1 + P(s)\,C(s)\,H(s)$, must have negative real parts, ensuring they lie in the left half of the complex plane. However, in frequency-domain analysis, compensator design is typically based on the loop transmission function $L(s) = P(s)\,C(s)\,H(s)$, which determines system stability, performance, and robustness.

12.7.2 Phase and Gain Margins, and Crossover Frequencies

The gain crossover frequency, or unity-gain frequency ω_{gc}, is the frequency at which the magnitude of the loop transmission equals unity (0 dB). The phase margin φ_m is then defined as the difference between $-180°$ and the phase of the loop transmission at ω_{gc}, representing the additional phase lag required to lose stability. Phase margin is directly related to system damping, overshoot in the time response, and robustness to parameter variations and modeling errors. A phase margin in the range of 30°–60° generally provides a good balance between adequate damping and robustness without an excessive response time. A higher phase margin enhances robustness but may lead to slower transient responses. To summarize:

$$|L(j\omega_{gc})| = 1$$
$$\varphi_m = 180° + \angle L(j\omega_{gc}) \tag{12.52}$$

The phase crossover frequency ω_{pc} is the frequency at which the phase of the loop transmission reaches $-180°$. The gain margin is then defined as the amount by which the system gain can be increased before reaching instability. It is calculated as $20\log_{10}(1/G)$, where G is the gain at ω_{pc}. A desirable gain margin is typically at least 6 dB to ensure stability and robustness against variations. To summarize:

$$\angle L(j\omega_{gc}) = -180°$$
$$g_m = \frac{1}{|L(j\omega_{pc})|}\ or\ G_m = 20\log_{10}\left(\frac{1}{|L(j\omega_{pc})|}\right) \tag{12.53}$$

In summary, the relationships among phase margin, gain margin, and cross frequencies are illustrated in Figure 12.22.

12.7.2.1 Lead Compensator

Typically, a lead–lag compensator is used to enhance system performance. The lag compensator increases low-frequency gain, reducing steady-state error, while the lead compensator introduces a positive phase contribution over a specific frequency range. This improves the phase margin,

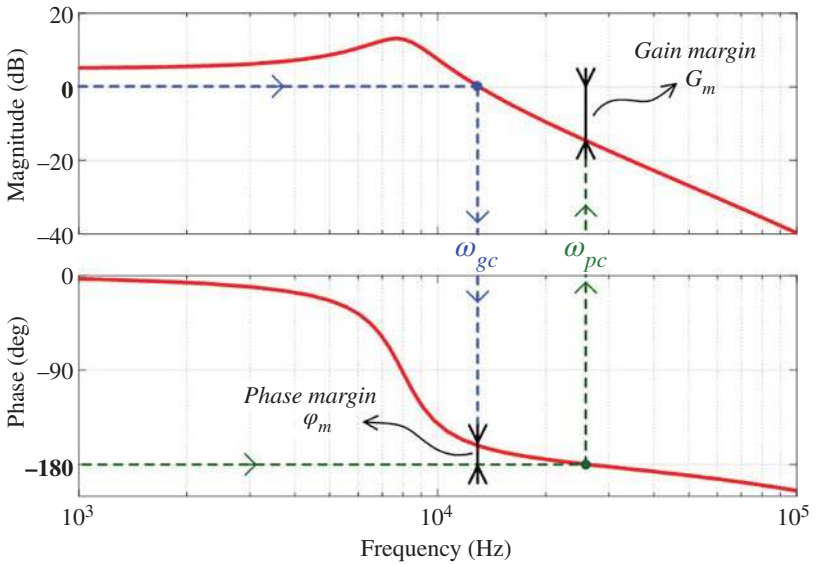

Figure 12.22 Phase margin, gain margin, and crossover frequencies.

enhancing the transient response by limiting overshoot and ensuring the robustness of the control system. The general transfer function of a lead compensator can be expressed as follows:

$$C_{lead} = \frac{\alpha\tau s + 1}{\tau s + 1}; \alpha > 1 \tag{12.54}$$

The zero of the lead compensator is placed closer to the origin than its pole, resulting in a phase lead over a specific frequency range. The lead compensator provides a maximum phase of ϕ_m at the frequency of ω_m as follows:

$$\phi_m = \sin^{-1}\left(\frac{\alpha - 1}{\alpha + 1}\right) \text{ at } \omega_m = \frac{1}{\tau\sqrt{\alpha}} \tag{12.55}$$

Knowing the required phase compensation ϕ_m, α can be obtained. Then, knowing ω_m, the value of τ can be obtained. The value of ω_m is set at the gain crossover frequency $\omega_{gc} = 2\pi f_{gc}$ of the loop to obtain the highest phase margin. The gain crossover frequency is selected based on the desired bandwidth, balancing response speed and robustness. Excessively large values of α can lead to excessive high-frequency noise amplification; a common choice is $\alpha = 10$. A simple rule of thumb to approximate the relationship between the damping ratio ζ of the dominant closed-loop poles and the phase margin ϕ_m of the loop transmission is:

$$\xi = \frac{\phi_m}{100} \tag{12.56}$$

In summary, the frequency of a lead compensator is illustrated in Figure 12.23.

12.7.2.2 Lag Compensator

The lag compensator can simply be implemented as a pure integrator, given by the transfer function:

$$C_{lag} = \frac{1}{\tau s} \tag{12.57}$$

This provides an infinite DC gain (at zero frequency), significantly improving the steady-state performance by eliminating steady-state error of step response. However, it introduces a phase

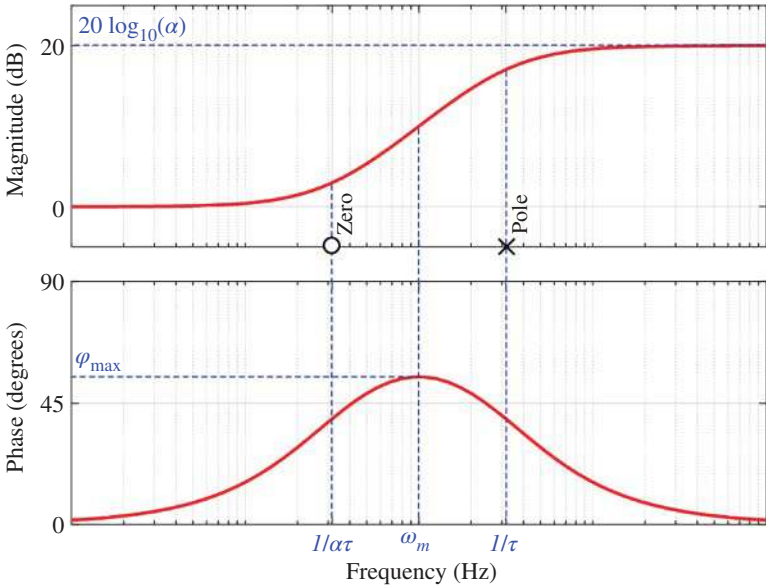

Figure 12.23 Frequency response of a lead compensator.

lag of −90°, which can negatively impact stability and transient response. By placing a zero at a higher frequency than the pole, the phase lag introduced at mid frequencies is minimized and primarily affects low frequencies. This design ensures that the phase margin of the system and thus its transient response and robustness are not significantly degraded. The transfer function of such a lag compensator is given by:

$$C_{lag} = \frac{\tau s + 1}{\tau s} \tag{12.58}$$

It is often used in systems requiring perfect tracking, such as position control systems, where zero steady-state error is critical. However, placing a pure integrator introduces infinite DC gain, which can lead to control saturation and excessive phase lag. To mitigate these issues, the pole can be placed slightly away from the origin but still close enough to maintain sufficient DC gain. The general transfer function of a lag compensator is given by:

$$C_{lag} = \frac{\tau s + 1}{\alpha \tau s + 1}; \alpha > 1 \tag{12.59}$$

The pole of the lag compensator is placed closer to the origin than the zero. In summary, the frequency of a lag compensator is illustrated in Figure 12.24.

12.7.3 Control Loop Design in the Case of DC Motors and Actuators

Since FOC transforms the control of an AC motor into emulation of that of a DC motor, the electromechanical system of a typical DC actuator or motor serves as an example for control system design. Figure 12.25 shows the modeling block diagram of a limited-angle torque motor [1].

The electrical dynamics include the resistance R and inductance L of the stator coil, while the mechanical dynamics consist of a mass-spring-damper system characterized by rotor inertia J, stiffness K_s, and damping coefficient K_d. These two subsystems interact through electromechanical coupling, where energy conversion occurs. In other words, the coil current i_c generates an electromagnetic torque $T_e = k_t\, i_c$ on the rotor, while the rotor velocity ω induces a back-EMF $E = k_b\, \omega$ in

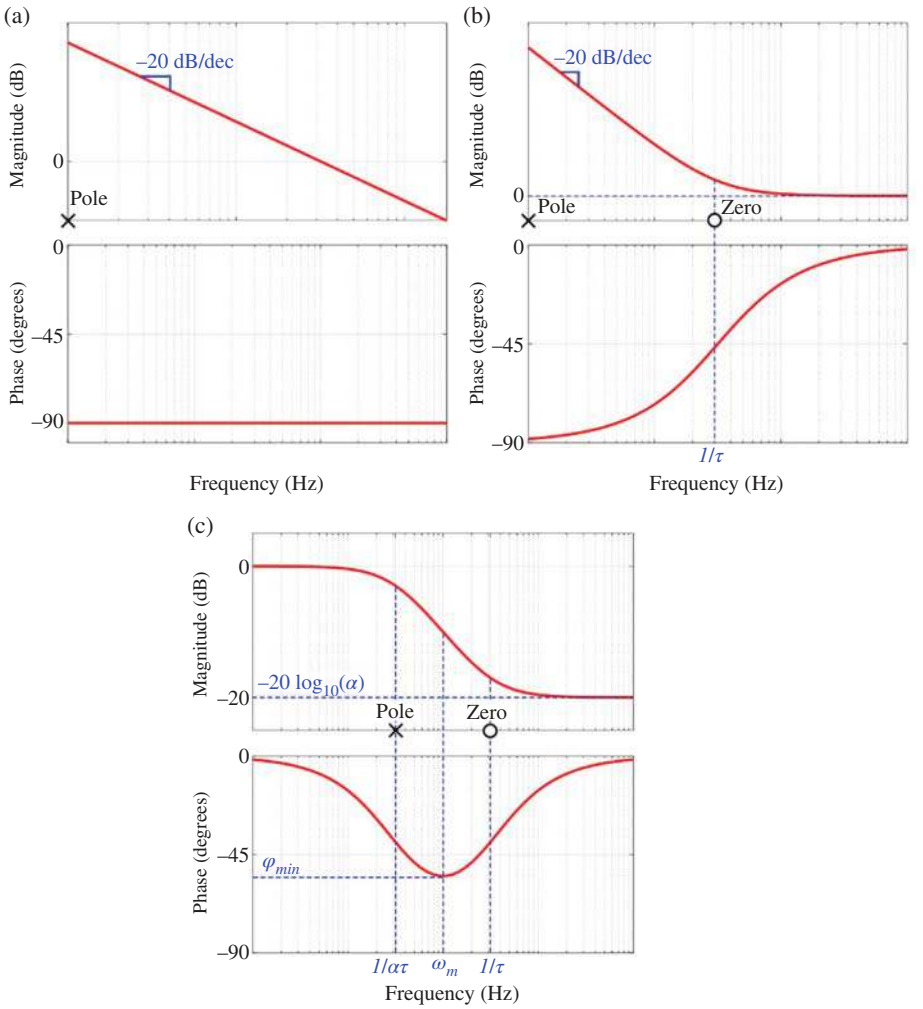

Figure 12.24 Frequency response of a lag compensator: (a) pure integrator, (b) pure integrator with added zero, (c) general form.

the stator coil. Due to the energy conservation principle, the torque constant k_t and the back-EMF constant k_b are equal. The governing equations describing the system dynamics are:

$$\begin{cases} v_c = E + Ri_c + L\dfrac{di_c}{dt} \\ E = k_b\omega \\ T_e = J\dfrac{d^2\theta}{dt^2} + K_d\dfrac{d\theta}{dt} + K_s \\ T_e = k_t i_c \end{cases} \tag{12.60}$$

Figure 12.26 illustrates the control system for a DC actuator with cascaded control loops. The innermost loop regulates the stator current, which is directly proportional to the electromagnetic torque generated by the actuator. This current (or torque) loop tracks the current (or torque) command generated by the velocity loop. Since the electrical dynamics of the system are much faster

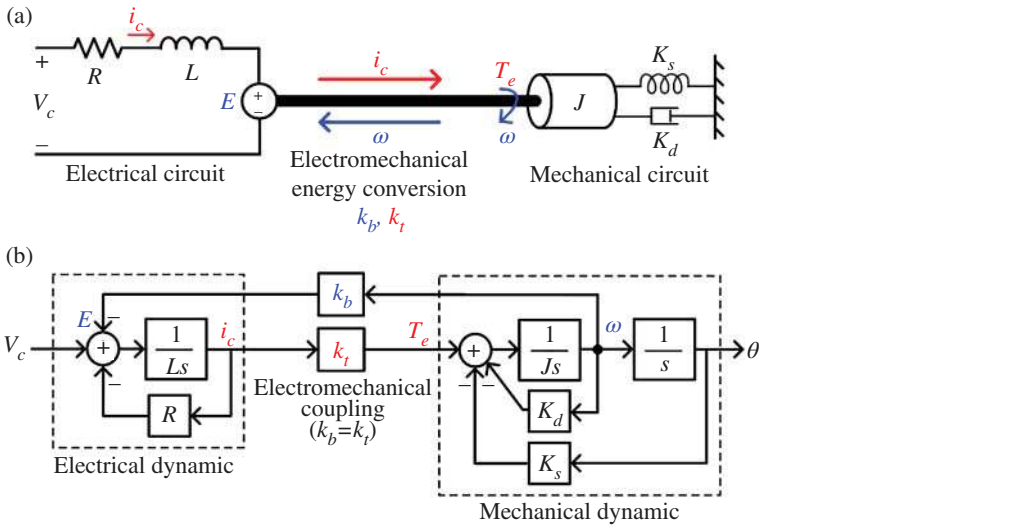

Figure 12.25 Limited angle torque actuator: (a) electromechanical circuit, (b) block diagram for small signal model.

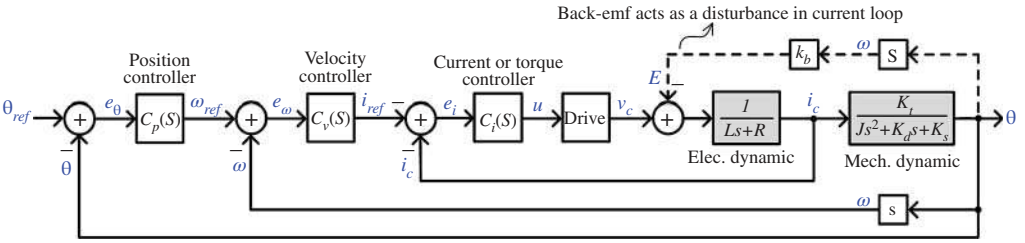

Figure 12.26 Cascaded control loops for a DC actuator.

than the mechanical dynamics, the current loop must be the fastest loop in the system, with the highest bandwidth. Typically, the bandwidth of the current loop is designed to be 10–20 times that of the velocity loop. This separation in bandwidth ensures dynamic decoupling between the two loops, allowing the velocity loop to treat the current loop—including the electrical dynamics—as a simple gain (the DC gain of the current loop). In other words, if the current loop is sufficiently fast, the electrical dynamics are effectively eliminated, and the current (or torque) can be commanded instantaneously. Without a current loop, the electrical time constant would introduce delays in converting the drive voltage applied to the stator terminals into current or torque, which is the input to the mechanical dynamics. As shown in Figure 12.26, the back-EMF acts as a disturbance to the current loop, but with sufficient disturbance rejection, it can be mitigated. Additionally, by eliminating the effects of electrical dynamics, the robustness of the control system is enhanced, making it less sensitive to temperature-dependent variations such as changes in coil resistance.

Finally, with the implementation of velocity and position loops, the mechanical dynamics are eliminated, enabling instantaneous command of velocity and position, ensuring fast reference tracking. The velocity loop, which is placed outside the current loop, regulates the velocity of the rotor by generating a torque command for the current loop. To maintain proper decoupling between the loops, the velocity loop must be slower than the current loop. The outermost loop is the position loop, which controls the position by generating a velocity reference for the velocity

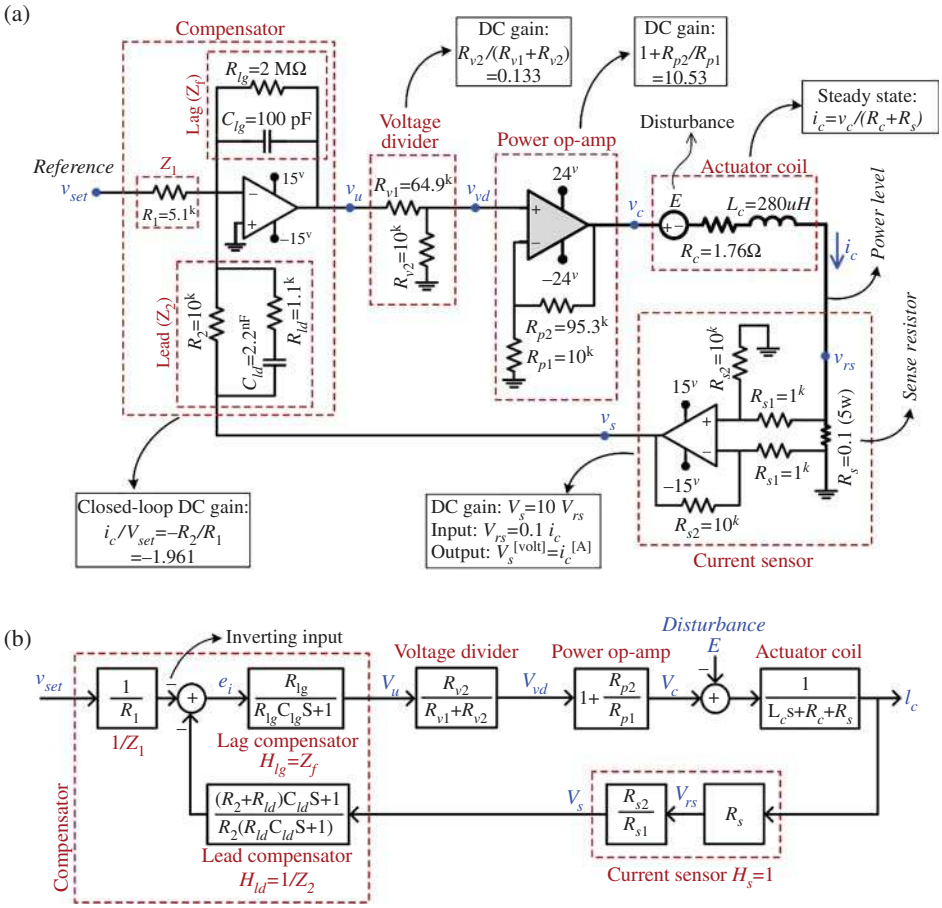

Figure 12.27 Current control loop for actuator: (a) realization using operational amplifiers, (b) block diagram.

loop. Similar to the relationship between the current and velocity loops, the position loop must be slower than the velocity loop to ensure proper decoupling. This hierarchical control structure allows each loop to be designed independently.

As the circuit and the block diagram shown in Figure 12.27, the current control loop can be implemented using an op-amp-based analog circuit [1, 2]. A power op-amp with a gain of $1 + R_{p2}/R_{p1} = 10.53$ is used to drive the actuator, capable of delivering a current of ±10 A. Since an op-amp's gain-bandwidth product is constant, increasing the closed-loop gain reduces the bandwidth; thus, selecting the lowest feasible gain is preferred to maintain a higher bandwidth. To match the compensator's maximum output voltage (±14.7 V) to the power op-amp's input range, a voltage divider with a gain of $R_{v2}/(R_{v1} + R_{v2}) = 0.133$ is employed. This ensures that the maximum output voltage of the compensator (±14.7 V) is properly matched to the power op-amp's input, resulting in a maximum drive voltage of $\pm 14.7\,\text{V} \times 0.133 \times 10.53 = \pm 20.6\,\text{V}$ at the outputs of the power op-amp which corresponds to the maximum output current of 20.6/1.86 = 10.7 A ensuring proper operation within the limits.

The coil current is measured by the voltage across a very small sense resistor ($R_s = 0.1\,\Omega$) placed in series with the coil. To avoid loading it, the voltage is buffered with a DC gain of R_{s2}/R_{s1}, which

is set to the inverse of the sense resistor $1/R_s = 10$, such that its output v_s is equal to the coil current i_c. The lead compensator is incorporated into the feedback path, helping to reduce overshoot in the output of the power op-amp, which could otherwise cause drive saturation. The relationship between the two inputs and the output of the compensator op-amp can be expressed as follows:

$$V_u = -\underbrace{Z_f}_{\text{lag}}\left(\frac{1}{Z_1}V_{set} + \underbrace{\frac{1}{Z_2}}_{\text{lead}}V_s\right) \tag{12.61}$$

Considering the inverting input, its block diagram can be represented as in Figure 12.27(b). The transfer function of the lag compensator is obtained as follows:

$$H_{lag}(s) = Z_f = \frac{R_{\text{lg}}}{R_{\text{lg}}C_{\text{lg}}s + 1} \tag{12.62}$$

The large resistor R_{lg} shifts the zero slightly further from the origin, effectively limiting the DC gain to prevent excessive current in the coil under unexpected conditions. If R_{lg} is very large, a pure integrator represented by the following transfer function is obtained:

$$\lim_{R_{\text{lg}}\to\infty} H_{lag}(s) = \frac{1}{C_{\text{lg}}s} \tag{12.63}$$

The transfer function of the lead compensator can be expressed as follows:

$$H_{lead}(s) = \frac{1}{Z_2} = \frac{1}{R_2}\frac{(R_2 + R_{\text{ld}})C_{\text{ld}}s + 1}{R_{\text{ld}}C_{\text{ld}}s + 1} = \frac{1}{R_2}\frac{\alpha\tau s + 1}{\tau s + 1} \tag{12.64}$$

where the time constant and pole-zero ratio of the lead compensator are given by $\tau = R_{ld}C_{ld}$, and $\alpha = 1 + R_2/R_{ld}$. The closed-loop DC gain is approximately R_2/R_1, and a value of ~2 is chosen to match the bounds of V_{set} (±5 V from DAC of a DSP where the position control loop can be implemented) to the current capability of the power op-amp ($\pm 5 \times 2 = \pm 10$ A). Next, selecting a pole-zero ratio of $\alpha = 10$, a maximum phase boost of $\phi_m \approx 55^\circ$ at frequency ω_m is introduced. Therefore, the resistor R_{ld} is determined as follows:

$$\alpha = 1 + \frac{R_2}{R_{\text{ld}}} \tag{12.65}$$

Hence

$$R_{ld} = \frac{R_2}{\alpha - 1} \approx 1.1\ \text{k}\Omega \tag{12.66}$$

The 10–90% rise time of the closed-loop response is given by $t_r \approx 2.2/\omega_{bw}$, where ω_{bw} is the bandwidth of the system in rad/sec. To achieve a rise time of $t_r < 50\,\mu$s, the required bandwidth is approximately ~7 kHz. A crossover frequency of $f_c = 20$ kHz, which is well above the electrical time constant, is picked to achieve a closed-loop bandwidth around $f_{bw} = 7.8$ kHz. Setting $\omega_m = \omega_{gc} = 2\pi f_{gc}$, the value of the capacitor C_{ld} is determined as follows:

$$\omega_m = \frac{1}{R_{\text{ld}}C_{\text{ld}}\sqrt{\alpha}} \tag{12.67}$$

Hence

$$C_{\text{ld}} = \frac{1}{\omega_m R_{\text{ld}}\sqrt{\alpha}} \approx 2.2\,nF \tag{12.68}$$

The last component to be determined is the capacitor C_{lg}, which is selected such that the gain of loop transmission is unity at gain crossover frequency ω_{gc} as follows:

$$|L(j\omega_{gc})| = \left| \underbrace{\left(\frac{1}{j\omega_{gc}C_{lg}}\right)}_{lag} \underbrace{\left(\frac{1}{R_2}\frac{j\omega_{gc}\alpha\tau+1}{j\omega_{gc}\tau+1}\right)}_{lead} \underbrace{\left(\frac{R_{v2}}{R_{v1}+R_{v2}}\right)\left(1+\frac{R_{p2}}{R_{p1}}\right)}_{Driver} \underbrace{\left(\frac{1}{j\omega_{gc}L_c+R_c+R_s}\right)}_{Actuator} \right| = 1 \tag{12.69}$$

Hence

$$C_{lg} \approx 100\ pF \tag{12.70}$$

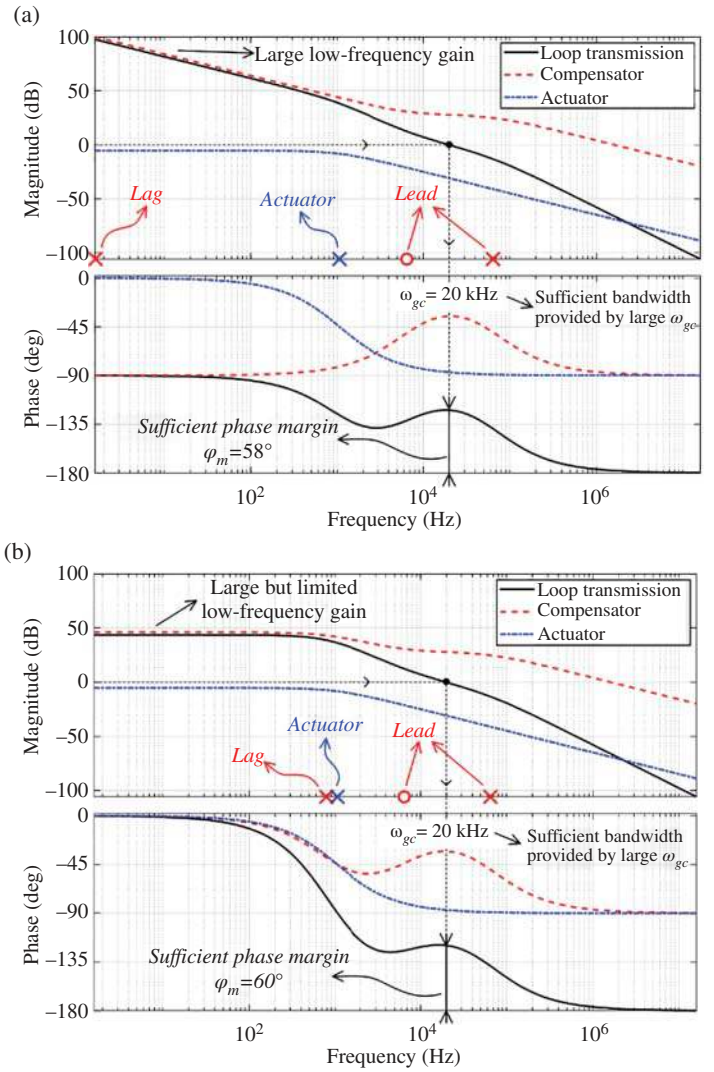

Figure 12.28 Frequency response of the "plant" (actuator coil), lead–lag compensator, and loop transmission: (a) lag compensator with pure integrator and (b) lag compensator with pole a bit further from the origin to limit the DC gain.

Figure 12.28 illustrates the frequency response of the loop transmission, the compensator, and the actuator plus driver for two cases: lag compensator with a pure integrator, and lag compensator with the pole slightly shifted from the origin. In the first case, the pure integrator provides infinite DC gain, while the second case limits the DC gain, preventing overcurrent while still maintaining sufficient low-frequency gain. Also, a sufficient phase margin φ_m of 58° and 60° for these two cases is obtained, ensuring stability, good transient response, and sufficient robustness.

12.7.4 Design Trade-Offs of Current Control Loop

Reference tracking is defined as the response from the reference input to the output, as follows [3]

$$\begin{cases} T = \dfrac{Y}{R} = \dfrac{FPC}{1+PCH} \\ T_{DC} = \lim\limits_{C\to\infty} T(0) = \dfrac{F(0)}{H(0)} \end{cases} \tag{12.71}$$

The corresponding frequency and step responses are shown in Figure 12.29a, representing a well-damped system with an expected bandwidth of approximately 8 kHz and zero steady-state error.

Disturbance rejection represents the transfer function from the disturbance D to the output y:

$$\begin{cases} \dfrac{Y}{D} = \dfrac{P}{1+PCH} \\ DC\ Gain:\ \lim\limits_{C\to\infty} \dfrac{P}{1+PCH} = 0 \end{cases} \tag{12.72}$$

Ideally, the DC gain of the disturbance rejection transfer function should be zero with an infinite loop gain to completely eliminate the disturbance which typically occurs at low frequencies. For instance, in the current control loop, the back-emf is often treated as a disturbance. A higher low-frequency gain improves disturbance rejection, but it can result in a lower phase margin which leads to reduced stability margins and robustness, so a balance is needed. As shown in Figure 12.29b, a great attenuation of the disturbance is obtained.

The sensitivity function S is defined as the transfer function from the noise N to the output y or, equivalently, from the reference R to the error e when $F = 1$:

$$S = \frac{Y}{N} = \frac{1}{1+PCH} \tag{12.73}$$

At low frequencies, S is close to zero due to the high loop gain, reflecting small steady-state error. At high frequencies, S approaches unity because the loop gain decreases. At mid frequencies, S exhibits a peak M_s at frequency ω_{ms}, indicating a region where the system is more sensitive to model variations. Sensitivity is a measure of robustness to parameter variations in the plant P. The impact of variations in the closed-loop transfer function T due to changes in P is proportional to S, as shown by:

$$\frac{dT}{dP} = S\frac{T}{P} \tag{12.74}$$

Hence

$$\frac{dT}{T} = S\frac{dP}{P} \tag{12.75}$$

If S is pushed too low at low frequencies (to reduce steady-state error and improve disturbance rejection), it rises at mid frequencies, leading to a higher peak M_s. This phenomenon is called the waterbed effect: pushing down in one region causes a rise elsewhere. It is also reflected in the

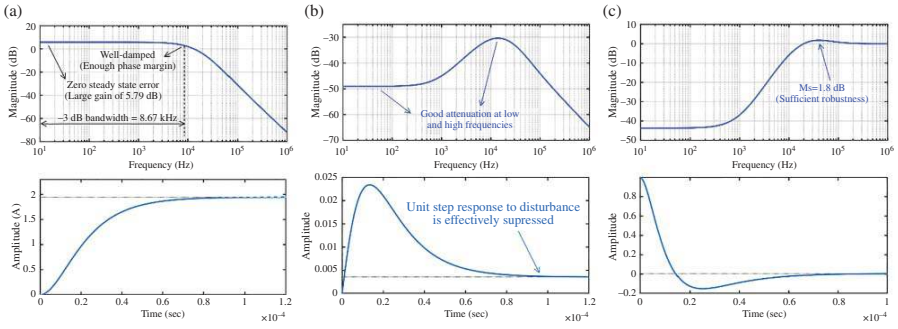

Figure 12.29 Design trade-offs: (a) reference tracking, (b) disturbance rejection, and (c) sensitivity.

fact that $S + T = 1$ for $F = H = 1$. A well-designed system keeps $M_s \leq 2$ dB to 3 dB. As shown in Figure 12.29c, a value of $M_s = 1.8$ dB ensures sufficient robustness to variations in coil resistance and inductance.

12.7.5 Responsiveness and Disturbance Rejection in FOC

After introducing various control methods, this chapter focuses on FOC as a case study to analyze its responsiveness and disturbance rejection capabilities. The chapter explores FOC's effectiveness by conducting both frequency domain analysis and real-time simulation, providing a comprehensive understanding of how the control strategy manages to respond to changes in command inputs while effectively rejecting disturbances.

12.7.5.1 Transfer Function Derivation

To form a simplified block diagram of FOC speed regulation, the effect of current control loop needs to be considered, and it is simplified as a first-order inertia part.

$$G_c(s) = \frac{1}{\tau_c s + 1} \tag{12.76}$$

Hence, the simplified block diagram can be drawn as Figure 12.30.

According to Figure 12.30, the open-loop transfer function of speed tracking is:

$$\begin{aligned} G_\Omega(s) &= G_{PI}(s) G_c(s) G_{plant}(s) \\ &= \frac{k_p s + k_i}{J\tau_c s^3 + (J + B\tau_c)s^2 + Bs} \end{aligned} \tag{12.77}$$

With unit feedback, the closed-loop transfer function can be obtained as:

$$\begin{aligned} \Phi_\Omega(s) &= \frac{G_\Omega(s)}{1 + G_\Omega(s)} \\ &= \frac{k_p s + k_i}{J\tau_c s^3 + (J + B\tau_c)s^2 + (B + k_p)s + k_i} \end{aligned} \tag{12.78}$$

Similarly, the open-loop transfer function regarding to load torque is:

$$\begin{aligned} G_{T_c}(s) &= G_{plant}(s) \\ &= \frac{1}{J_s + B} \end{aligned} \tag{12.79}$$

And its feedback loop is:

$$\begin{aligned} H_{T_c}(s) &= G_{PI}(s) G_c(s) \\ &= \left(k_p + k_i \frac{1}{s}\right)\left(\frac{1}{\tau_c s + 1}\right) \end{aligned} \tag{12.80}$$

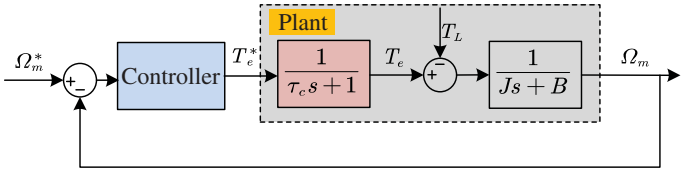

Figure 12.30 Simplified block diagram of a field-oriented controller.

Hence, the system closed-loop transfer function of load torque is:

$$\begin{aligned}\Phi_{T_L}(s) &= \frac{G_{T_L}(s)}{1 + G_{T_L}(s)H_{T_L}(s)} \\ &= \frac{s(\tau_c s + 1)}{(\tau_c s + 1)s(Js + B) + (k_p s + k_i)}\end{aligned} \tag{12.81}$$

12.7.5.2 Frequency Domain Analysis

Based on the transfer functions (12.78) and (12.81), the Bode plots can be drawn in Figure 12.31 to verify their performance before real implementation, and the simulation parameters are set as $J = 0.0025$, $\varsigma = 0.707$ $\omega = 20\pi$.

Figure 12.31a illustrates its speed tracking performance, demonstrating that the motor's speed closely follows the reference below a certain threshold. This indicates that the control system effectively manages to keep the motor's speed aligned with the desired setpoint within this frequency range. Figure 12.31b presents the disturbance rejection capabilities, where the Bode plot passes through the origin at a slope of 20 dB/decade, signifying the system's ability to fully eliminate the impact of constant disturbances. However, the Bode plot also reveals an increased amplitude in the medium frequency range, implying that if the disturbance is periodic and falls within this frequency range, the effectiveness of FOC in rejecting the disturbance will be compromised. This suggests that while FOC performs well in handling low-frequency disturbances, its rejection capabilities may degrade when faced with medium-frequency periodic disturbances.

To illustrate how system responsiveness varies with increasing control gain, the Bode plot of $\omega = 200\pi$ is drawn in Figure 12.32.

Figure 12.32 demonstrates that increasing the control gain bandwidth results in an extended tracking range, which translates to improved tracking performance. As the control gain increases, the system is capable of following the reference signal over a broader range of frequencies. In addition, Figure 12.35 exhibits a decrease in amplitude in the disturbance rejection Bode plot, indicating an overall enhancement in the system's ability to reject disturbances across the entire frequency spectrum. However, it is important to note that while disturbance rejection improves,

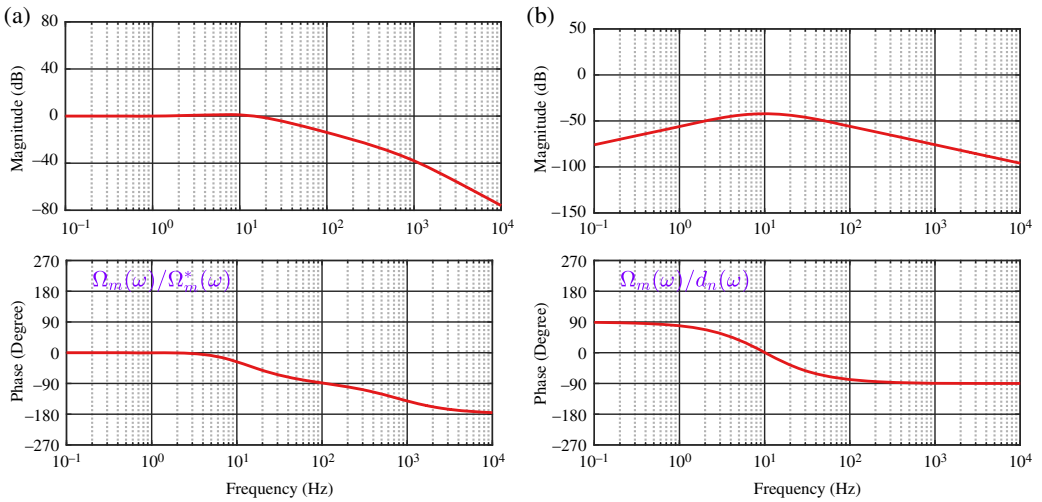

Figure 12.31 Bode plot of the field-oriented control system: (a) tracking performance (b) disturbance rejection.

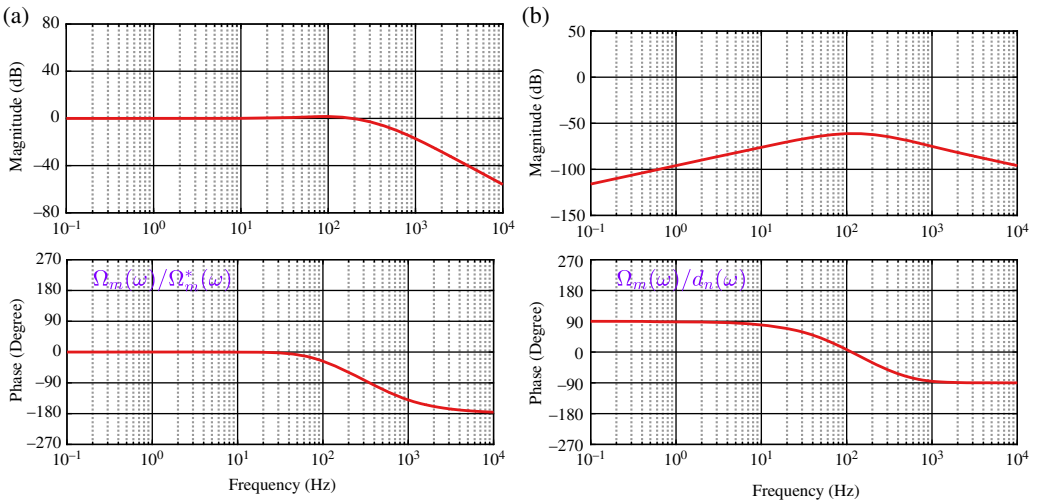

Figure 12.32 Bode plot of the field-oriented control system with increased control gain: (a) tracking performance, (b) disturbance rejection.

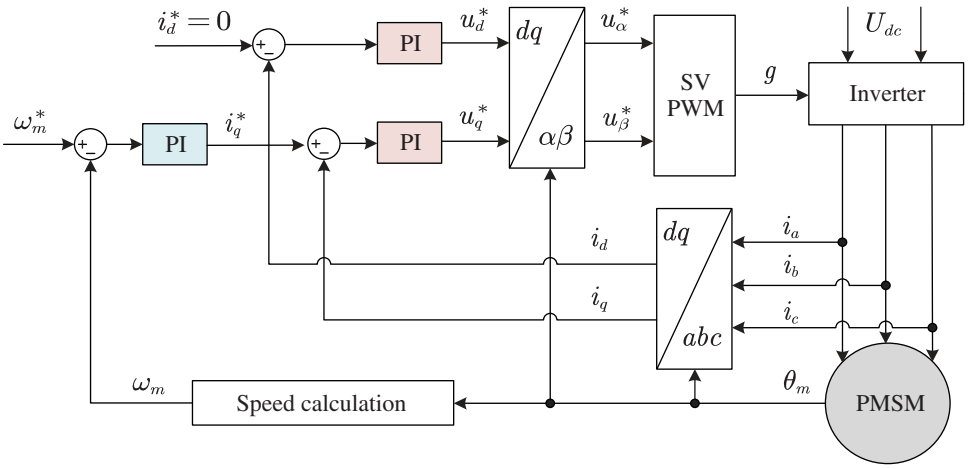

Figure 12.33 System block diagram for simulation.

the system remains less effective at handling disturbances in the medium frequency range compared to low-frequency disturbances. This analysis highlights the benefits of higher control gains in boosting both tracking and disturbance rejection performance at the same time.

12.7.6 Realtime Simulation

Based on the previous controller design, the whole system block diagram for simulation can be drawn as Figure 12.33 with parameters listed in Table 12.3.

A step load change shown in Figure 12.34 is added to the motor to test its disturbance rejection ability.

Figure 12.35 and Figure 12.36 show the speed response using a PI controller with different control gains: 40π for Figure 12.35 and 80π for Figure 12.36.

Table 12.3 Simulated motor parameters.

Symbols	Value
Number of pole pair p_n	4
Rotor PM flux ψ_f	0.232 Wb
d-axis inductance L_d	2.55 mH
q-axis inductance L_q	3.33 mH
Stator resistance R_s	0.33 Ω
Moment of inertia J	2.5 g/m^3

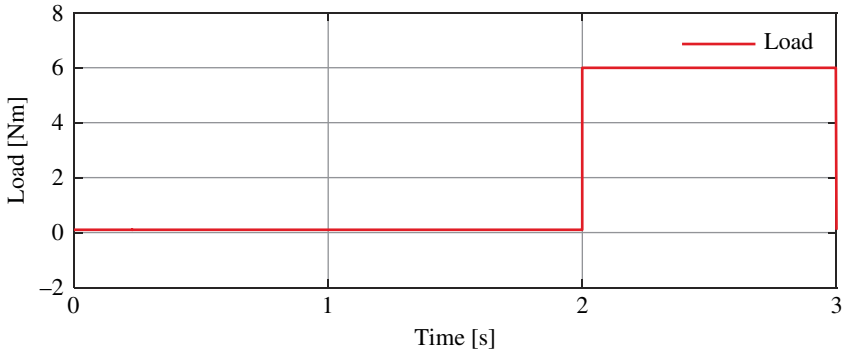

Figure 12.34 Load added to motor.

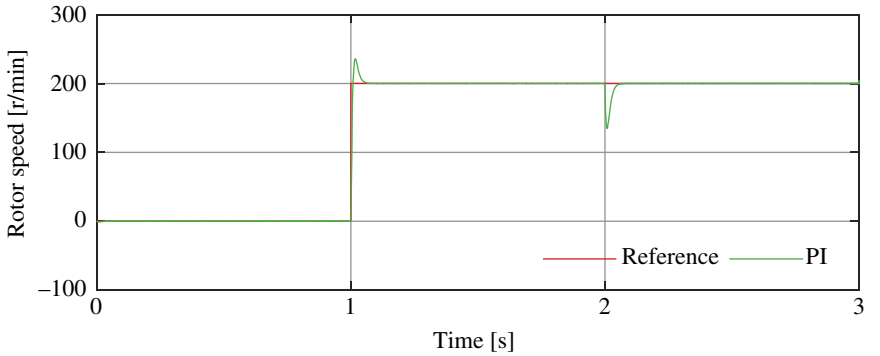

Figure 12.35 Rotor speed response in simulation.

As observed in the previous figures, the effect of the constant load is effectively eliminated, and by increasing the control bandwidth, the speed drop caused by the disturbance is minimized, indicating an enhanced disturbance rejection capability.

In practical applications, the speed reference for a motor may not always remain constant; it can vary over time depending on the operational requirements. To simulate such scenarios, the following analysis uses a speed reference with a sinusoidal waveform. This varying reference allows for a more comprehensive evaluation of the control system's ability to track dynamic changes in speed, providing insights into how effectively the system responds to fluctuating demands. By using a sinusoidal speed reference, the simulation tests the control system's performance in maintaining accuracy and stability even when the desired speed is continuously changing.

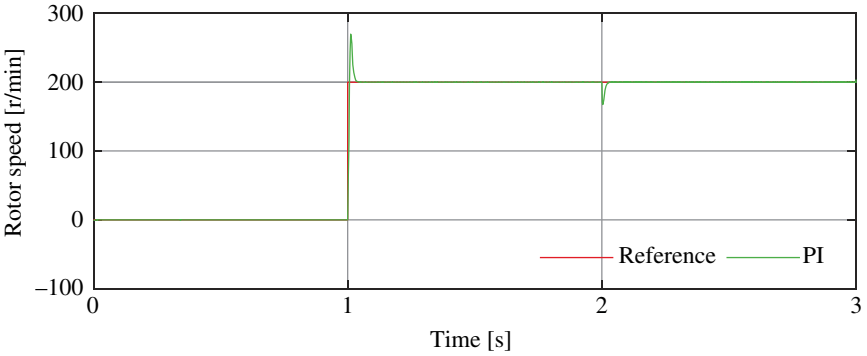

Figure 12.36 Rotor speed response with increased control gain

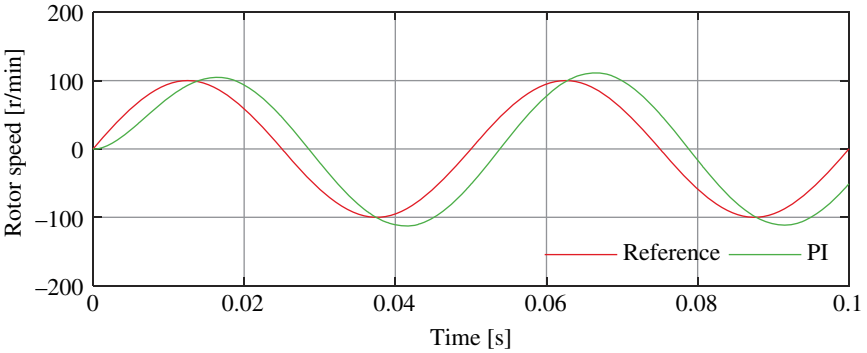

Figure 12.37 Rotor speed response of tracking a sinusoidal reference in simulation.

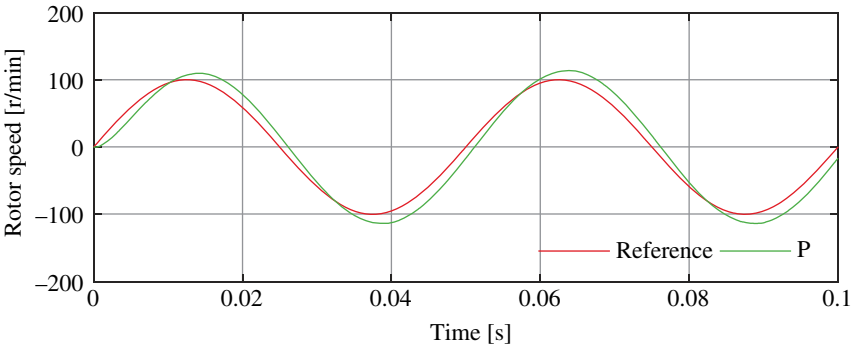

Figure 12.38 Rotor speed response of tracking with increased control gain.

Similarly, the PI controller is simulated with control gains of 40π and 80π and the results are recorded in Figure 12.37 and Figure 12.38.

12.8 Stability Analysis

Stability in control systems refers to the capability of a system to maintain its expected output behavior responding to inputs and disturbances. A control system is considered stable if, when subjected to a bounded input, its output also remains bounded, and the system eventually returns

to its equilibrium state after experiencing a disturbance. An "unstable" system is one in which a disturbance from intended state will grow with time, rather than decay away to zero.

In FOC, one of the primary factors contributing to system instability is the use of unsuitable control gains. Control gains determine the responsiveness of the system to errors between the desired and actual motor states, such as speed or torque. If the control gains are set too high, the system can become overly reactive, leading to oscillations and overshoot as it attempts to correct errors too aggressively. Conversely, if the control gains are too low, the system may respond sluggishly, failing to adequately correct deviations, which can also lead to instability. This delicate balance highlights the importance of appropriately tuning control gains to maintain stability while ensuring precise motor control. And the following case uses the Routh-Hurwitz criterion to obtain the stable range for observer bandwidth selection.

Stability is particularly important in PMSM control systems because these motors are widely used in scenarios requiring precise control of speed and torque, such as electric vehicles and industrial automation. Instability in these systems can lead to erratic motor behavior, reduced efficiency, or even mechanical damage. For instance, oscillations in motor speed can cause excessive wear on mechanical components, while overshoot in torque control can result in jerky and unpredictable motion. Therefore, ensuring stability in PMSM control is crucial for the reliable and predictable operation of these systems, making it a fundamental aspect of control system design.

12.8.1 Mathematical Foundation

Analyzing stability in control systems involves using mathematical tools that help determine whether a system will maintain its equilibrium when subjected to disturbances or changes in input. One of the central concepts in this analysis is the characteristic equation, which is a crucial factor in assessing system stability. The characteristic equation is derived from the denominator of system's transfer function, typically in the form of a polynomial. Its roots, known as the system's poles, are crucial in determining the system's response. Specifically, the location of these poles in the complex plane indicates whether the system will remain stable. To ensure system stability, all poles must have negative real parts, meaning they should be in the left half of the complex plane. It ensures that any disturbances or deviations from equilibrium will decay over time, allowing the system to return to its desired state.

12.8.1.1 A Simple Example

A simplified rendition of a feedback loop is shown in Figure 12.39.

This system features negative feedback, so that the 'error' between the command X and the feedback version of the signal Y is small (or zero). An important feature of the feedback signal is its phase relationship to the input to the forward path H. If that phase approaches 180° with a gain magnitude of at least unity, the feedback signal is now positive, and that causes the error to grow. The "phase margin", the difference between the actual phase and 180° when the magnitude of the feedback signal is one, is an important measure of stability.

To understand stability of this feedback system, it is necessary to establish the roots of the system function. That is:

$$F = \frac{H}{1 + KH} \tag{12.82}$$

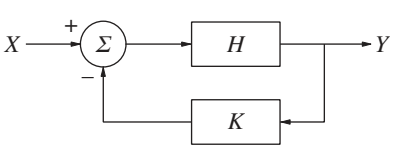

Figure 12.39 Feedback loop.

The poles of the system function are, of course, the roots of the denominator. As a simple example, suppose the forward system function is:

$$H = \frac{1}{(s+a)\ (s+b)} \tag{12.83}$$

The roots (poles) of the system function are, for positive values of the feedback gain K:

$$s = -\frac{a+b}{2} \pm \sqrt{\left(\frac{a+b}{2}\right)^2 - K} \tag{12.84}$$

One way of looking at what happens with dynamical systems like this is to plot the root locus: the path of the roots of the system as the loop gain is varied. For this system, the root locus is roughly as shown in Figure 12.40. The two roots start, with $K = 0$, at -a and -b, move together, merge, and then become complex. For the second order system as described here, the real part of the system response is constant, so a disturbance would have a frequency that increases with gain K, but which has a decay rate that is independent of K. But consider what happens if, somewhere in the loop, another pole appears, so that the forward system function is:

$$H = \frac{1}{(s+a)\ (s+b)\ (s+c)} \tag{12.85}$$

In this case, while we won't solve this problem rigorously, the root locus looks more like what is shown in Figure 12.41. In this case, the "fastest" of the roots gets faster, while the other two merge as in the second order case, but then move in the direction of positive real part, or instability. This sort of system will first become more responsive but then "oscillatory" and, for higher gains, unstable.

12.8.2 Routh-Hurwitz

One widely used tool to assess system stability is the Routh-Hurwitz criterion. This criterion provides a straightforward solution by determining whether all poles of the characteristic equation have negative real parts, without having to explicitly calculate the poles. By applying it, one can

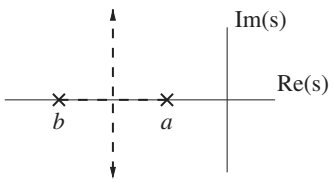

Figure 12.40 Root locus of a second-order system.

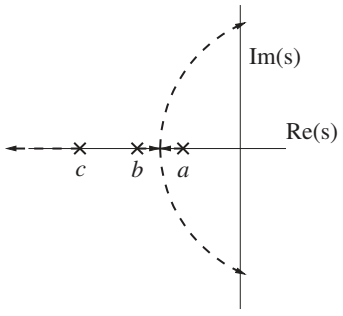

Figure 12.41 Root locus of the example third-order system.

Table 12.4 Routh table.

s^3	$a_3 = J\tau_c$	$a_1 = k_p$
s^2	$a_2 = J$	$a_0 = k_i$
s^1	$b_1 = (a_2a_1 - a_3a_0)/a_2$ $= k_p - \tau_c k_i$	0
s^0	$c_1 = (b_1 a_0 - 0)/b_1$ $= k_i$	0

analyze the signs and patterns in the coefficients of the characteristic equation to conclude whether the system is stable. This method is particularly valuable in control system design, as it allows engineers to quickly assess the stability of complex systems, ensuring that they meet the necessary stability requirements.

The first step in a Routh-Hurwitz analysis is to set up what is called the "Routh Table." This table focuses on the characteristic equation of the system: the denominator of the system function. It has a row for each coefficient of the system: for a third-order system, there are four rows. The top row consists of the coefficients of the highest order term and then the coefficients of every other term, in descending order. The second row has the terms not in the first row. So, for a fourth-order system the terms in the top row would be the coefficients of the fourth, second, and zeroth order terms, while the second row would have the coefficients of the third and first order terms. (If the second row is not as long as he first, as it would be with an even numbered order, the last coefficient is zero). Then, for each of the rest of the rows, each term is constructed as the negative of the determinant of a 2×2 matrix divided by the highest order entry in the row above. The left-hand column of that matrix is the value of the leading entries in the two rows above, and the right-hand column of that matrix is the value of the entries in the two rows above and to the right. The lowest order entries for the lower rows are zero. There is an example of this in the reference cited below for a fourth-order system and a third-order system is illustrated below.

Interpretation of the Routh table is that the system is stable if all of the entries in the first column have the same sign. That is, the number of right-hand plane roots is equal to the number of sign changes in the first column.

For the exemplar drive system described above, as described in (12.78) and (12.81) neglecting the viscous damping B, the characteristic equation of the system is

$$J\tau_c s^3 + Js^2 + k_p s + k_i \tag{12.86}$$

Hence, the Routh array can be listed as Table 12.4.

According to the criterion, to ensure system stability, every element in the first column of the Routh array must be positive. So, for the above case:

$$k_p - \tau_c k_i > 0 \tag{12.87}$$

Substituting the control gain setup into (30) yields

$$2\zeta\omega_o - \tau_c\omega_o^2 > 0 \tag{12.88}$$

By simplifying it, the stable condition for control bandwidth selection is:

$$\omega_o < 2\zeta/\tau_c \tag{12.89}$$

12.9 Problems

12.1 What are the meanings of the *dq* axis inductances in a PMSM, and why is this distinction unnecessary in induction machines?

12.2 Briefly describe the fundamental concept of FOC and analyze its advantages. What coordinate systems and transformations are used in vector control?

12.3 Analyze the physical significance of the motor model parameters in various coordinate transformations.

12.4 Briefly describe the fundamental concept of direct torque control and analyze its advantages.

12.5 Please provide a brief comparison between FOC and DTC.

12.6 Given the rated parameters of a three-phase induction motor as:

Symbols	Value
Number of pole pair p_n	3
Synchronous frequency f_s	50 Hz
Rotor resistance R_1	0.06 Ω
Stator leakage inductance X_1	0.34 Ω
Rotor leakage inductance X_2	0.33 Ω
Magnetizing reactance X_m	10.6 Ω

Ignore stator resistance, plot the torque-speed curves of the motor operating under constant flux control at 50 Hz and 100 Hz.

12.7 Given the inverter model as figure below:

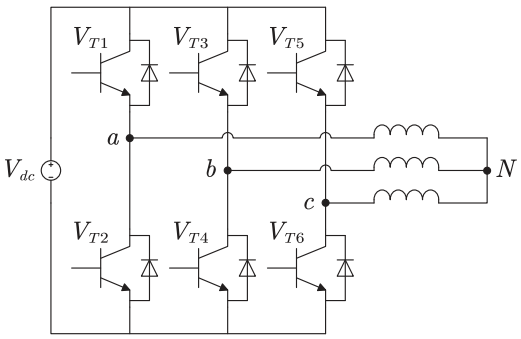

Analyze the phase voltages V_{aN}, V_{bN}, V_{cN} and line voltages V_{ab}, V_{ac}, V_{bc} of a three-phase load for all switching combinations in tabular form.

12.8 Establish a direct torque control simulation model for a synchronous motor, referring to Figure 12.18 for guidance.

12.9 Establish a field oriented control simulation model for a synchronous motor, referring to Figure 12.10 for guidance.

12.10 Given the parameters of PMSM as:

Symbols	Value
Number of pole pair p_n	5
Rotor PM flux ψ_f	0.34 Wb
d-axis inductance L_d	3.32 mH
q-axis inductance L_q	4.47 mH
Stator resistance R_s	0.22 Ω
Moment of inertia J	10.5 g/m^3

If the bandwidth method is used to specify the speed loop control gain and the current loop impact is neglected, apply the Routh-Hurwitz criterion to analyze the stability range of the bandwidth. Also, draw its Bode plots regarding speed tracking and disturbance rejection.

12.11 Given the parameters of the mechanical dynamic of the DC actuator discussed in the chapter as $k_t \approx 1.9$ mN.m/A, $J \approx 1.5\text{e}{-9}$ kg.m^2, $K_d \approx 4.5\text{e}{-07}$ N.sec/rad, and $K_s \approx 1.3$ mN/rad, for full-state feedback control of the position, obtain the feedback gain matrix K using Ackermann's formula to have the desired closed-loop poles with a natural frequency of $\omega_n = 2\pi f_n = 2\pi 500$ rad/sec, and damping of $\zeta = 0.8$. As the bandwidth of the current control loop (>8 kHz) is much larger than the bandwidth of the position loop (~500 Hz), current control loop can be treated as its DC gain as in the figure below. This gain is canceled out by its inverse in the position loop.

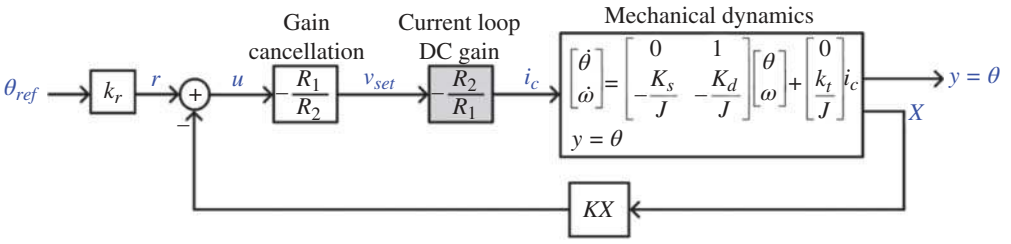

References

1 Mohammadi, S. (2022). "Modeling, design, identification, drive, and control of a rotary actuator with magnetic restoration," Ph.D. dissertation, Dept. Elect. Eng. Comput. Sci., Massachusetts Inst. Technol., Cambridge, MA, USA.

2 Mohammadi, S., Benner, W.R., Kirtley, J.L., and Lang, J.H. (2024). An actuator with magnetic restoration, Part II: Drive circuit and control loops. *IEEE Transactions on Energy Conversion* 39 (4): 2543–2558.

3 Astrom, K.J. and Murray, R.M. (2008). *Feedback Systems: An Introduction for Scientists and Engineers*. NJ: Princeton University Press.

Index

Electromagnetic Analysis of Electric Machines: First Principles, Modeling, and Design, First Edition.
James L. Kirtley, Christopher H. T. Lee, and Sajjad Mohammadi.

Companion website: www.wiley.com/go/kirtleyelectric

WILEY END USER LICENSE AGREEMENT

Go to www.wiley.com/go/eula to access Wiley’s ebook EULA.